The Acid Growth Theory: a Fundamental Concept Revisited

Dissertation zur

Erlangung der naturwissenschaftlichen Doktorwürde
(Dr. sc. nat.)

vorgelegt der

Mathematisch-naturwissenschaftlichen Fakultät der

Universität Zürich

von

Gorka Santos Fernandez

aus Spanien

Promotionskommission

Prof. Dr. Ueli Grossniklaus (Leitung der Dissertation)
Universität Zürich, Schweiz

Prof. Dr. Joop Vermeer
Université de Neuchâtel, Schweiz

Prof. Dr. Bradley Nelson
ETH Zürich, Schweiz

Prof. Dr. Christian Hardtke
Université de Lausanne, Schweiz

Zürich, 2020

Curriculum Vitae

Persönliche Angaben

Name	Santos Fernanadez
Vorname	Gorka
Geburtsdatum	31. January 1988
Heimatort	San Sebastian, PV

Ausbildung

2015– aktuell Doktorand MNF an der Universität Zürich

Ph.D. Thesis: *The Acid Growth Theory: a Fundamental Concept Revisited*

09.2006 - 06.2011 B.Sc. & M.Sc. Molekulargenetik an der UCM MADRID

Master Thesis: "*Rapid and reliable identification of biotypes B & Q in the whitefly Bemisia tabaci through ISSR (Inter-Simple Sequence Repeat)*"

Bachelor Thesis: "*Study of chromosome B's pathogenicity in Zea mais*"

09.1999 - 06.2006 Colegio Sagrado Corazón Mundaiz Ikastetxea

Publikationen (*denotes equal contribution)

- Moussu S*, Broyart C*, **Santos-Fernandez G***, Augustin S, Wehrle S, Grossniklaus U, Santiago J. 2020. Structural basis for recognition of RALF peptides by LRX proteins during pollen tube growth. *Proc Natl Acad Sci USA* **117**:7494-7503.
- Vogler H*, **Santos-Fernandez G***, Mecchia MA*, Grossniklaus U. 2019. To preserve or to destroy, that is the question: The role of the cell wall integrity pathway in pollen tube growth. *Curr Opin Plant Biol* **52**:131–139.
- Mecchia MA*, **Santos-Fernandez G***, Duss NN*, Somoza SC, Boisson-Dernier A, Gagliardini V, Martínez-Bernardini A, Fabrice TN, Ringli C, Muschietti JP, Grossniklaus U. 2017. RALF4/19 peptides interact with LRX proteins to control pollen tube growth in. *Science* **358**:1600–1603.

Acknowledgments

First of all, I would like to thank Prof. Ueli Grossniklaus for giving me the opportunity to accomplish my PhD in his laboratory and for creating such a nice working environment. I am grateful for his supervision, helpful discussions and his support. Furthermore, I am thankful for the freedom he granted me, which has helped me to achieve good results and reach the goals of my project.

Moreover, I want to thank Prof. Bradley Nelson (ETH, Zurich), Prof. Christian Hardtke (Unil, Lausanne) and Prof. Joop Vermeer (UZH, University of Zurich) for being part of my committee and for their essential guidance during the meetings. Without them and their experience, I could not have successfully conducted all the different and multidisciplinary experiments that I had to plan and perform during my thesis.

A special thanks goes to Dr. Hannes Vogler, for being always there as my guidance, a second mentor without whom, the good results wouldn't have been possible to reach due to his enthusiasm for science. Working and travelling with him, together with the long beer discussions, provided me with good advices, the ones which have marked me and will mark my future directions. Also in parallel, I would like to thanks Dr. Martin Mecchia for the time spent working working together on the 'RALF project'. It would be impossible to count all the ways that you've helped me in my progress.

Dear Lab colleagues, especially Alejandro, thank you for being there in the good and the bad moments, for making a bad day into a good one. Thank you for helping me with my experiments while laughing and sharing life experiences. I will miss you all.

For day to day scientific business, I am very thankful to the past and present members of the Sex club discussion group that I was allowed to be a part of: Evelyne, Nadine, Andrea, Andrea, Anna, Dario, Martin, Alejandro, Stefano, Katya, Nick and Nicky.

Furthermore, I would like to enormously thank the technical employees of our group, who are the scaffolds of the lab and are always open to help with any of my requests and questions: Valeria, Arturo, Christof, Daniela, Peter, Anja and Daniel. Additionally, I would like to thank Dani Bollier for the construction of the different pieces of the CFM, and the gardeners Kari and Christian for being always there behind the scenes.

For their friendship, outdoor trips, dinners, parties, aperos, chats, scientific discussions, inherited projects, conferences and running the SOLA, I would like to thank

everyone from the lab, and especially Nadine, Alejandro, Sofia, Ueli, Önder, Afif, Milka, Gautam, Christof, Ana Marcela and Arturo.

Apart from the Grossniklaus lab, I would like to send special thanks to the people from Prof. Bradley Nelson's group, mainly to Dr. Jan Burri — one of the nicest and blondest persons I know and the best companion to visit Kandersteg — for all the work we did together on the root project. Thanks also to Julia Santiago's group. Both to her and Steven Moussu. They made me more busy than usual during the last part of my PhD, but this collaboration taught me a lot about my own project, and it demonstrated how the power of the different groups together can reach goals efficiently.

From the deepest of my heart I would like to thank my family and Justine, my girlfriend, for putting up with all the long working hours, moody moments and giving me so much support. Thanks for making me who I am and for holding me either in the past or in my future.

Last, but not least, I am very grateful to many of my old and new friends. For those from San Sebastian, my place of birth, who visited me during this period in Zurich. To all my friends from Madrid, the city where I lived and studied. It has been always a pleasure to keep traveling and visiting you, guys. And specially to 'The Imparables', the group of friends I made when I arrived in Zurich. Without them and their continuous supportive pressure, together with the countdowns to hand in the thesis, probably this day would have taken a bit longer.

Zusammenfassung

Pflanzenwachstum und Entwicklung beeinflusst die landwirtschaftliche Produktion direkt. Beides, Entwicklung und Wachstum, ist abhängig von Zellteilung und Zellexpansion. Die Zellwand, die natürliche Barriere der Zelle, und Zellexpansion und Zellteilung sind direkt miteinander verknüpft. Die Zellwand besteht hauptsächlich aus Zellulose und Querverbindungen aus anderen Polysacchariden, deren Häufigkeit und Konformation beeinflussen die mechanischen Parameter der Zellwand, wie Elastizität oder Steifigkeit, und regulieren so die Zellexpansion. Während dem Wachstum einer Zelle müssen die Eigenschaften der Zellwand laufend angepasst werden, so dass die Zellexpansion nicht die Integrität der Zelle beeinträchtigt. Aus diesem Grund überwachen Rezeptoren in der Plasmamembran die Eigenschaften der Zellwand und übersetzen extrazelluläre Signale in Intrazelluläre Signalkaskaden, indem der Zellwandintegritäts-Signalweg (CWI) aktiviert wird, um die Regulierung der Zusammensetzung der Zellwand anzupassen.

Der pH-Wert ist ein Parameter, der die polymerische Struktur der Zellwand beeinflusst wie in der Acid Growth Theory (AGT) beschrieben wurde. Durch die Steigerung des Turgordruckes, führt Zellwandversauerung zu verstärkter Zellelongation. Obwohl die Mehrheit der wissenschaftlichen Gemeinde die AGT akzeptiert, wird sie immer noch kontrovers diskutiert; mehrere sich widersprechende Studien wurden publiziert und es gibt noch keine Evidenz für die allgemeine Anwendbarkeit der AGT. Das Hauptziel dieser Arbeit war die Validierung der AGT in verschiedenen experimentellen Systemen, wie Pollenschläuche von *Arabidopsis thaliana* und Wurzelzellen von *Brachypodium dystachion*.

In einem ersten Ansatz wurde *Arabidopsis* Pollen als Modellsystem genutzt, als tubuläre Strukturen eignen sich Pollenschläuche sehr gut, um Zellelongation auf der Ebene einer einzelnen Zelle zu untersuchen. Während diesem Projekt konnten wir aufzeigen, dass Rapid Alkalinisation Factors (RALF) Peptide mit Leucine Rich Repeat Extensine (LRX) Proteinen interagieren, LRX Proteine sind Zellwand-Glykoproteine. LRX-Proteine wurden als strukturelle Proteine beschrieben, aber wir konnten aufzeigen, dass sie, durch die Interaktion mit RALF-Peptiden, eine wichtige Rolle spielen für die Kontrolle der Zellwandintegrität. Ausserdem konnten wir durch eine Analyse der Protein Kristallisation demonstrieren, dass die Interaktion zwischen LRX und RALF eine pH-abhängige Interaktion ist; unter sauren Bedingungen, ist die Affinität der Bindungspartner, wegen eines spezifischen Faltstatus des RALF-Peptides höher.

In einem weiteren Ansatz wollten wir die AGT durch das Studium der Zellexpansion in *Brachypodium*-Wurzelzellen validieren. Die Zellexpansion in einer Mutante, die einen höheren Auxinspiegel und somit auch eine höhere Ansäuerung der Zellwand aufweist, *Bdtar21*, wurde analysiert, indem mit einem mikro-robotik-System die mechanischen Eigenschaften wachsender Pflanzenzellen charakterisiert wurden. Wir konnten demonstrieren, dass eine Reduktion des pH-Wertes einen direkten Einfluss hat auf die Elastizität und die Steifigkeit der Zellwand hat, und somit die AGT unterstützen.

Durch das Studium zweier Modellorganismen, *Arabidopsis thaliana* und *Brachypodium dystachion*, konnte ich aufzeigen, dass zumindest einige wichtige Interaktion zwischen Proteinen des Zellintegrität Signalwegs vom pH-Wert abhängig sind, der PH-Wird spielt deshalb eine wichtige Rolle für Zellelongation und Wachstum, dies stützt die AGT.

Abstract

Plant growth and development depends on cell division and expansion and has a direct impact on agricultural production. Thus, cells division and expansion are strictly connected with the cell wall, which forms a natural barrier. It consists mainly of cellulose and crosslinking polysaccharides whose abundance and conformation modulate mechanical parameters, such as stiffness and elasticity, and thus regulate cell expansion. During cell growth, cell wall properties have to be adjusted, assuring cell expansion without compromising cell integrity. Thus, plasma membrane-located receptors sense cell wall properties, transducing extracellular signals into intracellular cascades through the cell wall integrity (CWI) pathway that, in turn, leads to adjustments in the regulation and composition of the cell wall.

One parameter that has been shown to modify the polymeric structure of the cell wall is pH, as was described in the Acid Growth Theory (AGT). Cell wall acidification results into cell elongation due to an increase of the turgor pressure. Despite being accepted by the majority of the scientific community, the AGT is still controversial because of several contradicting studies published, and a proof for its universal applicability is still missing. Therefore, the main objective of this thesis has been to validate the AGT in different experimental systems such as *Arabidopsis thaliana* pollen tubes and *Brachypodium distachyon* root cells.

In a first approach, *Arabidopsis* pollen tubes have been used as model system, being a tubular structure very suitable for studying cell elongation at the single cell level. During this project, we could highlight interactions of Rapid ALkalinisation Factors (RALF) peptides, already known as actors of the CWI pathway, with Leucine Rich repeat eXtensine (LRX) proteins, a cell wall glycoprotein. So far, LRX proteins were described as having structural functions, but we found that they play an important signalling role during the control of CWI, though the interaction with RALF peptides. Moreover, we demonstrated that LRX-RALF interaction is pH-dependent, having a higher binding affinity under acidic pH, due a specific folding state of RALF, by protein crystallisation analyses.

The second approach we used to validate the AGT was to study cell expansion in *Brachypodium* root cells. Analysis of cell expansion in a mutant, *Bdtar2l*, exhibiting a higher auxin level and therefore a higher acidification of the cell wall, was performed. Using a micro-robotic system able to mechanically characterise growing plant cells, we

could demonstrate that a reduction in pH has a direct impact on the cell wall elasticity and stiffness, supporting the principle of the AGT.

Thus, during my doctoral studies, using two plant model organisms, *Arabidopsis* and *Brachypodium*, I was able to show that at least some important interactions between CWI signalling pathway proteins depend on a pH in the cell wall, which therefore plays a crucial role in cell elongation and growth, which in turn supports the AGT.

Content

1 Chapter 1 - INTRODUCTION

1.1 The Importance of the Elongation

One of the major concerns of plant biology is the better understanding of plant growth and cell morphogenesis mechanisms. In agriculture, these processes are crucial for efficient plant development during the growing season, resulting in higher plant biomass, which is essential for food production (Jones et al., *2015*), for the textile industry (Popp et al., *2014*) and more recently for the bioenergy production (Carlsson et al., *2011*). Thus, a better understanding of plant growth and cell elongation, does not only impact the field of plant science but also benefits the entire society.

Right after seed germination, plants grow through cells division followed by cell expansion. The rapid cell expansion provides a fast lengthening of axial organs (Mac-Leod and Thompson, *1979*; Obroucheva et al., *1995*) and is required in early germination for the survival of the young seedlings.

Plant cell expansion displays a regulated balance between flexibility and structural integrity of the cell, which is mainly controlled by the cell wall (Cosgrove, *2015*). The plant cell wall is a complex interconnected polymer network composed by large polysaccharides and cell wall proteins (for details see section 1.1.2). It surrounds and restrains the cell, allowing to build up an internal pressure due to the osmotic potential difference between inside and outside of the cell, called the turgor pressure. The interplay between cell wall and turgor pressure provides a mechanical rigidity and stability to the plant cells. Despite this rigidity, the cells must be able to expand during their development to form desired plant morphologies and sizes. Thus, when a cell grows, its wall stretches irreversibly as the cell enlarges due to the selective spatially localized cell wall loosening, the increase of the internal turgor pressure due to a higher osmotic water influx, and the integration of new cell wall material (Farrokhi et al., *2006*; Smith et al., *1998*).

These growth mechanisms have been observed in most of the cells exhibiting this rigid cell barrier, both in prokaryotes and in eukaryotes such as fungi and plants. Conversely, animal cells that do not have cell walls, rely on a cortical, contractile cytoskeleton, which is a complex, dynamic network of protein filaments and microtubules present in the cytoplasm, to control their mechanical properties and shapes (Durand-Smet et al., *2014*). This cytoskeleton provides mechanical resistance to deformation, induces shape changes during movement and is involved in the intracellular transport of vesicles and organelles. It is important to note that plant cells also possess a cytoskeleton that can indirectly control the structure and mechanical

properties of the cell wall (Baskin, *2001*; Kost and Chua, *2002*; Paredez et al., *2006*). However, its entire role within the plant cell dynamics needs further investigation. Therefore, the cell wall remains the principal barrier that controls plant cell elongation and makes the difference between an amazingly rapid cell expansion and a deadly cell explosion.

1.1.1 The Cell Wall

The cell wall fulfils very versatile tasks while being the principal barrier to protect the plant from physical damage and against plant viruses or other pathogens (Bellincampi et al., *2014*; Underwood, *2012*). The cell wall provides with both strength and flexibility to the cell (Cosgrove, *2015*). It withstands the turgor pressure, allowing the plant to remain rigid and erect preventing water loss to control the direction of cell growth (Gigli-Bisceglia et al., *2019*; Le Gall et al., *2015*; Moore et al., *2008*). Furthermore, the cell wall is permeable. Its porosity allows some small substances, like sucrose for example, to pass into the cell while keeping macromolecules, such as large proteins out. This phenomenon is mainly related with the cell wall components, which play a important role in all the different functions (Liu et al., *2019*; Read and Bacic, *1996*).

The cell wall is mainly composed of large polysaccharide molecules, such as cellulose, hemicelluloses and pectins (Cosgrove, *2005*; Wolf-Dieter, *1998*) (Fig. 1.1). Cellulose is a mostly unbranched (1,4)-linked β-D-glucan which is synthesised at the plasma membrane. Many of these cellulose molecules are arranged in a parallel manner but not evenly separated, as commonly depicted (Zhang et al., *2014*). Indeed, recent publications demonstrated that cellulose molecules make close contact with each other, forming junctions or bundles together with hemicelluloses, contributing substantially to the mechanical strength of the cell wall (Zhang et al., *2014*; Zhao et al., *2014*). Two main hemicelluloses appear to crosslink cellulose microfibrils: xyloglucan and arabinoxylan. Xyloglucan is the most abundant hemicellulosic polysaccharide in the primary cell wall. It has a backbone which is similar to the one of cellulose, where 3 out of 4 glucose residues are substituted by xylose. Thus, it is found to be the principal hemicellulose forming junctions with cellulose to maintain the mechanical stability (Park and Cosgrove, *2015*, *2012*). On the other hand, arabinoxylan consists of a (1,4)-linked β-D-xylan backbone decorated with arabinose branches. Although, like Xyloglucan, it is very similar to cellulose, both hemicelluloses are unable to form microfibrils by themselves. Hemicelluloses are synthesised in the Golgi apparatus, and like pectins, are transported

to the cell wall surface by vesicles for providing stability, strength and resistance for pathogen enzymatic attacks, like cellulases (Adani et al., *2011*). Pectins are a heterogeneous group of polysaccharides with distinctive domains thought to be covalently linked with each other, but the nature of the crosslink has not been determined yet (Ridley et al., *2001*; Vincken et al., *2003*). Pectins are mainly divided into rhamnogalacturonan I, homogalacturonan and xylogalacturonan. The latter two exhibit carboxyl groups that are often found methyl-esterified, which is a structural modification that prevents these pectins from linking with each other and thus from forming gels (Willats et al., *2001*). Arabinans and arabinogalactans are two neutral pectins also found in the cell wall. They have been proposed to promote cell wall flexibility by binding to cellulose (Lin et al., *2015*). Thus, in general, pectins function as a "glue" that holds the cell wall together and contribute to cell wall stiffness depending on the degree of methyl-esterification (Cosgrove, *2015*; Parre and Geitmann, *2005*).

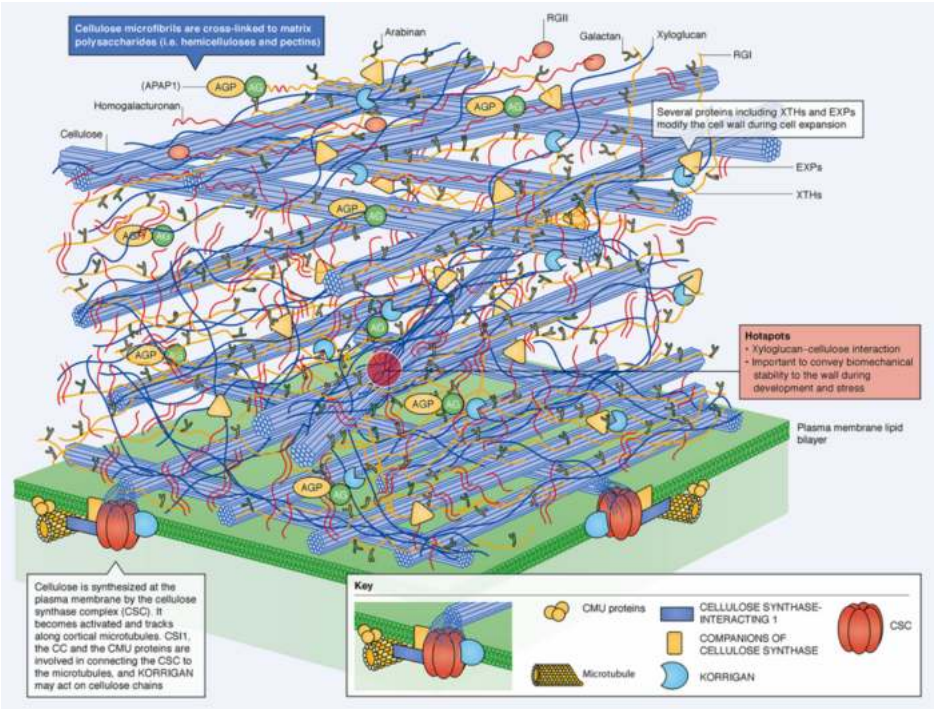

Fig. 1.1: A schematic overview of plant's cell wall. *Plant cells are surrounded by a strong polysaccharide-rich cell wall where cellulose hemicelluloses and pectins are the main components of the cell wall. Expansins (EXPs) and hydrolases (XTHs) can be also represented in this image. (Reprinted from (Lampugnani et al., 2018)).*

Even though these polysaccharides contribute about 90-95% of the material, the cell wall also contains a wide range of proteins that modify its mechanical properties and permeability (Albenne et al., *2013*), for example carbohydrate esterases (Nakamura et al., *2017*), polysaccharide lyases (Linhardt et al., *1987*) and expansins that act on the

carbohydrates (McQueen-Mason et al., *1992*). Another category of cell wall proteins, the oxido-reductases, mainly peroxidases, are essential to counterbalance many oxidation reactions occurring in the extracellular matrix that modify polymer networks involving carbohydrates and/or aromatic compounds (Passardi et al., *2004*). In addition, structural proteins like glycine-rich proteins, proline-rich proteins and hydroxyproline-rich glycoproteins, also called extensins, are present in the cell wall (Albenne et al., *2014*). This group of proteins is characterised by Ser-$Pro_{2–n}$ repeats (Borassi et al., *2015*; Showalter et al., *2016*). Intra- and intermolecular linkages formed by oxidative crosslinking of tyrosine in the context of a Tyr-X-Tyr sequence result in the formation of isodityrosines, di-isodityrosines, or pulcherosines (Brady et al., *1996*; Fry, *1982*; Holst and Varner, *1984*; Showalter et al., *2016*), which further strengthen the extensin structure. Extensin gene expression is induced or up-regulated in tissues under tensile stress (Shirsat et al., *1996*), strong mechanical pressure (Keller and Lamb, *1989*), upon wounding (Wycoff et al., *1995*) and pathogen infection (García-Muniz et al., *1998*). Furthermore, extensins have been found to produce chimeric proteins with Leucine-rich repeat (LRR) proteins, thus forming LRR-extensins (LRXs), which mediate protein–protein interactions in many different cellular processes (Baumberger et al., *2001*; Kobe and Deisenhofer, *1994*). Therefore, LRXs are candidates for having a regulatory or signaling function since the extensin domain can interact with the cell wall while the non-structural LRR domain provides an independent activity for cellular interactions (Xiao Liu et al., *2016a*).

Cellular interactions, like cell-cell communication during pathogen attacks, fertilisation or abiotic stress responses cause modifications of the cell wall (Bacete et al., *2018*). By using cell wall sensor molecules, the plant cell closely monitors the status of the cell wall and any modification is reported via signal-transduction mechanisms to the inside of the cell, where changes in gene expression and protein targeting are induced (Jones and Dangl, *2006*). This allows the plant cell to appropriately react to disturbances through the modification of the cell wall properties and to adjust, likewise, the cellular growth (Bellincampi et al., *2014*). Such a mechanism constantly senses the status of the cell wall and triggers intracellular physiological and biochemical responses that signal back to the cell wall to allow appropriate remodelling. This cell wall remodelling requires a large number of proteins with diverse biochemical activities (Cosgrove, *2014*). Thus, an elaborate cell wall integrity (CWI) surveillance system, consisting of a pathway of apoplastic proteins and transmembrane receptors, is in charge to detect changes in cell wall homeostasis. However, although the CWI pathway was postulated a while ago (Levin, *2005*; Ringli, *2010*) and some of the cytoplasmic components have been identified,

the involved ligand and the link between cell wall and plasma membrane stayed elusive until very recently.

1.1.2 The Cell Wall Integrity Pathway

It was long assumed that cell wall proteins have a largely structural function, like reinforcing bars used to give concrete a higher tensile strength. However, during the past 10 years, it has been shown that they also play an important role in the perception and transduction of extracellular signals as they react as extracellular sensors. Among these proteins, LRXs attracted much of the attention, because they were recently identified as a central element of the CWI pathway (Fabrice et al., *2018*). In *Arabidopsis thaliana* they form a family with eleven members, which are expressed in a tissue-specific manner. LRX1/2, LRX3/4/5, and LRX8/9/10/11 are predominantly expressed in root hairs, in the main root and the shoot, and in pollen, respectively (Herger et al., *2019*). As mentioned before, they are consist of two major domains, which are linked by a cysteine-rich repeat of 39–50 amino acids. The LRR domain, which contains 11 leucine-rich repeats (Baumberger et al., *2003*) is found in organisms throughout all kingdoms and represents a versatile domain implicated in binding interaction partners that range from small peptides to large proteins and non-proteinaceous small molecular compounds such as brassinosteroids (Hohmann et al., *2017*). This way, as it will be described in detail in Chapter 2, LRX proteins were shown to bind to a small group of peptides named Rapid ALkalinization Factors (RALFs) (Mecchia et al., *2017*; Pearce et al., *2001*). RALFs are peptide hormones that modify plant growth, fertilisation, and responses to pathogen infection by inducing several physiological responses, including alkalinization of the apoplast, hence their name (Campbell and Turner, *2017*; Ge et al., *2017*; Morato do Canto et al., *2014*; Murphy and De Smet, *2014*; Pearce et al., *2001*; Stegmann and Zipfel, *2017*). The *Arabidopsis RALF* gene family contains 34 members, some of which are broadly expressed, while others are found in specific tissues (Campbell and Turner, *2017*; Murphy and De Smet, *2014*) (Fig. 1.2 A). Furthermore, there is genetic and biochemical evidence that RALFs also bind the extracellular domain of some members of the transmembrane *Catharanthus roseus* RECEPTOR-LIKE KINASE1-LIKE (CrRLK1L) protein family (Dünser et al., *2019*; Ge et al., *2017*; Haruta et al., *2014*; Stegmann and Zipfel, *2017*), therefore providing a link between extracellular and intracellular signaling. Indeed, it was shown that this connection activates a phosphorylation cascade that eventually represses H^+-ATPase (proton pump) activity, thereby increasing the extracellular (apoplastic) pH and

reducing cell elongation (Chen et al., *2016*; Ge et al., *2017*; Haruta et al., *2014*). As it will be explained in the section 1.1.3, the Acid Growth Theory (AGT) suggests that acidification of the cell wall favours cell wall expansion, whereas alkalinization induces growth arrest (Cosgrove DJ in eLS,; Morato do Canto et al., *2014*; Rayle and Cleland, *1970*) (Fig. 1.2 B-C).

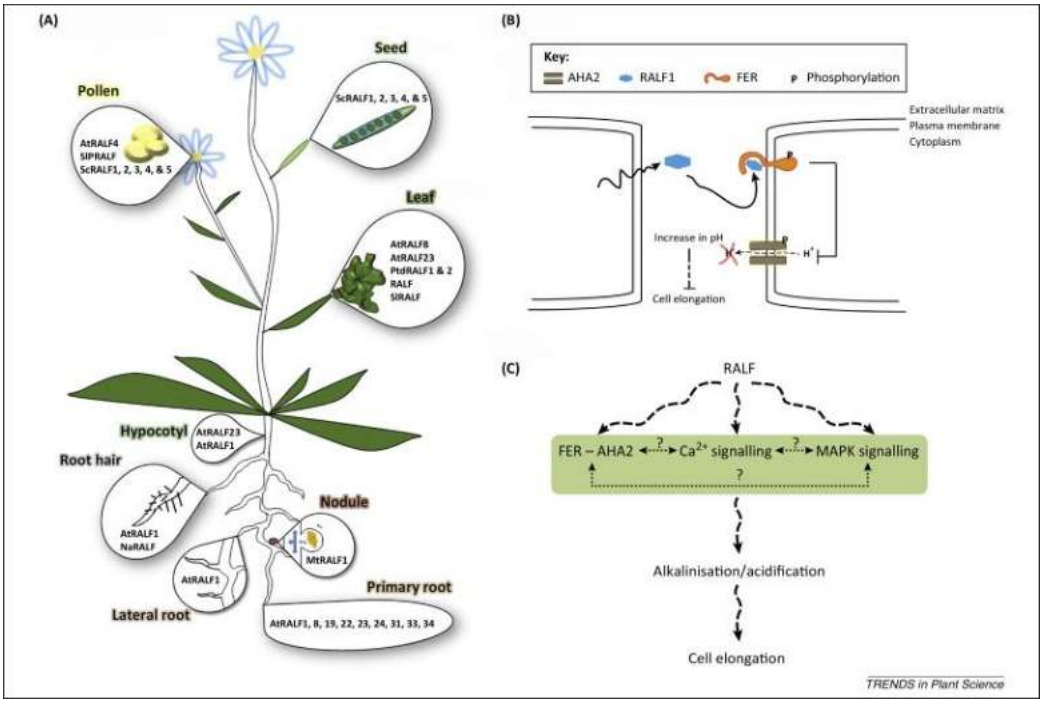

Fig. 1.2: Rapid ALkalinization Factor (RALF) peptides in plant growth and development. *(A) Schematic of a plant highlighting where RALFs have a role (combined observations from various species). (B) RALF binding to the FERONIA (FER) receptor and regulating H^+-ATPase 2 (AHA2) activity. (C) Summary of events downstream of RALF, without any specific order of events or interactions and indicating possible connections (broken line and '?'). (Reprinted form (Murphy and De Smet,* 2014*)).*

The CrRLK1Ls receptors consist of an extracellular domain which includes one or two malectin-like domains (Boisson-Dernier et al., *2011*), a transmembrane domain, and a cytoplasmic Ser/Thr kinase domain (Escobar-Restrepo et al., *2007;* Hématy et al., *2007*; Shiu and Bleecker, *2001*). In *Arabidopsis thaliana* more than 600 RLKs exist (Gish and Clark, *2011*), where the CrRLK1Ls form a family of 17 members with a very similar protein structure. The first evidence for a role of CrRLK1Ls in governing cell wall-related processes was the description of a cell wall integrity sensing function for THESEUS1 (THE1). The *the1* mutation mitigates the dark-grown hypocotyl elongation defects of various cellulose deficient mutants. The absence of a strong phenotypic effect in THE1 loss- and gain-of-function lines in the absence of cellulose-deficiency illustrated that THE1 monitors cell wall composition and actively represses growth in cellulose-deficient

mutants (Hématy et al., *2007*; Merz et al., *2017*). Following THE1, the CrRLK1L FERONIA (FER) was linked to a cell wall surveillance system. It was discovered that FER controls the disintegration of the pollen tube cell wall upon perception of the pollen tube at the synergid cells during fertilisation (Escobar-Restrepo et al., *2007*) (Section 1.2). However, due to the pleiotropic phenotypes of the *fer* mutant and the expression of FER in diverse vegetative tissues, it soon proved to be a central scaffold protein with a relay function in multiple processes for monitoring a wide range of plant responses (Feng et al., *2018*; Stegmann and Zipfel, *2017*).

After Haruta et al. showed in 2014 that FER was a receptor for RALF1 in roots (Haruta et al., *2014*), several CrRLK1L proteins binding different RALF peptides with varying specificities were described (Ge et al., *2017*; Gonneau et al., *2018*; Haruta et al., *2014*; Stegmann and Zipfel, *2017*), and additional FER cofactors were characterised. Employing co-immunoprecipitation and yeast two-hybrid assays, a physical link between FER and the LRR domain of LRX4 was reported (Dünser et al., *2019*). Indeed, Dünser et al. demonstrated that the vacuolar morphology is influenced by the extracellular pH, and that this adjustment depends on both FER and LRX function. Thus, LRX–FER-dependent cell wall sensing is required to coordinate extra- and intracellular adaptations (Dünser et al., *2019*). According to this, it was shown that FER interacts with the glycosylphosphatidylinositol-anchored proteins LORELEI (LRE) and LRE-LIKE GPI-AP1 (LLG1) in the endoplasmic reticulum. This interaction is crucial for the localisation of FER to the plasma membrane, implying that LRE and LLG1 act as chaperones for FER throughout the secretory pathway (Chao Li et al., *2015*). Furthermore, one member of a functionally redundant set of five ovule-expressed EARLY NODULIN-LIKE PROTEINs (ENODLs), ENODL14, was demonstrated to be required to anchor FER at the plasma membrane (Hou et al., *2016*). Finally, a yeast two-hybrid approach, together with different bimolecular fluorescence complementation assays, highlighted that RHO OF PLANTS (ROP)-GUANINE NUCLEOTIDE EXCHANGE FACTOR (GEF)1 also binds to FER (Duan et al., *2010*) (Fig. 1.3).

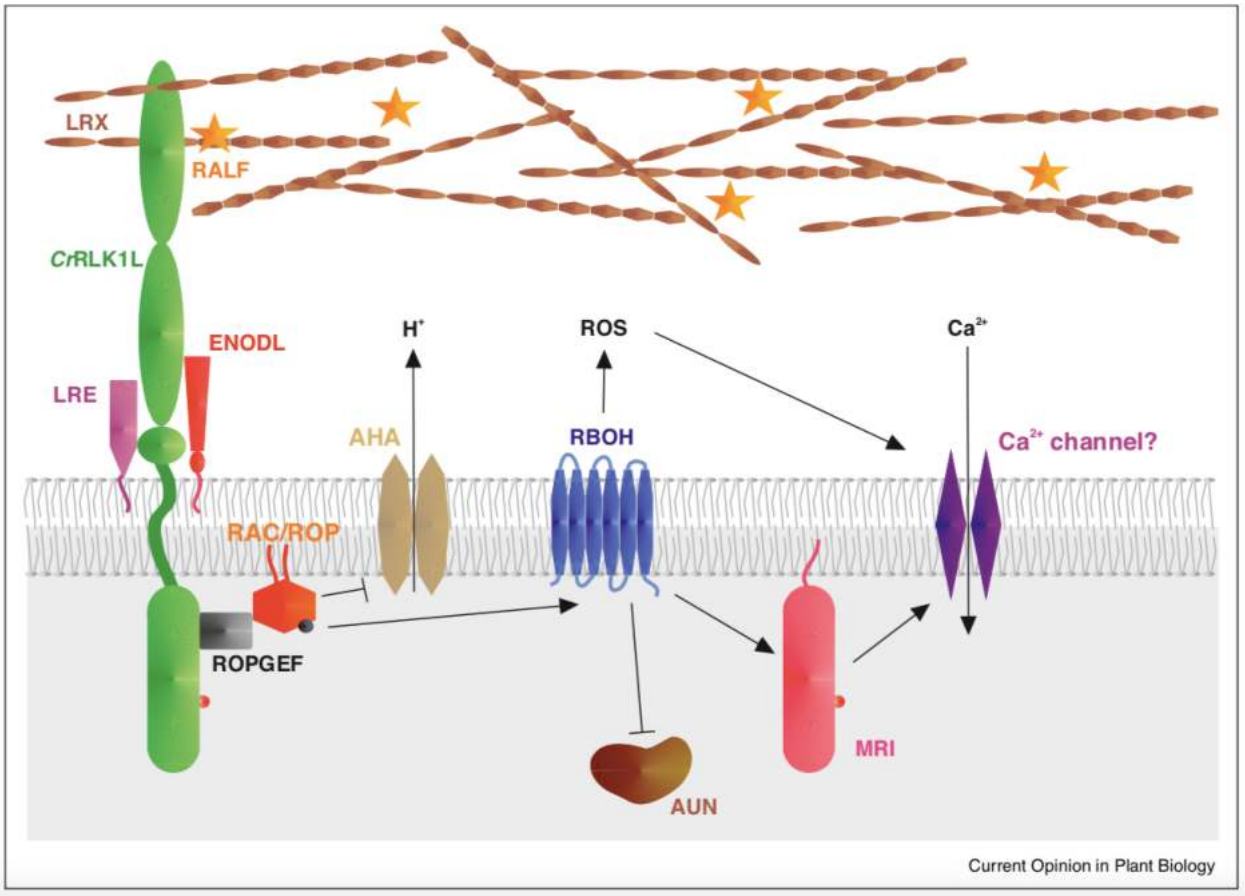

Fig. 1.3: Schematic representation of cell wall sensing by RAPID ALKALINIZATION FACTORs (RALFs) and downstream signaling components. *Cell-wall LRX proteins are recognised by RALF peptides, sensing alterations in the cell wall. To activate intracellular signaling pathways, they form a complex with CrRLK1L receptors and LRE/LLG co-receptors, inducing autophosphorylation of the CrRLK1L intracellular domain. Through signaling via ROPGEFs and RAC/ROPs, H^+-ATPases (AHA), calcium (Ca^{2+}) channels, and NADPH oxidases (RBOHs) are activated, which can modify cell wall properties by controlling H^+, Ca^{2+} and ROS levels, respectively. Moreover, CrRLK1L can activate intracellular phosphatases of the ATUNIS (AUN) family and cytoplasmic receptor-like kinases like MARIS (MRI). (Reprinted from (Vogler et al., 2019), Appendix, Chapter 7).*

In tip-growing root hairs, ROP proteins, also known as RAC (RAC/ROPs), interact with ROP-GEFs, which switch between an inactive GDP-bound and an active GTP-bound state to regulate the tip growth (Molendijk et al., *2001*) Thus, in response to upstream activation, ROP-GEF stimulates GDP–GTP exchange and activates RAC/ROPs on the plasma membrane, which in turn activate intracellular downstream processes that regulate cell growth (Molendijk et al., *2001*). As a consequence, FER can interact with plasma membrane H^+-ATPases of the AHA family (Yuan et al., *2017*), which are essential

both to control the membrane potential and to power ion transport across the plasma membrane in order to maintain polar growth in tip growing cells (Chen et al., *2018*; Hu et al., *2017*). In addition, after their activation, RAC/ROPs can modulate multiple secondary effectors that then in turn regulate cytoskeleton dynamics, Reactive Oxygen Species (ROS) production, cytosolic calcium (Ca^{2+}) homeostasis, and gene expression (Feiguelman et al., *2018*). Signal transduction processes usually rely on second messengers, small molecules like nitric oxide, ROS, and Ca^{2+}, whose levels and spatiotemporal patterns are specifically altered by external signals. These so-called signatures are detected and interpreted by the cell to elicit specific downstream responses. Thus, ROS-producing NADPH oxidases known as RESPIRATORY BURST OXIDASE HOMOLOGUEs (RBOHs) were characterised to be direct targets of these RAC/ROP proteins (Carol et al., *2005*, *2005*; Chao Li et al., *2015*), affecting also the Ca^{2+} influx (Wong et al., *2007*). As a consequence, FER mutants show altered Ca^{2+} signalling patterns, which are furthermore linked to changes in the perception of mechanical stimulations (Ngo et al., *2014*; Shih et al., *2014*). Nevertheless, even if Ca^{2+} channels may be regulated by ROS levels, the cross-regulatory interactions between ROS, Ca^{2+}, and H^{+} during cell growth are complex and need to be further investigated (Behera et al., *2018*; Boisson-Dernier et al., *2013*; Kaya et al., *2014*; Lassig et al., *2014*; Michard et al., *2017*).

Similar to FER, the CrRLK1Ls ANXUR (ANX)1/2 and BUDDHA'S PAPER SEAL (BUPS)1/2 are involved in CWI maintenance during pollen tube growth prior to reaching the ovules in *Arabidopsis* (Boisson-Dernier et al., *2013*; Ge et al., *2017*). Both ANX and BUPS act as RALF receptors, and the pollen tubes of their respective double mutants do not grow properly, frequently burst prematurely and produce an strong male sterility phenotype (Boisson-Dernier et al., *2009*; Ge et al., *2017*). Further analyses following an *anx1/2* sterility suppressor screen, identified another kinase as a positive regulator of the ANX-dependent pollen tube growth pathway (Boisson-Dernier et al., *2015*); the MARIS (MRI) kinase. MRI is a membrane-localized member of the Pto-interacting (Pti)-like subfamily, also known as RLCK-VIII. Interestingly, MRI loss-of-function mutants display pollen tube bursting like *anx1/2* plants, but the expression of the mutant form MRIR240C could rescue this phenotype, showing that MRIR240C is an overactive dominant MRI variant and that MRI plays an important positive role in the CWI pathway (Fig. 1.3). In the same *anx1/2* suppressor screen, the *atunis1* (*aun1*) mutant was recovered, rendering a member of the TYPE ONE PROTEIN PHOSPHATASE (TOPP) family inactive. AUN1 and its closest homolog AUN2 function redundantly as negative regulators of the ANX1/2- dependent CWI pathway (Franck et al., *2018*). Genetic experiments showed that

the mutant form of AUN1, AUN1D94N, can suppress diverse mutants of the pollen tube CWI pathway, placing AUN1/2 downstream of LRX, RALF, ANX and RBOH, but not of MRI (Fig. 1.3). Thus, it was proposed that the AUN1/2 phosphatases may counterbalance the kinase activity of MRI and/or regulate the phosphorylation status of common or different target proteins to regulate pollen tube growth (Franck et al., *2018*). However, how exactly AUN1/2 are activated and which target proteins they dephosophorylate requires further investigations. Moreover, AUN1/2 are localized both in the cytoplasm and the vegetative nucleus of growing pollen tubes, where they may have distinct functions. Indeed, TOPP4, another family member involved in gibberellic acid and auxin signaling, directly interacts with proteins at the plasma membrane and in the nucleus (Guo et al., *2015*; Qin et al., *2014*). Although many of the players involved in CrRLK1L signaling were initially identified through their role in plant reproduction, they or their homologs were found to play similar roles in diverse processes, including root growth, root hair development, cell expansion, innate immunity, and a variety of biotic and abiotic stress responses. It is thus probably only a matter of time until additional members of the ENODL and TOPP family will be implicated in other CrRLK1L-mediated signaling transduction processes (Vogler et al., *2019*).

Interestingly, rapid cell elongation leads to an increase in the strain rate, which activates cell wall synthesis via the CWI pathway and vice versa. In this process, the secondary messengers, like Ca^{2+}, play an important role, since they can be rapidly read out to respond back (Volotovski et al., *1998*). Thus, cells can start and stop this process quickly, in less than a minute in some cases, revealing that the molecular processes underlying irreversible wall expansion are dynamically controlled (Szymanski, *2009*). Such dynamic behaviour is reflected, at least in part, by changes in cell wall pH (Cosgrove, *2018*), which modulates the wall-loosening action of expansins (Cosgrove, *2015*) and potentially other wall-modifying agents that are activated by the phytohormone auxin in order to respond to specific biotic or abiotic stresses and to control the fine tune cellular growth by the AGT (Wu et al., *2008*).

1.1.3 The Acid Growth Theory

Plant growth and development are two physical processes occurring through the action of different parameters and in which plant hormones are known to play a critical role (Kende and Zeevaart, *1997*). Plant hormones, also known as phytohormones, are naturally produced by plant tissues and have been reported to regulate diverse

developmental processes, such as seed dormancy, seed germination and flowering, and they also affect cell elongation and cell division (Bedini et al., *2018*). Moreover, they have been shown to interact with each other antagonistically or cooperatively by complex crosstalks making their individual study difficult (Witzany, *2006*). For example, abscisic acid (ABA) and gibberellin (GA), act antagonistically in the control of seed dormancy and germination, where ABA positively regulates the induction and maintenance of dormancy, while GA enhances germination (Mittler and Blumwald, *2015*).

Among all the plant hormones, auxin has a central role because it orchestrates multiple developmental processes (Paque and Weijers, *2016*). Indeed, Gälweiler et al. showed already in 1998 by the use of PIN mutants, which are integral membrane proteins acting in the efflux of the auxin, that the disruption of the polar transport of this phytohormone leads to the failure of flower formation in *Arabidopsis* (Gälweiler et al., *1998*). Interestingly, local application of exogenous auxin to the naked inflorescences of *pin1* can induce the formation of floral primordia, highlighting the critical role of auxin in the flowering process (Cheng and Zhao, *2007*; Reinhardt et al., *2000*). Furthermore, auxin has also been shown to be important for the control of leaf senescence by over-expressing the *YUCCA6* gene, which is involved in the de novo auxin biosynthesis pathway in *Arabidopsis*. This mutant displayed a stay-green phenotype, associated with a delayed leaf senescence and an auxin hyper-accumulation, revealing the role of auxin in the natural ageing process of plant cells (Kim et al., *2011*). Nevertheless, despite its proven pluripotency, auxin is especially renowned for its capacity to promote cell elongation and has been found to be one of the main actors of the AGT (Hager et al., *1971*).

In the early 1970s, a physiological mechanism explaining cell expansion, the AGT was postulated (Hager et al., *1971*; Rayle and Cleland, *1977*, *1970*, *1992*). This theory proposes that the plant hormone auxin triggers the activation of plasma membrane (PM)-localised H^+-ATPases, resulting in acidification of the intercellular space (apoplast). Thereby, the low pH activates different proteins that act on carbohydrates, which leads to cell wall loosening and allows the cell to elongate due to the turgor pressure (Benjamins and Scheres, *2008*) (Fig. 1.4). This cell wall acidification results in a fast cell elongation, within minutes in classical assay systems like the hypocotyl of dicotyledons and the coleoptile of monocotyledons (Schopfer, *1989*; Takahashi et al., *2012*).

In addition, it is generally assumed that auxin promotes cell elongation by inducing the transcription of genes that encode cell wall remodelling factors (Sánchez-Rodríguez et al., *2010*; Wolf et al., *2012*). For instance, auxin promotes the expression of expansins, which are considered as primary facilitators of cell wall loosening. They

physically open up the fibrous network, allowing other cell wall remodelling enzymes, e.g. polygalacturonases, endoglucanases, and pectin methylesterases (PME), to access their respective substrates more easily (Catalá et al., *2000*).

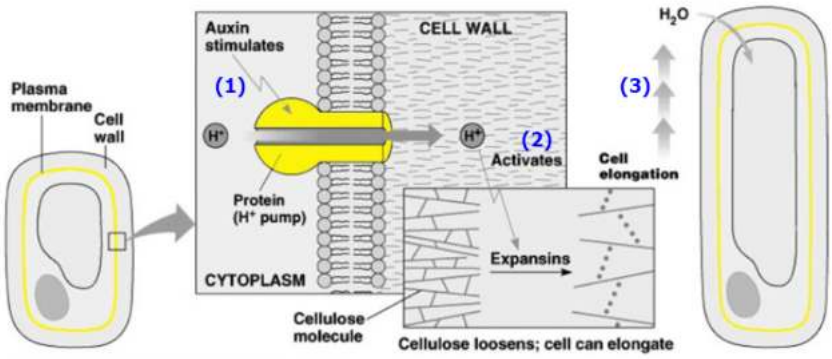

Fig. 1. 4: Control of cell expansion by auxin. Among the plant hormones, auxin has a central role because it orchestrates multiple developmental processes. *The effect of auxin on cell expansion is shown below: (1) auxin stimulates a proton pump, leading to the acidification of the apoplast; (2) low pH activates expansins, allowing cell wall loosening; (3) the cell elongates. (Modified from (Cosgrove,* 2005*)).*

The AGT has been a subject of debate ever since its first formulation, especially whether the theory is a universally applicable concept for plant cell elongation. Subsequent literature provided significant insight into the molecular mechanisms of auxin-triggered acid growth in plant shoots. By replacing auxin with low concentrations of fusicoccin, a fungal toxin which also directly activates the H^+-ATPases, increased growth of cells in the shoot was observed (Fendrych et al., *2016*; Lüthen et al., *1990*). In roots, however, the AGT remains controversial. Some of the strongest objections against the AGT are that in some elongating roots, researchers have observed that auxin treatments lead to alkalinization rather than acidification (Evans et al., *1980*; Lüthen and Böttger, *1993*). Furthermore, high auxin concentrations are indeed known to inhibit root cell expansion and overall root growth both in monocots and dicots (Chadwick and Burg, *1967*; Kutschera and Schopfer, *1985*). However, contrary to these observations and in line with the theory, it was shown that root growth is slightly promoted when auxin and its homologs are applied at very low concentrations to grass roots (Moloney et al., *1981*). These discrepancies are difficult to solve, even more when it has been reported that the application of auxin at high concentrations generally inhibits root growth in a model plant like *Arabidopsis* (Liu et al., *2015*). Thus, these controversial findings imply that our

knowledge about the role of pH in plant cell expansion is insufficient. Further investigations of the exact concentrations and the local distribution of protons within the cell wall and their effect on the mechanical properties of the latter are fundamental to better assess the validity of the AGT. So far, the AGT's biophysical component was traditionally only examined at systemic resolution and through non-genetic approaches. Thus, a proper correlation between biochemical factors, e.g. pH and auxin, with physical properties, e.g cell wall stiffness / elasticity, together with genetic information, is still needed.

Up to this point, new genetic, biochemical, biomechanical and microscopic tools and technologies have been developed and have been instrumental in providing new answers to the AGT, even though many questions remain unanswered. For example, it has been found very recently, that pectins also seem to act as cell wall modifying agents through the action of auxin. Auxin leads to a de-esterification of pectins, which decreases the rigidity of the cell wall and additionally contributes even further to the apoplastic acidification (Braybrook and Peaucelle, *2013*; Hocq et al., *2017*). These results were postulated according to the ability of the PME to generate secondary derivative compounds in the extracellular matrix, such as protons and methanol, which generally decrease the pH in any tissue. Unfortunately, there is still a lack of accurate apoplastic pH analyses with precise tools that can help visualise and quantify these small pH changes in the cell wall. In fact, most of the latest available pH probes work well for cytoplasmic pH measurements in plant cells, but not optimal in the cell wall (Gjetting et al., *2012*). Nevertheless, new imaging methods, for example, the use of the 8-hydroxypyrene.1,3,6-trisulphonic acid (HPTS) dye (Barbez et al., *2017*) to measure cell wall pH, could provide new answers since they record pH distributions at a very high resolution. This approach might therefore enable the researchers to track the acidification state of the cell wall in order to gain a better understanding of the cytomechanics behind cell elongation (See Section 1.4).

1.2 *Arabidopsis* pollen cells as a model system for investigating cell growth

So far, many experiments to better understand the AGT have been conducted at the tissue level, but for a deeper comprehension a much more profound analysis is needed. Therefore, studies at the single cell level can provide insights into the complex growth of plant tissues and organs. Since, plant cells are generally interconnected and forming tissues, it is often impossible to separate a single cell for analysis. To circumvent

this problem, individually growing pollen tubes of *Arabidopsis* and other species have been used as a model to study cellular growth for more than 50 years (Dashek and Rosen, *1966*; Kroh et al., *1970*; Smyth, *1990*).

In flowering plants (angiosperms) the mature male gametophyte contains a vegetative cell which harbours two sperm cells. It matures within the anthers of the plant into pollen grains that are subsequently dried and released with the aim of landing on the tip of a pistil, the stigma. Once there, after rehydration, the pollen grains germinate by the extrusion of a tube, which has one single objective: to deliver the two sperm cells attached to the vegetative nucleus to the female gametophyte, the ovule (Fig. 1.5 A). After germination, the pollen tubes elongate by tip-growth, penetrate the pistil tissue and grow through the nutrient-rich transmitting tract until they are attracted by the receptive ovules (Fig. 1.5 B). During this journey, the signalling between the pollen tube and the maternal tissues of the stigma, style, transmitting tract and ovule are fundamental to ensure optimal guidance via chemotactic cues (Herrero and Hormaza, *1996*; Márton et al., *2005*; Okuda et al., *2009*; Takeuchi and Higashiyama, *2012*). In the transmitting tract pollen tubes elongate extremely fast to ensure successful fertilisation. They can grow up to 30 cm in length in some plants like maize, despite their small diameter (15-20 μm), being among the fastest growing cells, if not the fastest, with average growth rates between 3-6 μm/min in *Arabidopsis* (Franck et al., *2017*; Lassig et al., *2014*). This rapid growth implies high tensile stress on the cell wall due to turgor pressure. Therefore, a precise control of cell wall deposition and remodelling through the CWI pathway is crucial to resist this stress and to maintain the shape of the pollen tube during growth. The continuous self-similar growth requires a non-expandable shank and a relatively soft apical region where cell expansion can occur. New cell wall material, mainly methyl-esterified pectins and, to a lesser extent, crystalline cellulose, is constantly added in this region. A few micrometers away from the pollen tube tip, in the transition zone between the spherical tip and the cylindrical shank, pectins become de-esterified by PMEs and gelled by Ca^{2+} cross-linking (Fraeye et al., *2010*). In addition, callose (1,3-P-glucan) polysaccharide is added to the cell wall, which leads to further reinforcement of the shank (Chebli et al., *2012*; Vogler, *2017*). Once the pollen tube arrives at the ovule, it penetrates an opening in the integuments, the micropyle, and reaches the embryo sac, which is composed by four cell-types in angiosperms: the two synergid cells, which are located at the micropylar opening of the ovule where the pollen tube enters; two gametes (the egg and the central cell); and three antipodal cells at the opposite extreme of the ovule's entrance. Pollen tube reception occurs at the filiform apparatus, a callose-rich complex formed by invaginations of the

synergid cell walls. After penetrating the embryo sac through one of the two synergids the two sperm cells are released. One sperm cell will fertilise the egg cell while the other one will fertilise the central cell, giving rise to the diploid embryo and the triploid endosperm for nurturing the embryo, respectively (Baroux et al., *2002*; Bleckmann et al., *2014*; Kessler et al., *2010*). This process is called double fertilisation (Fig. 1.5 C).

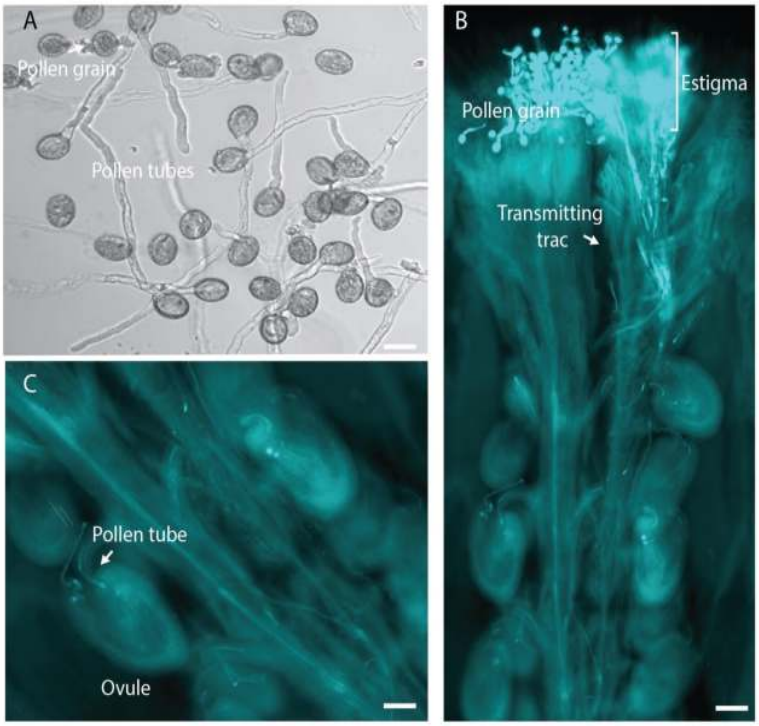

Fig. 1.5: Pollen tube growth analysis in vitro and in vivo. *(A) Pollen tubes grown in vitro and prepared for analysis. (B) Aniline blue staining of pistils 1-2 days after pollination. Pollen grains land on the stigma. After hydration, they germinate and form pollen tubes that penetrate the female tissues and grow through the transmitting tract towards the ovules.(C) When they arrive to the ovule, they penetrate through the micropyle and double fertilisation occurs. Scale bar 10 µm in (A), 100 mm in (B) and 150 mm in (C).*

Pollen tube reception at the synergids starts with growth arrest of the pollen tube, programmed cell death of the receptive synergid after which the pollen tube resumes growth at high speed only to burst and release the two sperm cells after arriving in the central cell. Essentially, all these steps are controlled by an extensive communication between the male and the female gametophytes which is to a great extent mediated by coordinated Ca^{2+} oscillations (Ngo et al., *2014*) and likely controlled by the important FER dependent signalling pathway (Escobar-Restrepo et al., *2007*). As previously mentioned, FER is expressed in the vegetative tissue of the mature *Arabidopsis* and accumulates in the

filiform apparatus of the synergids, being indispensable for pollen tube reception (Escobar-Restrepo et al., *2007*). Indeed, it was shown that the lack of FER, together with two CrRLK1L homologues, HERCULES RECEPTOR KINASE 1 (HERK1) and the recently discovered ANJEA (ANJ) (Galindo-Trigo et al., *2020*), prevents the proper communication between the female gametophyte and the arriving pollen tube. Thus, wild type pollen tubes which invade *fer* ovules, do not stop their growth and also fail to burst, leading to a pollen tube overgrowth inside the female gametophyte (Huck et al., *2003*). This phenotype is also mimicked in ovules lacking LRE, which acts as a cofactor of FER, HERK1 and ANJ (Capron et al., *2008*; Galindo-Trigo et al., *2020*; Chao Li et al., *2015*). Furthermore, these mutants display the same aberrant cytosolic Ca^{2+} pattern than *fer* during pollen tube reception (Xiao Liu et al., *2016b*), (Stegmann and Zipfel, *2017*), which is important for pollen tube rupture and affects to the CWI maintenance as a consequence (Duan et al., *2014*; Escobar-Restrepo et al., *2007*; Ngo et al., *2014*).

In order to comprehend the fundamental role of the different players in the CWI pathway, we took advantage of the tubular structure of the pollen tube. Their capacity to maintain a continuous apical elongation while controlling the integrity of the cell wall, together with the ability to react to different chemical and mechanical cues, places them in the spotlight to study cellular growth. Furthermore, it was reported that RALF1 binds the extracellular domain of FER increasing the apoplastic pH and reducing cell elongation in roots (Chen et al., *2016*; Haruta et al., *2014*). Thus, pollen tubes, with their respective CrRLK1L protein homologues like ANX1/2 (Boisson-Dernier et al., *2013*; Miyazaki et al., *2009*), have become fundamental to better understand cell elongation under the AGT.

All this information, together with the discovery of a new RALF peptide-binding interactor, LRX, will be profoundly characterised and described in Chapters 2 and 3.

1.3 *Brachypodium* roots as tissue model for investigating cell growth

Brachypodium distachyon is a fairly new plant model proposed in 2001 (Draper et al., *2001*), which has gained more and more popularity in recent years. It has emerged as a viable model system for studying biological issues related to the family of the grasses (*Poaceae*), which are of immense agricultural importance and include all our main cereal crops such as rice, corn, wheat and barley. The major challenges associated with these species include the large size of the plants, long generation times and demanding growth requirements (Jung et al., *2008*). In contrast, *Brachypodium* is a simpler monocotyledonous

system with a shorter stature, shorter generation time, smaller genome, the ability to self-pollinate, and it can be easily grown under simple conditions (Draper et al., *2001*). Therefore, *Brachypodium*, like *Arabidopsis*, is particularly useful for basic research that requires large numbers of individual plants, carefully controlled growth conditions, multiple generations, and genetic analyses (Brkljacic et al., *2011*). In addition, in the frame of our research project, previous studies described that these two model organisms show a different response to auxin. Interestingly, it has been reported that *Arabidopsis* root cells become shorter in response to both a decrease or an increase in auxin production (Liu et al., *2015*). However, in 2013, Pacheco-Villalobos et al. highlighted an increased root elongation in response to high levels of auxin in *Brachypodium* (Pacheco-Villalobos et al., *2013*). These differences to *Arabidopsis* and the simplicity of the *Brachypodium* model make it an ideal tool to validate the AGT and its universal applicability to cell expansion.

The final steps of auxin biosynthesis in *Arabidopsis* are controlled by two well characterised enzymes: the TRYPTOPHAN AMINOTRANSFERASE OF ARABIDOPSIS 1 (TAA1) and TAA1-RELATED (TAR) proteins, which catalyse the conversion of tryptophan to indole-3-pyruvic acid (IPA), and the family of YUCCA cytochrome P450s, which catalyse the conversion of IPA to indole-3-acetic acid (IAA), the major active form of auxin (Stepanova et al., *2008*; Won et al., *2011*)(Fig. 1.6 D). Three redundantly acting *TAA1/TAR* genes exist, whose progressive loss of function leads to ever reduced root growth and especially to the absence of a root in the triple mutant (Tao et al., *2008*). Phylogenetic analysis has identified bona fide TAA1/TAR homologous genes in monocotyledons. Whereas maize contains five members of this family , only two were found in *Brachypodium*. Thus, they were named TAA1-RELATED 1-LIKE (*BdTAR1L*) and *BdTAR2L*, with *BdTAR2L* being the dominantly expressed gene in the elongation zone of the root. Till the date, the major limitation to understand the AGT was the unavailability of suitable mutants that could help in its experimental verification. However, Pacheco-Villalobos et al. created a *Bdtar2l* mutant which, despite the observation that it is a loss-of-function allele, produced higher levels of auxin in this zone (Fig. 1.6 B). As a consequence, the cell elongation is greatly exaggerated, and the root as a whole is up to 160% the length of wild type, while size and activity of the root meristem are not affected in this mutant (Fig.1.6 A-C) (Pacheco-Villalobos et al., *2013*). Therefore, in contraposition to the dicotyledonous model system *Arabidopsis*, which has a highly counterintuitive phenotype as explained before, the *Bdtar2l* mutants offer a unique opportunity to address the validity of the AGT in the root.

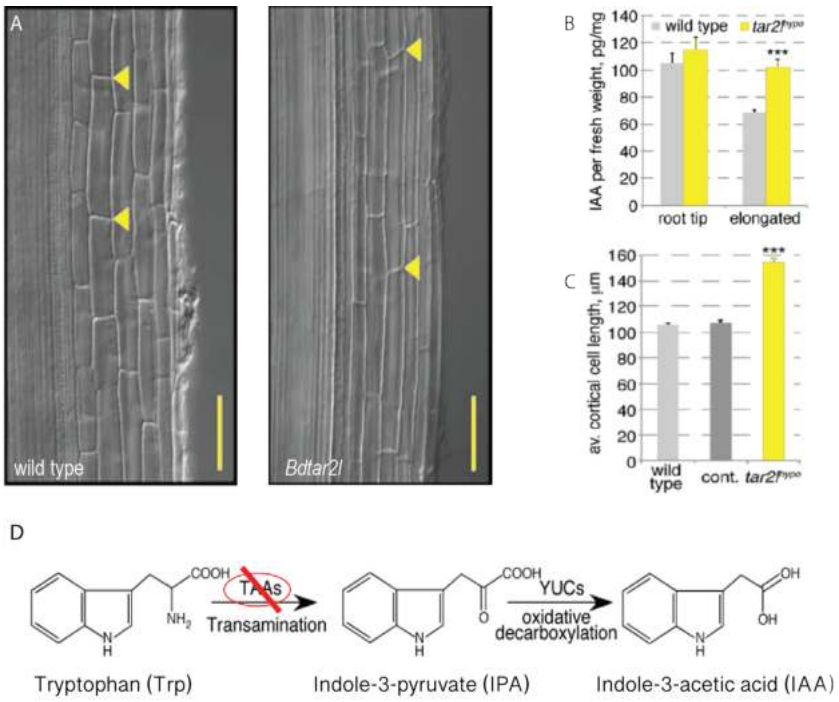

Fig. 1.6: Cellular root phenotypes of Bdtar2l mutants. *(A) Representative Nomarski optics images of mature root portions showing longer root cells in the mutant. (B) Free auxin (IAA) content in wild type and Bdtar2l root segments at 4 days after germination. (C) Quantification of mature cortex cell length at 4 days after germination. (D) The simplified indole-3-pyruvic acid (IPyA) pathway mutation in the IAA biosynthetic pathway of the Bdtar2l mutant. (Adapted form (Pacheco-Villalobos et al.,* 2013*)).*

We have now genetic and pharmacological tools, like the HPTS pH reporter or the IAA chemical, at our disposal to observe the effects of increased auxin levels either in systemic steady state or upon induction. However, as explained, the growth of walled cells is determined by the plastic response of the acidified wall to the mechanical force exerted by the turgor pressure. So, in order to totally comprehend the basis of the AGT, the force balance between turgor and tensile resistance of the plant cell wall has to be assessed as well as the mechanical properties of the cell surface at the multicellular level.

1.4 Cytomechanics - The Mechanical Basis of Cell Form and Structure

Biomechanical studies were largely faded from the focus of plant science with the rapid progress of genetics and molecular biology since the mid-twentieth century. However, the development of more sensitive measuring tools renewed the interest in plant biomechanics in recent years. Thus, mechanical characterisation has become an important and now frequently used tool for plant phenotyping (Pieruschka and Lawson,

2015). Indeed, biomechanical forces play an important role not only in cell growth but also in other biological functions, such as plant stability or resistance against pathogens (Bao et al., 2010; Spatz et al., 1990).

As already mentioned, cell walls provide shape and stability to the plant and have to be strong enough to withstand the high tensile forces generated by turgor pressure, which typically ranges from 0.3 to 1 MPa (Benkert et al., 1997; Cosgrove, 1997; Tomos and Leigh, 1999). Furthermore, the cell has to balance those forces, by inducing wall stress relaxation, to properly elongate and avoid rupture of the cell wall (Cosgrove, 1993; Cosgrove et al., 1984; Wolf et al., 2012). Therefore, to better understand growth at the mechanical level, the turgor pressure and the elastic properties of the cell wall need to be quantified.

Several different techniques have been employed to estimate the value of turgor pressure, but only the pressure probe, an oil-filled microcapillary which is inserted into the vacuole, allows direct pressure measurement (Benkert et al., 1997; Jones et al., 2015; Tomos and Leigh, 1999). Initially, this technique was used to measure turgor in algae with very large cells (Hüsken et al., 1978; Tomos and Leigh, 1999), but continuous development made it possible to use the pressure probe also for small cells, such as stomatal guard cells (Franks, 2003; C. Wei et al., 2001). However, due to its invasive nature, this method cannot be used repeatedly on the same cell (Fig. 1.7 A). In addition, an alternative method to measure the turgor pressure is ball tonometry, a large-scale indentation method (Lintilhac et al., 2000; Chunfang Wei et al., 2001), where a large spherical probe is applied to the cell with an imposed load while the contact area is measured (Fig. 1.7 B). Due to the large diameter of the indenter, which is much bigger than the thickness of the cell wall, the elasticity of the cell wall itself can be neglected. Thus, turgor pressure is determined by the ratio between the known load and the contact area between the sphere and the cell surface. Turgor pressure values measured with this method correlate well with the direct pressure probe measurements (Wang et al., 2006).

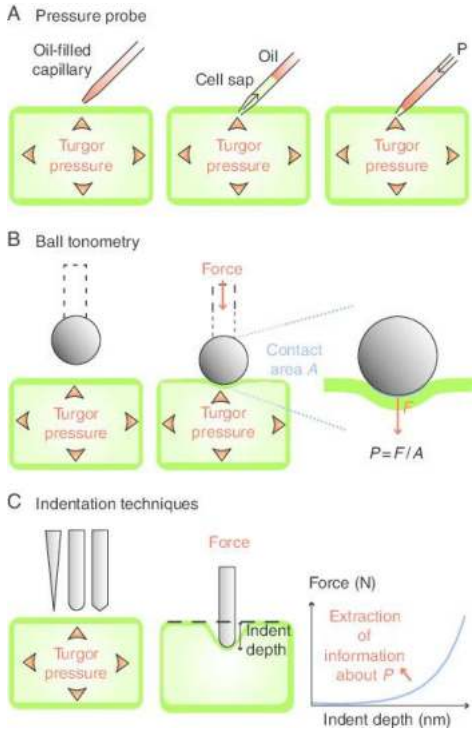

Fig. 1.7: Measurement of turgor with mechanical methods. *(A) Pressure probe, wherein the pressure is measured directly using a capillary for manipulating turgor pressure within a cell by injecting or removing a known volume of liquid. (B) Non-invasive ball tonometry based on the compression of individual plant cells with a large diameter sphere, wherein the surface of contact between the sphere and the cell is determined optically. The pressure (P) is defined as the force (F) exerted on a surface divided by the area (A) over which that force acts. (C) Different indentation methods, wherein the force-indentation curve gives stiffness. Schematic of a typical indentation experiment with loading a constant force (N=Newtons). (Reprinted from (Beauzamy et al., 2014)).*

In addition to turgor pressure, the elasticity/stiffness of the cell wall is a limiting factor that must be regulated to permit cellular growth (Cosgrove, *1993*; Cosgrove et al., *1984*; Wolf et al., *2012*). Thus, numerous methods have been developed to better understand the rigidity of the cell wall. One of the major techniques generally used to determine cell walls elasticity in their natural state, is the 'tensile test'. This test measures the deformation produced by the application of different pulling forces onto isolated cell walls or entire plant tissue blocks by the use of an extensometer (McQueen-Mason et al., *1992*; Schopfer, *2006*). However, although such measurements can give answers concerning mechanical properties, the extensions measured cannot always directly be related to the growth of living cells in a quantitative way because the applied stress is unidirectional in most cases, whereas the *in vivo* stress in the cell wall due to turgor

pressure is multidirectional. Furthermore, this approach is not suitable to measure local differences in mechanical cell wall properties (Geitmann, *2006*; Vogler et al., *2015*). To overcome the lack of precision of the 'tensile test', especially for local measurements, indentation techniques have been used to measure cell wall stiffness. Cells are locally indented using forces in the range of pico to milliNewtons to investigate the biomechanics at smaller scales and in a more localised manner (Fig. 1.8 C).

Most of the methods to measure forces at the microscale are cantilever-based. A force probe connected to a cantilever interacts with a sample, and the cantilever's deflection is measured using either optical, piezoresistive and piezoelectric methods (Fauver et al., *1998*). The atomic force microscope (AFM), in which the cantilever tip can be as small as a single atom, has already been used for various applications in the life and material sciences, and has become the dominating method for measuring forces in the nanoNewton range (Müller and Dufrêne, *2008*). However, the cantilever has to be flexible enough to be deflected by the sample, and sufficiently stiff to deform it, resulting in a narrow force range that can be measured by this technique. Therefore, the maximal forces provided by the AFM are often not sufficient enough to characterise the stretching and elongation of the rigid cell wall of plants (Burgert and Keplinger, *2013*; Felekis et al., *2011*). These shortcomings were addressed by developing related techniques using larger cantilevers, which allowed to measure larger biological structures, like pollen tubes (Geitmann and Parre, *2004*; Parre and Geitmann, *2005*). Nevertheless, these cantilever-based methods tend to be sensitive to off-axis forces leading to lateral deflections which sometimes induce slippages (Muntwyler, *2010*).

To overcome these problems, Bradley Nelson's group at the ETH Zurich, developed a 'MicroElectromechanical Systems' (MEMS)-based capacitative force sensors which have already been demonstrated to be useful for measuring the hardening of the zona pellucida after fertilisation of a mouse oocyte (Sun and Nelson, *2002*). In collaboration with the Nelson group, we developed the Cellular Force Microscope (CFM) by integrating MEMS-based force sensors with a micro-positioning system (Fig. 1.8 A-B) (Felekis et al., *2011*). Compared to other mechanical characterisation tools used for biological samples, such as the AFM (Arfsten et al., *2010*; Deng et al., *2011*; Pablo, *2018*), the CFM offers the possibility to apply multi-scale loads from the nano- to milliNewton range with significantly higher displacement, i.e., indentation depths in the range of several micrometers with nanometer-resolution. Therefore, the CFM has already been shown to be effective to characterise the cell wall stiffness of a large variety of different cell types, such as lily (*Lilium longiflorum*) and *Arabidopsis* pollen tubes (Fabrice et al., *2018*; Vogler et

al., *2013*) as well as epidermal tissue of onions (Routier-Kierzkowska et al., *2012*). Importantly, the 'apparent stiffness' measured by the CFM reflects additional parameters that contribute to the cellular mechanical properties such as the turgor pressure (Smith et al., *1998*; Wang et al., *2004*), the cell and indenter geometry (Bolduc et al., *2006*), as well as the pre-indentation mechanical stresses (Zamir and Taber, *2004*). Thus, in order to separate them, it is essential to fit the data with a mechanical model that captures these various influences. The modelling techniques commonly used in engineering to predict the mechanical behavior of complex structures is based on Finite Element Method (FEM) modelling. In this approach, the structubehaviourral system is divided into discrete areas, i.e. the elements, which are connected by characteristic key points (generally located at their corners), or nodes. The quantities of interest, i.e. stresses, strains, and displacements are evaluated at the nodes connecting different elements. Thus, the FEM technique produces approximate solutions to complex problems by calculating the behaviour of structures with complicated geometry and material properties. FEM modelling has already been used to model the elastic, temporary deformation of plant tissues and cells under the application of external loads (Bolduc et al., *2006*; Fayant et al., *2010*; Hamant et al., *2008*; Wang et al., *2006*). Therefore, the CFM, in combination with an FEM-based model, provides a powerful method to evaluate important mechanical parameters, such as turgor pressure and cell wall elasticity of single, growing cells and tissues (Fabrice et al., *2018*; Routier-Kierzkowska et al., *2012*; Vogler et al., *2013*; Weber et al., *2015*). However, FEM models depend on input parameters that are either difficult to measure, such as cell wall thickness, or that must be derived from cell populations other than those used for the stiffness measurements. The stretch ratio between turgid and plasmolysed cell diameters is such a case, since complete plasmolysis is not reversible. For these reasons, turgor pressure and cell wall elasticity derived from a FEM method-based approach always represent average values based on experiments performed on different cell populations. Ideally, however, we would like to know these parameters for every individual cell. For this purpose, Burri and colleagues developed a dual indentation method based on the CFM combining microcompression (similar to ball tonometry) with microindentation and which allows the turgor pressure to be measured directly while providing an analytical solution for the cell wall elasticity (Burri et al., *2019*).

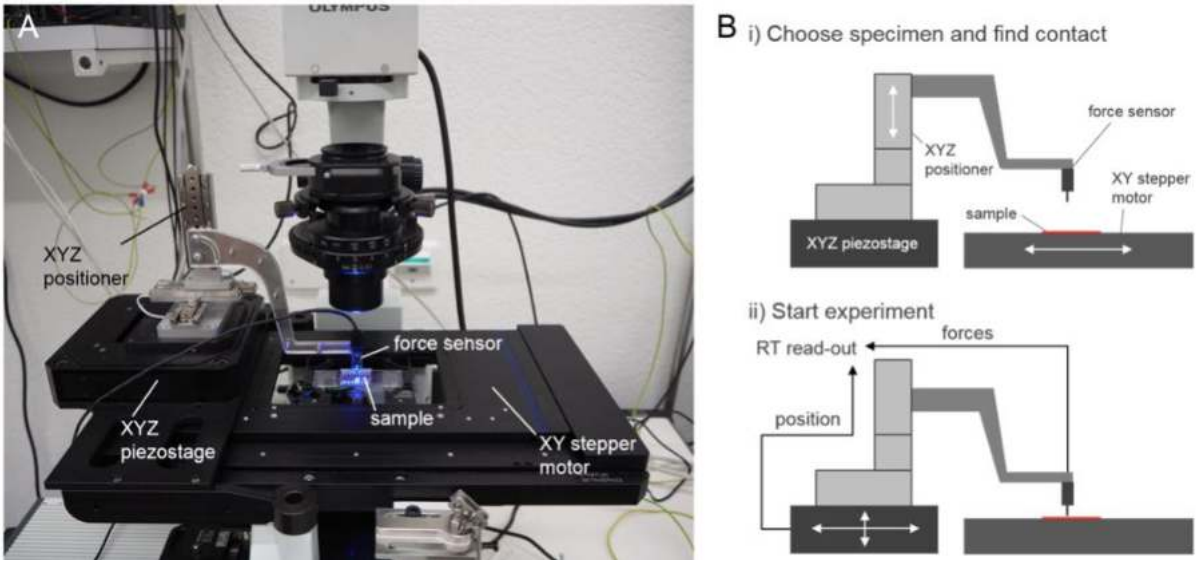

Fig. 1.8: The CFM allowing fluorescence imaging of intracellular reporters while simultaneously providing stable and precise micro-indentation experiments *(A) Configuration of the Cellular Force Microscope (CFM) integrated with an inverted microscope. (B) Experimental procedure: (i) Using the large travel range to find a suitable specimen and position the sensor close to it, (ii) indenting the sensor tip into the sample using the piezostage with real-time recording of position and force.*

Furthermore, regarding our research project and for better understanding the AGT, the CFM has been combined with fluorescence microscopy, allowing the simultaneous measurements of forces and the visualisation of intracellular reporters (Felekis et al., *2015*), like intra- and extra-cellular pH *in planta*. For that, in addition, a microfluidic lab-on-a-chip device (LOC) has been developed and integrated with the CFM to support seed germination, indentation measurements, and long-term fluorescence imaging for obtaining accurate profiles along the different *Brachypodium* roots, previously described. The CFM is therefore a suitable instrument to approach the AGT from a different angle and provide the biomechanical data that have been missing until now. The exact approach and the results gained from CFM analyses will be described in detail in Chapter 4.

2 Chapter 2 - RALF4/19 for mantaining the cell wall integrity

2.1 Introduction

All of Chapter 2 was published as Mecchia, Martin A., **Santos-Fernandez, Gorka**, Duss, Nadine N., Somoza, Sofía C., Boisson-Dernier, Aurélien, Gagliardini, Valeria, Martínez-Bernardini, Andrea, Fabrice, Tohnyui Ndinyanka, Ringli, Christoph, Muschietti, Jorge P. and Grossniklaus, Ueli to *Science* **358**, 1600-1603 (2017).

I contributed to this work as follows: I performed all the phenotypic characterisation and the seeds/silique counting, pollen tube's images of both the *in vitro* pollen germination and the fluorescent peptides' application analysis, the immunostaining and the *RALF4* and *RALF19* RNA extraction for ddPCR to analyse the cDNA levels in the open flowers of the different lines. GSF also analysed all the peptides' effect in pollen tubes for measuring the growth arrest phenotype together with all the Western blots to better characterise the protein interaction. Furthermore, I helped with the quantitative analysis of LRX8-RALF4 binding, the interpretation of the results, and the writing of the manuscript.

Thus, in this chapter an alternative interaction partner of RALF peptides is shown, the LEUCINE-RICH REPEAT EXTENSIN (LRX) family. As it was explained in '*Arabidopsis* pollen cells as a model system for investigating cell growth', until then, RALF peptides were shown to be the ligand of the CrRLK1L family members. However, with this discovery, we show another parallel ally for the recognition of this peptide by the pollen tube for growing while maintaining the CWI. This revelation will allow the scientific society to better understand the fundamental role of these small peptides while opening the possibility of investigating new and different developmental paths. For instance, new routes and branches that can lead to the global knowledge of the effect of these small peptide hormones to the plant in its integrity.

All supplemental data can be found in the Appendix.

PLANT SCIENCE

RALF4/19 peptides interact with LRX proteins to control pollen tube growth in *Arabidopsis*

Martin A. Mecchia,[1,2,3]* Gorka Santos-Fernandez,[1]* Nadine N. Duss,[1]* Sofía C. Somoza,[2] Aurélien Boisson-Dernier,[4] Valeria Gagliardini,[1] Andrea Martínez-Bernardini,[1] Tohnyui Ndinyanka Fabrice,[1]† Christoph Ringli,[1] Jorge P. Muschietti,[2,5]‡ Ueli Grossniklaus[1]‡

The communication of changes in the extracellular matrix to the interior of the cell is crucial for a cell's function. The extracellular peptides of the RAPID ALKALINIZATION FACTOR (RALF) family have been identified as ligands of receptor-like kinases of the *Cr*RLK1L subclass, but the exact mechanism of their perception is unclear. We found that *Arabidopsis* RALF4 and RALF19 redundantly regulate pollen tube integrity and growth, and that their function depends on pollen-expressed proteins of the LEUCINE-RICH REPEAT EXTENSIN (LRX) family, which play a role in cell wall development but whose mode of action is not understood. The LRX proteins interact with RALFs, monitoring cell wall changes, which are communicated to the interior of the pollen tube via the *Cr*RLK1L pathway to sustain normal growth.

RAPID ALKALINIZATION FACTORs (RALFs) are secreted peptides serving as extracellular signals that are transduced to the inside of the cell (*1*–*3*) (Fig. 1A). Spread throughout the plant kingdom, with 36 members in *Arabidopsis* (*1*), RALFs regulate developmental and physiological processes (*1*–*6*). FERONIA (FER), a member of the *Cr*RLK1L family of receptor-like kinases (RLKs) that is at the nexus between extracellular and intracellular events, is a receptor of several RALF peptides (*3*, *7*).

We used the pollen tube, which displays rapid and polarized growth, to study the function of RALF peptides in signal transduction (*1*). Although pollen tube growth depends on RALF peptides, the underlying mechanisms are unknown (*4*, *8*, *9*). Using publicly available expression data, we identified eight RALFs that were expressed in pollen (fig. S1), belonging to three phylogenetic clades (fig. S2). We focused on clade I with two members, *RALF4* and *RALF19* (fig. S3), and confirmed their specific expression by reverse transcription polymerase chain reaction (RT-PCR) and reporter gene analyses (fig. S4).

To investigate the biological function of *RALF4/19*, we generated plants expressing an artificial microRNA (amiRNA) (Fig. 1A), *amiRRALF4/19*, under a pollen-specific promoter (*10*); 50% and 25% of the independent T1 plants displayed short and intermediate silique lengths, respectively (n = 40). Droplet digital PCR (ddPCR) confirmed down-regulation of *RALF4* and *RALF19* in the *amiRRALF4/19* lines; expression of the non-targeted *RALF9* was unaffected (Fig. 1, A and B, and fig. S5D). The homozygous *amiRRALF4/19* line #23, with 10% of the wild-type seed set (Fig. 1, C and D), was used for further studies. Semi–in vivo pollen germination of *amiRRALF4/19* or wild-type pollen, on wild-type or *amiRRALF4/19* carpels, demonstrated that *amiRRALF4/19* pollen failed to grow on any carpel; this result indicates that the reduced *RALF4/19* expression in pollen was responsible for the low seed set (fig. S6). Moreover, in vivo only 3.5% of *amiRRALF4/19* pollen tubes reached the ovules (fig. S7). Nearly 70% of in vitro germinated pollen tubes of *amiRRALF4/19* plants burst, suggesting a role of *RALF4/19* in regulating pollen tube integrity and growth (Fig. 1, E and F). The observed in vivo and in vitro phenotypes of *amiRRALF4/19* line are reminiscent of double mutants affecting the redundant ANXUR1 (ANX1) and ANX2 *Cr*RLK1L*s* (*11*, *12*) and the redundant reactive oxygen species–producing NADPH oxidases RbohH and RbohJ (*13*) (Fig. 1C), respectively, and mutants affecting the receptor-like cytoplasmic kinase (RLCK) MARIS (MRI) (*14*), the latter three acting downstream of *ANX1/2* in the signal transduction pathway.

To investigate the relevance of *RALF4/19* for pollen tube growth, we characterized the insertion mutant *ralf4-1* (Fig. 1, B to F, fig. S8, and table S1). Homozygous *ralf4-1* plants were fertile (Fig. 1C and fig. S8) but 47% of in vitro germinated pollen tubes burst, versus 19% in the wild type (Fig. 1, E and F, and fig. S9), perhaps because of excessive growth soon after germination (fig. S9). These results suggest redundancy of *RALF4/19* for in vivo pollen tube growth. To confirm this, we complemented *amiRRALF4/19* lines with *rRALF4*, an amiRNA-resistant version of *RALF4* (Fig. 1A) driven by its own promoter (p*RALF4:rRALF4*), carrying mutations that reduce the interaction with *amiRRALF4/19* without affecting the RALF4 amino acid sequence (Fig. 1, A and B). Transgenic plants (*rRALF4* lines) had a restored, normal fertility (22 of 32 independent lines; Fig. 1, C and D). In contrast, *rRALF4* pollen tubes behaved like those of *ralf4-1* mutants (49% bursting) (Fig. 1, E and F). These results confirm that reduction of either *RALF4* or *RALF19* leads to pollen tube bursting in vitro, whereas in vivo *RALF4* and *RALF19* act redundantly.

Plants with *RALF4* overexpression showed a skewed segregation ratio in crosses with transgenic pollen (tables S2 and S3) as well as reduced pollen germination and seed set (fig. S10). Synthetic RALF4 peptide can repress pollen tube growth (*4*), although a scrambled RALF4 peptide, which contains the same amino acids but in random sequence, could not (fig. S11, A and B). Together, these results suggest that high levels of RALF4 affect pollen germination and pollen tube growth.

To determine whether RALF4/19 peptides bind to specific regions of growing pollen tubes, we added synthetic RALF4 and RALF19 labeled with fluorescein isothiocyanate (FITC) to in vitro growing wild-type pollen tubes. Both bound along the length of the pollen tubes, with stronger signals at the tip (Fig. 1, G and H). The FITC-RALF4 Scrambled peptide did not show binding at the tip (fig. S11, C and D). After incubation, FITC-labeled RALF4/19 peptides were observed in vesicles inside the cell, as reported for other peptides binding pollen tubes (*15*, *16*) and consistent with binding to receptors that become internalized after activation.

Pollen tube growth cannot occur unless the cell wall at the tip is sufficiently soft to allow cell expansion but rigid enough to resist turgor pressure (*17*–*20*). Because *amiRRALF4/19* pollen tubes showed impaired growth, we analyzed cell wall components and found that, relative to the wild type, *amiRRALF4/19* pollen tubes were deficient in callose deposition (Fig. 2, A and D), accumulated acidic pectin in bulges (Fig. 2, B and E, and fig. S12), and showed a broader distribution of esterified pectins, usually localized at the pollen tube tip (Fig. 2, C and F). These results indicate that down-regulation of *RALF4/19* leads to changes in cell wall composition that are correlated with the formation of bulges, where acidic pectins accumulate and pollen tubes burst.

RALF peptides can bind FER to regulate various signaling pathways (*3*, *7*, *21*). Because ANX1 and ANX2 show the highest similarity to FER (*22*) and because the *amiRRALF4/19* phenotype resembles that of mutants in the *ANX1/2* pathway (*11*, *12*), we performed genetic analyses to place *RALF4/19* in this signaling pathway. Overexpression of *ANX1* or *MRI* in pollen tubes represses pollen germination and pollen tube elongation (*13*, *14*). Expressing *ANX1-YFP* or *MRI-YFP* in an *amiRRALF4/19* background under a pollen-specific promoter showed that neither *ANX1* (31 independent lines)

[1]Department of Plant and Microbial Biology and Zurich-Basel Plant Science Center, University of Zurich, 8008 Zurich, Switzerland. [2]Instituto de Investigaciones en Ingeniería Genética y Biología Molecular, Dr. Héctor Torres (INGEBI-CONICET), Vuelta de Obligado 2490, C1428ADN Buenos Aires, Argentina. [3]Fundación Instituto Leloir, IIBBA-CONICET, Buenos Aires, Argentina. [4]Biocenter, Botanical Institute, University of Cologne, 50674 Cologne, Germany. [5]Departamento de Biodiversidad y Biología Experimental, Facultad de Ciencias Exactas y Naturales, Universidad de Buenos Aires, Int. Güiraldes 2160, Ciudad Universitaria, Pabellón II, C1428EGA Buenos Aires, Argentina.
*These authors contributed equally to this work. †Present address: Biozentrum, University of Basel, 4056 Basel, Switzerland.
‡Corresponding author. Email: grossnik@botinst.uzh.ch (U.G.); prometeo@dna.uba.ar (J.P.M.)

nor *MRI* (50 independent lines) could rescue the pollen tube bursting phenotype of *amiRRALF4/19* (Fig. 2, G to J); these results imply that the *ANX1* and *MRI* overexpression phenotypes depend on *RALFL4/19*. However, expression of a dominant version of MRI, MRI^{R240C}*-YFP*, which suppresses the *anx1/2* double mutant (*14*), also suppressed the *amiRRALF4/19* phenotype (39 of 46 independent lines; Fig. 2, G to J). These results indicate that *RALF4* and *RALF19* act upstream of *ANX1/2* in the signaling pathway, consistent with a putative function as ligands for the activation of ANX1/2.

A pollen-specific RALF was found to interact with an LRX protein from tomato pollen in a yeast two-hybrid screen (*8*). LRX proteins play a role in cell wall development, and *lrx* mutants show defects in tip-growing cells, such as root hairs (*23*). Four members of the LRX family (*LRX8* to *LRX11*) are expressed in pollen (*24*), and higher-order mutants show a pollen tube bursting phenotype reminiscent of *amiRRALF4/19* lines (*25*). This suggests that RALF4/19 peptides may control pollen tube growth in conjunction with LRX proteins. To test this hypothesis, we treated single, double, and triple *lrx* mutant pollen tubes with synthetic RALF4 peptides that repress wild-type pollen tube growth (fig. S11). Growth of wild-type and all *lrx* mutant pollen tubes was not affected when scrambled RALF4 peptides were used (Fig. 3A and movie S1). However, when RALF4 peptides were added, wild-type, single, and double but not triple *lrx* mutant pollen tubes stopped growing (Fig. 3A and movie S1), which demonstrates that *LRX* proteins are redundant and are required for growth inhibition by RALF4 peptides. Thus, the perception of RALF4 depends on the presence of pollen-expressed LRX proteins.

To test whether RALF peptides directly interact with LRX proteins, we performed coimmunoprecipitation experiments with several LRX-Citrine [CIT, a version of green fluorescent protein (GFP)] and RALF4–hemagglutinin (HA) fusion proteins in *Agrobacterium*-infiltrated *Nicotiana benthamiana* leaves. After immunoprecipitation with GFP-Trap agarose beads, mature RALF4-HA was detected when LRX8-CIT, LRX10-CIT, or LRX11-CIT were co-expressed (Fig. 3B and fig. S13). Complementary results were obtained using anti-HA agarose beads, showing coimmunoprecipitation of LRX8-CIT, LRX10-CIT, and LRX11-CIT (fig. S13). When coimmunoprecipitation was performed using a scrambled RALF4-HA peptide, no interaction was observed (fig. S13). A yeast two-hybrid assay

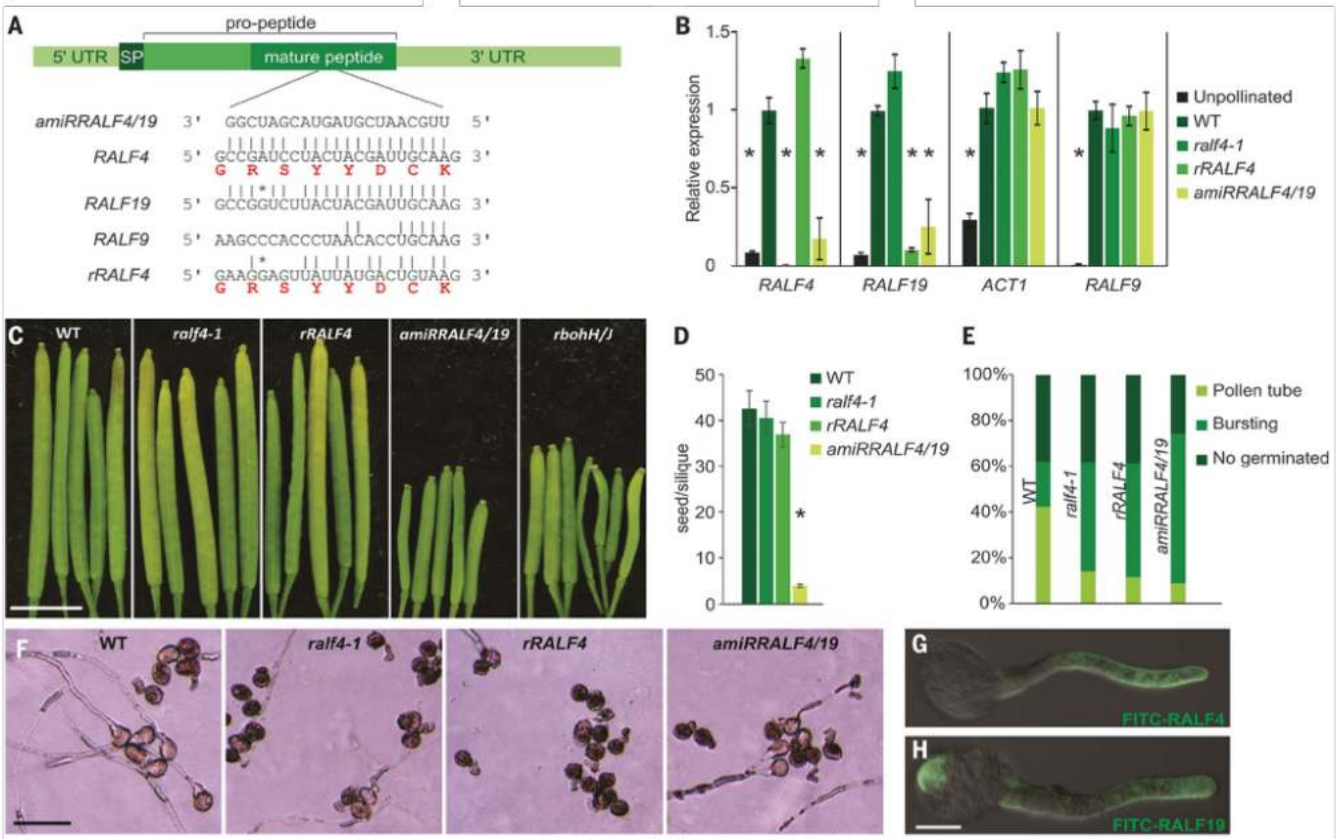

Fig. 1. *RALF4* and *RALF19* are important for pollen tube integrity and growth. (**A**) Sequence alignment of the mature amiRNA against *RALF4* and *RALF19* (*amiRRALF4/19*) with a target site in the coding regions of *RALF4* and *RALF19* mRNAs; asterisks indicate G:U base pairs. Alignment of *RALF9* and a resistant version of *RALF4* (*rRALF4*) shows that silent mutations prevent amiRNA regulation but do not change the amino acid sequence (red). SP, signal peptide. Amino acid abbreviations: C, Cys; D, Asp; G, Gly; K, Lys; R, Arg; S, Ser; Y, Tyr. (**B**) ddPCR of *RALF4* and *RALF19* levels in open flowers of wild-type (WT), *ralf4-1* mutant, *rRALF4*, and *amiRRALF4/19* plants. Unpollinated carpels were used as a control for pollen-specific expression. Expression was calculated as copies relative to *ARTUMES* (*AT1G61790*) mRNAs; WT was used as reference. *RALF9* and *ACT1* were used as internal reference genes. Data are means ± SEM of three biological replicates. *$P < 0.01$, one-way analysis of variance (ANOVA). (**C**) Siliques from the primary inflorescence of WT, *ralf4-1*, *rRALF4*, *amiRRALF4/19*, and *rbohH/J* mutant plants. Scale bar, 0.5 cm. (**D**) Seeds per silique of WT, *ralf4-1*, *rRALF4*, and *amiRRALF4/19* lines. Data are means ± SEM of three biological replicates ($n = 20$). *$P < 0.01$, one-way ANOVA. (**E**) Analysis of in vitro pollen germination of WT, *ralf4-1*, *rRALF4*, and *amiRRALF4/19*. (**F**) In vitro pollen germination of WT, *ralf4-1*, *rRALF4*, and *amiRRALF4/19*. Scale bar, 100 μm. (**G** and **H**) Binding of FITC-conjugated RALF peptides on WT pollen tubes. Both FITC-RALF4 (G) and FITC-RALF19 (H) peptides bind to growing pollen tubes. Scale bar, 10 μm.

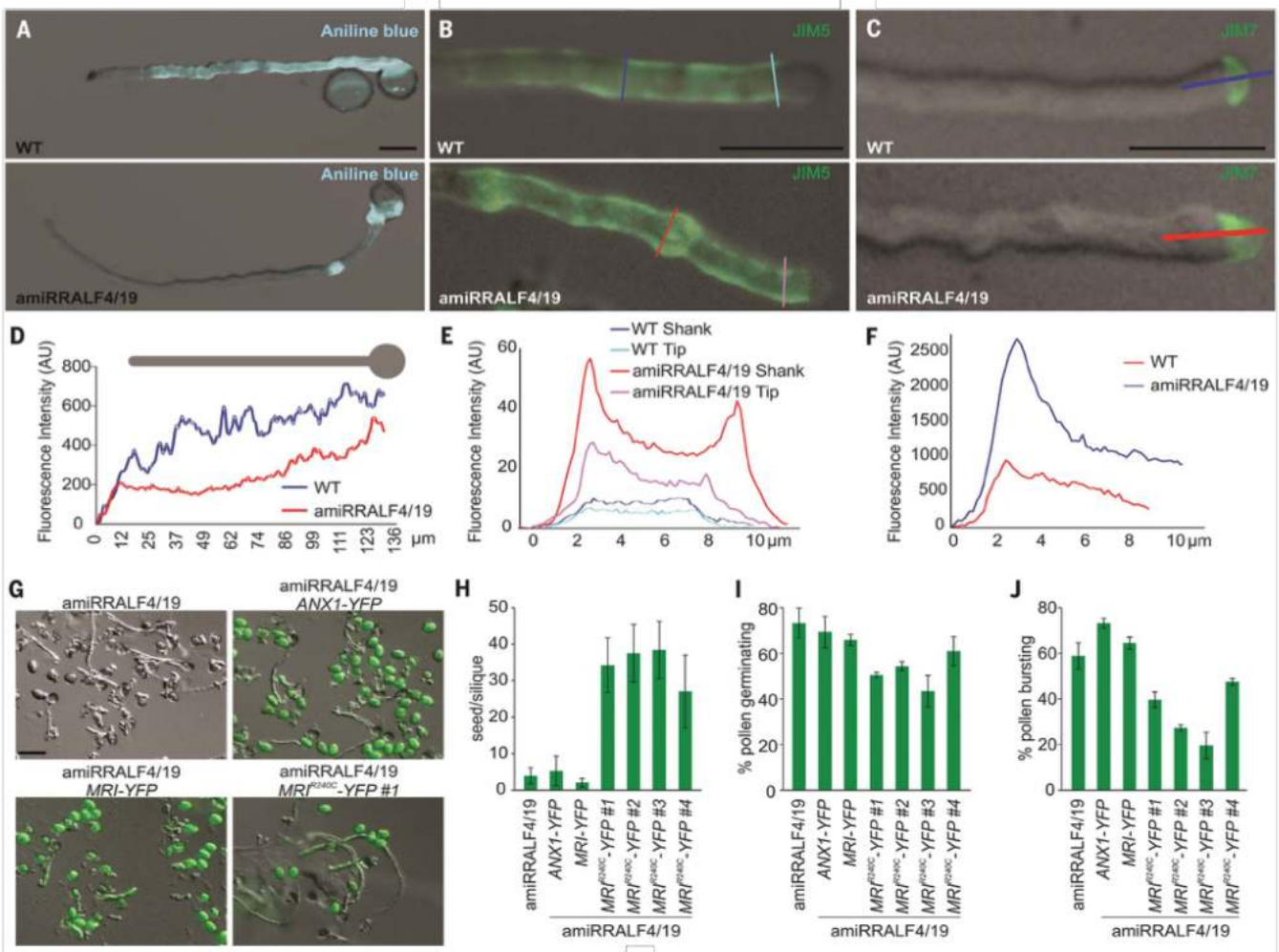

Fig. 2. *RALF4* and *RALF19* control cell wall composition and act upstream of *ANX1* and *MRI* in the *ANX1/2* pathway. (**A**) Aniline blue staining of callose deposition in WT and *amiRRALF4/19* pollen tubes. Scale bar, 20 µm. (**B**) JIM5 immunostaining of acidic pectins in WT and *amiRRALF4/19* pollen tubes. Scale bar, 20 µm. (**C**) JIM7 immunostaining of esterified pectins in WT and *amiRRALF4/19* pollen tubes. Scale bar, 20 µm. (**D**) Histogram of fluorescence intensity of aniline blue staining along pollen tubes of WT and *amiRRALF4/19* plants (n = 20). (**E**) Histogram of transversal sections of fluorescence accumulation in WT and *amiRRALF4/19* pollen tubes (n = 20). (**F**) Histogram of longitudinal sections of fluorescence accumulation in WT and *amiRRALF4/19* pollen tubes (n = 20). (**G**) In vitro pollen germination of *amiRRAL4/19* lines expressing *ANX1-YFP*, *MRI-YFP*, or *MRI^{R240C}-YFP*. Scale bar, 50 µm. (**H**) Number of seeds per silique of *amiRRALF4/19* lines expressing *ANX1-YFP*, *MRI-YFP*, or *MRI^{R240C}-YFP*. Data are means ± SEM of two biological replicates with 15 siliques analyzed per experiment. (**I**) Percentages of in vitro germinated pollen of *amiRRALF4/19* lines expressing *ANX1-YFP*, *MRI-YFP*, or *MRI^{R240C}-YFP*. Data are means ± SEM of two biological replicates with 200 pollen grains analyzed per experiment. (**J**) Percentages of bursting pollen tubes after in vitro germination of *amiRRALF4/19* lines expressing *ANX1-YFP*, *MRI-YFP*, or *MRI^{R240C}-YFP*. Data are means ± SEM of two biological replicates with 200 pollen tubes analyzed per experiment.

confirmed interactions of LRX8 and LRX9 with RALF4 (fig. S13), and quantification of the LRX8-RALF4 interaction by biolayer interferometry resulted in a dissociation constant K_D of 900 nM (fig. S14). Moreover, incubation of wild-type and *lrx8/9/11* pollen tubes with FITC-RALF4 peptides showed reduced binding of RALF4 to the triple mutant pollen tubes (Fig. 3, C to E). Thus, RALF4 interacts with LRX proteins to control pollen tube integrity and growth.

Our results show that RALF4/19 peptides and LRX proteins physically interact in the cell wall and are required to activate the *ANX1/2*-mediated signal transduction pathway regulating pollen tube growth. Both the RALF and LRX proteins are secreted by the pollen tube itself, whose integrity and growth they control. We propose that pollen tubes use autocrine signaling to explore their extracellular space, which may influence the composition, level, and modification of these secreted proteins, thereby providing information about the female tissues through which the pollen tubes grow and navigate. *Cr*RLK1Ls have two malectin domains that are thought to bind oligosaccharides (*26*) and interact with a variety of proteins. FER, for example, binds different RALF peptides and interacts with many other proteins, including RLKs, glycosylphosphatidylinositol-anchored proteins, phosphatases, and small guanosine triphosphatases (*27*, *28*). Thus, it seems that *Cr*RLK1Ls form a signaling hub by bringing together secreted peptides in the cell wall with various membrane-associated proteins to control specific cellular processes. Future investigations will elucidate how this multitude of interactions is regulated at the biochemical level

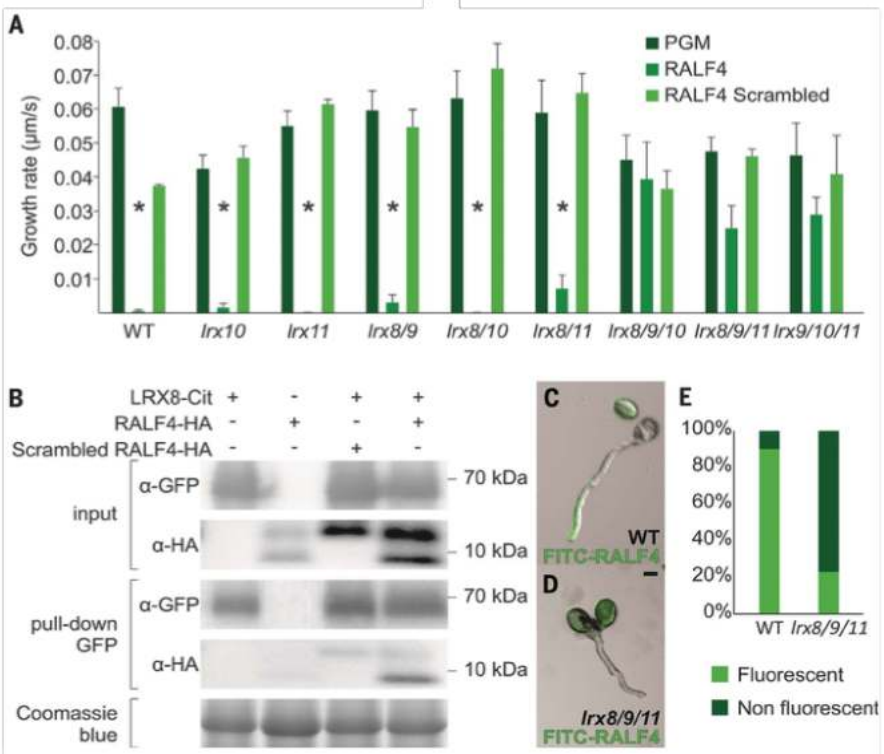

Fig. 3. RALF4 and RALF19 interact with LRX proteins to coordinate pollen tube integrity and growth. (**A**) Growth rate of WT and *lrx* single, double, and triple mutant pollen tubes in pollen germination medium (PGM), mature RALF4 synthetic peptides (250 nM), or RALF4 Scrambled synthetic peptides (250 nM) ($n = 29$). *$P < 0.05$, one-way ANOVA. (**B**) Western blot analysis of coimmunoprecipitated RALF4-HA after immunoprecipitation of LRX8-CIT using antibody against GFP (α-GFP). Predicted sizes: RALF4-HA and Scrambled RALF4-HA propeptide, 14.8 kDa; mature RALF4-HA, 8.3 kDa; LRX8-Cit, 70 kDa. (**C** and **D**) Binding of FITC-RALF4 conjugated peptides on WT (C) and *lrx8/9/11* triple mutant (D) pollen tubes. Scale bar, 10 µm. (**E**) Percentage of pollen tubes with FITC-RALF4 binding ($n = 50$).

to direct the diverse processes controlled by *Cr*RLK1L signaling pathways.

REFERENCES AND NOTES

1. E. Murphy, I. De Smet, *Trends Plant Sci.* **19**, 664–671 (2014).
2. G. Pearce, D. S. Moura, J. Stratmann, C. A. Ryan Jr., *Proc. Natl. Acad. Sci. U.S.A.* **98**, 12843–12847 (2001).
3. M. Stegmann *et al.*, *Science* **355**, 287–289 (2017).
4. A. Morato do Canto *et al.*, *Plant Physiol. Biochem.* **75**, 45–54 (2014).
5. R. Srivastava, J. X. Liu, H. Guo, Y. Yin, S. H. Howell, *Plant J.* **59**, 930–939 (2009).
6. J. Wu *et al.*, *Plant J.* **52**, 877–890 (2007).
7. M. Haruta, G. Sabat, K. Stecker, B. B. Minkoff, M. R. Sussman, *Science* **343**, 408–411 (2014).
8. P. A. Covey *et al.*, *Plant Physiol.* **153**, 703–715 (2010).
9. G. Y. Zhang, J. Wu, X. W. Wang, *Mol. Biol. Rep.* **37**, 3273–3281 (2010).
10. M. Schiøtt *et al.*, *Proc. Natl. Acad. Sci. U.S.A.* **101**, 9502–9507 (2004).
11. A. Boisson-Dernier *et al.*, *Development* **136**, 3279–3288 (2009).
12. S. Miyazaki *et al.*, *Curr. Biol.* **19**, 1327–1331 (2009).
13. A. Boisson-Dernier *et al.*, *PLOS Biol.* **11**, e1001719 (2013).
14. A. Boisson-Dernier, C. M. Franck, D. S. Lituiev, U. Grossniklaus, *Proc. Natl. Acad. Sci. U.S.A.* **112**, 12211–12216 (2015).
15. M. L. Mårton, A. Fastner, S. Uebler, T. Dresselhaus, *Curr. Biol.* **22**, 1194–1198 (2012).
16. S. Okuda *et al.*, *Mol. Plant* **6**, 1074–1090 (2013).
17. H. Vogler, D. Felekis, B. J. Nelson, U. Grossniklaus, *Plants* **4**, 167–182 (2015).
18. Y. Chebli, M. Kaneda, R. Zerzour, A. Geitmann, *Plant Physiol.* **160**, 1940–1955 (2012).
19. H. Hölte, *Plant Cell Physiol.* **56**, 224–231 (2015).
20. P. K. Hepler, C. M. Rounds, L. J. Winship, *Mol. Plant* **6**, 998–1017 (2013).
21. J. Chen *et al.*, *Proc. Natl. Acad. Sci. U.S.A.* **113**, E5519–E5527 (2016).
22. A. Boisson-Dernier, S. A. Kessler, U. Grossniklaus, *J. Exp. Bot.* **62**, 1581–1591 (2011).
23. N. Baumberger, C. Ringli, B. Keller, *Genes Dev.* **15**, 1128–1139 (2001).
24. N. Baumberger *et al.*, *Plant Physiol.* **131**, 1313–1326 (2003).
25. T. Ndinyanka Fabrice *et al.*, bioRxiv:10.1101/223008 (2017).
26. T. Schallus *et al.*, *Mol. Biol. Cell* **19**, 3404–3414 (2008).
27. C. Li *et al.*, *eLife* **4**, e06587 (2015).
28. H. Liao, R. Tang, X. Zhang, S. Luan, F. Yu, *Plant Cell Physiol.* **58**, 1143–1150 (2017).

ACKNOWLEDGMENTS

We thank H. Vogler and M. Jaciubek for advice on pollen tube assays and cloning strategies, respectively; A. Sede for help with genotyping; K. Locher and T. Pflüger for access to Monolith technology; T. Hander for help with the BLItz system; and C. Eichenberger, A. Bolaños, D. Guthörl, P. Kopf, and A. Frey for general laboratory support. Supported by the University of Zurich; Research and Technology Project MecanX (grant 145676 to U.G. and C.R.) funded by SystemsX.ch; Swiss National Science Foundation grants 3100308_160336 and CR32I3_156724 (U.G.); Deutsche Forschungsgemeinschaft grant BO 4470/1-1 (A.B.-D.), and Agencia Nacional de Promoción Científica y Tecnológica grants PICT2014 (J.P.M. and M.A.M.) and PICT2015 (J.P.M.). The stay of M.A.M. in U.G.'s laboratory was supported by an EMBO Short-Term Fellowship and the Company of Biologists. Supplement contains additional data.

SUPPLEMENTARY MATERIALS

www.sciencemag.org/content/358/6370/1600/suppl/DC1
Materials and Methods
Figs. S1 to S14
Tables S1 to S5
Movies S1 and S2
References (*29*–*41*)

1 August 2017; accepted 10 November 2017
10.1126/science.aao5467

Science

RALF4/19 peptides interact with LRX proteins to control pollen tube growth in *Arabidopsis*

Martin A. Mecchia, Gorka Santos-Fernandez, Nadine N. Duss, Sofia C. Somoza, Aurélien Boisson-Dernier, Valeria Gagliardini, Andrea Martínez-Bernardini, Tohnyui Ndinyanka Fabrice, Christoph Ringli, Jorge P. Muschietti and Ueli Grossniklaus

Science **358** (6370), 1600-1603.
DOI: 10.1126/science.aao5467originally published online December 14, 2017

Timing a switch in tissue integrity

In plants, sperm cells travel through the pollen tube as it grows toward the ovule. Successful fertilization depends on the pollen tube rupturing to release the sperm cells (see the Perspective by Stegmann and Zipfel). Ge *et al.* and Mecchia *et al.* elucidated the intercellular cross-talk that maintains pollen tube integrity during growth but destroys it at just the right moment. The signaling peptides RALF4 and RALF19, derived from the pollen tube, maintain its integrity as it grows. Once in reach of the ovule, a related signaling peptide, RALF34, which derives from female tissues, takes over and causes rupture of the pollen tube.

Science, this issue p. 1596, p. 1600; see also p. 1544

Science (print ISSN 0036-8075; online ISSN 1095-9203) is published by the American Association for the Advancement of Science, 1200 New York Avenue NW, Washington, DC 20005. The title *Science* is a registered trademark of AAAS.

3 Chapter 3 - Deeping in the LRX - RALF complex

3.1 Introduction

All of Chapter 3 was published as Moussu Steven, Broyart Caroline, **Santos-Fernandez Gorka**, Augustin Sebastian, Wehrle Sarah, Grossniklaus Ueli, Santiago Julia to *Proc Natl Acad Sci USA*, **117** (13), 7494-7503 (2020).

I contributed to this paper as follows: I analysed all the peptides' effect in pollen tubes for measuring the growth arrest phenotype and performed all the *in vitro* pollen tube assays to better understand the importance of RALFs' folded structure and their effects. Furthermore, I performed all the phenotypic characterization and the seeds/silique counting together with the *Arabidopsis* transformations to study the rescue of the *lrx* mutants' phenotype (pollen tube bursting) and the analysis of protein expression in these lines by Western blotting. In addition, I helped with the interpretation of the results and the writing of the 'Supplementary Materials' for the publication.

Importantly, the results of chapter 2, in addition with other published paper supporting our discoveries, like the Chunzhao Zhao's and colleagues (Zhao et al., *2018*) marked a before and an after in the way of understanding the RALFs' interaction with their partners. However, it raised plenty of new open questions such as: 'How could a small peptide be recognized by two different proteins? How does the binding of LRX affect the interaction with the CrRLK1L family? Do these proteins interact together?'

Thus, to better understand the interaction of these peptides, it was necessary to deeply understand its diverse structure. This is what the next chapter is all about; a deep description of the structural bases of both RALF and LRX, and their close affinity interactions.

Note that all supplemental data can be found in the Appendix.

Structural basis for recognition of RALF peptides by LRX proteins during pollen tube growth

Steven Moussu[a,1], Caroline Broyart[a,1], Gorka Santos-Fernandez[b,c,1], Sebastian Augustin[a], Sarah Wehrle[d], Ueli Grossniklaus[b,c], and Julia Santiago[a,2]

[a]The Plant Signaling Mechanisms Laboratory, Department of Plant Molecular Biology, University of Lausanne, 1015 Lausanne, Switzerland; [b]Department of Plant and Microbial Biology, University of Zurich, 8008 Zurich, Switzerland; [c]Zurich-Basel Plant Science Center, University of Zurich, 8008 Zurich, Switzerland; and [d]Institute of Bioengineering, École Polytechnique Fédérale de Lausanne, 1015 Lausanne, Switzerland

Edited by Julian I. Schroeder, Cell and Developmental Biology Section, Division of Biological Sciences, University of California San Diego, La Jolla, CA, and approved February 11, 2020 (received for review January 8, 2020)

Plant reproduction relies on the highly regulated growth of the pollen tube for sperm delivery. This process is controlled by secreted RALF signaling peptides, which have previously been shown to be perceived by *Catharanthus roseus* RLK1-like (*Cr*RLK1Ls) membrane receptor-kinases/LORELEI-like GLYCOLPHOSPHATIDYLINOSITOL (GPI)-ANCHORED PROTEINS (LLG) complexes, or by leucine-rich repeat (LRR) extensin proteins (LRXs). Here, we demonstrate that RALF peptides fold into bioactive, disulfide bond-stabilized proteins that bind the LRR domain of LRX proteins with low nanomolar affinity. Crystal structures of LRX2–RALF4 and LRX8–RALF4 complexes at 3.2- and 3.9-Å resolution, respectively, reveal a dimeric arrangement of LRX proteins, with each monomer binding one folded RALF peptide. Structure-based mutations targeting the LRX–RALF4 complex interface, or the RALF4 fold, reduce RALF4 binding to LRX8 in vitro and RALF4 function in growing pollen tubes. Mutants targeting the disulfide-bond stabilized LRX dimer interface fail to rescue *lrx* infertility phenotypes. Quantitative biochemical assays reveal that RALF4 binds LLGs and LRX cell-wall modules with drastically different binding affinities, and with distinct and mutually exclusive binding modes. Our biochemical, structural, and genetic analyses reveal a complex signaling network by which RALF ligands instruct different signaling proteins using distinct targeting mechanisms.

Arabidopsis | cell-wall integrity | pollen tube | structure biology | peptide signaling

In flowering plants, sexual reproduction depends on the directional growth of pollen tubes to deliver the sperm cells to the female gametes. The polarized, rapid growth of the pollen tube depends on the highly dynamic remodeling of their cell wall. The redundant signaling peptides RALF4 and RALF19 ensure pollen tube integrity and growth by interacting with two distinct protein families, the malectin-domain *Cr*RLK1L membrane receptor kinases (1–4), and the cell-wall monitoring leucine-rich repeat (LRR) extensin proteins (LRXs) (5, 6). Together with ANXUR1/2 and BUDDHA'S PAPER SEAL1/2 (BUPS1/2), the pollen-expressed LORELEI-like GLYCOLPHOSPHATIDYLINOSITOL (GPI)-ANCHORED PROTEINS2 (LLG2) and LLG3 are also required for monitoring pollen tube integrity and are part of the same signaling complex (2, 7). Recent structural data of the ternary RALF23–LLG2–FERONIA (FER) (8) complex suggests a shared mechanism for recognition of RALF peptides by LLG proteins, where the N-terminal region of the peptide is responsible for inducing an allosteric change in LLG to nucleate assembly with the corresponding *Cr*RLK1L receptor (9). LRXs and RALF4/19 functions seem to be directly connected with the regulation of extracellular matrix composition to allow for proper cell-wall homeostasis during pollen tube growth. Deregulation of both RALF4/19 and LRX proteins translates into the unstructured deposition of pectin and changes in wall mechanical properties, leading to defective pollen tubes (5, 6).

While *Cr*RLK1L/LLGs and LRXs are required for proper pollen tube growth, their relative contribution to specific RALF peptide sensing remains to be investigated. Here, we mechanistically dissect how pollen-expressed RALF peptides differentially interact with secreted LRX and membrane-anchored LLG proteins, respectively. Our work reveals that RALFs are folded signaling proteins precisely sensed by LRX proteins, whose bioactivity is determined by their oligomeric state to control pollen tube cell-wall integrity.

Results

There are 37 RALF peptides in *Arabidopsis* (10), with RALF4/19 being involved in the regulation of pollen tube integrity and growth (3, 5). Mature RALF4/19 peptides are 51 amino acids long and contain four invariant cysteines. We hypothesized that they may be folded proteins, stabilized by intramolecular disulfide bridges. Hence, for biochemical and structural analyses, we expressed RALF4/19 as thioredoxin A fusion proteins by secreted expression in insect cells. We observed secretion of RALF4/19 into the growth cell medium only when coexpressed with members of the LRX family, but neither as a stand-alone protein nor in the presence of the *Cr*RLK1L ANXUR1 (ANX1) (11, 12) (*SI Appendix*, Fig. S1). Efficient secretion of RALF4/19 required the N-terminal half of LRX8/11 (*SI Appendix*, Fig. S1). RALF4/19 formed stable complexes with $LRX8_{33–400}$ (amino acids 33 to 400) and $LRX11_{45–415}$ in size-exclusion chromatography (SEC) experiments

Significance

Plant reproduction relies on proper pollen tube growth to reach the female gametes. This process is highly regulated by a family of secreted signaling peptides that are recognized by cell-wall monitoring proteins to enable plant fertilization. Here, we report that these signaling peptides are sensed both by specific cell-wall and membrane-anchored proteins, which together enable cell-wall remodeling and, consequently, pollen tube growth.

Author contributions: S.M., C.B., G.S.-F., U.G., and J.S. designed research; S.M., C.B., G.S.-F., S.A., S.W., and J.S. performed research; S.M., C.B., G.S.-F., S.A., U.G., and J.S. analyzed data; J.S. wrote the paper; S.M. wrote materials and methods, figure legends, and revisions and comments; C.B. provided comments on the paper; G.S.-F. provided comments and figure legends; and U.G. provided comments and corrections in the manuscript.

The authors declare no competing interest.

This article is a PNAS Direct Submission.

Data deposition: The atomic coordinates and structure factors have been deposited in the Protein Data Bank, http://www.wwpdb.org/ (PDB ID codes 6QXP, 6QWN, and 6TME).

[1]S.M., C.B., and G.S.-F. contributed equally to this work.

[2]To whom correspondence may be addressed. Email: julia.santiago@unil.ch.

This article contains supporting information online at https://www.pnas.org/lookup/suppl/doi:10.1073/pnas.2000100117/-/DCSupplemental.

First published March 12, 2020.

(*SI Appendix*, Fig. S1). The presence of both proteins in the respective complexes was verified by mass spectrometry (*SI Appendix*, Fig. S2). Next, we biochemically mapped the RALF4 binding site to the predicted LRR core of LRX8 and LRX11 (*SI Appendix*, Fig. S1).

To quantify the interaction of RALF4 and LRX8, we first dissociated the complex at low pH (*Materials and Methods*) (Fig. 1*A*). The LRX8–RALF4 complex could be fully reconstituted when shifting the pH to 5.0 (13, 14) (Fig. 1*A*). To characterize the interaction of LRX8 with RALF4, we titrated the RALF4 protein isolated from insect cells ($RALF4_{folded}$ hereafter) into a solution containing isolated $LRX8_{49–400}$ using isothermal titration calorimetry (ITC). We found that RALF4 tightly binds the LRR core of LRX8 with ~3.5-nM affinity and a binding stoichiometry (N) of ~1 (Fig. 1 *B* and *D* and *SI Appendix*, Fig. S3). Next, we used a label-free surface biosensor based on grating-couple interferometry (GCI) (*Materials and Methods*) (15) to study the binding kinetics between LRX8 and the folded RALF4 peptide (Fig. 1*C* and *SI Appendix*, Fig. S1). In GCI experiments, LRX8 binds $RALF4_{folded}$ with a dissociation constant (K_d) of ~0.5 nM, in good agreement with the ITC experiments. This tight interaction of the peptide to the cell-wall monitoring protein is characterized by a fast association ($k_a \sim 4{\cdot}10^5\ M^{-1}\ s^{-1}$) and a very slow dissociation rate ($k_d \sim 2{\cdot}10^4\ s^{-1}$) (Fig. 1*C* and *SI Appendix*, Fig. S1). To assess whether the RALF4 tertiary structure is a major binding determinant, we measured the binding affinity of mutant RALF4 peptides, in which we replaced two (Cys86 and Cys105) or all four cysteines by alanine in a synthetic peptide ($RALF_{CC}$, $RALF_{CCCC}$)

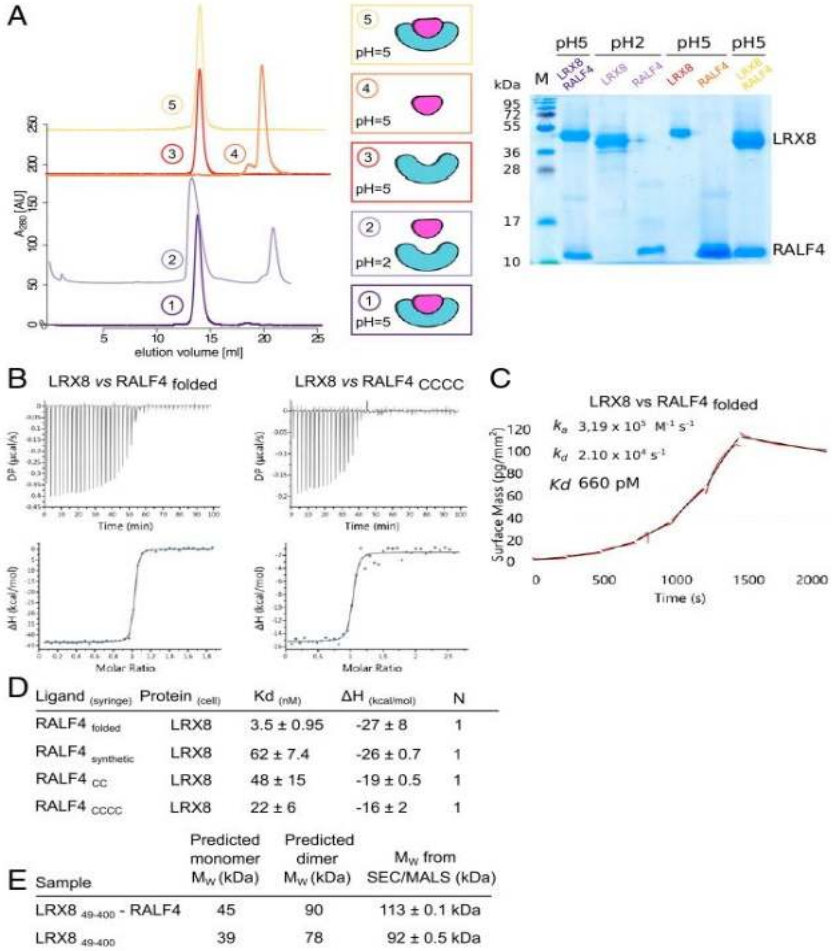

D

Ligand (syringe)	Protein (cell)	Kd (nM)	ΔH (kcal/mol)	N
$RALF4_{folded}$	LRX8	3.5 ± 0.95	-27 ± 8	1
$RALF4_{synthetic}$	LRX8	62 ± 7.4	-26 ± 0.7	1
$RALF4_{CC}$	LRX8	48 ± 15	-19 ± 0.5	1
$RALF4_{CCCC}$	LRX8	22 ± 6	-16 ± 2	1

E

Sample	Predicted monomer M_W (kDa)	Predicted dimer M_W (kDa)	M_W from SEC/MALS (kDa)
$LRX8_{49-400}$ - RALF4	45	90	113 ± 0.1 kDa
$LRX8_{49-400}$	39	78	92 ± 0.5 kDa

Fig. 1. Dimeric LRX proteins bind $RALF_{folded}$ peptides with high affinity. (*A*) Folded RALF4 peptide can be obtained by complex dissociation. LRX8–RALF4 complex purification, dissociation, and reconstitution. SEC graphs of the different steps are plotted on the *Left*. From bottom to top: LRX8–RALF4 purified complex at pH 5.0 (dark purple); dissociated LRX8–RALF4 complex at pH 2.0 (light purple). Orange and red runs represent RALF4 and LRX8 peaks, respectively, dialyzed back to pH 5.0. The SEC for the reconstituted complex, using the previously separated proteins, is shown in yellow. Schematics of the different steps, and SDS gel of the corresponding peaks, are shown alongside. (*B*) ITC of LRX8 vs. $RALF4_{folded}$ and $RALF4_{CCCC}$. Raw thermograms of ITC experiments are plotted. (*C*) Binding kinetics of LRX8 vs. $RALF4_{folded}$ obtained from GCI experiments. The sensogram with recorded data are shown in red with the respective fits in black. The summary table contains the corresponding association rate constant (k_a), dissociation rate constant (k_d), and the dissociation constant K_d. (*D*) ITC table summaries of LRX8 vs. RALF4 peptides. K_d (dissociation constant) indicates the binding affinity between the two molecules considered (in nanomoles). The N indicates the reaction stoichiometry ($n = 1$ for a 1:1 interaction). The values indicated in the table are the mean ± SD of two or three independent experiments. (*E*) Table of SEC–MALS analysis of apo–LRX8 and LRX8–RALF4 complex. The predicted and measured values are reported in the table for comparison. Values indicated in the table are the mean ± SD of two or three independent measurements.

(Fig. 1 *B* and *D* and *SI Appendix*, Fig. S1). $RALF4_{CC}$ and $RALF_{CCCC}$ bind LRX8 with ~10-fold reduced affinity, suggesting that LRX8 preferentially senses the folded RALF4 signaling protein but still binds the linearized peptide with nanomolar affinity (Fig. 1 *B* and *D* and *SI Appendix*, Figs. S1 and S3). A synthetic, wild-type (WT) RALF4 peptide ($RALF4_{synthetic}$) bound LRX8 with lower affinity, K_d of ~60 nM (Fig. 1*D* and *SI Appendix*, Fig. S1), in agreement with previous findings (5). We then compared the folding state of insect cell-expressed $RALF4_{folded}$ with the different synthetic peptides using near-UV circular dichroism spectra (CD). In these experiments, we observed a spectrum characteristic for a disulfide-bond stabilized protein for $RALF4_{folded}$ but not for the $RALF_{CCCC}$ (*SI Appendix*, Fig. S4). The spectrum of $RALF4_{synthetic}$ indicates a partially folded state (*SI Appendix*, Fig. S4).

Next, we assessed the stoichiometry of LRX–RALF complexes. We found LRX8 and LRX11 to be homodimers in the presence or absence of $RALF4_{folded}$ as judged by analytical SEC and multiangle light scattering (MALS) experiments (Fig. 1*E* and *SI Appendix*, Fig. S5). The MALS data are consistent with a 2 + 2 complex, with each glycosylated LRX protomer binding one RALF4 molecule.

The fact that LRX proteins appear to specifically sense $RALF_{folded}$ peptides prompted us to investigate LRX–RALF complex structures. Diffracting crystals were obtained for LRX2–RALF4 and the pollen-specific LRX8–RALF4 complex, determined at 3.2-Å and 3.9-Å resolution, respectively (*SI Appendix*, Table S1). LRX2–RALF4 crystals contain four RALF4-bound dimers in the asymmetric unit, which closely align with each other, and with the LRX8–RALF4 complex (root mean square deviation [r.m.s.d.] is ~0.8 Å comparing 357 pairs of corresponding C_α atoms) (Fig. 2*A* and *SI Appendix*, Fig. S6). We thus used the higher resolution LRX2–RALF4 structure to further analyze the signaling complex. A structural homology search with the program DALI (16) revealed that the LRX2 protein is closely related to the extracellular domain of known LRR receptor kinases, such as the immune receptor FLS2 (*DALI Z*-score of 33.5, r.m.s.d. of ~1.7 comparing 299 corresponding C_α atoms). LRX2 comprises 11 LRRs sandwiched by canonical N- and C-terminal capping domains and a cysteine-rich protrusion that represents the N-terminal part of the extensin domain (Fig. 2 *A* and *D*). The LRX2 and LRX8 complex structures confirm that LRX proteins form constitutive dimers, covalently linked by a conserved disulfide bond (Fig. 2*A* and *SI Appendix*, Figs. S6 and S7). One RALF4 peptide is bound to each LRX protomer in the dimer, consistent with our MALS and ITC experiments in solution (Figs. 1 *B*, *D*, and *E* and

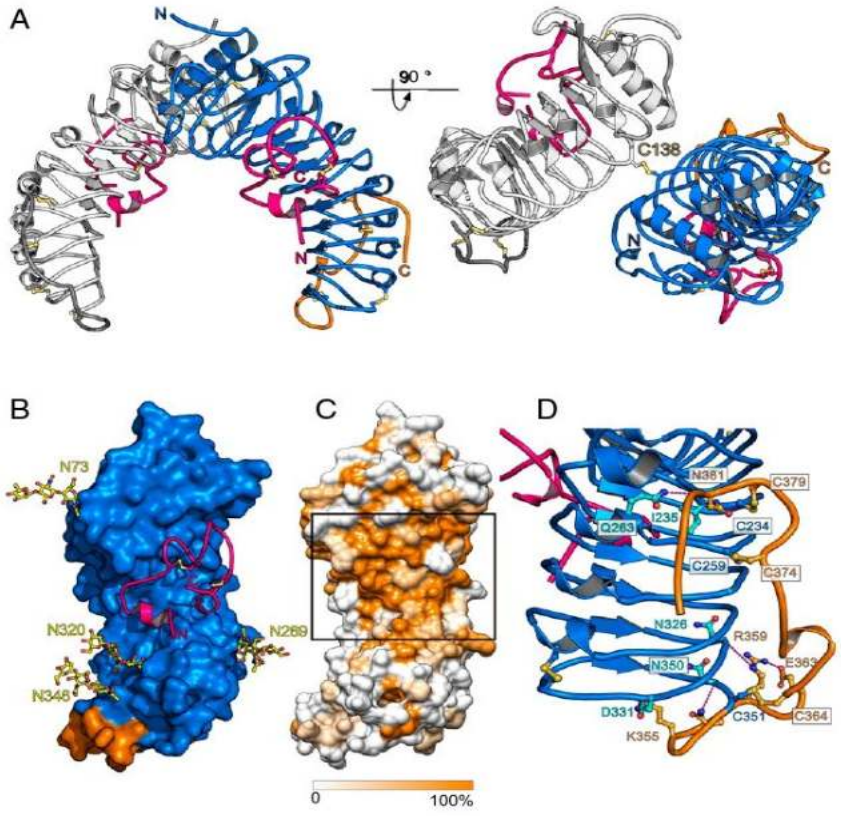

Fig. 2. The LRR core of LRX proteins provides a conserved homodimer interface, a RALF binding pocket, and a stabilized connection to the extensin domain. (*A*) Front and 90° *x* axis rotated view of the covalently linked LRX2 homodimer in complex with RALF4 (ribbon diagram). The LRR domain is depicted in blue, the cysteine-rich tail in orange, and the RALF4 peptide is highlighted in pink. The disulfide bridge covalently linking the two LRX protomers is highlighted in yellow. (*B*) Surface view of LRX2 (color code as in *A*) along with a cartoon representation of the RALF4 peptide (pink), highlighting the LRX2's RALF4 binding pocket. *N*-glycosylations are depicted in yellow. (*C*) Surface representation of LRX2 colored according to the LRX family amino acid conservation. The black rectangle underlines the conservation of the LRX's RALF binding pocket. (*D*) Cartoon representation of the C-terminal part of the LRR core and the Cys tail of LRX2 (color code as in *A*). Each connecting disulfide bond is formed between a Cys from the LRR domain (depicted in blue) and the Cys-rich tail (highlighted in orange). Interface residues making polar contacts are shown as sticks and hydrogen bonds are depicted as dotted lines (in magenta).

2*A*). The LRR core provides a binding platform for $RALF4_{folded}$ (Fig. 2*B* and *SI Appendix*, Fig. S6). Despite the moderate resolution of our complex structures, we located difference electron density accounting for the entire RALF4 folded peptide, again supporting its tight interaction with LRX proteins (*SI Appendix*, Fig. S8). The mature RALF4 protein consists of a short N-terminal alpha-helix, followed by a long loop region that is shaped by two disulfide bonds and a final one-turn 3_{10}-helix at the C terminus. The rather unstructured RALF4 peptide adopts a defined conformation when binding to the LRX LRR domain by making extensive contacts with the binding pocket (Fig. 2*B* and *SI Appendix*, Figs. S6 and S7). The RALF binding pocket is highly conserved among the known LRX family members, suggesting that other LRX proteins may bind different RALF peptides in a similar conformation (Fig. 2*C* and *SI Appendix*, Fig. S7). This particular binding configuration exposes the least conserved regions of the peptide to the solvent (*SI Appendix*, Fig. S9). In our structures, we also captured the cysteine-rich tail that links the C-terminal LRR capping domain of LRX2 and LRX8 to the cell-wall anchored extensin domain. The cysteine-rich linker adopts similar conformations in the LRX2 and LRX8 structures (*SI Appendix*, Fig. S6). The cysteine-rich tail folds back onto the LRR domain and connects via a ladder of disulfide bridges with LRRs 7 to 11. Several conserved polar and hydrophobic residues further stabilize this LRR–linker interface (Fig. 2*D* and *SI Appendix*, Fig. S7). This suggests that the RALF4 binding domain of LRX proteins is tightly connected to its extensin domain.

We next dissected the RALF4–LRX8 binding mode. Few interactions between the N-terminal alpha-helix (residues 64 to 69) of $RALF4_{folded}$, which is a major determinant for LLG binding (9) with the LRR core of LRXs are mediated by RALF4 residues Tyr63, Ile64, and Tyr66 and LRX8 residues Gln314 ($Gln296^{LRX2}$), Phe221($Phe202^{LRX2}$), Glu266 ($Glu248^{LRX2}$), and Glu313 ($Glu295^{LRX2}$) (Fig. 3*A* and *SI Appendix*, Fig. S10). A RALF4 Tyr63Ala/Tyr66Ala double mutant still bound LRX8 with wild-type affinity, suggesting that the N-terminal helix in RALF peptides is not a major determinant for high-affinity binding to LRX proteins (Fig. 3*B*, see below). The loop region in $RALF4_{folded}$ (residues 70 to 101) is structurally stabilized and oriented by the Cys76–Cys86 and Cys99–Cys105 disulfide bonds, required for high-affinity binding to LRX8 (Figs. 1 *B* and *D* and 3*A* and *SI Appendix*, Fig. S3). We identified the conserved RALF4 Tyr83 and Tyr84 to be part of this loop region and directly contacting the LRR core of LRX8 and LRX2 (Fig. 3*A*). Titration of a $RALF4_{Y83A.Y84A}$ mutant peptide to LRX8 in ITC assays resulted in a much weaker binding affinity ($K_d \sim 1.4$ μM) when compared to wild-type RALF4 (Fig. 3*B* and *SI Appendix*, Fig. S11). Thus, the loop region forming part of the RALF4–LRX complex interface in our structures is critical for RALF4 binding in vitro.

To confirm the binding mode of RALF4 to LRX8, we mutated the LRX surface in contact with the RALF4 loop region. Coexpression of LRX8 Phe109Ala/His150Ala ($Phe90^{LRX2}$/$His131^{LRX2}$) and wild-type RALF4 led to a reduced expression of the LRX8 protein in insect cells and secretion of the RALF4 peptide was not detected. This suggests that the mutations in the RALF–LRX loop interface inhibit the formation of a stable LRX8–RALF4 complex. Similar results were obtained in planta, where LRX8 and RALF4 mutant proteins targeting the complex interface failed to interact in coimmunoprecipitation experiments in tobacco (*SI Appendix*, Fig. S11). To determine whether RALF4 binding to LRX is critical to regulate pollen tube growth and integrity, we complemented a *lrx* quadruple mutant (*lrx8,9,10,11*) with the full-length $LRX8_{F109A.H150A}$ mutant expressed under the control of the native LRX8 promoter (*SI Appendix*, Fig. S12). The mutant failed to rescue the pollen tube growth defect and fertility phenotype (Fig. 3*C*) despite the proper localization of the C-terminal $LRX8_{F109A.H150A}$–mCitrine fusion protein to the cell wall (*SI Appendix*, Fig. S13).

Altogether, our experiments show that the disulfide bond-stabilized loop in $RALF4_{folded}$ is a major determinant for LRX binding and that binding of the peptide to LRX is required to control pollen tube growth. Based on these findings, we compared the bioactivity of synthetic, folded, and cysteine-mutated RALF4 signaling peptides in pollen tube growth assays. Addition of RALF4 peptides represses pollen tube growth, suggesting that high levels of RALF4 can also deregulate cell-wall integrity and/or sensing, leading to growth arrest (5, 17). The inhibitory effect of RALF4 peptides on pollen tube elongation was quantified using two peptide concentrations: 50 and 100 nM (Fig. 3*D*). Addition of a sequence-permutated version of RALF4 ($RALF4_{scrambled}$) had no effect on pollen tube growth, whereas $RALF4_{folded}$ completely inhibited growth at both concentrations. The synthetic and cysteine-mutated RALF4 peptides partially suppressed pollen tube growth (Fig. 3 *D* and *E*), in good agreement with our structural and quantitative biochemical data (Figs. 1 *B–D* and 2*A*).

It has previously been reported that the *Cr*RLK1Ls FER and THESEUS1 (8, 18) are receptors for RALF peptides with binding affinities in the nanomolar (nM) to the micromolar (μM) range (3, 19–21). Together with FER, the GPI-anchored protein LORELEI, expressed in the female gametophyte, is also required for fertilization (22, 23) and it copulls down with the receptor kinase in vitro (24). In addition, FER has been reported to coimmunoprecipitate with LLG1 in the presence of RALF peptides (24). These data have been supported by the recent crystal structure of the ternary FER–LLG2–RALF23 complex, where the N-terminal region of RALF23 (YISY motif) (25) is recognized by LLG proteins, inducing a conformational change promoting the interaction with the FER receptor-like kinase (9). We thus quantified the direct binding of $RALF4_{folded}$ to the ectodomains of the pollen-expressed LLG2/3 (2, 7), which have also been reported to be part of *Cr*RLK1L–LLG complexes (2). We quantified the interactions in acidic and alkaline conditions since oscillatory influx of H^+ is thought to be important for tip growth of the pollen tube (26, 27), and RALFs have been reported to alkalinize the apoplast space (28). We found that LLG3 binds $RALF4_{folded}$ with K_ds of ~11 μM at pH 5.0, ~4,000 times weaker than to LRX8 at the same pH (Fig. 3*F*). We next quantified the interaction of $RALF4_{folded}$ with LRX8 and LLG2/3 at pH 7.5. We determined a K_d for RALF4–LRX8 to be ~0.1 μM (Fig. 3*F*). $RALF4_{folded}$ bound LLG2 and LLG3 with dissociation constants of ~0.5 μM and ~1.5 μM, respectively (Fig. 3*F* and *SI Appendix*, Fig. S17). Thus, pH alterations modulate the interaction of $RALF4_{folded}$ with LRX8 and LLGs, with LRX proteins consistently recognizing $RALF4_{folded}$ with higher affinity.

Next, we compared the binding modes for $RALF4_{folded}$ interacting with LRX8 or LLGs. We found that mutations in the RALF4 YISY motif (Tyr63Ala/Tyr66Ala mutant), did not interfere with $RALF4_{folded}$ binding to LRX8, but disrupted the interaction with LLGs, consistent with previous structural and biochemical work (Fig. 3 *B* and *F* and *SI Appendix*, Fig. S18) (9). The mutant $RALF4_{folded\ Y63A.Y66A}$ protein completely inhibited pollen growth to a similar extent as wild-type $RALF4_{folded}$, suggesting that RALF4-mediated pollen tube growth arrest may be exclusively regulated by LRX proteins (Fig. 3 *D* and *E*). Taken together, our findings suggest that LLGs and LRX proteins sense RALF peptides with mechanistically distinct peptide binding modes. Despite the similar phenotypes induced by mutations in ANX1, BUPS2, LLG2, LLG3, RALF4/19, and pollen-expressed LRX proteins (2, 3, 5–7, 11), we could not observe any simultaneous interactions between $RALF4_{folded}$, LRX proteins, and LLGs or *Cr*RLK1Ls (*SI Appendix*, Figs. S14–S16). Thus, $RALF4_{folded}$ appears to interact in a mutually exclusive manner with either LRXs or LLGs.

We next characterized the LRX homodimer, which we find stabilized by a central disulfide bridge in our two complex structures (Figs. 2*A* and 4*A* and *SI Appendix*, Fig. S6). The disulfide

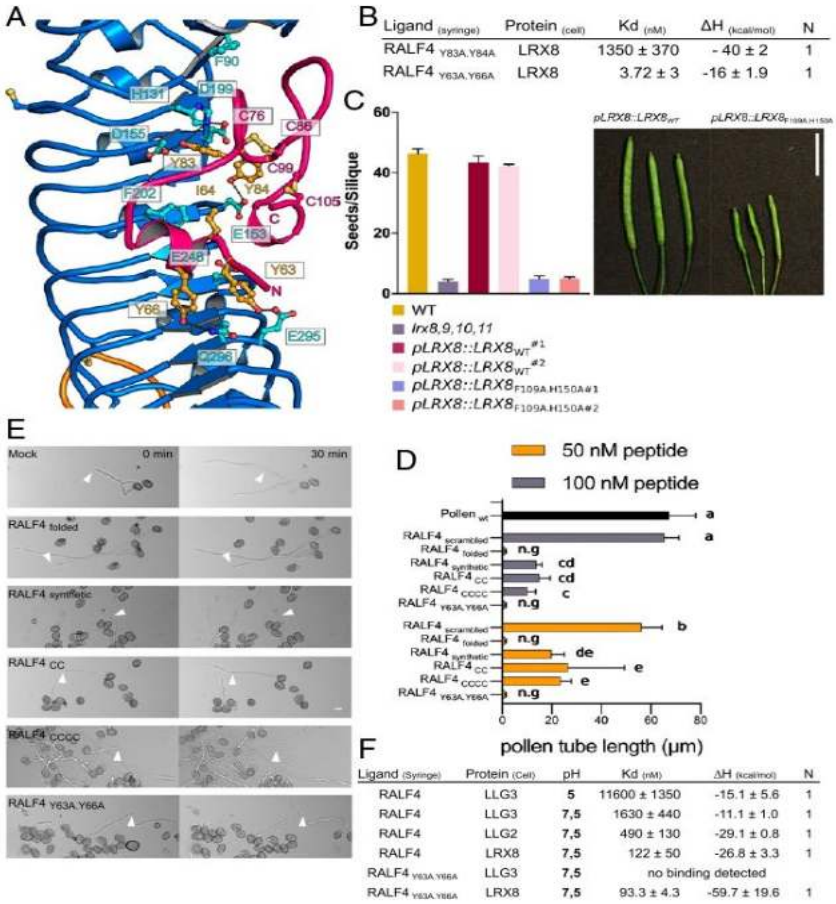

Fig. 3. LRX8 bioactivity depends on the interaction with folded RALFs. (*A*) Close-up view of the LRX2–RALF4 binding pocket. A large surface of the RALF4 peptide (in pink) directly interacts with the LRR core (in blue) of LRX2. Polar contacts of RALF4 with LRX2 are shown as dotted lines (in gray). The two disulfide bridges responsible for the folding of the peptide, C76–C86 and C99–C105, are depicted as sticks in light orange. (*B*) ITC table summaries of LRX8 vs. $RALF4_{Y83A.Y84A}$ and $RALF4_{Y63A.Y66A}$ mutants. Table summaries show the dissociation constant (K_d), binding stoichiometries (N), and thermodynamic parameters. The values indicated in the table are the mean ± SD of two or three independent experiments. (*C*) Complementation assay of *lrx8,9,10,11* with point mutated $LRX8_{F109A.H150A}$ driven by its endogenous promoter. (*C, Left*) Seeds per silique of WT, *lrx8,9,10,11*, $pLRX8::LRX8_{WT}$ lines 1 and 2, and $pLRX8::LRX8_{F109A.H150A}$ in the *lrx8,9,10,11* quadruple mutant background, for two independent lines. Data are means ± SEM of 10 siliques. For LRX8 mutant transgenic lines, 16 independent lines were analyzed. (*C, Right*) Silique images of the corresponding lines. (Scale bar, 10 mm.) (*D*) Growth rate of wild-type pollen tubes after the addition of $RALF4_{scrambled}$, $RALF4_{folded}$, $RALF4_{synthetic}$, $RALF4_{CC}$, $RALF4_{CCCC}$, and $RALF4_{Y63A.Y66A}$ peptides at different concentrations after 30 min. Data were analyzed by one-way ANOVA followed by Tukey's test as post hoc, considering $P \leq 0.05$ as significantly different; data shown are mean ± SEM of three biological replicates, $n = 28$ each. Same letters represent samples that are not different between each other; n.g, no growth after peptide addition. (*E*) Effect of RALF4 peptides on wild-type pollen tubes growing in semisolid medium at two time points after adding them to a concentration of 50 nM. Arrowheads indicate the position of the tip of selected pollen tubes at time point 0 min. (Scale bar, 10 µm.) (*F*) Binding matrix of $RALF4_{folded}$ and $RALF4_{Y63A.Y66A}$ peptides vs. LRX8 and LLG2/3 membrane proteins in acidic and alkaline conditions. ITC table summary with dissociation constants (K_d), binding stoichiometries (N), and thermodynamic parameters (ΔH).

bond contributes to a dimer interface formed by highly conserved hydrophobic and polar amino acids (642-Å^2 buried surface area) (Fig. 4 *A* and *B* and *SI Appendix*, Figs. S6 and S7 and Table S2). We probed the LRX8 dimer interface by mutational analysis: LRX8 still behaves as a dimer in solution when the disulfide bond was disrupted by mutating Cys157 ($Cys138^{LRX2}$) to Ala, suggesting that the intermolecular disulfide bond is not essential for the structural integrity of the LRX dimer. Simultaneous mutation of Tyr87 ($Phe68^{LRX2}$) to Ala and Ala133 ($Ala114^{LRX2}$) to Phe resulted in a monomer–dimer equilibrium, which we could quantitatively shift to a LRX8 monomer by additionally introducing the Cys157Ala mutation (Fig. 4 *C* and *D* and *SI Appendix*, Fig. S19). Both dimeric and monomeric LRX8 forms retain the capacity to bind RALF4, with the monomer binding the folded peptide with wild-type affinity (~2.5 nM) (Fig. 4*E* and *SI Appendix*, Fig. S19). Crystallographic analysis of the $LRX8_{monomer}$–$RALF4_{folded}$ complex yielded a 2.3-Å resolution structure of the complex with excellent stereochemistry (*SI Appendix*, Table S1). In the $LRX8_{monomer}$ complex, $RALF4_{folded}$ binds to the LRX binding surface in a conformation similar to the wild-type $LRX8_{dimer}$ (r.m.s.d. is ~0.65 Å comparing 327 residues of corresponding Cα atoms) (*SI Appendix*, Fig. S20). Thus, our biochemical and structural data reveal that mutations affecting the dimer interface of LRX8 specifically alter the oligomeric state of the cell-wall protein, while leaving its interaction with RALF peptides intact.

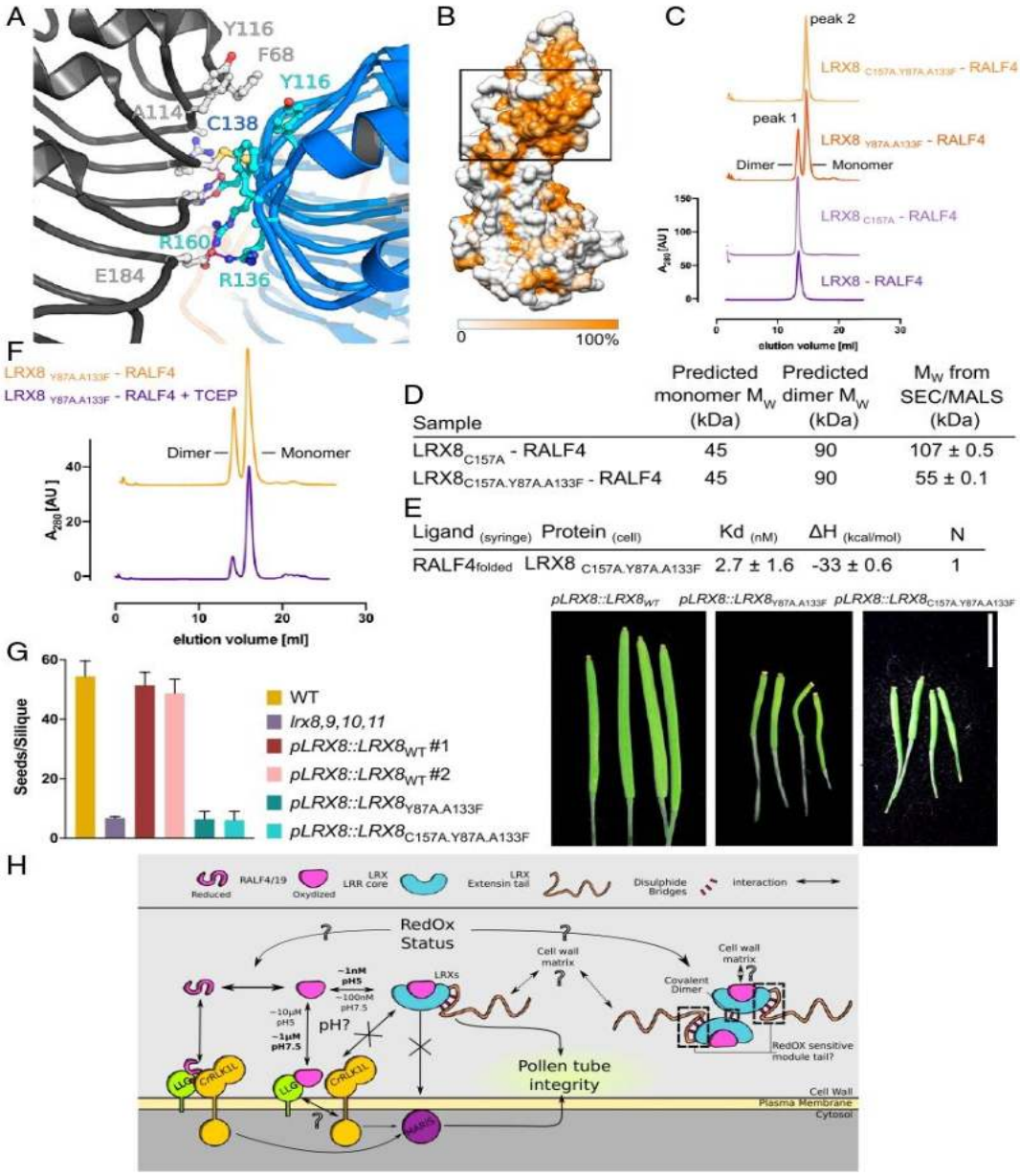

Fig. 4. LRX8 functional mechanism requires homodimerization to control pollen tube growth. (*A*) Close-up view of the dimer interface in LRX2. Details of the interactions between the two protomers (depicted in blue and gray) are highlighted. The Cys (C138) mediating the disulfide bond formation is depicted in yellow. The ionic and hydrogen bonds are shown as dotted lines (in magenta). (*B*) Side surface representation of LRX2 colored according to LRX family sequence conservation. The black rectangle depicts the LRX dimer interface. (*C*) The dimer interface of LRX proteins is stabilized by a central disulfide bridge. SEC runs of wild-type LRX8–RALF4, $LRX8_{C157A}$–RALF4, $LRX8_{Y87A.A133F}$–RALF4, and $LRX8_{C157A.Y87A.A133F}$–RALF4. Peaks 1 and 2 correspond to the dimeric and monomeric forms of LRX8, respectively. (*D*) SEC–MALS summary table for the $LRX8_{C157A}$–RALF4 and $LRX8_{C157A.Y87A.A133F}$–RALF4 complexes in solution at pH 5.0, along with the predicted molecular weights. The values indicated in the table are the mean ± SD of two independent measurements. (*E*) ITC of $LRX8_{C157A.Y87A.A133F}$ vs. $RALF4_{folded}$. The table summarizes the biophysical values obtained. K_d, (dissociation constant), binding stoichiometries (N), and thermodynamic parameters (ΔH). (*F*) Shift of the monomer–dimer equilibrium under reducing conditions in solution. $LRX8_{Y87A.A133F}$–RALF4 run in the absence (orange) and presence (purple) of TCEP. (*G*) Complementation assays of *lrx8,9,10,11* with LRX8 oligomeric mutants. (*G*, *Left*) Seeds per silique of WT, *lrx8,9,10,11*, *pLRX8::LRX8*$_{WT}$ lines 1 and 2, *pLRX8::LRX8*$_{Y87A.A133F}$ and *pLRX8*::$LRX8_{C157A.Y87A.A133F}$ in the *lrx8,9,10,11* quadruple mutant background. Data are means ± SEM of 10 siliques. For LRX8 mutant transgenic lines, 16 independent lines were analyzed. (Scale bar, 10 μm.) (*G*, *Right*) Siliques images of the corresponding lines. (*H*) Working model and open questions about RALF-mediated autocrine signaling during pollen tube growth. Physical interactions are depicted by double arrows and genetic relationships by single arrows. Straight lines indicate what is known, and dotted lines indicate speculative relationships. Affinity ranges are marked next to the interaction arrows. Legends of the different components are shown on *Top*.

To assess the role of the dimer interface and its central cysteine in a changing redox environment, we incubated purified LRX8 and LRX8–RALF4 complex with increasing concentrations of the reducing agent dithiothreitol (DTT) under denaturing conditions. In both cases, the dimer could be converted into monomers (*SI Appendix*, Fig. S21). In addition, we could also quantitatively shift the oligomeric equilibrium of $LRX8_{Y87A.A133F}$ toward the monomeric species in the presence of a reducing agent in SEC experiments (Fig. 4*F*). Consistent with these observations, we could detect both oligomeric species of a myc-tagged $LRX8_{1–400}$, when transiently expressed in tobacco leaves, in the absence of DTT (*SI Appendix*, Fig. S21).

Next, we asked whether the oligomeric state of LRX proteins has functional relevance in planta. We transformed the quadruple *lrx8,9,10,11* mutant with monomeric LRX8 ($LRX8_{C157A.Y87A.A133F}$) and the monomer–dimer variant ($LRX8_{Y87A.A133F}$) under the control of the native *LRX8* promoter (*SI Appendix*, Fig. S12). Both LRX8 variants were secreted into the cell wall and we could detect expression of both mutants' proteins in pollen (*SI Appendix*, Figs. S12 and S13). Like the previously tested $LRX8_{F109A.H150A}$ mutant (Fig. 3*C*), these oligomeric variants failed to complement the sterility phenotype of the *lrx8,9,10,11* quadruple mutant (Fig. 4*G*), suggesting that both the RALF binding capacity and the dimeric state of LRX8 are required to facilitate the rapid growth of the pollen tube to the ovule.

Discussion

Our work reveals that RALF peptides can exist as small folded signaling proteins, placing them together with other cysteine-rich signaling peptides in plants, such as the LURE peptides controlling pollen tube guidance or the EPF peptides controlling stomatal patterning (29, 30). In the case of RALF peptides, the isolated protein may already be folded, as suggested by a recent NMR study (31), and is fully structured when bound with high affinity to LRX proteins (Fig. 2). It is of note that RALF4, when bound to LRX, adopts a defined conformation exposing a highly basic surface patch, which we speculate could mediate targeted interactions with other proteins or cell-wall components (*SI Appendix*, Fig. S8). Binding of RALFs to the LRR region could thus affect the overall conformation of the LRX extensin domain, which our structures reveal to be tightly linked to the LRR core. The identity of these interacting factors will be a key question to address in future studies.

Polarized tip growth of pollen tubes has been reported to be driven by waves of acidic pH and reactive oxygen species (ROS) production to allow for the proper cell-wall dynamics (26, 32–35). This correlates with our biochemical findings, where both parameters modulate RALF sensing by LRXs (Figs. 1 and 3) and the oligomeric state of LRX proteins (Fig. 4*H*). A putative redox-controlled oligomerization of LRX proteins would add an additional layer to the modulation of RALF sensing and signaling. In this respect, it is noteworthy that cell-wall thioredoxins have been identified as putative LRX interactors (36).

Our and previous structural and biochemical data support two distinct targeting mechanism for RALF peptides toward the LRX and *Cr*RKL1L–LLGs signaling modules (9). We demonstrate that these binding events are mutually exclusive in the context of pollen tube growth and, consequently, we did not observe formation of tertiary complexes containing RALFs, LRXs, LLGs, or *Cr*RLK1Ls proteins. This suggests that RALF peptides trigger two parallel, converging but mechanistically distinct signaling pathways. On the one hand, RALF4/19 peptides can signal via the *Cr*RLK1Ls–LLGs to control processes inside the pollen tube through the cytoplasmic receptor-like kinase MARIS (5, 37); on the other hand, RALF4/19 may signal to control processes outside the cell through their interaction with LRXs in the cell wall. This is consistent with the finding that, unlike mutants with reduced RALF4/19 activity (5), mutants lacking multiple pollen-expressed LRXs cannot be suppressed by dominant active MARIS (*SI Appendix*, Fig. S22) (38). That indicates that also based on genetic evidence, RALF4/19 peptides function in different but converging pathways to fine tune pollen tube integrity.

Our binding data between RALFs, LRXs, and LLGs, together with previous studies (20), suggest that this autocrine signaling cascade could be additionally regulated by pH fluctuations in the cell wall to modulate pollen tube growth (13, 21, 26, 27). Our in vitro data clearly suggest that LRX proteins represent high-affinity sensors for RALFs at acidic pH, while LLGs show a binding preference under neutral/alkaline conditions (Fig. 4*H*). Our structural, quantitative biochemical, and physiological experiments suggest that LRX proteins preferentially bind folded rather than linear RALF peptides. The N-terminal α-helix conserved among all RALF family members does not play a major role in LRX recognition but has previously been shown to be critical and sufficient for *Cr*RLK1Ls–LLGs complex formation (9). An attractive hypothesis would thus be that cell-wall pH and redox changes alter the conformations and oligomeric states of both RALF ligands and their sensors, allowing different signaling complexes to form (Fig. 4*H*). RALF peptides may exist in a fully folded oxidized state preferentially bound by LRX proteins. However, in response to a changing cell-wall environment, they may acquire a reduced linearized state preferentially bound by LLG-containing complexes (Fig. 4*H*). This point should be considered in future studies aimed at dissecting the contributions of LRXs and *Cr*RLK1Ls to the diverse RALF-mediated signaling processes in plants. The RALF signaling system emerges as a unique signaling cascade, in which one family of ligands is recognized by two structurally distinct receptor families, that are differentially modulated but together shape a core developmental process in plants.

Materials and Methods

Protein Expression and Purification. Codon-optimized synthetic genes for expression in *Spodoptera frugiperda* (Invitrogen GeneArt), coding for *Arabidopsis thaliana* LRX2 (residues 1 to 385; At1g62440), LRX8 (residues 33 to 400, 49 to 400, and 49 to 373; At3g19020), LRX11 (residues 45 to 415, 64 to 415, and 64 to 388; At4g33970); LLG2 (residues 24 to 135; At2g20700), LLG3 (residues 24 to 137; At4g28280), BUPS2 (residues 40 to 439; At2g21480) domains were cloned into a modified pFastBac (Geneva Biotech) vector, providing a TEV (tobacco etch virus protease) cleavable C-terminal StrepII-9xHis tag. LRX8 (49 to 400) fused to a noncleavable Avi-tag was also cloned into a modified pFastBac vector harboring the *Drosophila BiP* secretion signal peptide (39–41). *Spodoptera frugiperda* codon-optimized RALF4 (residues 58 to 110; At1g28270) and RALF19 (residues 58 to 110; At2g33775) mature peptide sequences were N-terminally fused to TRX A (Thioredoxin A) in a pFastBac vector driven by a 30 K signal peptide (42). For protein expression, *Trichoplusia ni* Tnao38 cells (43) were coinfected with a combination of LRX and RALF virus with a multiplicity of infection (MOI) of 3 and incubated for 1 d at 28 °C and 2 d at 22 °C at 110 rpm. The secreted complexes were purified from the supernatant by sequential Ni^{2+} (HisTrap excel; GE Healthcare; equilibrated in 25 mM KP_i pH 7.8, 500 mM NaCl) and StrepII (Strep-Tactin Superflow high capacity [IBA Lifesciences] equilibrated in 25 mM Tris pH 8.0, 250 mM NaCl, 1 mM EDTA) affinity chromatography. All proteins were incubated with TEV protease to remove the tags. Proteins were further purified by SEC on a Superdex 200 increase 10/300 GL column (GE Healthcare), equilibrated in 20 mM sodium citrate pH 5.0, 150 mM NaCl. For crystallization and biochemical experiments, proteins were concentrated using Amicon Ultra concentrators (Millipore, molecular weight cut-off 3,000 and 30,000). Proteins were analyzed for purity and structural integrity by sodium dodecyl sulfate– polyacrilamide gel electrophoresis and mass spectrometry. The BirA enzyme was cloned into a modified pETM11 vector providing an N-terminal 6xHis tag and a TEV site. The enzyme was purified from *Escherichia coli* by Ni^{2+} affinity chromatography.

Mass Spectrometry. For LC-MS/MS analysis of LRX8–RALF4, 5 μL of complex (1 mg/mL) was diluted in 20 μL of the following buffer: 50 mM ammonium bicarbonate, 10 mM TCEP (triscarboxyethylphosphine) and 40 mM chloroacetamide. Samples were incubated 45 min in the dark at room temperature (RT), and then digested with 0.1 μg of sequencing-grade trypsin or chymotrypsin

(Promega). Samples were incubated at 37 °C for 4 h, and digestion reaction was stopped with 2 μL of 10% formic acid. They were then diluted 10× with loading buffer (2% acetonitrile, 0.05% trifluoroacetic acid) and injected on a Fusion Tribrid orbitrap mass spectrometer (Thermo Fisher Scientific) interfaced to a Dionex RSLC 3000 nano-HPLC. Peptides were separated on a 65-min gradient from 4 to 76% acetonitrile in 0.1% formic acid at 0.25 μL/min on an in-home packed C18 column (75-μm internal diameter × 40 cm, 1.8 μm, Reprosil Pur, Dr. Maisch). Full MS survey scans were performed at 120,000 resolution. In data-dependent acquisition controlled by Xcalibur 4.1 software (Thermo Fisher), a top speed precursor selection strategy was applied to maximize acquisition of peptide tandem MS spectra with a maximum cycle time of 1.5 s. higher-energy collisional dissociation (HCD) (normalized collision energy: 32%) or electron-transfer/higher-energy collisional dissociation (supplemental HCD activation energy: 25%) fragmentation mode were used with a precursor isolation window of 1.6 *m/z*. MS/MS spectra were acquired at a 15,000 resolution, and peptides selected for MS/MS were excluded from further fragmentation during 60 s. For data analysis, tandem mass spectra were searched using PEAKS software (version 8.5, Bioinformatics Solutions Inc.) against a custom database containing common contaminants and the sequences of the proteins of interest. Mass tolerances used were 10 ppm for the precursors and 0.02 Da for collision-induced dissociation fragments. Activities of proteases considered were semitrypsin or semichymotrypsin (one specific cut) with two missed cleavages. Carbamidomethylation of cysteine was specified as a fixed modification. N-terminal acetylation of protein and oxidation of methionine were specified as variable modifications. PEAKS results were imported into the software Scaffold 4.8.5 (Proteome Software Inc.) for validation of MS/MS-based peptide (minimum 90% probability) and protein (min 95% probability) identifications, dataset alignment, as well as parsimony analysis to discriminate homologous hits.

For LC-MS/MS analysis of LRX11–RALF4, 10 μL of complex (10 mg/mL) was diluted in 20 μL of the following buffer: 8 M urea, 50 mM TEAB (triethylammonium bicarbonate), 5 mM TCEP (triscarboxyethylphosphine), and 20 mM chloroacetamide. After 1 h incubation at RT, the sample was then diluted adding 90 μL of 50 mM TEAB, split into two aliquots of 55 μL and digested with 0.2 μg of trypsin or chymotrypsin. Samples were incubated at 37 °C for 2.5 h, and digestion reaction was stopped with 1 μL of 10% formic acid and 200 μL of loading buffer. They were injected on a Fusion Tribrid orbitrap mass spectrometer interfaced to a Dionex RSLC 3000 nano-HPLC, as above. Full MS survey scans were performed at 120,000 resolution. In data-dependent acquisition controlled by Xcalibur 4.1 software, a top speed precursor selection strategy was applied to maximize acquisition of peptide tandem MS spectra with a maximum cycle time of 0.6 s. HCD (normalized collision energy: 32%) fragmentation mode was used with a precursor isolation window of 1.6 *m/z*. MS/MS spectra were acquired in the linear trap and peptides selected for MS/MS were excluded from further fragmentation during 60 s. For data analysis, tandem mass spectra were searched using Mascot (Matrix Science, version 2.6.2) against a custom database containing common contaminants and the sequences of the proteins of interest. Mass tolerances used were 10 ppm for the precursors and 0.5 Da for collision-induced dissociation fragments. Activities of proteases considered were semitrypsin (one specific cut) or chymotrypsin, with two or three missed cleavages, respectively. Carbamidomethylation of cysteine was specified as a fixed modification, and oxidation of methionine as variable modification. Mascot results were imported into the software Scaffold for validation of MS/MS-based peptide (minimum 95% probability) and protein (minimum 95% probability) identifications, dataset alignment, as well as parsimony analysis to discriminate homologous hits.

MALS. MALS was used to assess the monodispersity and molecular weight of the apo LRXs and in complex with RALF4. Samples containing 100 μg of protein were injected into a Superdex 200 increase 300/10 GL column (GE Healthcare) using an HPLC system (Ultimate 3000, Thermo Fisher Scientific) at a flow rate of 0.5 mL min^{-1}, coupled in-line to a multiangle light scattering device (miniDAWN TREOS, Wyatt). Static light scattering was recorded from three different scattering angles. The scatter data were analyzed by ASTRA software (version 6.1, Wyatt). Experiments were done in duplicate with SD indicated in the figures.

Protein Complex Dissociation. LRX–RALF complexes were obtained in vivo by coexpression in insect cells. The apo proteins were obtained by complex dissociation in vitro using a low pH buffer. After purification of the LRX–RALF complex (see above), the protein complex was incubated for 1 h at 4 °C in the following buffer: 20 mM citric acid pH 2, 150 mM NaCl. Next, the dissociated proteins were separated by gel filtration, using a Superdex 200 increase 10/300 GL column (GE Healthcare) equilibrated in the same buffer. Each protein was then collected separately and dialyzed against 20 mM citric acid pH 5, 150 mM NaCl. To test whether proteins were still folded and functional, proteins were again run in a Superdex 200 increase 10/300 GL column (GE Healthcare) in 20 mM citric acid pH 5, 150 mM NaCl. We also tested, for each batch of dissociated protein, that the complex would be fully reconstituted when mixing the proteins in equimolar proportions. Additionally, we tested the in vivo activity in pollen tube growth assays of the dissociated peptide (folded) versus a synthetic linear version of RALF4 of the same sequence.

ITC. Experiments were performed at 25 °C using a MicroCal PEAQ-ITC (Malvern Instruments) with a 200-μL standard cell and a 40-μL titration syringe. LRX8 protein and RALF peptides were gel filtrated into either pH 5 ITC buffer (20 mM sodium citrate pH 5.0, 150 mM NaCl) or pH 7.5 ITC buffer (20 mM Hepes pH 7.5, 150 mM NaCl). For the RALF vs. LRX interactions, a typical experiment consisted of injecting 1 μL of a 100-μM solution of the RALF peptides into 10 μM LRX8 (49 to 400) solution in the cell at 150-s intervals. The experiments using RALF, *Cr*RLK1Ls, and LLGs were typically performed with 10 μM protein in the cell and 100 μM ligand in the syringe, and an injection pattern of 2 μL. ITC data were corrected for the heat of dilution by subtracting the mixing enthalpies for titrant solution injections into protein-free ITC buffer. Experiments were done at least in duplicates and data were analyzed using the MicroCal PEAQ-ITC Analysis Software provided by the manufacturer. All ITC runs used for data analysis had an N ranging between 0.8 and 1.3. The N values were fitted to 1 in the analysis.

Protein Biotinylation. A total of 25 μM of LRX8 (49 to 400) were biotinylated with the biotin ligase BirA (2 μM) (40) for 1 h at 30 °C, in a volume of 200 μL. The buffer used in the reaction was: 25 mM Tris pH 8, 150 mM NaCl, 5 mM MgCl2, 2 mM 2-mercaptoethanol, 0.15 mM biotin, 2 mM ATP. Biotinylated proteins were purified by SEC in 20 mM Hepes pH 7.5, 150 mM NaCl.

GCI. GCI experiments were performed with the Creoptix WAVE system using 4 PCP WAVE chips (thin quasiplanar polycarboxylate surface [Creoptix]). Chips were first conditioned with borate buffer (100 mM sodium borate pH 9.0, 1 M NaCl [Xantec]). Then, the chips were activated with 1:1 mix of 400 mM *N*-(3-dimethylaminopropyl)-*N*′-ethylcarbodiimide hydrochloride and 100 mM *N*-hydroxysuccinimide (Xantec). Streptavidin (1.5 mg/mL [Sigma]) in 10 mM sodium acetate pH5 (Sigma) was immobilized on the chip surface until saturation was reached, followed by passivation of the surface with bovine serum albumin (BSA) (5 mg/mL [Sigma]) in 10 mM sodium acetate pH 5, and a final quenching step with 1 M ethanolamine pH8 (Xantec). Then, biotinylated LRX8 (ligand) (200 to 300 μg/mL) was captured on the streptavidin surface until the desired density was reached. Two different kinetic analyses were performed to measure the binding of $RALF4_{folded}$ (analyte) to LRX8: a regeneration-free kinetic and a normal kinetic. Both experiments were performed at 25 °C with a 1:2 dilution series from a maximum concentration of 10 nM $RALF4_{folded}$, in 20 mM citrate pH 5, 250 mM NaCl, 0.01% Tween-20, 0.1% BSA. Blank injections were used for double referencing and a dimethyl sulfoxide (DMSO) calibration curve for bulk correction. Analysis and correction of the obtained data were performed using the Creoptix WAVE control software (correction applied: X and Y offset; DMSO calibration; double referencing). A one-to-one binding model was used for both experiments.

Crystallization and Data Collection. Crystals of the $LRX2_{29–385}$–RALF4 and $LRX8_{33–400}$–RALF4 complexes developed at room temperature in hanging drops composed of 1.0 μL of protein solution (20 mg/mL) and 1.0 μL of the following crystallization buffers, respectively: 20% (wt/vol) polyethylene glycol (PEG) 3350, 0.1 M Bis-Tris pH 5 and 0.2 M sodium acetate and 17.5% (wt/vol) PEG 8000, 0.1 M Bis-Tris pH 7 and 0.2 M sodium citrate. Drops were suspended above 0.6 mL of crystallization buffer. For data collection, LRX2–RALF4 crystals were transferred into crystallization buffer supplemented with 15% (vol/vol) ethylene glycol and snap frozen in liquid nitrogen. In the case of the LRX8–RALF4 complex, crystals were snap frozen in the presence of 15% glycerol as cryoprotectant.

Crystals of the $LRX8_{C157A.Y87A.A133F}$ mutant in complex with RALF4, grew in 0.3 M ammonium sulfate and 20% (wt/vol) PEG 4000. Crystals of the monomer were cryoprotected using 15% (vol/vol) ethylene glycol and snap frozen in liquid nitrogen. The 3.2-Å, 3.9-Å, and 2.3-Å native datasets, respectively, were collected at beam-line PXIII of the Swiss Light Source. Data processing and scaling were done in XDS (version June 2017) (44).

Circular Dichroism. Near-UV spectra (250 to 400 nm) were acquired using a Chirascan V100 spectrophotometer (Applied Photophysics) equipped with a 150 W Xenon arc lamp, on a 6.5 μM (1 mg/mL) sample in a quartz cuvette of

1-cm light path (Hellma). Buffer and samples were measured 10 times each. Signal from the buffer was subtracted from the samples and values were then normalized to the absorbance at 278 nm (highest in all cases).

Structure Determination and Refinement. The structure of the LRX2–RALF4 complex (PDB ID: 6QXP) was determined by molecular replacement using the program PHASER, implemented in the Phenix MRage pipeline (45). Search models were selected using the program HHPRED (46) and tested iteratively in the MRage pipeline. A solution using a fragment of the LRR ectodomain of the plant immune receptor FLS2 (PDB ID: 4MNA) yielded a solution with eight molecules in the asymmetric unit. The search model, which showed 28% sequence identity with LRX2 target was further improved using the program CHAINSAW in CCP4 (47, 48). The final solution was used for noncrystallographic symmetry averaging and density modification in the program PHENIX.RESOLVE (49). The resulting map was readily interpretable and the LRX2–RALF4 complex structure was built and completed by iterative round of manual model building in COOT (50) and restrained TLS in phenix.refine. The structure of LRX8–RALF4 (PDB ID: 6QWN) was solved by molecular replacement in PHASER (51) and using the LRX2–RALF4 as search model. The structure of $LRX8_{C157A.Y87A.A133F}$–RALF4 (PBD ID: 6TME) was determined by molecular replacement in PHASER, using the LRX2–RALF4 complex as search model. The LRX8–RALF4 and $LRX8_{C157A.A133F.Y87A}$–RALF4 structures were also built and completed by iterative round of manual modeling in COOT and restrained refinement in phenix.refine. Inspection of the final models with phenix.molprobity (52) reveal good stereochemistry (*SI Appendix*, Table S1). Diagrams were prepared with PYMOL (https://pymol.org/2/) or CHIMERA (53). Structure-based sequence alignments include a secondary structure assignment calculated with the program DSSP (54). The two-dimensional (2D) ligand-interaction diagram was generated with LIGPLOT (55).

Transient Protein Expression in Tobacco Leaves. *Nicotinia benthamiana* plants were grown for 3 wk prior to agroinfiltration. Appropriate *Agrobacterium tumefaciens* cultures were grown in yeast extract broth media at 28 °C until reaching an optical density of 0.6. Cultures were centrifuged for 10 min at 4,000 rpm. Cells were resuspended in fresh infiltration media (50 mM MES, 2 mM NaH_2PO4, 0.5% [m/v] saccharose, 100 μM acetosyringone, pH 5.6) and left on the shaker for 2 h in the dark. For coinfiltration of two *Agrobacterium* strains, infiltration media with the appropriate *Agrobacterium* strains harboring the desired constructs were mixed in a 1:1 vol/vol ratio. Infiltration was performed with a syringe. Plants were grown for 2 more days prior to material collection. Leaves were cut and flash frozen in liquid nitrogen. For the plasmolysis experiments, an acetosyringone concentration of 500 μM was used, and plants were imaged 6 d after infiltration. Plants were then infiltrated with a 30% glycerol solution to induce plasmolysis and imaged right after. For LRX8-mCitrine WT and mutants, the excitation and emission wave lengths used were 514 nM and 525 to 550, respectively. For the plasma membrane marker Lti6-mCherry the excitation wavelength was 561 nm and the emission was between 595 and 645 nm. Leaves were imaged with a SP8 Leica confocal microscope. Images were adjusted using ImageJ.

In Vitro Redox Sensitivity Experiments. To determine the importance of disulfide bridge formation in the LRX homodimers, samples were incubated at 95 °C for 5 min in Laemmli buffers containing DTT 0, 1, 3, 5, or 20 mM, respectively. They were subsequently run on denaturing SDS gels for further size identification. In solution, reducing assays were performed by incubating the $LRX8_{Y87A.A133F}$ protein with and without 5 mM TCEP for 1 h at RT. Samples were then run by size-exclusion chromatography on a Superdex 200 increase 10/300 GL column (GE Healthcare), equilibrated in 20 mM sodium citrate pH 5.0, 150 mM NaCl, in the presence or absence of TCEP.

Protein Extraction, Coimmunoprecipitation, and Western Blot Analysis. Transiently expressed LRX8 and RALF4 proteins in tobacco were extracted as follow: 300 mg of plant material were crushed in liquid nitrogen and resuspended in 600 μL of extraction buffer (150 mM Tris pH 7.5; 150 mM NaCl; 10% [vol/vol] glycerol; 10 mM EDTA, 0.5% IGEPAL, cOmplete protease inhibitor [Roche]). Samples were centrifuged at 15,000 rpm for 20 min, and the supernatant was then centrifugated twice more to discard residual pellet debris. A total of 50 μL of input sample was kept at this stage, the rest was incubated for 1 h at 4 °C with anti-myc or anti-HA magnetic beads (μMACS, Milteny Biotech). Immunoprecipitation was performed according to manufacturer's specifications, using the extraction buffer for column washes. Standard Laemmli buffer (56) was added to the input and immunoprecipitated samples prior to gel loading. Finally, Western blot analysis was performed with horseradish peroxidase-coupled anti-myc and anti-HA antibodies (MACS, Milteny Biotech) at 1:2,000 dilution. Detection was performed using WesternBright Sirius (Advansta). Images were taken with a LAS500 BlotImager. For Western blot detection of expressed proteins in insect cells (supernatant and pellet fractions) we used anti-His HRP conjugated from Roche in a 1:2,000 dilution.

Pollen Germination In Vitro Assays. Open flowers were incubated at 22 °C for 30 min in moist incubation boxes. Then, pollen was bound to xilane-coated slides containing germination medium (0.01% boric acid [wt/vol], 5 mM CaCl 2, 5 mM KCl, 1 mM $MgSO_4$, 10% sucrose, pH 7.5). Pollen grains were preincubated in moist incubation boxes for 30 to 45 min at 30 °C and then transferred to 22 °C from 30 min to 2 h as indicated. After 2 h of in vitro pollen germination, peptides were added to pollen germination medium to a concentration of 50 nM and 100 nM. The effect on pollen tube growth was imaged using a Leica DM 6000 microscope and analyzed using the ImageJ 1.40g software (http://rsb.info.nih.gov/ij). $RALF4_{synthetic}$, $RALF4_{scrambled}$, $RALF4_{C86A.C105A}$, and $RALF4_{C76A.C86A.C99A.C105A}$ synthetic peptides were obtained from PHTD Peptides Industrial Co, Ltd. and Genscript (see sequences below). The rest of the peptides were expressed and produced in insect cells complexed with LRX8 and dissociated as indicated above.

Sequences of the Synthetic Peptides. Sequence of $RALF4_{synthetic}$: RRYIGYDALKKNNVPCSRRGRSYYDCKKRRRNNPYRRGCSAITHCYRYAR

Sequence of $RALF4_{scrambled}$: PTYNSCRRKCKRDRGYAARRYKRYRYVNADIKRNHSGYPCRICSRLYGRN

Sequence of $RALF4_{C86A.C105A}$ ($RALF4_{CC}$): RRYIGYDALKKNNVPCSRRGRSYYDAKKRRRNNPYRRGCSAITHAYRYAR

Sequence of $RALF4_{C76A.C86A.C99A.C105A}$ ($RALF4_{CCCC}$): RRYIGYDALKKNNVPASRRGRSYYDAKKRRRNNPYRRGASAITHAYRYAR

Sequence of $RALF4_{Y83A.Y84A}$: RRYIGYDALKKNNVPCSRRGRSAADCKKRRRNNPYRRGCSAITHCYRYAR.

Generation of Transgenic Lines. All transgenic lines were generated using the floral dip method (57) with the *A. tumefaciens* strain GV3101. The construct pLAT52:MRIR240C-YFP, described previously (37), was used for *A. thaliana* transformation. The construct expressions in pollen tubes were checked and imaged using a Leica DM 6000 microscope. Amplification of LRX8 full-length from transgenic lines was performed using the following primers: Fw-5′: ATG ACC CGA AGA ACA ATG GAG, Rev-5′: ATG GTG TCT CAG GCT TTG GAC TAG. To detect the expression of LRX8-myc mutants, Western blot analysis was performed with horseradish peroxidase-coupled anti-myc (MACS, Milteny Biotech) at 1:2,000 dilution. Seed per silique phenotypes were checked in T1 plants.

Data and Materials Availability. All data are available in the main text or in *SI Appendix, Supplementary Materials*.

ACKNOWLEDGMENTS. We thank V. Olieric for providing beam time and the staff at beam line PXIII of the Swiss Light Source, Villigen, for technical assistance during data collection. We also thank Fabio Spiga and Rony Nehme from Creoptix (Switzerland) for technical assistance when performing and analyzing the GCI experiments. We thank Cyril Lipp (University of Zurich) for help with plant care. Funding: Supported by the University of Lausanne, the University of Zurich, European Research Council grant agreement no. 716358 (J.S.), Swiss National Science Foundation grants 31003A_173101 (J.S.) and CR3213_156724 (U.G.), the Programme Fondation Philanthropique Famille Sandoz (J.S.), and European Molecular Biology Organization long-term fellowship 1004-2017 (S.M.).

1. A. Boisson-Dernier, S. A. Kessler, U. Grossniklaus, The walls have ears: The role of plant CrRLK1Ls in sensing and transducing extracellular signals. *J. Exp. Bot.* **62**, 1581–1591 (2011).
2. Z. Ge *et al.*, LLG2/3 are co-receptors in BUPS/ANX-RALF signaling to regulate *Arabidopsis* pollen tube integrity. *Curr. Biol.* **29**, 3256–3265.e5 (2019).
3. Z. Ge *et al.*, *Arabidopsis* pollen tube integrity and sperm release are regulated by RALF-mediated signaling. *Science* **358**, 1596–1600 (2017).
4. S. Moussu, S. Augustin, A.-O. Roman, C. Broyart, J. Santiago, Crystal structures of two tandem malectin-like receptor kinases involved in plant reproduction. *Acta Crystallogr. D Struct. Biol.* **74**, 671–680 (2018).
5. M. A. Mecchia *et al.*, RALF4/19 peptides interact with LRX proteins to control pollen tube growth in *Arabidopsis*. *Science* **358**, 1600–1603 (2017).
6. T. N. Fabrice *et al.*, LRX proteins play a crucial role in pollen grain and pollen tube cell wall development. *Plant Physiol.* **176**, 1981–1992 (2018).

7. H. Feng *et al.*, LORELEI-LIKE GPI-ANCHORED PROTEINS 2/3 regulate pollen tube growth as chaperones and coreceptors for ANXUR/BUPS receptor kinases in Arabidopsis. *Mol. Plant* **12**, 1612–1623 (2019).
8. J.-M. Escobar-Restrepo *et al.*, The FERONIA receptor-like kinase mediates male-female interactions during pollen tube reception. *Science* **317**, 656–660 (2007).
9. Y. Xiao *et al.*, Mechanisms of RALF peptide perception by a heterotypic receptor complex. *Nature* **572**, 270–274 (2019).
10. L. Campbell, S. R. Turner, A comprehensive analysis of RALF proteins in green plants suggests there are two distinct functional groups. *Front. Plant Sci.* **8**, 37 (2017).
11. A. Boisson-Dernier *et al.*, Disruption of the pollen-expressed FERONIA homologs ANXUR1 and ANXUR2 triggers pollen tube discharge. *Development* **136**, 3279–3288 (2009).
12. S. Miyazaki *et al.*, ANXUR1 and 2, sister genes to FERONIA/SIRENE, are male factors for coordinated fertilization. *Curr. Biol.* **19**, 1327–1331 (2009).
13. E. Barbez, K. Dünser, A. Gaidora, T. Lendl, W. Busch, Auxin steers root cell expansion via apoplastic pH regulation in *Arabidopsis thaliana*. *Proc. Natl. Acad. Sci. U.S.A.* **114**, E4884–E4893 (2017).
14. K. S. K. Gjetting, C. K. Ytting, A. Schulz, A. T. Fuglsang, Live imaging of intra- and extracellular pH in plants using pHusion, a novel genetically encoded biosensor. *J. Exp. Bot.* **63**, 3207–3218 (2012).
15. P. Kozma, A. Hamori, K. Cottier, S. Kurunczi, R. Horvath, Grating coupled interferometry for optical sensing. *Appl. Phys. B* **97**, 5–8 (2009).
16. L. Holm, C. Sander, Dali: A network tool for protein structure comparison. *Trends Biochem. Sci.* **20**, 478–480 (1995).
17. A. Morato do Canto *et al.*, Biological activity of nine recombinant AtRALF peptides: Implications for their perception and function in Arabidopsis. *Plant Physiol. Biochem.* **75**, 45–54 (2014).
18. K. Hématy *et al.*, A receptor-like kinase mediates the response of Arabidopsis cells to the inhibition of cellulose synthesis. *Curr. Biol.* **17**, 922–931 (2007).
19. M. Haruta, G. Sabat, K. Stecker, B. B. Minkoff, M. R. Sussman, A peptide hormone and its receptor protein kinase regulate plant cell expansion. *Science* **343**, 408–411 (2014).
20. M. Stegmann *et al.*, The receptor kinase FER is a RALF-regulated scaffold controlling plant immune signaling. *Science* **355**, 287–289 (2017).
21. M. Gonneau *et al.*, Receptor Kinase THESEUS1 is a rapid alkalinization factor 34 receptor in *Arabidopsis*. *Curr. Biol.* **28**, 2452–2458.e4 (2018).
22. X. Liu *et al.*, The role of LORELEI in pollen tube reception at the interface of the synergid cell and pollen tube requires the modified eight-cysteine motif and the receptor-like kinase FERONIA. *Plant Cell* **28**, 1035–1052 (2016).
23. A. Capron *et al.*, Maternal control of male-gamete delivery in *Arabidopsis* involves a putative GPI-anchored protein encoded by the LORELEI gene. *Plant Cell* **20**, 3038–3049 (2008).
24. C. Li *et al.*, Glycosylphosphatidylinositol-anchored proteins as chaperones and co-receptors for FERONIA receptor kinase signaling in *Arabidopsis*. *eLife* **4**, e06587 (2015).
25. G. Pearce, Y. Yamaguchi, G. Munske, C. A. Ryan, Structure-activity studies of RALF, rapid alkalinization factor, reveal an essential–YISY–motif. *Peptides* **31**, 1973–1977 (2010).
26. J. A. Feijó, J. Sainhas, G. R. Hackett, J. G. Kunkel, P. K. Hepler, Growing pollen tubes possess a constitutive alkaline band in the clear zone and a growth-dependent acidic tip. *J. Cell Biol.* **144**, 483–496 (1999).
27. M. A. Messerli, G. Danuser, K. R. Robinson, Pulsatile influxes of H+, K+ and Ca2+ lag growth pulses of *Lilium longiflorum* pollen tubes. *J. Cell Sci.* **112**, 1497–1509 (1999).
28. G. Pearce, D. S. Moura, J. Stratmann, C. A. Ryan, Jr, RALF, a 5-kDa ubiquitous polypeptide in plants, arrests root growth and development. *Proc. Natl. Acad. Sci. U.S.A.* **98**, 12843–12847 (2001).
29. G. Lin *et al.*, A receptor-like protein acts as a specificity switch for the regulation of stomatal development. *Genes Dev.* **31**, 927–938 (2017).
30. X. Zhang *et al.*, Structural basis for receptor recognition of pollen tube attraction peptides. *Nat. Commun.* **8**, 1331 (2017).
31. R. O. Frederick *et al.*, Function and solution structure of the *Arabidopsis thaliana* RALF8 peptide. *Protein Sci.* **28**, 1115–1126 (2019).
32. G. B. Monshausen, T. N. Bibikova, M. A. Messerli, C. Shi, S. Gilroy, Oscillations in extracellular pH and reactive oxygen species modulate tip growth of *Arabidopsis* root hairs. *Proc. Natl. Acad. Sci. U.S.A.* **104**, 20996–21001 (2007).
33. A. Boisson-Dernier *et al.*, ANXUR receptor-like kinases coordinate cell wall integrity with growth at the pollen tube tip via NADPH oxidases. *PLoS Biol.* **11**, e1001719 (2013).
34. H. Kaya *et al.*, Ca2+-activated reactive oxygen species production by *Arabidopsis* RbohH and RbohJ is essential for proper pollen tube tip growth. *Plant Cell* **26**, 1069–1080 (2014).
35. M. Potocký, M. A. Jones, R. Bezvoda, N. Smirnoff, V. Zárský, Reactive oxygen species produced by NADPH oxidase are involved in pollen tube growth. *New Phytol.* **174**, 742–751 (2007).
36. C. Zhao *et al.*, Leucine-rich repeat extensin proteins regulate plant salt tolerance in *Arabidopsis*. *Proc. Natl. Acad. Sci. U.S.A.* **115**, 13123–13128 (2018).
37. A. Boisson-Dernier, C. M. Franck, D. S. Lituiev, U. Grossniklaus, Receptor-like cytoplasmic kinase MARIS functions downstream of *Cr*RLK1L-dependent signaling during tip growth. *Proc. Natl. Acad. Sci. U.S.A.* **112**, 12211–12216 (2015).
38. C. M. Franck *et al.*, The protein phosphatases ATUNIS1 and ATUNIS2 regulate cell wall integrity in tip-growing cells. *Plant Cell* **30**, 1906–1923 (2018).
39. M. G. Cull, P. J. Schatz, Biotinylation of proteins in vivo and in vitro using small peptide tags. *Meth. Enzymol.* **326**, 430–440 (2000).
40. M. Fairhead, M. Howarth, Site-specific biotinylation of purified proteins using BirA. *Methods Mol. Biol.* **1266**, 171–184 (2015).
41. E. Smakowska-Luzan *et al.*, An extracellular network of *Arabidopsis* leucine-rich repeat receptor kinases. *Nature* **553**, 342–346 (2018).
42. M. Futatsumori-Sugai, K. Tsumoto, Signal peptide design for improving recombinant protein secretion in the baculovirus expression vector system. *Biochem. Biophys. Res. Comm.* **391**, 931–935 (2010).
43. Y. Hashimoto, S. Zhang, S. Zhang, Y.-R. Chen, G. W. Blissard, Correction: BTI-Tnao38, a new cell line derived from Trichoplusia ni, is permissive for AcMNPV infection and produces high levels of recombinant proteins. *BMC Biotechnol.* **12**, 12 (2012).
44. W. Kabsch, Integration, scaling, space-group assignment and post-refinement. *Acta Crystallogr. D Biol. Crystallogr.* **66**, 133–144 (2010).
45. G. Bunkóczi *et al.*, Phaser MRage: Automated molecular replacement. *Acta Crystallogr. D Biol. Crystallogr.* **69**, 2276–2286 (2013).
46. J. Söding, A. Biegert, A. N. Lupas, The HHpred interactive server for protein homology detection and structure prediction. *Nucleic Acids Res.* **33**, W244–W248 (2005).
47. N. Stein, CHAINSAW: A program for mutating pdb files used as templates in molecular replacement. *J. Appl. Cryst.* **41**, 641–643 (2008).
48. R. Schwarzenbacher, A. Godzik, S. K. Grzechnik, L. Jaroszewski, The importance of alignment accuracy for molecular replacement. *Acta Crystallogr. D Biol. Crystallogr.* **60**, 1229–1236 (2004).
49. P. D. Adams, *et al.*, PHENIX: A comprehensive Python-based system for macromolecular structure solution. *Acta Cryst. D Biol. Crystallogr.* **66**, 213–221 (2010).
50. P. Emsley, K. Cowtan, Coot: Model-building tools for molecular graphics. *Acta Crystallogr. D Biol. Crystallogr.* **60**, 2126–2132 (2004).
51. A. J. McCoy *et al.*, Phaser crystallographic software. *J. Appl. Crystallogr.* **40**, 658–674 (2007).
52. V. B. Chen *et al.*, MolProbity: All-atom structure validation for macromolecular crystallography. *Acta Crystallogr. D Biol. Crystallogr.* **66**, 12–21 (2010).
53. E. F. Pettersen *et al.*, UCSF Chimera: A visualization system for exploratory research and analysis. *J. Comput. Chem.* **25**, 1605–1612 (2004).
54. W. G. Touw *et al.*, A series of PDB-related databanks for everyday needs. *Nucleic Acids Res.* **43**, D364–D368 (2015).
55. A. C. Wallace, R. A. Laskowski, J. M. Thornton, LIGPLOT: A program to generate schematic diagrams of protein-ligand interactions. *Protein Eng. Des. Sel.* **8**, 127–134 (1995).
56. U. K. Laemmli, Cleavage of structural proteins during the assembly of the head of bacteriophage T4. *Nature* **227**, 680–685 (1970).
57. S. J. Clough, A. F. Bent, Floral dip: A simplified method for Agrobacterium-mediated transformation of *Arabidopsis thaliana*. *Plant J.* **16**, 735–743 (1998).

4 Chapter 4 - The acid growth theory still revisited

4.1 Introduction

The AGT states that the plant hormone auxin activates plasma-bound proton pumps (e.g.,H^+-ATPases), leading to apoplastic acidification. The reduced pH increases the efficiency of cell wall loosening agents (e.g. expansin), which reduces the cell wall stiffness, resulting in turgor-driven cell expansion (Hager et al., *1971*; Rayle and Cleland, *1977*, *1970*, *1992*). As previously explained, in contrast to the situation in the shoot where the acid growth theory is well documented and supported by the literature (Spartz et al., *2014*; Takahashi et al., *2012*), its applicability to roots is still under debate due to the controversial results observed in previous publications (Arsuffi and Braybrook, *2017*; Evans et al., *1980*; Lüthen and Böttger, *1993*)(Section 1.1.3). Indeed, with experiments using the *Bdtar2l* mutant of *Brachypodium*, which expresses higher levels of auxin and has larger root cells as a consequence, Pacheco-Villalobos et al. demonstrated that the strong root elongation phenotype of this line cannot be associated with cell wall acidification driven by proton pumps. More specifically, focusing on the first centimetre of the root tip, they highlighted an overall root alkalisation in the mutant with no significant difference in the proton pump gene expression level when compared to the wild type (WT). Taken together, these results are in direct opposition to the AGT (Pacheco-Villalobos et al., *2016*). For *Arabidopsis*, however, Barbez et al. could validate, in 2017, the direct link between auxin and pH acidification in the roots by the use of a novel fluorescent molecular marker for subcellular monitoring of the apoplastic pH distribution, the 8-hydroxypyrene-1,3,6-trisulfonic acid trisodium salt (HPTS) (Barbez et al., *2017*). Remarkably, they added an additional level of precision in their study by performing a deeper independent analysis focusing on different root zones, which were known to have a different gene expression profile (Birnbaum et al., *2003*). More concretely, three main spatial phases were defined according to the developmental stages of root cells (Fig. 4.1 A). The division zone (DZ), which includes the meristem, is the first zone from the root tip and as its name indicates, it is were cells divide and undergo physiological changes to prepare for fast elongation, which will occur in the elongation zone (EZ). In this area, the cell length quadruples in only a few hours (Verbelen et al., *2006*). The EZ is followed by the maturation zone (MZ), also known as differentiation zone, where the cells progressively stop their elongation and start producing root hairs. Thus, by this approach, Barbez et al. could also show that in *Arabidopsis* the pH changed according to the different root zones. Indeed they highlighted that pH was more acidic during cellular elongation in the EZ, but increased

when the root cells reached their final length in the differentiation zone (Barbez et al., 2017). These observations raise the question as to whether the discrepancies in the AGT could originate either from species-specific differences or from differences in spatial and temporal resolution.

Therefore, in order to comprehensively validate in a coherent experimental system to what degree the AGT can explain cell elongation in the root, we focused on the different growth processes of root cells in the monocotyledonous *Brachypodium*, comparing WT with the *Bdtar2l* mutant. As outlined before (Section 1.3), this mutant provides a suitable system to study the AGT as it has an allelic mutation in the auxin biosynthetic gene *BdTAR2L*, which leads to higher levels of auxin in roots and shows longer roots cells as a consequence. Interestingly, this line, also generates longer but overall thinner root cells than the WT and produces shorter and less abundant root hairs when mature. As a result, *Bdtar2l* also exhibits a reduced root diameter (Pacheco-Villalobos et al., 2013). To confirm the hypothesis that a high spacial resolution is an essential criterion for the validation of the AGT, we decided to perform pH measurements using the segmentation approach described in Barbez and colleagues (Barbez et al., 2017) (Fig. 4.1 B). Following this system, we could show that the zone differentiation based on the cell physiological state, is a key parameter to explain the AGT in *Brachypodium* roots. Interestingly, the preliminary results using the HPTS molecular marker showed higher acidification levels in the EZ of *Bdtar2l* which together with the auxin over-accumulation, supports this part of the AGT, while being in direct opposition with what it was shown by Pacheco-Villalobos et al. (Pacheco-Villalobos et al., 2016). However, it is important to remind that their results were obtained when measuring the first centimetre of the root in its totality. In comparison, in our approach, the EZ has been characterised within the 2 first millimetres, and thus, in the absence of root hairs.

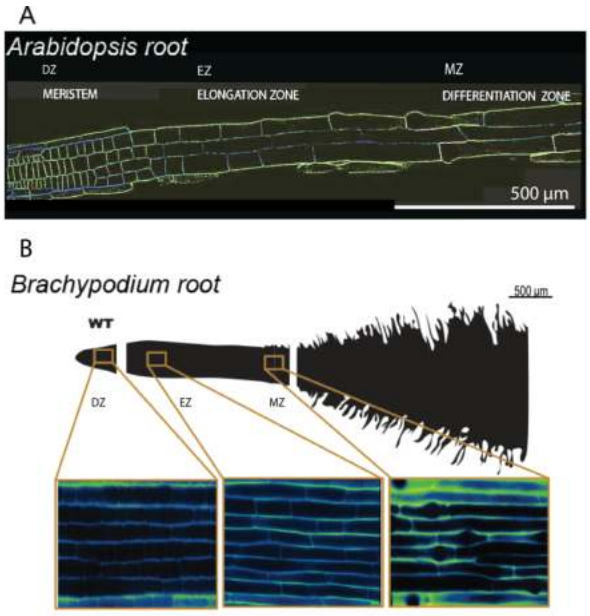

Fig. 4.1: Schematic representation of the different root zones under HPTS fluorescent pH indicator. *(A) Arabidopsis's different root zones' visualisation using the HPTS fluorescent pH dye. Adapted from (Barbez et al., 2017) (B) Brachypodium's different root zones' schematic characterisation. Division Zone (DZ), Elongation Zone (EZ) and Maturation Zone (MZ).*

On the other hand, the study of the AGT requires correlation between biochemical factors, e.g. pH and auxin responses, with physical properties, e.g cell wall stiffness/elasticity. As explained and according to the theory, an increase of the apoplast acidification leads to the cell wall loosening, which should reduce the cell wall stiffness, as a consequence, to allow the cell expansion driven by the turgor pressure. Thus, in order to gain more insight into the function of auxin in *Brachypodium* and to better understand how it affects cell wall stiffness, we combined genetic, biochemical and mechanical experiments in our study. The mechanical properties at the multicellular level of *Brachypodium* roots were extracted both using an extensometer and through micro-indentation experiments performed with the CFM (See Section 1.4). Importantly, the stiffness values obtained from CFM measurements do not only reflect the elastic properties of the cell wall but also the turgor pressure (Smith et al., *1998*; Wang et al., *2004*), the cell and the indenter geometry (Bolduc et al., *2006*), and the pre-indentation mechanical stresses (Zamir and Taber, *2004*). For this reason, we will refer to the measured stiffness as 'apparent stiffness' (Zamir and Taber, *2004*). To facilitate seed germination, long-term fluorescence imaging and indentation measurements, a microfluidic lab-on-a-chip device (LOC) was developed and integrated with the CFM. Thus, the causal relation

of the different mechanical analysis performed by the extensometer and the CFM, together with the auxin activity and the cell wall pH measured with the help of the LOC, have been analysed and are essential to understand the AGT. According to our preliminary results, we could show that the *Bdtar2l* mutant's EZ, known to express more auxin (Pacheco-Villalobos et al., *2013*), has a lower pH and exhibits smaller apparent stiffness than the WT. These results defend that higher auxin levels will increase the cell wall loosening due to an increase of cell wall acidification, agreeing therefore with the AGT.

In addition, our preliminary results suggested that the AGT is supported more specifically in the EZ where the cells are predisposed to elongate, and not in the MZ where they get mature. The apparent stiffness in the MZ was unfortunately not accurately measurable by the CFM due to an enormous number of root hairs in the WT. In order to correct these artefactual results, we used a mathematical model based on the finite element method (FEM) and derived from our extensometer results, to better characterise the mechanical parameters that cannot be visualised with the currently used techniques. FEMs are used to extract material properties in both engineering and biology, such as shear stress, which cannot be measured physically, and have already been shown to be useful in cell wall-membrane structure analyses (Moore et al., *1969*). Indeed, Vogler and colleagues demonstrated that FEM-based models allowed to estimate the elastic modulus of the cell wall as well as the turgor pressure of growing pollen tubes (Vogler et al., *2013*). Thus, in this chapter, we have also used this numerical method to analyse the different stresses that the *Brachypodium* roots are able to withstand when stretched by the extensometer. Despite having thinner roots, we realised that the MZ of the *Bdtar2l* mutant can tolerate more shear stresses while showing less elasticity than the WT.

As all the experiments performed on the EZ of *Brachypodium* roots support the AGT while the analysis performed on the MZ does not, we consider it important to clearly identify the different root zones along the longitudinal root axis. This, together with the development of adapted mechanophysical and mathematical methods, is the key to the proper assessment of the AGT in this specific tissue.

4.2 Material and Methods

Cellular Force Microscopy on Roots

For the purpose of this experiment, the CFM was integrated with an inverted optical microscope allowing fluorescence imaging of intracellular reporters while

providing high spatial precision and force resolution. The system offers a sub-microNewton force sensing, with a precise position control (±2 nm resolution) and a large travel range (135 mm×85 mm). The ability to measure small displacements during the micro-indentations and still be able to scan along the entire specimen is especially crucial when measuring centimetre long roots. Forces were measured using a dual-axis micromechanical systems (MEMS)-based capacitive force sensor with a flat probe (50×50 μm) and a force range of ±1500 μN (FT-S10000; FemtoTools AG). The force sensors were mounted on an xyz positioner (SLC-2475-S; Smar-Act) for rough positioning prior to the experiment. Coarse positioning of the microscopy sample slide was performed with an xy microscope stage (M-687.UO; Physik Instrumente (PI) GmbH & Co.) and the fine position control during the experiments was conducted with an xyz piezo stage (P-563.3CD PIMars; PI). The axes of the piezo stage were controlled by an analog output module (NI-9022; National Instruments (NI)) and the forces at and positions of the micro-indenter were read out with an analog input module (NI9215; NI). Closed-loop control of the microindentation was implemented in LabVIEW™ and executed by a real-time computer with an integrated field-programmable gate array (FPGA) (NI cRIO9024; NI) (Fig. 4.2).

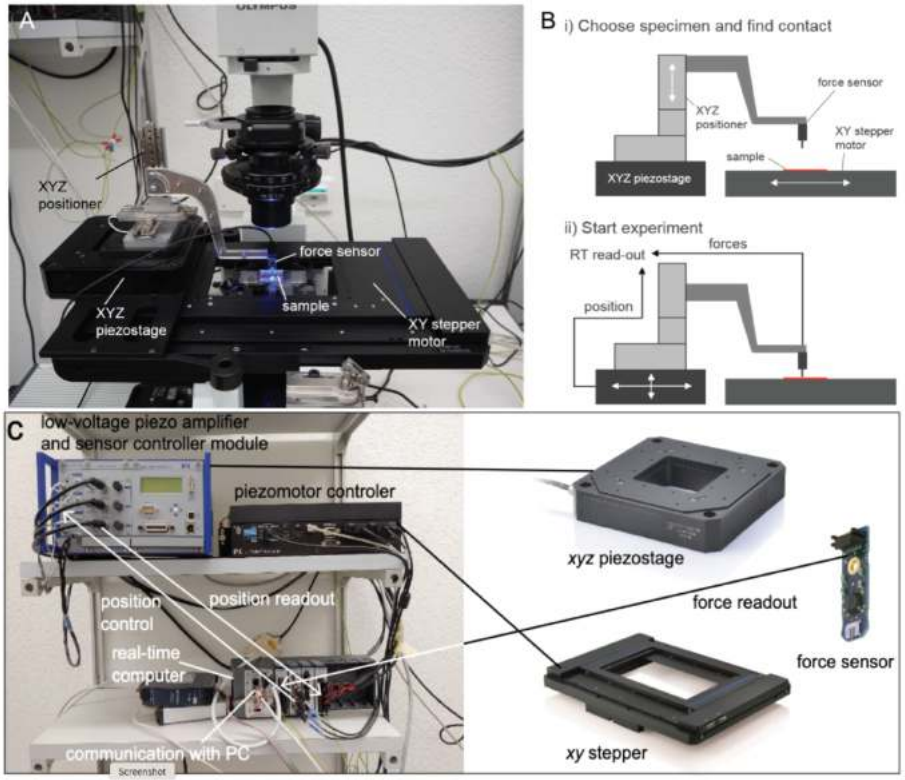

Fig. 4.2: The Cellular Force Microscope (CFM) integrated with an inverted microscope. *(A) System configuration. (B) Experimental procedure: 1. The xy stage with its large travel range is used to find a suitable specimen and then the sensor probe is positioned close to*

it with the xyz positioner. 2. The sensor probe is driven into the sample using the xyz piezo stage with a real-time recording of position and force. (C) Hardware configuration and information flow.

The Root Chip: A Lab-on-a-chip Device for Mechanical Characterisation of Roots

Fixing the root hairs on a glass slide by hand turned out to be vastly time-consuming, and to guarantee direct contact with the glass slide for optimal results required multiple attempts and root samples. Therefore, we went for a higher throughput method with additional upsides. We designed and fabricated a lab-on-a-chip (LOC) device to integrate with the CFM for the mechanical characterisation of root hairs (Fig. 4.3 A). In this LOC, the *Brachypodium* seeds are placed in the seed reservoir of the chip and the growing roots are guided along microchannels with a slightly smaller height than the roots' diameter (Fig. 4.3 B). This guarantees direct contact with the glass slide, which is crucial for accurate micro-indentation measurements. Furthermore, this prevents the root from growing out of focus, allowing long-term microscopic observation of the entire root. Openings along the microchannels offer an easy access to the root with the force sensor. An improved second version offers a thicker, elevated seed reservoir to plant the seed after germination, whereas the rest of the LOC is thin (~2 mm), so that the even a short force probe can reach and measure the root (Fig. 4.3 C).

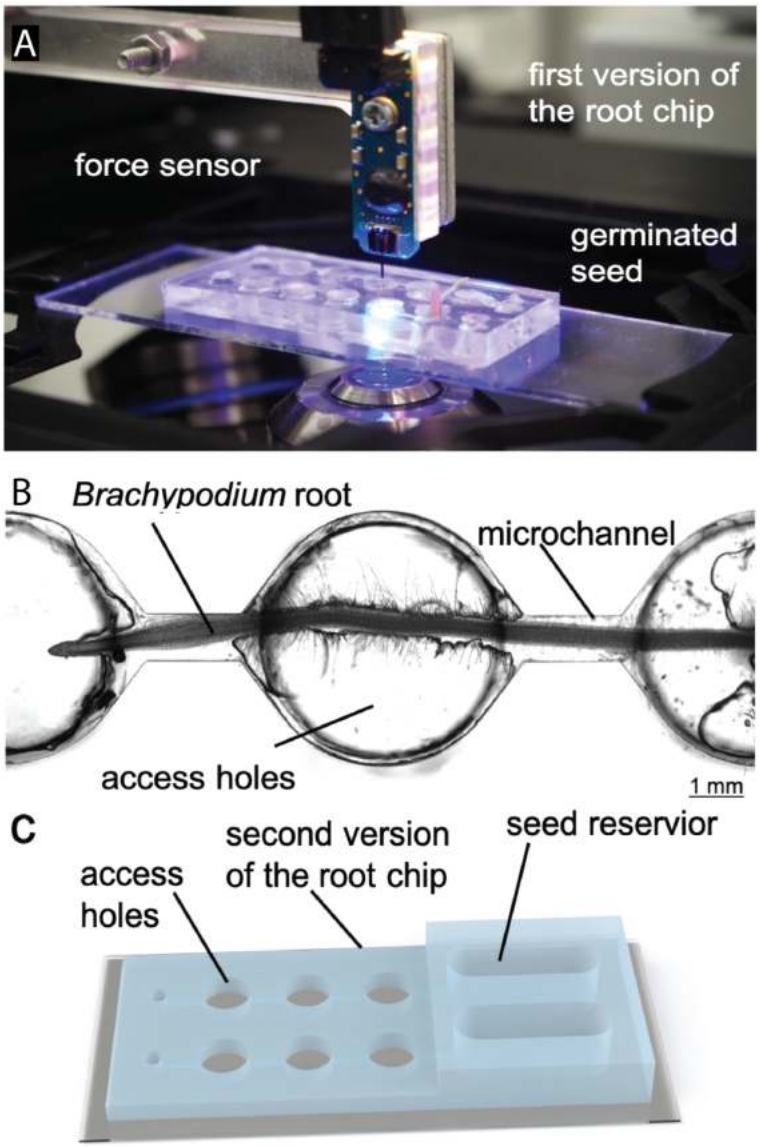

Fig. 4.3: Lab-on-a-chip Device for Mechanical Characterisation of Brachypodium distachyon roots. *(A) A germinated Brachypodium seed in the first version of the microfluidic root chip integrated with the CFM. (B) Microscopic image of a root growing in the root chip. (C) 3D rendering of the improved second version of the root chip.*

Measuring pH in Live Roots Using a Fluorescent pH Indicator

In order to study the biomechanical factors involved in root growth, the use of the new fluorescent pH indicator 8-hydroxypyrene-1,3,6-trisulfonic acid trisodium salt (HPTS) (Barbez et al., *2017*) (Fig 4. 4) in *Brachypodium* roots was established. Since root growth is not restricted to one direction, long-term confocal imaging to see the temporal changes in pH is challenging. The LOC device developed for the mechanical characterisation of roots also facilitates imaging by restricting growth into one direction

and keeping the roots in the focal plane. Openings along the microchannels allowed external manipulation, for example, for adding dyes.

For a better understanding of root cell growth, the root was divided into different zones according to cell size and the visualised differentiation state, namely the division zone (DZ), close to the meristem, the elongation zone (EZ), were the cells start to elongate (from ~500 μm to 1 mm from the root tip in the wt, and from ~500 μm to 2 mm from the root tip in the *Bdtar2l*) and the maturation zone (MZ), were the cells start producing root hairs (Fig. 4.4 A-C).

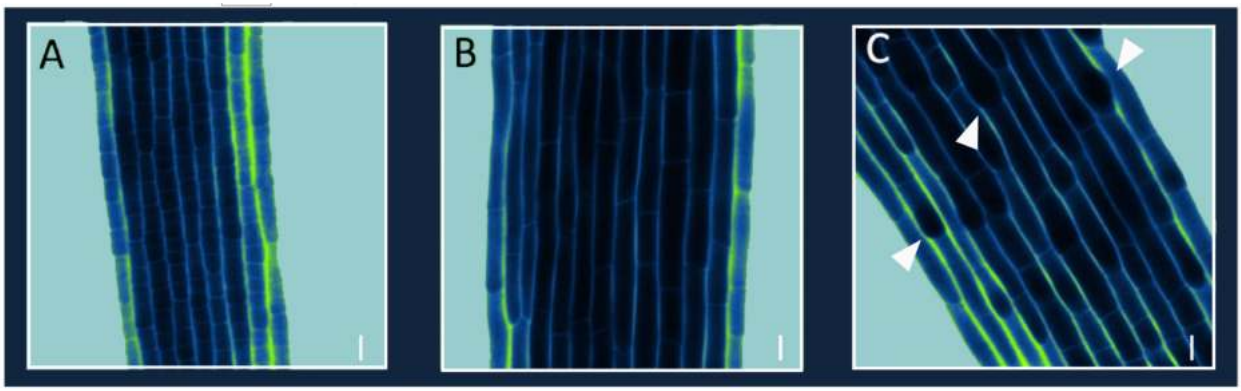

Fig. 4.4: E.g. of 8-hydroxypyrene-1,3,6-trisulfonic acid trisodium salt (HPTS) fluorescent pH indicator analysis on wild type roots. *(A) Root division zone. (B) Elongation zone. (C) Beginning of the Maturation zone where the initial bulges of the root hairs can be visualised (white arrowheads). Scale bar, 10 µm.*

The HPTS is a ratiometric pH-sensitive fluorophore from the group of chemicals known as arylsulfonates, soluble in water and used as a pH indicator with a pKa of ~7.3. Ratiometric indicators are able to shift the peak wavelength of either their excitation or emission curve upon binding a ion of interest, permitting a very accurate quantification. As a ratiometric or dual-wavelength ion indicators, the HPTS has the ability to quantitatively measure extracellular H^+ concentrations. Thus, the fluorescent signals for the protonated HPTS form (Excitation 405 nm, emission peak 514 nm), as well as the deprotonated HPTS form (excitation 458 nm, emission peak, 514 nm) were detected as shown in the literature (Barbez et al., *2017*; Overly et al., *1995*). To obtain a reliable measure of the apoplastic pH in *Brachypodium* roots, we performed a previous *in vitro* calibration of the HPTS dye using MS media that contained buffers adjusted to known pH values between 5 and 8 (130 mM KCl, 1 mM MgCl2, 15 mM Mes, 15 mM Hepes, pH 5-9)(Bright et al., *1987*) on a microscope slide. The 458/405 ratios were then used to plot a calibration curve from which a best-fitting regression curve was calculated (Fig. 4.5). Images were acquired using a Leica SP5 Laser Scanning Confocal Microscope (LSCM) with a HCX

APO L 40×/0.5-W objective and a Leica HyD hybrid detector. Image analysis was performed using ImageJ 1.40g software (http://rsb.info.nih.gov/ij), and data were statistically evaluated with Microsoft Excel 2016. All experiments were performed in at least three biological replications.

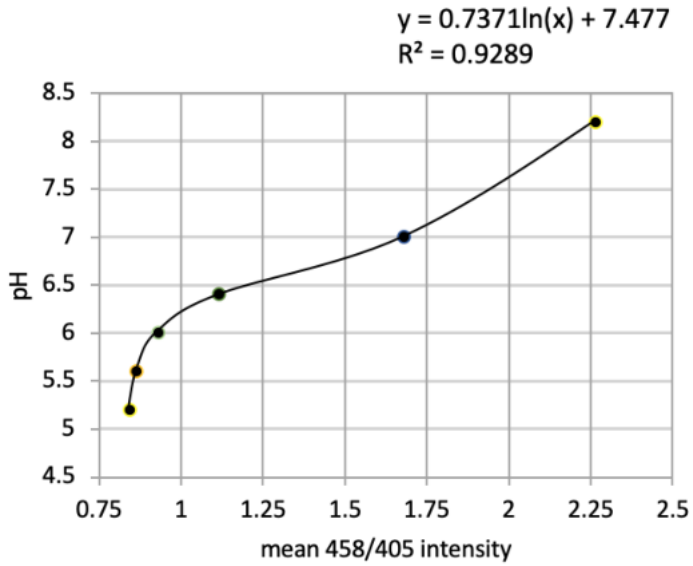

Fig. 4.5: In vivo HPTS calibration in medium with pH 5–8. *The equation derived from regression analysis is shown on top of the graph, which enables pH calculation from the obtained 458/405 values.*

Uniaxial tension test analysis performed by an extensometer

Uniaxial tension tests produced by extensometers were used extensively and most notably in the discovery of the cell wall modifying protein expansins (McQueen-Mason et al., *1992*). Thus, following the established experimental methods, we used uniaxial tension tests to characterise the mechanical properties of *Brachypodium* roots in order to better understand the physics behind this tissue. As the classical extensometer setup, the root was clamped into the extensometer by the root tip, to apply a calibrated tension to measure the deformation of the first remaining centimetre (Fig 4.6 A). The elongation of the roots in response to this tensile force was then recorded as a stress-strain profile (Fig. 4.6 B). Subsequently, we calculated the elastic modulus E, which is a measure of stiffness and thus a characteristic property of linear elastic materials. E is defined as the ratio of stress (force per unit area) and strain (proportional deformation):

$$E = \frac{stress}{strain} = \frac{F/A}{\Delta l / l_o}$$

This way, the biophysical measurements of E, a measure of stiffness, can be compared between specimen.

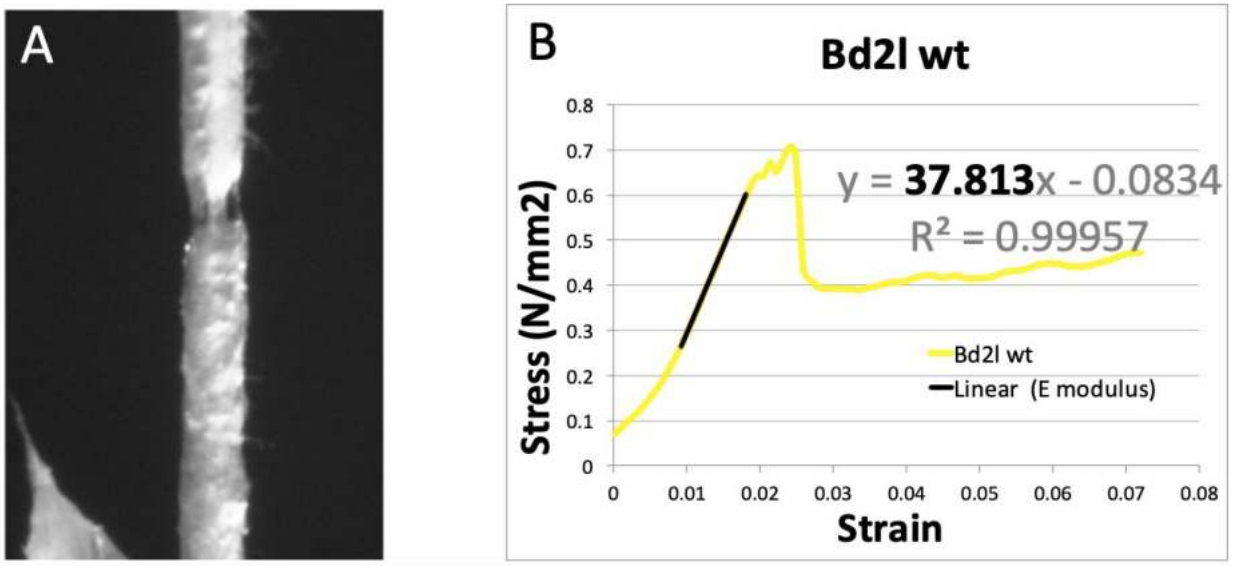

Fig.. 4.6: Uniaxial tension tests. *(A) A wild type root under tension by an extensometer. (B) Typical stress vs. strain curve recorded from the root shown in (A).*

All the measurements for obtaining the mechanical properties at a nanometric scale were performed using an Instron 600DX extensometer model, tracked by the BLUEHILL® UNIVERSAL Next Generation Materials Testing Software and recorded by a BIC-AF2-Z14 Autofocus Video Microscope Camera. The instrument was used at 2% of its capacity to apply maximum forces of 0.5 N.

Note that, since samples are clamped at the tip, these analyses can only be performed for the MZ.

Finite element method(FEM)-based model on uniaxial tension test

In parallel, for the FEM analyses, a 1 cm long mesh consisting of a single solid inner cylinder (diameter ~100 μm in the WT, ~50 μm in the mutant) perfectly encased in a larger hollow outer cylinder (diameter ~500 μm WT, ~350 μm *Bdtar2l*) was modelled. These cylinders represent the inner layers, containing the endodermis and the vascular tissues, and outer layers, form by the epidermis and cortex (Vaughan-Hirsch et al., *2018*), of the *Brachypodium* roots and were discretised using quadratic brick elements within the finite element package, ABAQUS/STANDARD (Simulia, http://www.3ds.com). The roots were modelled using the isotropic Saint Venant-Kirchhoff hyperelastic material model with the Poisson ratios set to 0.2. The elastic modulus of the inner cylinder and the effective elastic modulus of the entire root (both cylinders) were determined

experimentally by tensile tests, as explained before. To simulate the yielding behavior of the outer cylinder as observed in the experiments, the outer cylinder was divided into two separate meshes along its cross section at the centre of the axial axis of the root. The upper and lower cross-sectional surfaces (or edges) of these meshes were joined using a surface-to-surface constraint which yielded above a threshold value given by the experimental measurement of the ultimate tensile strength of the outer cylinder. A tensile test was then simulated on the root using a quasi-static model by applying equivalent displacement boundary conditions on the top and bottom edges of the root until the outer layer yielded. As a result, a sensitivity analysis on the effect of the frictional coefficient on the shear stress was measured for the WT and mutant roots. The frictional coefficient describes the ratio of the force of friction between two bodies, defined as the force resisting the relative motion between two surfaces. Shear stress is defined as the force that causes deformation of a material by slippage along the plane parallel to the normal stress (Fig. 4.7).

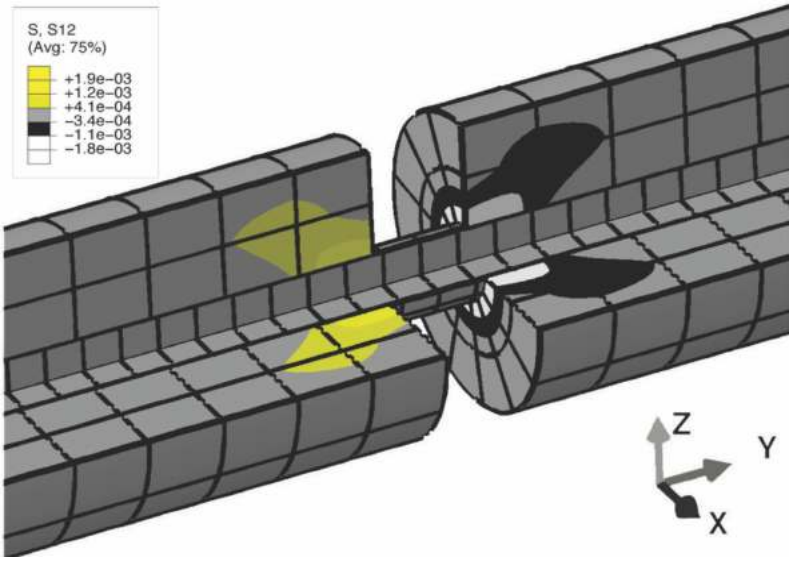

Fig. 4.7: FEM-based Brachypodium root model. *FEM-based analysis showing the friction forces in MPa on a root after the break of the outer layer while loading.*

Root and Root Chip Preparation for analysis and experimentation

All the roots were grown after the lemma of mature seeds was carefully peeled off with forceps before seed sterilisation in 1 ml of 70 % ethanol per seed for 1 min. After ethanol removal, seeds were soaked in a solution of 1.3 % sodium hypochlorite plus one drop of Tween-20 (P9416, Merck) per 50 ml for 5 min and afterward rinsed three times with sterile deionised water. The sterilised seeds were stratified for 2 days at 4 °C to ensure synchronous germination on vertically oriented 10 or 24 cm square plates of half-

strength Murashige-Skoog (MS) media (2.45 g/L MS salts with vitamins, 1% sucrose, 1% agar, pH 5.7, pH 3 and pH 5,7 + 5 μM of Indole-3-acetic acid (IAA), the most common, naturally occurring, plant hormone of the auxin) in a growth chamber under continuous light with an intensity of 100 μE to 120 μE at 22 °C. For extensometer loadings, roots were emerged in half-strength MS liquid media before preparation, to avoid the drying of the samples while preparing them.

LOC devices were loaded with the same media in a concentration of 1 mM for the HPTS. MS media was preheated up to 60 °C and filled into the LOC devices, which were loaded with a P1000 pipette from one end to the other by letting some liquid escape from the small hole at the end of the LOC under the fume hood. Once the medium was solidified, plants were transplanted from the surface of the square plates to the seed reservoir of the LOC with the root tip facing the guide channel. Plants were grown vertically oriented under continuous light with an intensity of 100 μE to 120 μE at 22 °C.

4.3 Results

Cells in the EZ of *Bdtar2l* exhibit stronger elongation compared to the WT

In order to accurately identify the different zones in the *Brachypodium* roots, we generated different cell size measurements within the first 2 mm of the root from the root tip in both the WT and the *Bdtar2l* mutant. Our measurements demonstrated an increase in average cell size from the DZ (~50 μm cell size) to the EZ (~100 μm) and the MZ (>150 μm) in both lines fitting with the developmental stages in the root. Furthermore, we did not appreciate any significant difference between WT and *Bdtar2l* in the first 500 μm corresponding to the DZ. At ~700 μm, in the EZ, we observed a significant difference in cell length between the WT and the mutant as expected. Finally, at a distance of more than 1.5 mm from the root tip, our measurements did not show any significant different between the WT and the mutant cell length.

Based on these results, we were able to clearly differentiate the different cell zones according to the root cell size to perform precise analyses for the AGT validation (Fig. 4.8).

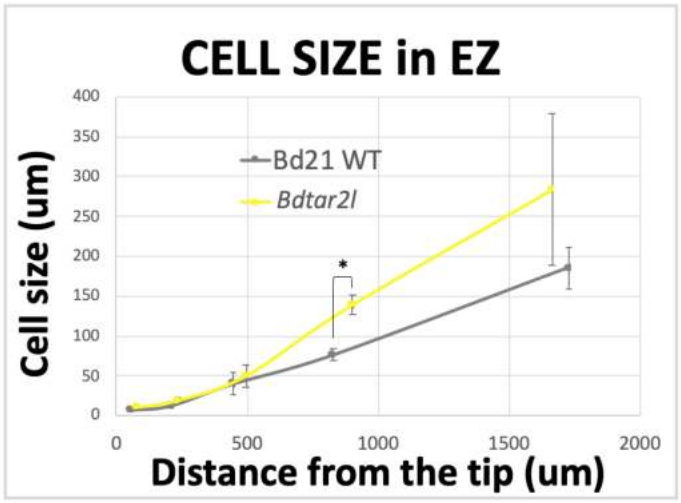

Fig. 4.8: Different cell size comparison between WT and Bdtar2l mutant when measured according to the distance form the tip. *Cell size was measured and compared to establish the different roots zones. According to our visualisation analyses the DZ is established around the fist 500 µm form the tip for both (~50 µm cell size), followed by the EZ (~100 µm) and the MZ (≥150 µm).*

The distribution of pH levels in *Brachypodium* roots supports the AGT

To validate whether the observed significant difference in EZ cell elongation between the WT and the *Bdtar2l* mutant is correlated with cell wall acidification, we performed a pH analysis using the HPTS dye on the different roots zones. The obtained intensity ratio results, which correspond to the pH level (low ratio equals low pH and vice-versa), showed significant differences (p value <0.05) between the WT and the *Bdtar2l* mutant, in the DZ and more pronounced in the EZ, were the cells rapidly elongate. Indeed, in the auxin over-accumulated *Bdtar2l* mutant, both developmental zones exhibited lower pH (~5,8) when compared to the WT's (~6,5 and ~6 for the DZ and the EZ respectively). Together with the significantly longer cells in *Bdtar2l*, this is in agreement with the AGT, which states that cell wall acidification increases cell elongation (Fig. 4.9 A-C).

Concerning the acidification level of the MZ, no significant results (p value = 0.6932) have been observed, despite a tendency of lower ratio values in the WT (ratio <1) compared to the mutant (ratio of 1.1) (Fig. 4.9 C). Furthermore, in relation with the developmental zone shift from the DZ to the EZ and from the EZ to the MZ, we did not observe a significant pH change neither in the WT nor in the *Bdtar2l* mutant. These results highlight the necessity of using additional measurements such as mechanophysical analyses to better understand the current pH results. Nevertheless, the pH measurements

confirmed that the examination of root cells by development zones is a good approach to evaluate the AGT more accurately.

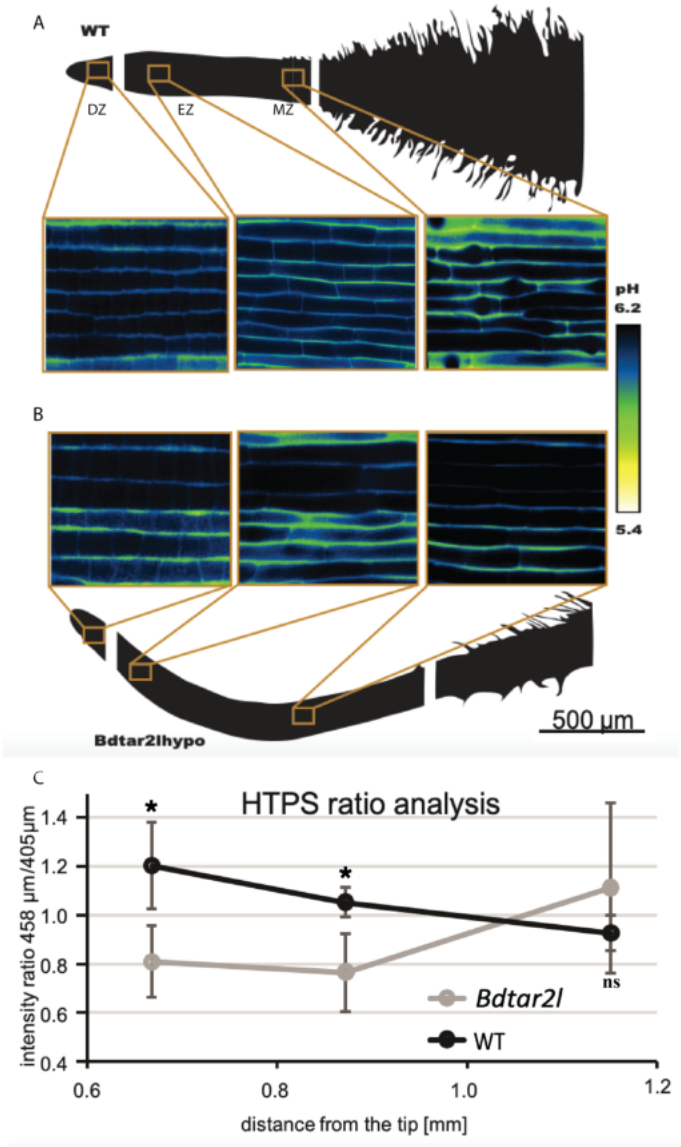

Fig. 4.9: Ratio-metric comparison of fluorescent pH-indicator HPTS on wild-type (WT) and Bdtar2l roots in the different zones. *2D representation of (A) WT and (B) Bdtar2l root in black and white, divided into the three different zones (division zone (DZ), elongation zone (EZ), and maturation zone (MZ)) together with their corresponding pH values measured using the pH indicator HPTS (from acidic pH yellow to basic pH blue colour gradient). (C) HPTS ratio-metric analysis in mutant and WT roots. The values were plotted according to the distance from the tip and are proportional to pH values. Data were analysed by a Student's t test, considering $P \leq 0.05$ as significantly different; data shown are mean ± SEM*

The AGT is supported by reduced stiffness and pH in the EZ of the *Bdtar2l* mutant

To see if the observed decrease in pH had an influence on the mechanical properties, we used the CFM to measure the apparent stiffness of cells in the different root zones both in the WT and the *Bdtar2l* mutant. The AGT states that an decrease in the apoplast pH leads to the cell wall loosening, which, as a consequence, allows the cells to expand. Thus, we expected to see a reduction in cell wall stiffness in the EZ of both lines. In addition, this effect should be more pronounced in the *Bdtar2l* mutant.

We could show that in the WT, the EZ (apparent stiffness = 193.2 N/m) was significantly stiffer than the EZ of the *Bdtar2l* mutant (170.3 N/m), which stipulates that an increase in auxin enhances cell wall loosening due to acidification of the cell wall. This is in line with our expectations. Furthermore, these results correlate with the HPTS' results, showing that the accumulation of the phytohormone auxin in the EZ acidifies the cell wall, leading to a decrease in stiffness in this area and therefore to cell elongation.

When comparing the MZ of both lines we observed higher apparent stiffness in the mutant (apparent stiffness = 187.1 N/m) compared to the WT (142.6 N/m). This surprising results might be biased due to the presence of the large amount of root hairs in the WT's MZ, which may interfere with our measurements. Despite this problem, we expect that the measurements performed in the MZ of *Bdtar2l* are accurate due to the absence of the long root hairs. Therefore, our results show none significant difference in between the EZ and the MZ of the *Bdtar2l* mutant. Interestingly, these results agree with the ones of the HPTS dye, which showed the same acidification levels in both areas. Apparently, due to an increase of the auxin levels in the *Bdtar2l*, the maladjusted hormonal growth control has an important effect in the EZ-MZ transition and leads to an extended EZ in the mutant. Or, in other words: in *Bdtar2l* the cells remain longer in the EZ, which consequently extends their elongation phase.

On the other hand, the MZ of the WT (142.6 N/m) showed smaller apparent stiffness than its EZ (193.2 N/m). Since difficulties appeared when measuring this zone, due the the root hairs, further analyses with a different tool than the CFM are needed in this area (Fig. 4. 10).

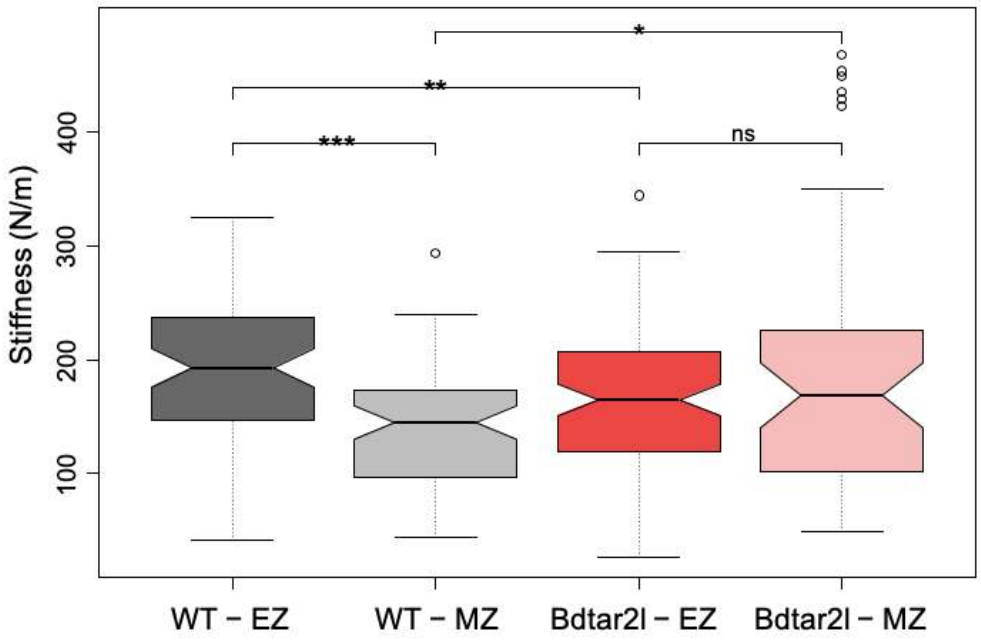

Fig. 4. 10: Stiffness analysis along the root. *Differences in apparent stiffness according to different zones (EZ vs. MZ) in wild type (WT) and mutant roots. EZ = approx. the first millimetre in the wt, 2 mm in the Bdtar2l, MZ=from the EZ up to 3 mm. Data were analysed by one-way ANOVA followed by Tukey's test as post hoc; n= 18-24 with 8-10 technical replicates by zone. ∗p <0.05; ∗∗p <0.01; ∗∗∗p <0.001; ns, no significant. Boxplot shows 1st and 3rd quartiles (box), median (thick line) and the most dispersed values within 1.5 times the interquartile range (whiskers).*

The AGT stipulates that the cell wall acidification, due to the auxin expression, is the principal cause of the cell wall loosening. According to our previous results, we already correlated the cell wall loosening with the reduction of the cell wall stiffness. So, in order to validate that the high concentration of auxin and the cell wall acidification correlate directly with a decrease in the cell wall stiffness, we measured this mechanical property on different roots treated either by low pH or by external application of auxin at high concentration.

As expected, a related effect can be observed when growing WT and *Bdtar2l* roots either at low pH or at high concentrations of IAA (Fig. 4.11 A-B). According to our results, in both cases the WT's EZ shows a similar significant reduction of the apparent stiffness (~90 N/m) when compared to the untreated control (142.6 N/m). Furthermore, the same response can be observed in the *Bdtar2l* mutant's EZ (187.1 N/m) when it is growth at pH 3 (apparent stiffness = 107.6 N/m), supporting therefore the AGT (Fig. 4.11 A). However, the MZ of both plants' roots seems not to be affected neither to a decrease of

pH nor an increase of IAA. Interestingly, our results don't show any significant difference in the apparent stiffness in this area, which fits with the HPTS ratio-metric analysis, and suggest therefore the idea that only the cells which are in the EZ, are predisposed to elongate since they react to both treatments (Fig. 4.11 B).

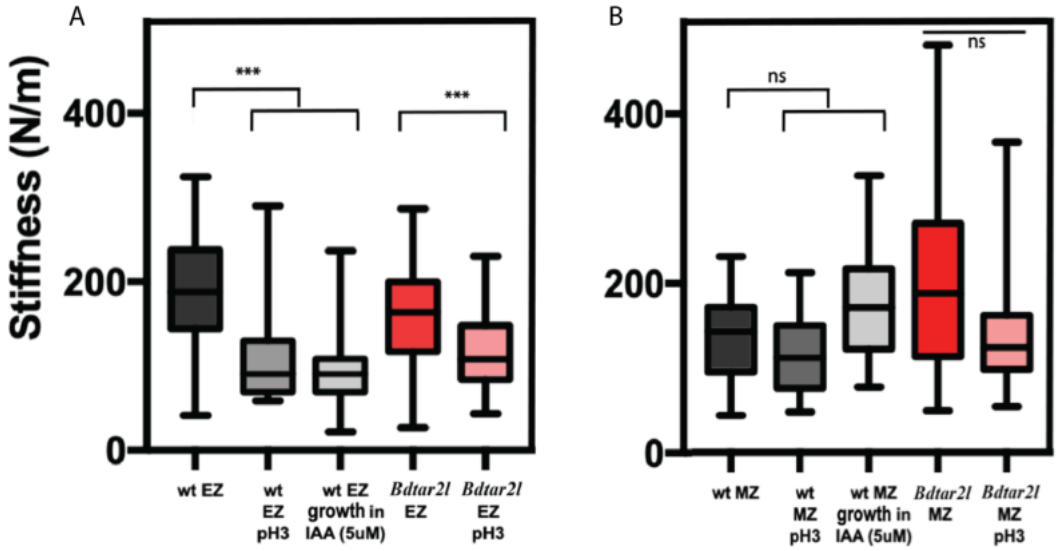

Uniaxial tension tests show higher elasticity in WT's MZ in accordance with the preliminary results obtained by the CFM

Due to the lack of reliable apparent stiffness measurements in the MZ of the WT, uniaxial tension tests performed by an extensometer, were used to compare the mechanical properties of WT and *Bdtar2l* roots in this zone. The CFM and extensometer provide different mechanical information since they operate at different scales, however, both techniques are useful to characterise linked mechanical parameters. From a general point of view, the mechanical properties describe how a material (*Brachypodium* roots in our case) deforms when a force is applied. In contraposition with the micro indentation experiments already performed, which apply local known forces to measure the local specific stiffness after a deformation, the classical uniaxial tension test setup involves clamping a known length of a sample (first cm of the MZ) for then applying a calibrated tension. This tension generates a deformation that is measured in order to obtain the elastic modulus E (Young's modulus). This way, the uniaxial tensile test formally describes the relationship between stress (force/cross sectional area) and strain (relative change in length), thus the stress-strain pattern can be used to characterise a different but related description of the micro-mechanical properties already acquired by the CFM.

Therefore, according with the uniaxial tension test, the elongation of the root in response to a tensile force was recorded as a stress-strain profile, from which the E

modulus was calculated and then compared between the different lines. This analysis showed a significantly higher E value for the *Bdtar2l* mutant (45.3 MPa) than for the WT (37.3 MPa) in the MZ, revealing a higher elasticity in the WT, which is in agreement with the CFM data, therefore validating both techniques reciprocally despite the artefactual values obtained with the CFM due to the root hairs (Fig. 4.12 A-B).

Furthermore, in order to better understand how the diameter of the different roots and the properties of the different layers affected the previously obtained experimental results from the entire root (both layers), we decided to measure the inner cylinder of the *Brachypodium* roots, which is protected by the endodermis and known to be formed by the vascular tissues. As expected, when comparing the E modulus of the WT (158.5 MPa) and the *Bdtar2l* (311.5 MPa) of the inner cylinders, the results were similar to those when the entire root was pulled. Thus, the higher elastic modulus of the *Bdtar2l* mutant suggests that —assuming same turgor pressure— the diameter should be lower, which is what we see in the experiments.

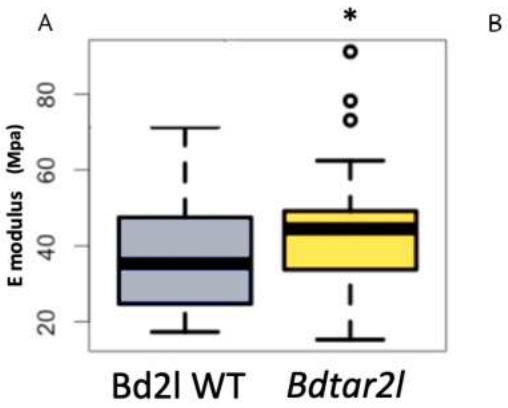

B

	Mean E modulus (N/mm2)= Mpa	n	T-test P-value
Bd2l WT	37.3 ± 8.15	42	* 0.03
Bdtar2l	45.3 ± 9.6	27	
Inner cylinder WT	158.5 ± 52.16	36	*** <0.001
Inner cylinder *Bdtar2l*	311.5 ± 61.5	26	

Fig. 4. 12: E modulus comparison of wild-type (WT) and Bdtar2l roots' MZ of the entire root (both cylinders) and the inner cylinder. *(A) WT and Bdtar2l roots elastic modulus comparison. (B) Table with the E modulus results and the statistical analysis for the entire root (both cylinders) and the inner cylinder of WT and Bdtar2l. Data were analysed by one-way ANOVA followed by Tukey's test as post hoc; ∗p <0.05; ∗∗p <0.01; ∗∗∗p <0.001.*

In order to better study the interaction between the inner and outer cylinders we made a FEM based model to estimate the shear stresses for a range of frictional coefficients. The results showed that higher load resistance in the mutant is associated with a lower elasticity, which can influenced the root geometry and shape. Indeed, a difference in deformation pattern was observed between the WT and the mutant roots while the pulling forces were applied, with the WT being more elastic. Thus, the FEM model shows a 5% higher shear stress for the same frictional coefficient, that acts to resist

the motion between the inner and out cylinders, in the *Bdtar2l* mutant when compared to wild type. Higher shear stress means higher resistance to loading due to the geometry of the MZ of the *Bdtar2l* mutant, which contains a significant reduced diameter and longer root cells. (Fig. 4.13).

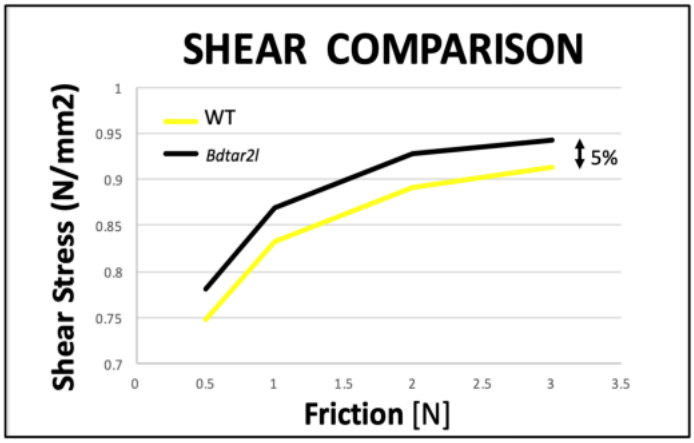

Fig. 4. 13: Shear stress comparison between the WT and Bdtar2l. *The different outer and inner tissue layers's share forces compared under the same friction analysis. FEM model output based on data presented in Fig 4.12.*

4.4 Discussion and Conclusion

With this study we could show that the AGT can be validated in the EZ of *Brachypodium* roots by using a remarkable segmentation approach together with the mechanical characterisation and the fluorescent imaging. Until now, the AGT was poorly understood in root cells due to controversial studies and the lack of suitable methods. Thus, a significant part of this work has been to develop and optimise new approaches to better comprehend this concept. We combined a CFM approach with a tensile test analysis, in order to correlate the change in cell growth to a pH gradient while measuring the mechanical properties of the cell wall. Tensile tests performed by extensometers have already been shown to be useful in the discovery of the cell wall modifying protein expansin in the last century (McQueen-Mason et al., *1992*). But now, combined with FEM-based modelling, they helped us to better understand the different stresses occurring in the roots under different conditions. Therefore, the new tools we developed, in combination with those already established, and the precise characterisation of root developmental zones, may allow to standardise root growth analysis, which may provide a better understanding of the AGT. Indeed, the root segmentation by a zone parameter has been already described in many important crops, such as wheat (Li et al., *2019*), maize (Moreno-Ortega et al., *2017*) and barley (Sarabia et al., *2020*). In addition, we can easily

imagine that this method could also be applied to other longitudinally organised plant organs such as lateral roots, some monocot leaves and/or internodes in the future.

As explained, according to our results, we could validate the AGT in the EZ. The mutant's EZ, expressing more auxin, having a lower pH according to the HPTS, and becoming softer, supports the idea behind the AGT; an increase of auxin leads to an increase in cell wall loosening due to a reduction in pH as observed also in our analyses and when applying high concentrations of auxin externally. Therefore, the decrease in stiffness, due to both the effect of the expansin activity and a de-methyl-esterification of pectin prior to organ outgrowth, is driven by the increase of auxin (Braybrook and Peaucelle, *2013*; Hocq et al., *2017*). Contrarily, we realised that in WT roots the EZ is stiffer than the MZ, in contrast to our expectations since according to the AGT, the cell which elongate increases the cell wall loosening and thus, should be less stiff. However, as explained, the MZ contains larger amount of root hairs than the EZ, which may affect the compression experiments by falsely suggesting softer cells in this part of the root.

When examining the *Bdtar2l* mutant, we found no significant difference in either pH or stiffness measurements between the EZ and the MZ , revealing a very conserved phenotype of long cells. The nonsignificant difference between these two zones may be explained by the absence of a strong decrease in auxin concentration in the MZ. A consequence of this phenomenon could be that the cells remain in the developmental program for elongation for a longer time, which leads to thinner roots with only few root hairs (Pacheco-Villalobos et al., *2013*).

We were again confronted with the same problem of long root hairs in the WT when we compared the MZ of WT and *Bdtar2l* with the CFM approach. Therefore, we could not take the obtained results as granted and we performed additional analysis using an extensometer to avoid any interference in the data measurements. According to our results and as expected due the thicker cells of the WT's MZ, the uniaxial tension tests showed more elastic roots than the *Bdtar2l*'s. However, we showed in parallel that the MZ is not affected by the external low pH and high auxin concentration application and, therefore, confirm a relationship absence with the AGT. Thus, this may suggest that just the cells in the EZ are the only ones predisposed to elongation because they are affected by the increase in auxin levels.

To summarise, according to our preliminary results, we could show that higher expression of auxin decreases the pH and consequently increases the cell wall elasticity by cell wall loosening in the elongating cells. This cell wall loosening may have to continue or even increase to reach the MZ, where cells will expand to start producing

root hairs for better nutrient uptake (Bates and LYNCH, *1996*; Gilroy and Jones, *2000*). At this stage different key genes involved in the modulation of auxin levels will get expressed, allowing the cells to stop their growth and get mature (Birnbaum et al., *2003*; Kyndt et al., *2012*; Moubayidin et al., *2013*). In the mutant, regulation of root cell growth is maladjusted and has an important effect in the EZ-MZ transition, maintaining a constant stiffness along the root, as well as higher shear stresses between the inner and outer cylinders when the root is pulled. Thus, the cell wall's stronger rigidity in the mutant MZ may constrain the cells to keep elongating and prevent them from expanding. As a consequence, only some softer cells will mature and produce root hairs. Still, most of the biological systems are analogous to the chicken and the egg paradigm; thus, the question whether cell elongation occurs due to cell wall softening in the EZ, or due to an increase of rigidity of the apoplast downstream in the cell lineage, i.e. in the MZ, remains open and requires further investigation.

Even-though our system helps in the better comprehension of the AGT, the broad spread of different phenotypes observed in WT and mutant roots requires a larger data set to formulate well-founded statements. To clear up the inconsistencies between the EZ-MZ, the pH has to be measured concomitantly with the cellular apparent stiffness and the elongation rate, together with the local IAA levels measured by synthetic promoter DR5 reporter system, for example (Chen et al., *2013*; Gallavotti et al., *2008*). Furthermore, according to our zone segmentation, it would be important to specifically asses the full transcriptomic, metabolic and proteomic profiles of the individual zones to better understand the discrepancies in between the different areas. Such experiments provided already interesting information about zone-specific protein expression in wheat roots (Li et al., *2019*) or transcriptome gradients in barley roots, where in the latter Hill et all. revealed even root-zone-specific responses to salt exposure (Hill et al., *2016*).

Unfortunately, according to our mechanophysical analyses, the CFM appears not to be the ideal tool to characterise root cells individually in the MZ since the large number of root hairs, especially in the WT, may influence the measurements and lead to artefacts. Furthermore, the uniaxial tension tests, that have been proven to be suitable in the MZ, are not able to provide the elasticity in the EZ, since this area gets clamped and provides just the mechanical properties of the rest first centimetre length of the root, the MZ. Hence, parallel analyses with the Automated Confocal Micro-Extensometer, for example, which has been shown to enable in vivo quantification of mechanical properties with cellular resolution in *Arabidopsis* (Robinson et al., *2017*), could provide us with more accurate sub-cellular data in the future. A future in which more precise pH apoplastic

sensors and subcellular auxin reporters for our model plant may be developed and will allow us, together with the already established CFM, to create spatially better resolved stiffness and elongation maps in *Brachypodium* roots.

5 Chapter 5 - General discussion and future perspectives

All findings presented in this thesis are discussed in detail at the end of each chapter. This section will attempt to summarise the most important findings and put the results into a bigger context in order to discuss some open questions and future perspectives.

Arabidopsis and *Brachypodium* models: a perfect combination for understanding the AGT and its universal applicability

Arabidopsis thaliana has served as a plant model system for more than 40 years and is widely considered the preeminent model plant (Koornneef and Meinke, *2010*; Krämer, *2015*). The well characterised developmental processes, involving the different, well described cell types, helped us to better understand at what level the Acid Growth Theory can explain cell elongation. As discussed in Chapter 1, the *Arabidopsis* pollen tube is a widely used model ideally suited to study cellular processes underlying polarised cell growth. The observed apical expansion makes pollen tubes the perfect system to comprehend the fine-tuned deposition of plasma membrane and cell wall components during cell elongation generated by the interplay between the expansive force of turgor pressure and the controlled loosening of the cell wall, which is thought to be induced by a reduction of the cell wall's pH. Therefore, to avoid a cellular burst, the balance between the turgor-driven expansion and the cell wall synthesis is principally controlled by some plasma membrane-located receptors which belong to the cell wall integrity (CWI) signalling pathway. In 2014, Haruta and colleagues showed that FER, one of the main actors of the CWI pathway, was able to bind RALF1, which leads to the inhibition of plasma membrane H^+-ATPase activity, which in turn increases the apoplastic pH. They also showed that the addition of RALF1 peptide correlates to an immediate arrest of root growth, which is consistent with the dogma of the Acid Growth Theory (Haruta et al., *2014*). Thus, the study of these peptides has become essential to understand how the AGT controls cell growth.

On the other hand, a second system was used to understand AGT at the multicellular level; the root of *Brachypodium* distachyon. As explained, *Brachypodium* is a fairly new plant model which has has developed into a viable model system to study biological issues relevant to grasses and hence to a whole range of important crops (Brkljacic et al., *2011*). More specifically, for our purpose, it has become essential for understanding the still controversial AGT. To this end, we took advantage of an allelic mutant in a key auxin biosynthetic gene, *BdTAR2L*, which produce higher levels of auxin

specifically in the root cell elongation zone (Pacheco-Villalobos et al., *2013*). As we showed, this promotes cell elongation is associated to an increase of acidification, which together with an increase of the cell wall loosening leads to a decrease in cell wall stiffness and produces longer root cells as a consequence. Thus, the use of both models provided us with a wider overview to understand the AGT's universal applicability and becomes an excellent system to study at what degree the AGT can explain cell elongation both at cellular and multicellular level.

RALF4/19 peptides interact with LRX proteins to control pollen tube growth in *Arabidopsis*

The pollen tubes of *Arabidopsis* allowed us to study cell wall modifications at the single cell level, while focusing on the different protein interactions that are involved in the adaptation of cell wall loosening. As shown in Chapter 2, RALF peptides interact with LRX proteins to control cell growth and are required to activate the CrRLK1L-mediated signal transduction pathway to regulate pollen tube development in *Arabidopsis* (Mecchia et al., *2017*). The RALF-CrRLK1L module and some of the components working up- and downstream of the RLK are conserved in many other processes like the establishment of cell morphology, defense against pathogen attacks and abiotic stress responses (Dünser et al., *2019*; Stegmann et al., *2017*; Yang et al., *2015*). All this is achieved through the coordination of many intracellular pathways, which subsequently regulate H^+, Ca^{2+}, and ROS levels both in the cytosol and the apoplast to modulate the cell wall integrity in response (Thor, *2019*; Vogler et al., *2019*; Voxeur and Höfte, *2016*).

In order to understand how the H^+ concentration in the cell wall affects the different players of the CWI pathway, we generated different binding affinities' experiments of RALF peptides with crystallised LRX and CrRLK1L/LLGs membrane proteins in acidic and alkaline conditions (Chapter 3). Our latest binding data between RALFs and its different receptors, together with the results of previous studies (Ge et al., *2017*; Gonneau et al., *2018*; Mecchia et al., *2017*), suggest that CWI pathway could be additionally regulated by pH fluctuations in the cell wall (Höfte and Voxeur, *2017*; Moussu et al., *2020*). Altogether, these findings suggest that RALFs have the capacity to instruct different signalling proteins to coordinate cell wall remodelling during cell elongation according to the pH. Both our structural and physiological experiments support that folded rather than linear RALF peptides represent the bioactive ligands for both LRX and CrRLK1L/LLG (Moussu et al., *2020*; Xiao et al., *2019*). So, after this RALF expression, we defend that RALF peptides may bind to LRX in a fully folded oxidised

state preferentially. However, in response to a changing cell-wall environment, they may acquire a reduced linearised state to join different receptors, like CrRLK1Ls. RALF alters the activity of plasma membrane H^+-ATPases, Ca^{2+} concentration and ROS expression, which may indirectly affect different proteins involved in regulating cell elongation like other RLKs, for example. However, this hypothesis is still under investigation.

The role of auxin for the CWI maintenance during plant cell growth needs further examination

According to the AGT, auxin promotes cell elongation by cell wall acidification and the induction of cell wall remodelling enzymes (McQueen-Mason et al., *1992*) ,(Cosgrove, *2000*; Majda and Robert, *2018*). Although this phenomenon reminds controversial and not well defined yet, auxin's intracellular functionality and regulation is well characterised. The nuclear auxin pathway (NAP) is the machinery that controls auxin gene expression (Pierre-Jerome et al., *2014*). Without auxin, the transcriptional functions of the auxin response factors (ARF) are inhibited by union with the Aux/IAA proteins through heterodimerization (Li et al., *2016*). When auxin enters the nucleus, this union gets uncoupled, and Aux/IAAs are bound by the SCF-type ubiquitin protein ligase complexes (Weijers and Wagner, *2016*), leading to their subsequent degradation. The liberated ARF transcription factors can now modulate auxin-related gene expression via its DNA binding domain (Paque and Weijers, *2016*).

In 2010, Duan and colleagues showed that the CrRLK1L FER functions in a RAC/ROP signaling pathway and mediates the auxin-regulated root hair development, as explained (Duan et al., *2010*). But, 10 years later, and despite the well known characterisation of IAA's intracellular functionality, a real interconnection between auxin-induced gene expression and the cell wall integrity pathway is still missing. However, in 2018, Schoenaers et al. were able to show that plasma membrane-associated protein ERULUS (ERU), a new CrRLK1L family member, is an auxin-induced *Arabidopsis* receptor-like kinase whose expression is directly regulated by ARF7 and ARF19 transcription factors (Schoenaers et al., *2018*). Furthermore, ERU regulates cell wall composition at the tip of apically growing cells and modulates pectin dynamics through negative control of pectin methylesterase (PME) activity depending on Ca^{2+} concentrations (Schoenaers et al., *2017*). So, either expressed in roots or in pollen tubes, ERU connects the auxin and the CWI pathways. While the interaction of IAA with ERU has been well explained, the connection with other members of the CWI pathway is still missing and needs further investigation. So far, nothing is known about interaction

between ERU and other members of the CrRLK1L protein family, such as FER, ANX or THE, for example. Does ERU interact with RALF or the RALF-CrRLK1L module? Does the auxin-induced ERU contribute to the strong interaction between RALF and LRX through the induction of other proteins? These are just some examples of open questions, which may hopefully be answered in the near future.

Brachypodium roots as a tissue model for investigating cell growth and phytohormone interaction

The importance of having a model organism to better understand cell expansion becomes obvious from the example of the heavily debated acid growth in roots when compared to the well established and documented acid growth theory in plant shoots (Fendrych et al., *2016*; Rayle and Cleland, *1970*; Spartz et al., *2014*; Takahashi et al., *2012*). As explained, a scientific report using the HPTS pH marker for subcellular monitoring of the apoplastic pH distribution, showed that acidification is promoted by auxin in *Arabidopsis* (Barbez et al., *2017*). In the case of *Brachypodium* roots, however, cell elongation was more associated with alkalisation (Pacheco-Villalobos et al., *2016*). So far, these discrepancies could have been due to spatial, temporal or species-specific differences. Thanks to our work we demonstrated that these disagreements could be solved by a standardised and accurate approach for the different root zone identification. When the WT's and *Bdtar2l*'s EZs are compared, the resulting apparent stiffness decreases due to a cell wall acidification, supporting the AGT in this area. Furthermore, related to the differences between species, it has been shown several times that the auxin pathway interacts with ethylene, but this fact might differ substantially in *Brachypodium*. On one hand, auxin upregulates AMINOCYCLOPROPANE-1-CARBOXYLATE (ACC) SYNTHASE, an enzyme that catalyses the synthesis of ACC, the precursor of ethylene (Abel et al., *1995*). On the other hand, ethylene can influence the expression of *TAR* and *YUCCA* genes both in *Arabidopsis* and *Brachypodium* (Pacheco-Villalobos et al., *2013*; Stepanova et al., *2008*; Won et al., *2011*). It was shown that TAA/TAR is involved in the auxin biosynthesis pathway in both plants. However, while in *Arabidopsis* the down-regulation of TAA1 reduces the amount of auxin and therefore root growth is impaired (Stepanova et al., *2008*; Tao et al., *2008*), the *Bdtar2l* mutant has an increased root length and displays increased auxin levels. According to Pacheco-Villalobos et al., in the *Bdtar2l* mutant both root phenotype and auxin levels, could be restored by the addition of the ethylene precursor ACC. Surprisingly, this was not due to a change in *BdTAR2L* expression, but rather to the fact that the ACC-treated roots displayed reduced levels of YUCCA expression, the last

enzyme involved in tryptophan-dependent auxin biosynthesis (Pacheco-Villalobos et al., *2013*) (Fig. 5.1 A). As, ethylene is linked to the auxin biosynthesis intermediate IPA via VAS1-like enzymes (Pacheco-Villalobos et al., *2016*; Zheng et al., *2013*), lower levels of IPA in *Bdtar2l* mutants result in lower levels of ethylene. Thus, it was postulated that the decease of ethylene de-represses the rate-limiting YUCCA step in auxin biosynthesis and results in higher levels of auxin as long as *BdTAR2L* expression does not drop below a certain threshold (Pacheco-Villalobos et al., *2013*) (Fig. 5.1 B).

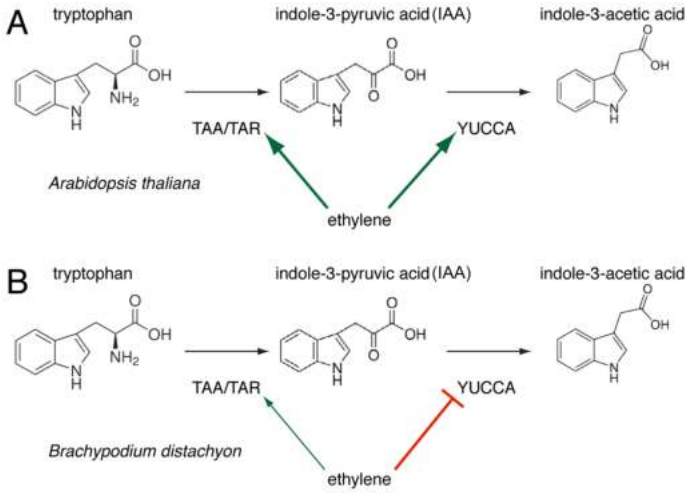

Fig. 5. 1: Auxin-ethylene crosstalk model proposed by Pacheco-Villalobos et al. in 2013. *Ethylene promotes YUCCA expression in Arabidopsis (A), while it suppresses YUCCA in Brachypodium (B). Adapted from (Pacheco-Villalobos et al., 2013).*

Interestingly, many experiments have shown that correct auxin effluxes are crucial for normal root development, which is inhibited by the addition of external auxin (Hobbie and Estelle, *1995*; Ivanchenko et al., *2008*; Marchant et al., *1999*; Swarup et al., *2001*; Yu et al., *2015*). Furthermore, general root growth inhibition is coupled with an increase in ethylene levels both in *Arabidopsis* and rice, a closer relative to *Brachypodium* (Iqbal et al., *2017*; Juan Li et al., *2015*; Růzicka et al., *2007*; Vaseva et al., *2018*). In the case of rice, however, it was concluded that the auxin-induced inhibition of root growth was not directly caused by the expression of ethylene, but rather that the roots needed a certain level of ethylene to cope with auxin to maintain the seminal root growth (Yin et al., *2011*). In addition, in 2014, Ma et al. also showed in rice that ethylene inhibits root growth largely through ABA function (Ma et al., *2014*), in contraposition to what was observed in *Arabidopsis* (Beaudoin et al., *2000*; Cheng et al., *2009*; Ghassemian et al., *2000*). Therefore, the study of the auxin-ethylene crosstalk, their gradient-interaction with the other phytohormones in the different plants models and how this affects cell wall acidification may provide deeper insights into the general validity of the AGT.

Cytomechanics: the comeback of the forgotten approach

Plant biomechanics is a field of research that not only combines physics, engineering, mathematics, and chemistry with botany and forestry science, but also includes diverse aspects of plant physiology, cell biology, biochemistry, ecology, as well as developmental and molecular biology. During cell growth and differentiation, plant cells increase in size to form different tissues. These growth and shape changes involve the stretching and deformation of cell wall material whose mechanical properties in turn control the process (Bidhendi and Geitmann, *2018*). Thus, the integration of biochemical and biomechanical signaling processes becomes crucial for many developmental steps as it allows cells to coordinate their behaviour. While a wealth of information is available about the signaling processes associated with biochemical hints, knowledge of the molecular underpinnings of the perception and processing of biomechanical cues is only emerging.

Biomechanical studies aim to understand the relationship between the mechanical properties of biological structures and their function. In cytomechanical investigations, this approach is brought down to the scale of cells and subcellular structures. As explained, in plant cells the interactions between turgor pressure, the cell wall, and the cytoskeleton are considered of primary importance. Until now, plenty of research publications made use of cytomechanics analyses to better understand plant's behaviour in plenty of different fields and species. For instance, Vogler et al. helped to resolve some still open questions in plant sexual reproduction by the characterisation of cell wall stiffness of lily and *Arabidopsis* pollen tubes (Fabrice et al., *2018*; Vogler et al., *2013*). Furthermore, in order to provide a comprehensive insight of work input, energy storage and release in plants, cytomechanical studies also helped in the breaking down of the hunting mechanism of the carnivorous Venus flytrap (*Dionaea muscipula*) (Burri et al., *2019*). Finally, to explore the relationship between genetics and cell expansion during germination of the mature *Arabidopsis* embryo, different mathematical models have been produced providing therefore novel considerable information in plant development (Montenegro-Johnson et al., *2015*). These are just some examples of the broad use that plant biomechanics can bring to complex biological studies. Following the principle of the presented multidisciplinary works, which take in account that to investigate the plant mechanical forces is essential to better understand questions related with plant development, we could show that the different mechanical parameters play an important role in the cell wall elongation and that this is specially influenced by the pH of the cell

wall. Through this thesis, we provided an integration of biological studies with engineering technology and physical and mathematical modelling, to show their strong value to better understand the cell elongation through AGT. Indeed, the results obtained in the root model, combining mechanical characterisation together with fluorescent imaging, allowed us to get a novel preliminary insights into the growth regulation of *Brachypodium* roots and to confirm the acid growth in this tissue.

AGT, what is next?

Despite the good combination of the two plant models in this study, the challenges faced during this interdisciplinary project sparkled up the necessity to develop new mutant lines in order to merge the different conclusion obtained when the models were studied independently. Mutants of FER, RALF and LRX in *Brachypodium* would allow a direct comparison of the effects of these proteins between the *Brachypodium* and *Arabidopsis* roots. The different derived phenotypes could be easily characterised by the use of the LOC device, which would allow us, in parallel, to properly track and analyse the effect of the addition of the RALF synthetic peptides during the different developmental stages of the *Brachypodium* roots. The effects of these mutants and the addition of external RALF peptides on auxin levels in both the WT and the *Bdtar2l* mutant will help to better understand the AGT. On the other hand, the study of the different phytohormones in the different plant models and how they affect the cell wall acidification specifically must be performed. Thus, the generation of mutants for specific key genes involved in the biosynthesis of the different phytohormones together with their external addition and the analysis of the different lines proposed, grown under different pH conditions, may be the solution to better understand the AGT from a much broader point of view.

According to our work, the development of new tools for mechanical characterisations at the micro-scale and the new imaging techniques developed, helped us to provide deeper information about the AGT. However, it is appreciable that further experiments are needed to clarify the real role of auxin and the pH according to our study. To this end, a higher application of a combination of genetic, physiological, biochemical, and biophysical approaches for comparative tests of WT and *Bdtar21* mutants are required. Therefore, it is essential to measure the pH of the WT and the *Bdtar2l* mutants under the different conditions already applied like acidic pH (pH 3) and hight concentration of IAA. Furthermore, new lines with the already explained DR5-auxin

reporter system together with new genetically encoded pH probes, like the novo pH-Lemon, for example, a fluorescent protein-based pH reporter already shown to be useful for acidic compartments (Burgstaller et al., *2019*), can provide with a deeper perception of the specific function of auxin *in vivo* to analyse the AGT in a more defined manner. Indeed, it would be interesting to cross these lines with the already existing *Bdtar2l*, to analyse their response under the application of different CFM's compression forces. This experiment would help to acquire a better knowledge of the intracellular auxin expression under tension and to know how the resultant cell wall pH variation can affect the cell wall loosening in a more specific and precise manner. Finally, to fully answer the still open question whether the AGT is absolute or not in the *Brachypodium* roots, it will be necessary to obtain a bigger comprehensive data set involving more morphological analyses, steady-state transcriptome, cell wall composition, proton pump activity, and cell wall elasticity of the different mutants' elongating cells. Altogether, this will allow us to establish causal links between all these parameters and the auxin activity to deliver a final and conclusive proof of the AGT's applicability to both tissue and single cell elongation. Even if the project seems too ambitious, there are still plenty of questions to resolve, nevertheless our results can always be a good base for further studies.

References

Abel S, Nguyen MD, Theologis A. 1995. The PS-IAA4/5-like family of early auxin-inducible mRNAs in *Arabidopsis thaliana*. *J Mol Biol* **251**:533–549.

Adani F, Papa G, Schievano A, Cardinale G, D'Imporzano G, Tambone F. 2011. Nanoscale structure of the cell wall protecting cellulose from enzyme attack. *Environ Sci Technol* **45**:1107–1113.

Albenne C, Canut H, Hoffmann L, Jamet E. 2014. Plant cell wall proteins: A large body of data, but what about runaways. *Proteomes* **2**:224–242.

Albenne C, Canut H, Jamet E. 2013. Plant cell wall proteomics: The leadership of *Arabidopsis thaliana*. *Front Plant Sci* **4**:111.

Arfsten J, Leupold S, Bradtmöller C, Kampen I, Kwade A. 2010. Atomic force microscopy studies on the nanomechanical properties of *Saccharomyces cerevisiae*. *Colloids Surf B Biointerfaces* **79**:284–290.

Arsuffi G, Braybrook SA. 2017. Acid growth: An ongoing trip. *J Exp Bot* **69**:137–146.

Bacete L, Mélida H, Miedes E, Molina A. 2018. Plant cell wall-mediated immunity: Cell wall changes trigger disease resistance responses. *Plant J* **93**:614–636.

Bao G, Kamm RD, Thomas W, Hwang W, Fletcher DA, Grodzinsky AJ, Zhu C, Mofrad MRK. 2010. Molecular biomechanics: The molecular basis of how forces regulate cellular function. *Mol Cell Biomech* **3**:91–105.

Barbez E, Dünser K, Gaidora A, Lendl T, Busch W. 2017. Auxin steers root cell expansion via apoplastic pH regulation in. *Proc Natl Acad Sci U S A* **114**:E4884–E4893.

Baroux C, Spillane C, Grossniklaus U. 2002. Evolutionary origins of the endosperm in flowering plants. *Genome Biology* **3**:reviews1026.1.

Baskin TI. 2001. On the alignment of cellulose microfibrils by cortical microtubules: A review and a model. *Protoplasma* **215**:150–171.

Bates TR, LYNCH JP. 1996. Stimulation of root hair elongation in *Arabidopsis thaliana* by low phosphorus availability. *Plant, Cell & Environment* **19**:529–538.

Baumberger N, Doesseger B, Guyot R, Diet A, Parsons RL, Clark MA, Simmons MP, Bedinger P, Goff SA, Ringli C, Keller B. 2003. Whole-genome comparison of leucine-rich repeat extensins in *Arabidopsis* and rice. A conserved family of cell wall proteins form a vegetative and a reproductive clade. *Plant Physiol* **131**:1313–1326.

Baumberger N, Ringli C, Keller B. 2001. The chimeric leucine-rich repeat/extensin cell wall protein LRX1 is required for root hair morphogenesis in *Arabidopsis thaliana*. *Genes Dev* **15**:1128–1139.

Beaudoin N, Serizet C, Gosti F, Giraudat J. 2000. Interactions between abscisic acid and ethylene signaling cascades. *Plant Cell* **12**:1103–1115.

Beauzamy L, Nakayama N, Boudaoud A. 2014. Flowers under pressure: Ins and outs of turgor regulation in development. *Ann Bot* **114**:1517–1533.

Bedini A, Mercy L, Schneider C, Franken P, Lucic-Mercy E. 2018. Unraveling the initial plant hormone signaling, metabolic mechanisms and plant defense triggering the endomycorrhizal symbiosis behavior. *Front Plant Sci* **9**:1800.

Behera S, Xu Z, Luoni L, Bonza MC, Doccula FG, De Michelis MI, Morris RJ, Schwarzländer M, Costa A. 2018. Cellular Ca^{2+} signals generate defined pH signatures in plants. *Plant Cell* **30**:2704.

Bellincampi D, Cervone F, Lionetti V. 2014. Plant cell wall dynamics and wall-related susceptibility in plant–pathogen interactions. *Front Plant Sci* **5**:228.

Benjamins R, Scheres B. 2008. Auxin: The looping star in plant development. *Annu Rev Plant Biol* **59**:443–465.

Benkert R, Obermeyer G, Bentrup F-W. 1997. The turgor pressure of growing lily pollen tubes. *Protoplasma* **198**:1–8.

Bidhendi AJ, Geitmann A. 2018. Finite element modeling of shape changes in plant cells. *Plant Physiol* **176**:41.

Birnbaum K, Shasha DE, Wang JY, Jung JW, Lambert GM, Galbraith DW, Benfey PN. 2003. A gene expression map of the *Arabidopsis*; root. *Science* **302**:1956.

Bleckmann A, Alter S, Dresselhaus T. 2014. The beginning of a seed: Regulatory mechanisms of double fertilization. *Front Plant Sci* **5**:452.

Boisson-Dernier A, Franck CM, Lituiev DS, Grossniklaus U. 2015. Receptor-like cytoplasmic kinase MARIS functions downstream of crRLK1L-dependent signaling during tip growth. *Proc Natl Acad Sci U S A* **112**:12211–12216.

Boisson-Dernier A, Kessler SA, Grossniklaus U. 2011. The walls have ears: The role of plant crRLK1Ls in sensing and transducing extracellular signals. *J Exp Bot* **62**:1581–1591.

Boisson-Dernier A, Lituiev D, Nestorova A, Franck C, Thirugnanarajah S, Grossniklaus U. 2013. ANXUR receptor-like kinases coordinate cell wall integrity with growth at the pollen tube tip via NADPH oxidases. *PLOS Biol* **11**:e1001719.

Boisson-Dernier A, Roy S, Kritsas K, Grobei MA, Jaciubek M, Schroeder JI, Grossniklaus U. 2009. Disruption of the pollen-expressed *feronia* homologs *ANXUR* and *ANXUR* triggers pollen tube discharge. *Development* **136**:3279.

Bolduc J-F, Lewis LJ, Aubin C-É, Geitmann A. 2006. Finite-element analysis of geometrical factors in micro-indentation of pollen tubes. *Biomech Model Mechanobiol* **5**:227–236.

Borassi C, Sede AR, Mecchia MA, Salgado Salter JD, Marzol E, Muschietti JP, Estevez JM. 2015. An update on cell surface proteins containing extensin-motifs. *J Exp Bot* **67**:477–487.

Brady JD, Sadler IH, Fry SC. 1996. Di-isodityrosine, a novel tetrametric derivative of tyrosine in plant cell wall proteins: A new potential cross-link. *Biochem J* **315**:323–327.

Braybrook SA, Peaucelle A. 2013. Mechano-chemical aspects of organ formation in *Arabidopsis thaliana*: The relationship between auxin and pectin. *PLOS ONE* **8**:e57813.

Bright G, Fisher G, Rogowska J, Taylor D. 1987. Fluorescence ratio imaging microscopy: Temporal and spatial measurements of cytoplasmic pH. *J Cell Biol* **104**:1019–1033.

Brkljacic J, Grotewold E, Scholl R, Mockler T, Garvin DF, Vain P, Brutnell T, Sibout R, Bevan M, Budak H, Caicedo AL, Gao C, Gu Y, Hazen SP, Holt BF, Hong S-Y, Jordan M, Manzaneda AJ, Mitchell-Olds T, Mochida K, Mur LAJ, Park C-M, Sedbrook J, Watt M, Zheng SJ, Vogel JP. 2011. *Brachypodium* as a model for the grasses: Today and the future. *Plant Physiol* **157**:3.

Burgert I, Keplinger T. 2013. Plant micro- and nanomechanics: Experimental techniques for plant cell-wall analysis. *J Exp Bot* **64**:4635–4649.

Burgstaller S, Bischof H, Gensch T, Stryeck S, Gottschalk B, Ramadani-Muja J, Eroglu E, Rost R, Balfanz S, Baumann A, Waldeck-Weiermair M, Hay JC, Madl T, Graier WF, Malli R. 2019. PH-lemon, a fluorescent protein-based pH reporter for acidic compartments. *ACS Sensors* **4**:883–891.

Burri JT, Vogler H, Munglani G, Läubli NF, Grossniklaus U, Nelson BJ. 2019. A microrobotic system for simultaneous measurement of turgor pressure and cell-wall elasticity of individual growing plant cells. *IEEE Robot Autom Lett* **4**:641–646.

Campbell L, Turner SR. 2017. A comprehensive analysis of RALF proteins in green plants suggests there are two distinct functional groups. *Front Plant Sci* **8**:37.

Capron A, Gourgues M, Neiva LS, Faure J-E, Berger F, Pagnussat G, Krishnan A, Alvarez-Mejia C, Vielle-Calzada J-P, Lee Y-R, Liu B, Sundaresan V. 2008. Maternal control of male-gamete delivery in *Arabidopsis* involves a putative GPI-anchored protein encoded by the *LORELEI* gene. *Plant Cell* **20**:3038.

Carlsson A, Yilmaz J, Green A, Stymne S, Hofvander P. 2011. Replacing fossil oil with fresh oil - with what and for what. *Eur J Lipid Sci Technol* **113**:812–831.

Carol RJ, Takeda S, Linstead P, Durrant MC, Kakesova H, Derbyshire P, Drea S, Zarsky V, Dolan L. 2005. A rhoGDP dissociation inhibitor spatially regulates growth in root hair cells. *Nature* **438**:1013–1016.

Catalá C, Rose JK, Bennett AB. 2000. Auxin-regulated genes encoding cell wall-modifying proteins are expressed during early tomato fruit growth. *Plant Physiol* **122**:527–534.

Chadwick AV, Burg SP. 1967. An explanation of the inhibition of root growth caused by indole-3-acetic acid. *Plant Physiol* **42**:415–420.

Chebli Y, Kaneda M, Zerzour R, Geitmann A. 2012. The cell wall of the *Arabidopsis* pollen tube—spatial distribution, recycling, and network formation of polysaccharides. *Plant Physiol* **160**:1940.

Chen J, Yu F, Liu Y, Du C, Li X, Zhu S, Wang X, Lan W, Rodriguez PL, Liu X, Li D, Chen L, Luan S. 2016. FERONIA interacts with ABI2-type phosphatases to facilitate signaling cross-talk between abscisic acid and RALF peptide in *Arabidopsis*. *Proc Natl Acad Sci U S A* **113**:E5519.

Chen W, Gong P, Guo J, Li H, Li R, Xing W, Yang Z, Guan Y. 2018. Glycolysis regulates pollen tube polarity via rho GTPase signaling. *PLOS Genet* **14**:e1007373.

Chen Y, Yordanov YS, Ma C, Strauss S, Busov VB. 2013. DR5 as a reporter system to study auxin response in populus. *Plant Cell Rep* **32**:453–463.

Cheng W, Chiang M, Hwang S, Lin P. 2009. Antagonism between abscisic acid and ethylene in *Arabidopsis* acts in parallel with the reciprocal regulation of their metabolism and signaling pathways. *Plant Mol Biol* **71**:61–80.

Cheng Y, Zhao Y. 2007. A role for auxin in flower development. *Journal of Integrative Plant Biology* **49**:99–104.

Cosgrove DJ. 2018. Diffuse growth of plant cell walls. *Plant Physiol Plant physiology* **176**:16–27.

Cosgrove DJ. 2015. Plant cell wall extensibility: Connecting plant cell growth with cell wall structure, mechanics, and the action of wall-modifying enzymes. *J Exp Bot* **67**:463–476.

Cosgrove DJ. 2014. Plant cell growth and elongation eLS. American Cancer Society.

Cosgrove DJ. 2005. Growth of the plant cell wall. *Nat Rev Mol Cell Biol* **6**:850–861.

Cosgrove DJ. 2000. Loosening of plant cell walls by expansins. *Nature* **407**:321–326.

Cosgrove DJ. 1997. ASSEMBLY AND ENLARGEMENT OF THE PRIMARY CELL WALL IN PLANTS. *Annu Rev Cell Dev Biol* **13**:171–201.

Cosgrove DJ. 1993. Wall extensibility: Its nature, measurement and relationship to plant cell growth. *New Phytol* **124**:1–23.

Cosgrove DJ, Van Volkenburgh E, Cleland RE. 1984. Stress relaxation of cell walls and the yield threshold for growth. *Planta* **162**:46–54.

Dashek WV, Rosen WG. 1966. Electron microscopical localization of chemical components in the growth zone of lily pollen tubes. *Protoplasma* **61**:192–204.

Deng Y, Sun M, Shaevitz JW. 2011. Direct measurement of cell wall stress stiffening and turgor pressure in live bacterial cells. *Phys Rev Lett* **107**:158101.

Draper J, Mur LAJ, Jenkins G, Ghosh-Biswas GC, Bablak P, Hasterok R, Routledge APM. 2001. *Brachypodium distachyon*; a new model system for functional genomics in grasses. *Plant Physiol* **127**:1539.

Duan Q, Kita D, Johnson EA, Aggarwal M, Gates L, Wu H-M, Cheung AY. 2014. Reactive oxygen species mediate pollen tube rupture to release sperm for fertilization in *Arabidopsis*. *Nat Commun* **5**:3129.

Duan Q, Kita D, Li C, Cheung A, Wu H. 2010. FERONIA receptor-like kinase regulates RHO GTPase signaling of root hair development. *Proc Natl Acad Sci U S A* **107**:17821–17826.

Durand-Smet P, Chastrette N, Guiroy A, Richert A, Berne-Dedieu A, Szecsi J, Boudaoud A, Frachisse J-M, Bendahmane M, Hamant O, Asnacios A. 2014. A comparative mechanical analysis of plant and animal cells reveals convergence across kingdoms. *Biophys J* **107**:2237–2244.

Dünser K, Gupta S, Herger A, Feraru MI, Ringli C, Kleine-Vehn J. 2019. Extracellular matrix sensing by FERONIA and leucine-rich repeat extensins controls vacuolar expansion during cellular elongation in *Arabidopsis thaliana*. *EMBO J* **38**:e100353.

Escobar-Restrepo J-M, Huck N, Kessler S, Gagliardini V, Gheyselinck J, Yang W-C, Grossniklaus U. 2007. The FERONIA receptor-like kinase mediates male-female interactions during pollen tube reception. *Science* **317**:656.

Evans ML, Mulkey TJ, Vesper MJ. 1980. Auxin action on proton influx in corn roots and its correlation with growth. *Planta* **148**:510–512.

Fabrice TN, Vogler H, Draeger C, Munglani G, Gupta S, Herger AG, Knox P, Grossniklaus U, Ringli C. 2018. LRX proteins play a crucial role in pollen grain and pollen tube cell wall development. *Plant Physiol* **176**:1981.

Farrokhi N, Burton RA, Brownfield L, Hrmova M, Wilson SM, Bacic A, Fincher GB. 2006. Plant cell wall biosynthesis: Genetic, biochemical and functional genomics approaches to the identification of key genes. *Plant Biotechnology Journal* **4**:145–167.

Fauver D, Dunaway L, Lilienfeld DH, Craighead HG, Pollack GH. 1998. Microfabricated cantilevers for measurement of subcellular and molecular forces. *IEEE Transactions on Biomedical Engineering* **45**:891–898.

Fayant P, Girlanda O, Chebli Y, Aubin C-E, Villemure I, Geitmann A. 2010. Finite element model of polar growth in pollen tubes. *Plant Cell* **22**:2579–2593.

Feiguelman G, Fu Y, Yalovsky S. 2018. ROP GTPases structure-function and signaling pathways. *Plant Physiol* **176**:57–79.

Felekis D, Muntwyler S, Vogler H, Beyeler F, Grossniklaus U, Nelson BJ. 2011. Quantifying growth mechanics of living, growing plant cells in situ using microbotics. *Micro & Nano Letters* **6**:311–316.

Felekis D, Vogler H, Mecja G, Muntwyler S, Nestorova A, Huang T, Sakar MS, Grossniklaus U, Nelson BJ. 2015. Real-time automated characterization of 3D morphology and mechanics of developing plant cells. *Int J Rob Res* **34**:1136–1146.

Fendrych M, Leung J, Friml J. 2016. TIR1/AFB-aux/IAA auxin perception mediates rapid cell wall acidification and growth of *Arabidopsis* hypocotyls. *Elife* **5**:e19048.

Feng W, Kita D, Peaucelle A, Cartwright HN, Doan V, Duan Q, Liu M-C, Maman J, Steinhorst L, Schmitz-Thom I, Yvon R, Kudla J, Wu H-M, Cheung AY, Dinneny JR. 2018. The FERONIA receptor kinase maintains cell-wall integrity during salt stress through Ca^{2+} signaling. *Curr Biol* **28**:666–675.e5.

Fraeye I, Colle I, Vandevenne E, Duvetter T, Van Buggenhout S, Moldenaers P, Van Loey A, Hendrickx M. 2010. Influence of pectin structure on texture of pectin–calcium gels. *Innovative Food Science & Emerging Technologies* **11**:401–409.

Franck CM, Westermann J, Boisson-Dernier A. 2017. Imaging Ca^{2+} dynamics in wild-type and NADPH oxidase-deficient mutant pollen tubes with yellow cameleon and confocal laser scanning microscopy plant germline development: Methods and protocols In: Schmidt A, editor. New York, NY: Springer New York. pp. 103–116.

Franck CM, Westermann J, Bürssner S, Lentz R, Lituiev DS, Boisson-Dernier A. 2018. The protein phosphatases ATUNIS1 and ATUNIS2 regulate cell wall integrity in tip-growing cells. *Plant Cell* **30**:1906.

Franks PJ. 2003. Use of the pressure probe in studies of stomatal function. *J Exp Bot* **54**:1495–1504.

Fry SC. 1982. Isodityrosine, a new cross-linking amino acid from plant cell-wall glycoprotein. *Biochem J* **204**:449–455.

Galindo-Trigo S, Blanco-Touriñán N, DeFalco TA, Wells ES, Gray JE, Zipfel C, Smith LM. 2020. CrRLK1L receptor-like kinases HERK1 and ANJEA are female determinants of pollen tube reception. *EMBO Rep* **21**:e48466.

Gallavotti A, Yang Y, Schmidt RJ, Jackson D. 2008. The relationship between auxin transport and maize branching. *Plant Physiol* **147**:1913.

García-Muniz N, Martínez-Izquierdo JA, Puigdomènech P. 1998. Induction of mRNA accumulation corresponding to a gene encoding a cell wall hydroxyproline-rich glycoprotein by fungal elicitors. *Plant Mol Biol* **38**:623–632.

Gälweiler L, Guan C, Müller A, Wisman E, Mendgen K, Yephremov A, Palme K. 1998. Regulation of polar auxin transport by atPIN1 in *Arabidopsis*; vascular tissue. *Science* **282**:2226.

Ge Z, Bergonci T, Zhao Y, Zou Y, Du S, Liu M-C, Luo X, Ruan H, García-Valencia LE, Zhong S, Hou S, Huang Q, Lai L, Moura DS, Gu H, Dong J, Wu H-M, Dresselhaus T, Xiao J, Cheung AY, Qu L-J. 2017. *Arabidopsis*; pollen tube integrity and sperm release are regulated by RALF-mediated signaling. *Science* **358**:1596.

Geitmann A. 2006. Experimental approaches used to quantify physical parameters at cellular and subcellular levels. *Am J Bot* **93**:1380–1390.

Geitmann A, Parre E. 2004. The local cytomechanical properties of growing pollen tubes correspond to the axial distribution of structural cellular elements. *Sex Plant Reprod* **17**:9–16.

Ghassemian M, Nambara E, Cutler S, Kawaide H, Kamiya Y, McCourt P. 2000. Regulation of abscisic acid signaling by the ethylene response pathway in *Arabidopsis*. *Plant Cell* **12**:1117–1126.

Gigli-Bisceglia N, Engelsdorf T, Hamann T. 2019. Plant cell wall integrity maintenance in model plants and crop species-relevant cell wall components and underlying guiding principles. *Cellular and Molecular Life Sciences*.

Gilroy S, Jones DL. 2000. Through form to function: Root hair development and nutrient uptake. *Trends Plant Sci* **5**:56–60.

Gish LA, Clark SE. 2011. The RLK/pelle family of kinases. *Plant J* **66**:117–127.

Gjetting SK, Ytting CK, Schulz A, Fuglsang AT. 2012. Live imaging of intra- and extracellular pH in plants using pHusion, a novel genetically encoded biosensor. *J Exp Bot* **63**:3207–3218.

Gonneau M, Desprez T, Martin M, Doblas VG, Bacete L, Miart F, Sormani R, Hématy K, Renou J, Landrein B, Murphy E, Van De Cotte B, Vernhettes S, De Smet I, Höfte H. 2018. Receptor kinase THESEUS1 is a rapid alkalinization factor 34 receptor in *Arabidopsis*. *Curr Biol* **28**:2452–2458.e4.

Guo X, Qin Q, Yan J, Niu Y, Huang B, Guan L, Li Y, Ren D, Li J, Hou S. 2015. TYPE-ONE PROTEIN PHOSPHATASE4 regulates pavement cell interdigitation by modulating PIN-FORMED1 polarity and trafficking in *Arabidopsis*. *Plant Physiol* **167**:1058.

Hager A, Menzel H, Krauss A. 1971. Versuche und hypothese zur primärwirkung des auxins beim streckungswachstum. *Planta* **100**:47–75.

Hamant O, Heisler MG, Jönsson H, Krupinski P, Uyttewaal M, Bokov P, Corson F, Sahlin P, Boudaoud A, Meyerowitz EM, Couder Y, Traas J. 2008. Developmental patterning by mechanical signals in *Arabidopsis*. *Science* **322**:1650.

Haruta M, Sabat G, Stecker K, Minkoff BB, Sussman MR. 2014. A peptide hormone and its receptor protein kinase regulate plant cell expansion. *Science* **343**:408–411.

Herger A, Gupta S, Kadler G, Franck CM, Boisson-Dernier A, Ringli C. 2019. LRR-extensins of vegetative tissues are a functionally conserved family of RALF1 receptors interacting with the receptor kinase FERONIA. *bioRxiv* 783266.

Herrero M, Hormaza JI. 1996. Pistil strategies controlling pollen tube growth. *Sex Plant Reprod* **9**:343–347.

Hématy K, Sado P-E, Van Tuinen A, Rochange S, Desnos T, Balzergue S, Pelletier S, Renou J-P, Höfte H. 2007. A receptor-like kinase mediates the response of *Arabidopsis* cells to the inhibition of cellulose synthesis. *Curr Biol* **17**:922–931.

Hill CB, Cassin A, Keeble-Gagnère G, Doblin MS, Bacic A, Roessner U. 2016. De novo transcriptome assembly and analysis of differentially expressed genes of two barley genotypes reveal root-zone-specific responses to salt exposure. *Sci Rep* **6**:31558.

Hobbie L, Estelle M. 1995. The axr4 auxin-resistant mutants of *Arabidopsis thaliana* define a gene important for root gravitropism and lateral root initiation. *Plant J* **7**:211–220.

Hocq L, Pelloux J, Lefebvre V. 2017. Connecting homogalacturonan-type pectin remodeling to acid growth. *Trends Plant Sci* **22**:20–29.

Hohmann U, Lau K, Hothorn M. 2017. The structural basis of ligand perception and signal activation by receptor kinases. *Annu Rev Plant Biol* **68**:109–137.

Holst G-J van, Varner JE. 1984. Reinforced polyproline II conformation in a hydroxyproline-rich cell wall glycoprotein from carrot root. *Plant Physiol* **74**:247.

Hou Y, Guo X, Cyprys P, Zhang Y, Bleckmann A, Cai L, Huang Q, Luo Y, Gu H, Dresselhaus T, Dong J, Qu L-J. 2016. Maternal ENODLs are required for pollen tube reception in *Arabidopsis*. *Curr Biol* **26**:2343–2350.

Höfte H, Voxeur A. 2017. Plant cell walls. *Curr Biol* **27**:R865–R870.

Hu C, Vogler H, Aellen M, Shamsudhin N, Jang B, Burri JT, Läubli N, Grossniklaus U, Pané S, Nelson BJ. 2017. High precision, localized proton gradients and fluxes generated by a microelectrode device induce differential growth behaviors of pollen tubes. *Lab Chip* **17**:671–680.

Huck N, Moore JM, Federer M, Grossniklaus U. 2003. The *Arabidopsis*; mutant feronia; disrupts the female gametophytic control of pollen tube reception. *Development* **130**:2149.

Hüsken D, Steudle E, Zimmermann U. 1978. Pressure probe technique for measuring water relations of cells in higher plants. *Plant Physiol* **61**:158–163.

Iqbal N, Khan NA, Ferrante A, Trivellini A, Francini A, Khan MIR. 2017. Ethylene role in plant growth, development and senescence: Interaction with other phytohormones. *Front Plant Sci* **8**:475.

Ivanchenko MG, Muday GK, Dubrovsky JG. 2008. Ethylene–auxin interactions regulate lateral root initiation and emergence in *Arabidopsis thaliana*. *Plant J* **55**:335–347.

Jones JDG, Dangl JL. 2006. The plant immune system. *Nature* **444**:323–329.

Jones MB, Finnan J, Hodkinson TR. 2015. Morphological and physiological traits for higher biomass production in perennial rhizomatous grasses grown on marginal land. *GCB Bioenergy* **7**:375–385.

Jung K-H, An G, Ronald PC. 2008. Towards a better bowl of rice: Assigning function to tens of thousands of rice genes. *Nat Rev Genet* **9**:91–101.

Kaya H, Nakajima R, Iwano M, Kanaoka MM, Kimura S, Takeda S, Kawarazaki T, Senzaki E, Hamamura Y, Higashiyama T, Takayama S, Abe M, Kuchitsu K. 2014. Ca^{2+}-activated reactive oxygen species production by *Arabidopsis* rbohh and rbohj is essential for proper pollen tube tip growth. *Plant Cell* **26**:1069.

Keller B, Lamb C. 1989. Specific expression of a novel cell wall hydroxyproline-rich glycoprotein gene in lateral root initiation. *Genes Dev* **3**:1639–1646.

Kende H, Zeevaart JAD. 1997. The five "classical" plant hormones. *Plant Cell* **9**:1197–1210.

Kessler SA, Shimosato-Asano H, Keinath NF, Wuest SE, Ingram G, Panstruga R, Grossniklaus U. 2010. Conserved molecular components for pollen tube reception and fungal invasion. *Science* **330**:968.

Kim JI, Murphy AS, Baek D, Lee S-W, Yun D-J, Bressan RA, Narasimhan ML. 2011. YUCCA6 over-expression demonstrates auxin function in delaying leaf senescence in *Arabidopsis thaliana*. *J Exp Bot* **62**:3981–3992.

Kobe B, Deisenhofer J. 1994. The leucine-rich repeat: A versatile binding motif. *Trends Biochem Sci* **19**:415–421.

Koornneef M, Meinke D. 2010. The development of *Arabidopsis* as a model plant. *Plant J* **61**:909–921.

Kost B, Chua N-H. 2002. The plant cytoskeleton: Vacuoles and cell walls make the difference. *Cell* **108**:9–12.

Krämer U. 2015. Planting molecular functions in an ecological context with *Arabidopsis thaliana*. *Elife* **4**:e06100.

Kroh M, Miki-Hirosige H, Rosen W, Loewus F. 1970. Incorporation of label into pollen tube walls from myoinositol-labeled lilium longiflorum pistils. *Plant Physiol* **45**:92–94.

Kutschera U, Schopfer P. 1985. Evidence against the acid-growth theory of auxin action. *Planta* **163**:483–493.

Kyndt T, Denil S, Haegeman A, Trooskens G, De Meyer T, Van Criekinge W, Gheysen G. 2012. Transcriptome analysis of rice mature root tissue and root tips in early development by massive parallel sequencing. *J Exp Bot* **63**:2141–2157.

Lampugnani ER, Khan GA, Somssich M, Persson S. 2018. Building a plant cell wall at a glance. *J Cell Sci* **131**:jcs207373.

Lassig R, Gutermuth T, Bey TD, Konrad KR, Romeis T. 2014. Pollen tube NAD(P)H oxidases act as a speed control to dampen growth rate oscillations during polarized cell growth. *Plant J* **78**:94–106.

Le Gall H, Philippe F, Domon J-M, Gillet F, Pelloux J, Rayon C. 2015. Cell wall metabolism in response to abiotic stress. *Plants (Basel, Switzerland)* **4**:112–166.

Levin DE. 2005. Cell wall integrity signaling in *Saccharomyces cerevisiae*. *Microbiol Mol Biol Rev* **69**:262.

Li C, Yeh F-L, Cheung AY, Duan Q, Kita D, Liu M-C, Maman J, Luu EJ, Wu BW, Gates L, Jalal M, Kwong A, Carpenter H, Wu H-M. 2015. Glycosylphosphatidylinositol-anchored proteins as chaperones and co-receptors for FERONIA receptor kinase signaling in *Arabidopsis*. *Elife* **4**:e06587.

Li J, Xu H-H, Liu W-C, Zhang X-W, Lu Y-T. 2015. Ethylene inhibits root elongation during alkaline stress through AUXIN1 and associated changes in auxin accumulation. *Plant Physiol* **168**:1777–1791.

Li L, Xu Y, Ren Y, Guo Z, Li J, Tong Y, Lin T, Cui D. 2019. Comparative proteomic analysis provides insights into the regulatory mechanisms of wheat primary root growth. *Sci Rep* **9**:11741.

Li S-B, Xie Z-Z, Hu C-G, Zhang J-Z. 2016. A review of auxin response factors (ARFs) in plants. *Front Plant Sci* **7**:47.

Lin D, Lopez-Sanchez P, Gidley MJ. 2015. Binding of arabinan or galactan during cellulose synthesis is extensive and reversible. *Carbohydr Polym* **126**:108–121.

Linhardt RJ, Galliher PM, Cooney CL. 1987. Polysaccharide lyases. *Appl Biochem Biotechnol* **12**:135–176.

Lintilhac PM, Wei C, Tanguay JJ, Outwater JO. 2000. Ball tonometry: A rapid, nondestructive method for measuring cell turgor pressure in thin-walled plant cells. *J Plant Growth Regul* **19**:90–97.

Liu S, Hu Q, Luo S, Li Q, Yang X, Wang X, Wang S. 2015. Expression of wild-type ptrIAA14.1, a poplar aux/IAA gene causes morphological changes in *Arabidopsis*. *Front Plant Sci* **6**:388.

Liu X, Günther Pomorski T, Liesche J. 2019. Non-invasive quantification of cell wall porosity by fluorescence quenching microscopy. *Bio-protocol* **9**:e3344.

Liu X, Wolfe R, Welch LR, Domozych DS, Popper ZA, Showalter AM. 2016a. Bioinformatic identification and analysis of extensins in the plant kingdom. *PLOS ONE* **11**:e0150177.

Liu X, Wolfe R, Welch LR, Domozych DS, Popper ZA, Showalter AM. 2016b. Bioinformatic identification and analysis of extensins in the plant kingdom. *PLOS ONE* **11**:e0150177.

Lüthen H, Bigdon M, Böttger M. 1990. Reexamination of the acid growth theory of auxin action. *Plant Physiol* **93**:931–939.

Lüthen H, Böttger M. 1993. The role of protons in the auxin-induced root growth inhibition - a critical reexamination. *Bot Acta* **106**:58–63.

Ma B, Yin C-C, He S-J, Lu X, Zhang W-K, Lu T-G, Chen S-Y, Zhang J-S. 2014. Ethylene-induced inhibition of root growth requires abscisic acid function in rice (*Oryza sativa L.*). *PLOS Genet* **10**:e1004701.

Mac-Leod RD, Thompson A. 1979. Development of lateral root primordia in vicia faba, pisum sativum, zea mays and phaseolus vulgaris: Rates of primordium formation and cell doubling times. *Ann Bot* **44**:435–449.

Majda M, Robert S. 2018. The role of auxin in cell wall expansion. *Int J Mol Sci* **19**:951.

Marchant A, Kargul J, May ST, Muller P, Delbarre A, Perrot-Rechenmann C, Bennett MJ. 1999. AUX1 regulates root gravitropism in *Arabidopsis* by facilitating auxin uptake within root apical tissues. *EMBO J* **18**:2066–2073.

Márton ML, Cordts S, Broadhvest J, Dresselhaus T. 2005. Micropylar pollen tube guidance by egg apparatus 1 of maize. *Science* **307**:573.

McQueen-Mason S, Durachko DM, Cosgrove DJ. 1992. Two endogenous proteins that induce cell wall extension in plants. *Plant Cell* **4**:1425.

Mecchia MA, Santos-Fernandez G, Duss NN, Somoza SC, Boisson-Dernier A, Gagliardini V, Martínez-Bernardini A, Fabrice TN, Ringli C, Muschietti JP, Grossniklaus U. 2017. RALF4/19 peptides interact with LRX proteins to control pollen tube growth in. *Science* **358**:1600–1603.

Merz D, Richter J, Gonneau M, Sanchez-Rodriguez C, Eder T, Sormani R, Martin M, Hématy K, Höfte H, Hauser M-T. 2017. T-DNA alleles of the receptor kinase THESEUS1 with opposing effects on cell wall integrity signaling. *J Exp Bot* **68**:4583–4593.

Michard E, Simon AA, Tavares B, Wudick MM, Feijó JA. 2017. Signaling with ions: The keystone for apical cell growth and morphogenesis in pollen tubes. *Plant Physiol* **173**:91.

Mittler R, Blumwald E. 2015. The roles of ROS and ABA in systemic acquired acclimation. *Plant Cell* **27**:64–70.

Miyazaki S, Murata T, Sakurai-Ozato N, Kubo M, Demura T, Fukuda H, Hasebe M. 2009. ANXUR1 and 2, sister genes to FERONIA/SIRENE, are male factors for coordinated fertilization. *Curr Biol* **19**:1327–1331.

Molendijk AJ, Bischoff F, Rajendrakumar CSV, Friml J, Braun M, Gilroy S, Palme K. 2001. *Arabidopsis thaliana* rop GTPases are localized to tips of root hairs and control polar growth. *EMBO J* **20**:2779–2788.

Moloney MM, Elliott MC, Cleland RE. 1981. Acid growth effects in maize roots: Evidence for a link between auxin-economy and proton extrusion in the control of root growth. *Planta* **152**:285–291.

Montenegro-Johnson TD, Stamm P, Strauss S, Topham AT, Tsagris M, Wood ATA, Smith RS, Bassel GW. 2015. Digital single-cell analysis of plant organ development using 3DCellAtlas. *Plant Cell* **27**:1018.

Moore JP, Vicré-Gibouin M, Farrant JM, Driouich A. 2008. Adaptations of higher plant cell walls to water loss: Drought vs desiccation. *Physiol Plant* **134**:237–245.

Moore R, Davids N, Friedenberg R. 1969. Study of a biological model of membrane function by finite element analysis. *Biosystems Mathematical Modelling and Analysis of Biological Systems* **3**:156–168.

Morato do Canto A, Ceciliato PHO, Ribeiro B, Ortiz Morea FA, Franco Garcia AA, Silva-Filho MC, Moura DS. 2014. Biological activity of nine recombinant atRALF peptides: Implications for their perception and function in *Arabidopsis*. *Plant Physiology and Biochemistry* **75**:45–54.

Moreno-Ortega B, Fort G, Muller B, Guédon Y. 2017. Identifying developmental zones in maize lateral root cell length profiles using multiple change-point models. *Front Plant Sci* **8**:1750.

Moubayidin L, Di Mambro R, Sozzani R, Pacifici E, Salvi E, Terpstra I, Bao D, Dijken A van, Dello Ioio R, Perilli S, Ljung K, Benfey PN, Heidstra R, Costantino P, Sabatini S. 2013. Spatial coordination between stem cell activity and cell differentiation in the root meristem. *Dev Cell* **26**:405–415.

Moussu S, Broyart C, Santos-Fernandez G, Augustin S, Wehrle S, Grossniklaus U, Santiago J. 2020. Structural basis for recognition of RALF peptides by LRX proteins during pollen tube growth. *Proc Natl Acad Sci USA* **117**:7494.

Muntwyler SD. 2010. Microforce-sensing probes and methodologies for micromechanical and dimensional metrology (PhD thesis). ETH.

Murphy E, De Smet I. 2014. Understanding the RALF family: A tale of many species. *Trends Plant Sci* **19**:664–671.

Müller DJ, Dufrêne YF. 2008. Atomic force microscopy as a multifunctional molecular toolbox in nanobiotechnology. *Nature Nanotechnology* **3**:261–269.

Nakamura AM, Nascimento AS, Polikarpov I. 2017. Structural diversity of carbohydrate esterases. *Biotechnology Research and Innovation* **1**:35–51.

Ngo QA, Vogler H, Lituiev DS, Nestorova A, Grossniklaus U. 2014. A calcium dialog mediated by the FERONIA signal transduction pathway controls plant sperm delivery. *Dev Cell* **29**:491–500.

Obroucheva NV, Antipova OV, Gorbova EN, Kotova LM. 1995. Relationship between initiation of cell elongation and cell division in radicles of germinating seeds. *Plant Soil* **173**:311–316.

Okuda S, Tsutsui H, Shiina K, Sprunck S, Takeuchi H, Yui R, Kasahara RD, Hamamura Y, Mizukami A, Susaki D, Kawano N, Sakakibara T, Namiki S, Itoh K, Otsuka K, Matsuzaki M, Nozaki H, Kuroiwa T, Nakano A, Kanaoka MM, Dresselhaus T, Sasaki N, Higashiyama T. 2009. Defensin-like polypeptide LUREs are pollen tube attractants secreted from synergid cells. *Nature* **458**:357–361.

Overly CC, Lee KD, Berthiaume E, Hollenbeck PJ. 1995. Quantitative measurement of intraorganelle pH in the endosomal-lysosomal pathway in neurons by using ratiometric imaging with pyranine. *Proc Natl Acad Sci USA* **92**:3156.

Pablo P de. 2018. Atomic force microscopy of virus shells. *Semin Cell Dev Biol* **73**:199–208.

Pacheco-Villalobos D, Díaz-Moreno SM, Schuren A van der, Tamaki T, Kang YH, Gujas B, Novak O, Jaspert N, Li Z, Wolf S, Oecking C, Ljung K, Bulone V, Hardtke CS. 2016. The effects of high steady state auxin levels on root cell elongation in *Brachypodium*. *Plant Cell* **28**:1009.

Pacheco-Villalobos D, Sankar M, Ljung K, Hardtke C. 2013. Disturbed local auxin homeostasis enhances cellular anisotropy and reveals alternative wiring of auxin-ethylene crosstalk in *Brachypodium distachyon* seminal roots. *PLOS Genet* **9**:e1003564.

Paque S, Weijers D. 2016. Q&A: Auxin: The plant molecule that influences almost anything. *BMC Biology* **14**:67.

Paredez AR, Somerville CR, Ehrhardt DW. 2006. Visualization of cellulose synthase demonstrates functional association with microtubules. *Science* **312**:1491.

Park YB, Cosgrove DJ. 2015. Xyloglucan and its interactions with other components of the growing cell wall. *Plant Cell Physiol* **56**:180–194.

Park YB, Cosgrove DJ. 2012. Changes in cell wall biomechanical properties in the xyloglucan-deficient *xxt1/xxt2* mutant of *Arabidopsis*. *Plant Physiol* **158**:465.

Parre E, Geitmann A. 2005. More than a leak sealant. The mechanical properties of callose in pollen tubes. *Plant Physiol* **137**:274.

Passardi F, Penel C, Dunand C. 2004. Performing the paradoxical: How plant peroxidases modify the cell wall. *Trends Plant Sci* **9**:534–540.

Pearce G, Moura DS, Stratmann J, Ryan J C A. 2001. RALF, a 5-kDa ubiquitous polypeptide in plants, arrests root growth and development. *Proc Natl Acad Sci U S A* **98**:12843–12847.

Pierre-Jerome E, Jang SS, Havens KA, Nemhauser JL, Klavins E. 2014. Recapitulation of the forward nuclear auxin response pathway in yeast. *Proc Natl Acad Sci U S A* **111**:9407.

Pieruschka R, Lawson T. 2015. Phenotyping in plants. Preface. *J Exp Bot* **66**:5385–5387.

Popp J, Lakner Z, Harangi-Rákos M, Fári M. 2014. The effect of bioenergy expansion: Food, energy, and environment. *Renewable and Sustainable Energy Reviews* **32**:559–578.

Qin Q, Wang W, Guo X, Yue J, Huang Y, Xu X, Li J, Hou S. 2014. *Arabidopsis* DELLA protein degradation is controlled by a type-one protein phosphatase, TOPP4. *PLOS Genet* **10**:e1004464.

Rayle DL, Cleland R. 1977. Chapter 6 control of plant cell enlargement by hydrogen ions current topics in developmental biology In: Moscona AA, Monroy A, editors. 11. Academic Press. pp. 187–214.

Rayle DL, Cleland R. 1970. Enhancement of wall loosening and elongation by acid solutions. *Plant Physiol* **46**:250.

Rayle DL, Cleland RE. 1992. The acid growth theory of auxin-induced cell elongation is alive and well. *Plant Physiol* **99**:1271.

Read SM, Bacic A. 1996. Cell wall porosity and its determination plant cell wall analysis In: Linskens HF, Jackson JF, editors. Berlin, Heidelberg: Springer Berlin Heidelberg. pp. 63–80.

Reinhardt D, Mandel T, Kuhlemeier C. 2000. Auxin regulates the initiation and radial position of plant lateral organs. *Plant Cell* **12**:507–518.

Ridley BL, O'Neill MA, Mohnen D. 2001. Pectins: Structure, biosynthesis, and oligogalacturonide-related signaling. *Phytochemistry* **57**:929–967.

Ringli C. 2010. Monitoring the outside: Cell wall-sensing mechanisms. *Plant Physiol* **153**:1445.

Robinson S, Huflejt M, Barbier de Reuille P, Braybrook S, Schorderet M, Reinhardt D, Kuhlemeier C. 2017. An automated confocal micro-extensometer enables in vivo quantification of mechanical properties with cellular resolution. *Plant Cell* **29**:2959–2973.

Routier-Kierzkowska A-L, Weber A, Kochova P, Felekis D, Nelson BJ, Kuhlemeier C, Smith RS. 2012. Cellular force microscopy for in vivo measurements of plant tissue mechanics. *Plant Physiol* **158**:1514–1522.

Růzicka K, Ljung K, Vanneste S, Podhorská R, Beeckman T, Friml J, Benková E. 2007. Ethylene regulates root growth through effects on auxin biosynthesis and transport-dependent auxin distribution. *Plant Cell* **19**:2197–2212.

Sarabia LD, Boughton BA, Rupasinghe T, Callahan DL, Hill CB, Roessner U. 2020. Comparative spatial lipidomics analysis reveals cellular lipid remodelling in different developmental zones of barley roots in response to salinity. *Plant, cell & environment* **43**:327–343.

Sánchez-Rodríguez C, Rubio-Somoza I, Sibout R, Persson S. 2010. Phytohormones and the cell wall in *Arabidopsis* during seedling growth. *Trends Plant Sci* **15**:291–301.

Schoenaers S, Balcerowicz D, Breen G, Hill K, Zdanio M, Mouille G, Holman TJ, Oh J, Wilson MH, Nikonorova N, Vu LD, De Smet I, Swarup R, De Vos WH, Pintelon I, Adriaensen D, Grierson C, Bennett MJ, Vissenberg K. 2018. The auxin-regulated crRLK1L kinase ERULUS controls cell wall composition during root hair tip growth. *Curr Biol* **28**:722–732.e6.

Schoenaers S, Balcerowicz D, Costa A, Vissenberg K. 2017. The kinase ERULUS controls pollen tube targeting and growth in *Arabidopsis thaliana*. *Front Plant Sci* **8**:1942.

Schopfer P. 2006. Biomechanics of plant growth. *Am J Bot* **93**:1415–1425.

Schopfer P. 1989. PH-dependence of extension growth in *Avena* coleoptiles and its implications for the mechanism of auxin action. *Plant Physiol* **90**:202.

Shih H-W, Miller ND, Dai C, Spalding EP, Monshausen GB. 2014. The receptor-like kinase FERONIA is required for mechanical signal transduction in *Arabidopsis* seedlings. *Curr Biol* **24**:1887–1892.

Shirsat AH, Bell A, Spence J, Harris JN. 1996. The brassica napus extA extensin gene is expressed in regions of the plant subject to tensile stresses. *Planta* **199**:618–624.

Shiu S-H, Bleecker AB. 2001. Receptor-like kinases from *Arabidopsis* form a monophyletic gene family related to animal receptor kinases. *Proc Natl Acad Sci USA* **98**:10763.

Showalter AM, Keppler BD, Liu X, Lichtenberg J, Welch LR. 2016. Bioinformatic identification and analysis of hydroxyproline-rich glycoproteins in populus trichocarpa. *BMC Plant Biol* **16**:229.

Smith AE, Moxham KE, Middelberg APJ. 1998. On uniquely determining cell–wall material properties with the compression experiment. *Chem Eng Sci* **53**:3913–3922.

Smyth D. 1990. *Arabidopsis thaliana*: A model plant for studying the molecular basis of morphogenesis. *Functional Plant Biol* **17**:323–331.

Spartz AK, Ren H, Park MY, Grandt KN, Lee SH, Murphy AS, Sussman MR, Overvoorde PJ, Gray WM. 2014. SAUR inhibition of PP2C-d phosphatases activates plasma membrane H+-ATPases to promote cell expansion in *Arabidopsis*. *Plant Cell* **26**:2129.

Spatz HC, Speck T, Vogellehner D. 1990. Contributions to the biomechanics of plants.; II. Stability against local buckling in hollow plant stems. *Bot Acta* **103**:123–130.

Stegmann M, Monaghan J, Smakowska-Luzan E, Rovenich H, Lehner A, Holton N, Belkhadir Y, Zipfel C. 2017. The receptor kinase FER is a RALF-regulated scaffold controlling plant immune signaling. *Science* **355**:287.

Stegmann M, Zipfel C. 2017. Complex regulation of plant sex by peptides. *Science* **358**:1544.

Stepanova AN, Robertson-Hoyt J, Yun J, Benavente LM, Xie D-Y, Doležal K, Schlereth A, Jürgens G, Alonso JM. 2008. TAA1-mediated auxin biosynthesis is essential for hormone crosstalk and plant development. *Cell* **133**:177–191.

Sun Y, Nelson BJ. 2002. Biological cell injection using an autonomous microrobotic system. *Int J Rob Res* **21**:861–868.

Swarup R, Friml J, Marchant A, Ljung K, Sandberg G, Palme K, Bennett M. 2001. Localization of the auxin permease AUX1 suggests two functionally distinct hormone transport pathways operate in the *Arabidopsis* root apex. *Genes Dev* **15**:2648–2653.

Szymanski DB. 2009. Plant cells taking shape: New insights into cytoplasmic control. *Curr Opin Plant Biol* **12**:735–744.

Takahashi K, Hayashi K-i, Kinoshita T. 2012. Auxin activates the plasma membrane H+-ATPase by phosphorylation during hypocotyl elongation in *Arabidopsis*. *Plant Physiol* **159**:632–641.

Takeuchi H, Higashiyama T. 2012. A species-specific cluster of defensin-like genes encodes diffusible pollen tube attractants in *Arabidopsis*. *PLOS Biol* **10**:e1001449.

Tao Y, Ferrer J-L, Ljung K, Pojer F, Hong F, Long JA, Li L, Moreno JE, Bowman ME, Ivans LJ, Cheng Y, Lim J, Zhao Y, Ballaré CL, Sandberg G, Noel JP, Chory J. 2008. Rapid synthesis of auxin via a new tryptophan-dependent pathway is required for shade avoidance in plants. *Cell* **133**:164–176.

Thor K. 2019. Calcium—nutrient and messenger. *Front Plant Sci* **10**:440.

Tomos AD, Leigh RA. 1999. THE PRESSURE PROBE: A versatile tool in plant cell physiology. *Annu Rev Plant Physiol Plant Mol Biol* **50**:447–472.

Underwood W. 2012. The plant cell wall: A dynamic barrier against pathogen invasion. *Front Plant Sci* **3**:85.

Vaseva II, Qudeimat E, Potuschak T, Du Y, Genschik P, Vandenbussche F, Van Der Straeten D. 2018. The plant hormone ethylene restricts *Arabidopsis* growth via the epidermis. *Proc Natl Acad Sci U S A* **115**:E4130.

Vaughan-Hirsch J, Goodall B, Bishopp A. 2018. North, east, south, west: Mapping vascular tissues onto the arabidopsis root. *Curr Opin Plant Biol* **41**:16–22.

Verbelen J-P, De Cnodder T, Le J, Vissenberg K, Baluska F. 2006. The root apex of *Arabidopsis thaliana* consists of four distinct zones of growth activities: Meristematic zone,

transition zone, fast elongation zone and growth terminating zone. *Plant Signal Behav* **1**:296–304.

Vincken J-P, Schols HA, Oomen RJFJ, McCann MC, Ulvskov P, Voragen AGJ, Visser RGF. 2003. If homogalacturonan were a side chain of rhamnogalacturonan i. Implications for cell wall architecture. *Plant Physiol* **132**:1781.

Vogler H. 2017. An introduction to male germline development plant germline development: Methods and protocols In: Schmidt A, editor. New York, NY: Springer New York. pp. 3–15.

Vogler H, Draeger C, Weber A, Felekis D, Eichenberger C, Routier-Kierzkowska A, Boisson-Dernier A, Ringli C, Nelson B, Smith R, Grossniklaus U. 2013. The pollen tube: A soft shell with a hard core. *Plant J* **73**:617–627.

Vogler H, Felekis D, Nelson JB, Grossniklaus U. 2015. Measuring the mechanical properties of plant cell walls. *Plants (Basel)* **4**.

Vogler H, Santos-Fernandez G, Mecchia MA, Grossniklaus U. 2019. To preserve or to destroy, that is the question: The role of the cell wall integrity pathway in pollen tube growth. *Curr Opin Plant Biol* **52**:131–139.

Volotovski I, Sokolovsky S, Molchan O, Knight M. 1998. Second messengers mediate increases in cytosolic calcium in tobacco protoplasts. *Plant Physiol* **117**:1023–1030.

Voxeur A, Höfte H. 2016. Cell wall integrity signaling in plants: "To grow or not to grow that's the question". *Glycobiology* **26**:950–960.

Wang CX, Wang L, Thomas CR. 2004. Modelling the mechanical properties of single suspension-cultured tomato cells. *Ann Bot* **93**:443–453.

Wang R, Jiao Q-Y, Wei D-Q. 2006. Mechanical response of single plant cells to cell poking: A numerical simulation model. *Journal of Integrative Plant Biology* **48**:700–705.

Weber A, Braybrook S, Huflejt M, Mosca G, Routier-Kierzkowska A-L, Smith RS. 2015. Measuring the mechanical properties of plant cells by combining micro-indentation with osmotic treatments. *J Exp Bot* **66**:3229–3241.

Wei C, Lintilhac PM, Tanguay JJ. 2001. An insight into cell elasticity and load-bearing ability. Measurement and theory. *Plant Physiol* **126**:1129.

Wei C, Steudle E, Tyree MT, Lintilhac PM. 2001. The essentials of direct xylem pressure measurement. *Plant, Cell & Environment* **24**:549–555.

Weijers D, Wagner D. 2016. Transcriptional responses to the auxin hormone. *Annu Rev Plant Biol* **67**:539–574.

Willats WGT, McCartney L, Mackie W, Knox JP. 2001. Pectin: Cell biology and prospects for functional analysis. *Plant Mol Biol* **47**:9–27.

Witzany G. 2006. Plant communication from biosemiotic perspective: Differences in abiotic and biotic signal perception determine content arrangement of response behavior. Context determines meaning of meta-, inter- and intraorganismic plant signaling. *Plant Signal Behav* **1**:169–178.

Wolf S, Hématy K, Höfte H. 2012. Growth control and cell wall signaling in plants. *Annu Rev Plant Biol* **63**:381–407.

Wolf-Dieter R. 1998. The molecular analysis of cell wall components. *Trends Plant Sci* **3**:27–32.

Won C, Shen X, Mashiguchi K, Zheng Z, Dai X, Cheng Y, Kasahara H, Kamiya Y, Chory J, Zhao Y. 2011. Conversion of tryptophan to indole-3-acetic acid by TRYPTOPHAN AMINOTRANSFERASES OF *ARABIDOPSIS* and YUCCAs in *Arabidopsis*. *Proc Natl Acad Sci U S A* **108**:18518–18523.

Wong HL, Pinontoan R, Hayashi K, Tabata R, Yaeno T, Hasegawa K, Kojima C, Yoshioka H, Iba K, Kawasaki T, Shimamoto K. 2007. Regulation of rice NADPH oxidase by binding of Rac GTPase to its N-terminal extension. *Plant Cell* **19**:4022.

Wu J-Z, Lin Y, Zhang X-L, Pang D-W, Zhao J. 2008. IAA stimulates pollen tube growth and mediates the modification of its wall composition and structure in torenia fournieri. *J Exp Bot* **59**:2529–2543.

Wycoff KL, Powell PA, Gonzales RA, Corbin DR, Lamb C, Dixon RA. 1995. Stress activation of a bean hydroxyproline-rich glycoprotein promoter is superimposed on a pattern of tissue-specific developmental expression. *Plant Physiol* **109**:41.

Xiao Y, Stegmann M, Han Z, DeFalco TA, Parys K, Xu L, Belkhadir Y, Zipfel C, Chai J. 2019. Mechanisms of RALF peptide perception by a heterotypic receptor complex. *Nature* **572**:270–274.

Yang T, Wang L, Li C, Liu Y, Zhu S, Qi Y, Liu X, Lin Q, Luan S, Yu F. 2015. Receptor protein kinase FERONIA controls leaf starch accumulation by interacting with glyceraldehyde-3-phosphate dehydrogenase. *Biochem Biophys Res Commun* **465**:77–82.

Yin C, Wu Q, Zeng H, Xia K, Xu J, Li R. 2011. Endogenous auxin is required but supraoptimal for rapid growth of rice (*Oryza sativa L.*) seminal roots, and auxin inhibition of rice seminal root growth is not caused by ethylene. *J Plant Growth Regul* **30**:20–29.

Yu C, Sun C, Shen C, Wang S, Liu F, Liu Y, Chen Y, Li C, Qian Q, Aryal B, Geisler M, Jiang DA, Qi Y. 2015. The auxin transporter, osAUX1, is involved in primary root and root hair elongation and in cd stress responses in rice (*Oryza sativa L.*). *Plant J* **83**:818–830.

Yuan W, Zhang D, Song T, Xu F, Lin S, Xu W, Li Q, Zhu Y, Liang J, Zhang J. 2017. *Arabidopsis* plasma membrane H+-ATPase genes *AHA2* and *AHA7* have distinct and overlapping roles in the modulation of root tip H+ efflux in response to low-phosphorus stress. *J Exp Bot* **68**:1731–1741.

Zamir EA, Taber LA. 2004. On the effects of residual stress in microindentation tests of soft tissue structures. *Journal of Biomechanical Engineering* **126**:276–283.

Zhang T, Mahgsoudy-Louyeh S, Tittmann B, Cosgrove DJ. 2014. Visualization of the nanoscale pattern of recently-deposited cellulose microfibrils and matrix materials in never-dried primary walls of the onion epidermis. *Cellulose* **21**:853–862.

Zhao C, Zayed O, Yu Z, Jiang W, Zhu P, Hsu C-C, Zhang L, Tao WA, Lozano-Durán R, Zhu J-K. 2018. Leucine-rich repeat extensin proteins regulate plant salt tolerance in. *Proc Natl Acad Sci U S A* **115**:13123–13128.

Zhao Z, Crespi VH, Kubicki JD, Cosgrove DJ, Zhong L. 2014. Molecular dynamics simulation study of xyloglucan adsorption on cellulose surfaces: Effects of surface hydrophobicity and side-chain variation. *Cellulose* **21**:1025–1039.

Zheng Z, Guo Y, Novák O, Dai X, Zhao Y, Ljung K, Noel J, Chory J. 2013. Coordination of auxin and ethylene biosynthesis by the aminotransferase VAS1. *Nat Chem Biol* **9**:244–246.

6 Chapter 6 - Appendix

6.1 Introduction

As more members of the 'RALF-FER artery' are being discovered while writing this thesis, it is important to summarise all the different players known till the date for the CWI maintenance in tip-growing plant cells. So, the next chapter is a perfect actualised review which touch the rest of the main characters of this interesting route. This remains entirely important since, as the reader has already realised and can compare bellow, the RALF-CrRLK1L module and some of the components working up- and downstream are conserved in many other developmental and physiological signaling processes. Furthermore, in addition to this, chapters 2 and 3's supplemental material can be also found to close an interesting travel which has taken me the 5 years of my research career in order to help in the better understanding of the total comprehension of the AGT.

Available online at www.sciencedirect.com

ScienceDirect

Current Opinion in Plant Biology

To preserve or to destroy, that is the question: the role of the cell wall integrity pathway in pollen tube growth

Hannes Vogler[1], Gorka Santos-Fernandez[1], Martin A Mecchia[1] and Ueli Grossniklaus

In plants, cell-shape is defined by the cell wall, a complex network of polymers located outside the plasma membrane. During cell growth, cell wall properties have to be adjusted, assuring cell expansion without compromising cell integrity. Plasma membrane-located receptors sense cell wall properties, transducing extracellular signals into intracellular cascades through the cell wall integrity (CWI) pathway that, in turn, leads to adjustments in the regulation and composition of the cell wall. Using pollen tube growth as a single celled model system, we describe the importance of RAPID ALKALINIZATION FACTOR (RALF) peptides as sensors of cell wall integrity. RALF peptides can mediate the communication between cell wall components and plasma membrane-localized receptor-like kinases (RLKs) of the *Cr*RLK1L family. The subsequent activation of intracellular pathways regulates H^+, Ca^{2+}, and ROS levels in the cell and apoplast, thereby modulating cell wall integrity. Interestingly, the RALF-*Cr*RLK1L module and some of the components working up- and downstream of the RLK is conserved in many other developmental and physiological signaling processes.

Address
Department of Plant and Microbial Biology and Zurich-Basel Plant Science Center, University of Zurich, Zollikerstrasse 107, 8008 Zurich, Switzerland

Corresponding author: Grossniklaus, Ueli (grossnik@botinst.uzh.ch)
[1] These authors contributed equally to this review.

Current Opinion in Plant Biology 2019, **52**:131–139

This review comes from a themed issue on **Cell biology**

Edited by **Eva Benkova** and **Yasin Dagdas**

https://doi.org/10.1016/j.pbi.2019.09.002

Introduction

A pollen tube's life is stressful. On the way to deliver its cargo, the two sperm cells, to the ovule, it has to find the right direction while dealing with many obstacles. Therefore, the perception and processing of extracellular signals, chemical and mechanical, is of great importance for pollen tubes to successfully perform their tasks. In about half the flowering plant taxa, the challenge starts right after the pollen grain lands on the stigma. Molecularly diverse self-incompatibility systems preclude 'self' pollen from fertilization by preventing germination or by inhibiting pollen tube growth in the pistil [1,2]. Once a pollen grain has been accepted as suitable, the pollen tube germinates and starts growing through the pistil into the stylar tissue towards the ovary. In the ovary, the pollen tube grows within a specialized tissue, the transmitting tract, from which it eventually exits and finds its way to the micropylar opening of a receptive ovule. As the pollen tube enters the micropyle, it encounters the synergid cells of the female gametophyte, and an extended cross-talk involving receptor-like kinase-mediated signaling and calcium (Ca^{2+}) oscillations ensures that, under normal conditions, only one pollen tube enters the ovule, eventually leading to successful double fertilization [3–6].

Several peptide signaling factors have been identified that are crucial for guiding the pollen tube through the different tissues and to actively modulate its growth. The most prominent pollen tube guidance molecules are the LURE proteins [7,8]. Rapid ALkalinization Factor (RALF) is the new kid on the block. The RALFs comprise a large family of peptides that lead to the alkalinization of the growth medium and modulate cell expansion through the cell wall integrity (CWI) pathway [9]. The pollen tube cell wall with its astonishing properties allowing extremely rapid tip growth plays a central role for successful fertilization. Not only does it act as a barrier between the cell and the extracellular environment to control the exchange of molecules, its mechanical properties also determine the growth behavior of the pollen tube via the CWI pathway. Here, we discuss selected, recent findings that shed light onto the mechanisms underlying the CWI pathway in pollen tubes.

The cell wall acts as an interface between extracellular and intracellular signaling

Plant cell walls are mainly composed of the polysaccharides cellulose, hemicelluloses, and pectins, resulting in a high tensile strength but also providing enough flexibility for cell expansion. The cell wall needs to be flexible enough to permit rapid growth yet preserve its integrity while defying mechanical adversities. During the rapid growth of pollen tubes, which elongate exclusively at their tip, the cell wall needs to remain intact while navigating through the different female tissues. However, at the end of its journey upon successful pollen tube

reception, it must burst to release the two sperm cells. Without rupture, double fertilization will not take place. Therefore, a growing pollen tube lives on the edge with the risk of premature bursting. Turgor pressure drives cell expansion at the tip by putting the cell wall under stress. As a consequence, there is a wall thinning phase, which needs to be compensated by the delivery of new cell wall material via the exocytotic pathway. If these processes are out of phase, the pollen tube would either lyse due to overthinning or experience growth arrest due to overthickening of the cell wall. In the yeast *Saccharomyces pombe*, Davì *et al.* used an original approach to measure the dynamics of growth-induced cell wall thinning and could show that thickening negatively influenced growth [10]. To avoid this, a fine-tuned balance between cell wall synthesis and turgor-driven expansion is crucial. Such a mechanism must constantly sense the status of the cell wall and trigger intracellular physiological and biochemical responses that signal back to the cell wall. A CWI pathway has been postulated a while ago [11,12] and the cytoplasmic components have been identified, but the ligand and the link between cell wall and plasma membrane stayed elusive until very recently.

In addition to the polysaccharide network, the cell wall contains proteins that were thought to have a largely structural function, like reinforcing bars used to give concrete a higher tensile strength. However, it became clear that they are much more than that and play an important role in the perception and transduction of extracellular signals. Among these proteins, the LEUCINE-RICH REPEAT EXTENSINs (LRXs) attracted much attention, because they were recently identified as a central element of the CWI pathway [13•]. Pollen tube-expressed LRX8, LRX10, and LRX11 have been shown to directly interact with RALF4 *in planta* (and RALF19 in a yeast two-hybrid system) [14••]. Both LRXs and RALFs are secreted by the pollen tube, indicating autocrine signaling to explore the extracellular environment. Genetic and biochemical evidence implies a connection of RALF4/19 with ANXUR1 (ANX1), ANX2, BUDDHA'S PAPER SEAL1 (BUPS1), and BUPS2,

Figure 1

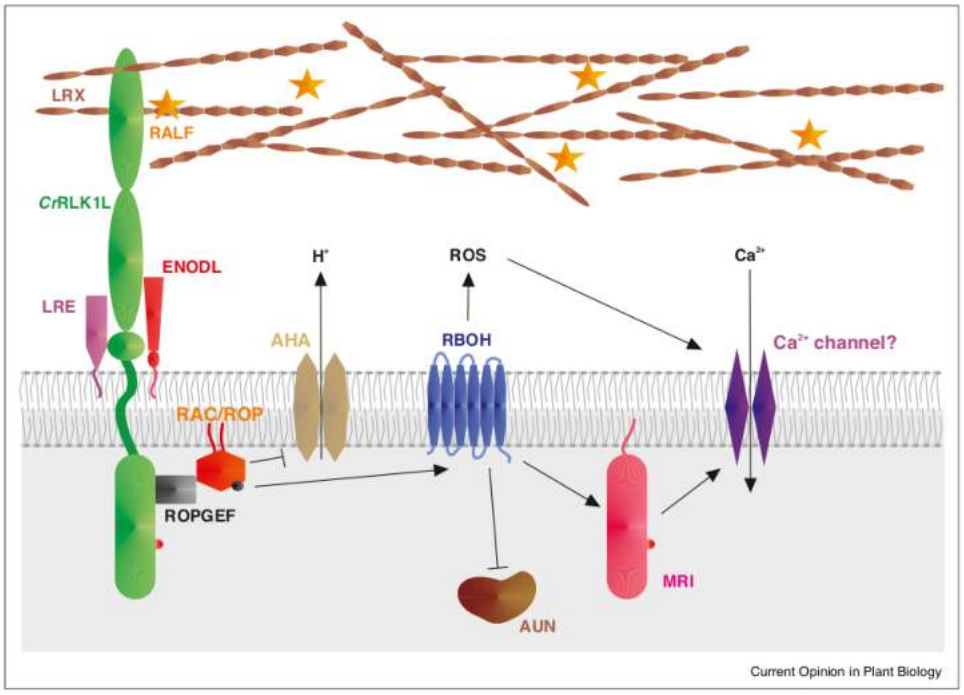

Schematic representation of cell wall sensing by RAPID ALKALINIZATION FACTORs (RALFs) and downstream signaling components.
Cell-wall LRX proteins are recognized by RALF peptides, sensing alterations in the cell wall. To activate intracellular signaling pathways, they form a complex with *Cr*RLK1L receptors and LRE/LLG co-receptors, inducing autophosphorylation of the *Cr*RLK1L intracellular domain. Through signaling via ROPGEFs and RAC/ROPs, H^+-ATPases (AHA), Ca^{2+} channels, and NADPH oxidases (RBOHs) are activated, which can modify cell wall properties by controlling H^+, Ca^{2+} and ROS levels, respectively. Moreover, *Cr*RLK1L can activate intracellular phosphatases of the ATUNIS (AUN) family and cytoplasmic receptor-like kinases like MARIS (MRI).

which are all members of the *Catharanthus roseus* RECEPTOR-LIKE KINASE1-LIKE (*Cr*RLK1L) family, thereby providing a link between extracellular and intracellular signaling [14••,15••] (Figure 1).

Transducing signals across the membrane

During pollen tube growth, LRX protein dimers are required for the sensing of RALF peptides to control pollen tube integrity [14••,16]. Mutations in pollen-expressed LRX proteins lead to premature bursting of the pollen tubes [13•,17,18], similar to what is observed when downregulating the pollen-specific RALF4/19 peptides [14••,15••]. Recently, it was shown that LRX-RALF interactions are also relevant for abiotic stress control and plant growth regulation [19•,20•], pointing out the importance of RALF peptides as signaling molecules that sense changes in the cell wall. RALFs are small peptides that alkalinize the culture medium of cells in suspension culture and repress growth if added to the growth medium [21]. Being present throughout the plant kingdom [21], they coordinate cell wall-related processes, like polarized cell growth, leaf and root growth, and innate immunity [14••,15••,19•,20•,22,23]. RALFs are secreted as proRALF polypeptides and processed by SITE-1 PROTEASE (S1P), releasing mature 5 kDa RALF peptides into the apoplast [24]. Once in the apoplast, RALF peptides can act as an autocrine signal, like the pollen tube-expressed RALF4/19 peptides [14••,15••], or as a paracrine signal, like ovule-expressed RALF34, which regulates pollen tube integrity [15••]. It was reported that RALF1 binds the extracellular domain of FERONIA (FER) and activates a phosphorylation cascade that represses H^+-ATPase activity, thereby increasing the extracellular (apoplastic) pH and reducing cell elongation in the root [22,25]. FER belongs to the *Cr*RLK1L subfamily of receptor-like kinases (RLKs), key regulators involved in sensing cell wall changes occurring during development or induced by environmental stimuli [22,26–31]. *Cr*RLK1Ls are transmembrane receptors with an extracellular domain, consisting of one or two malectin-like domains [32], a transmembrane domain, and a cytoplasmic Ser/Thr kinase domain [27,33] (Figure 1). FER can also directly interact with LRX4, controlling cell expansion, suggesting the formation of an LRX4/RALF1/FER complex, linking the cell wall with components of signal transduction across the membrane [19•] (Table 1). Similar to FER, THESEUS1 (THE1) interacts with RALF34 to control pericycle divisions during lateral root initiation [27,34], and during pollen tube growth, several RALF and *Cr*RLK1L members are implied in controlling cell wall stiffness and integrity. Pollen-expressed RALF4/19 peptides interact with the pollen-specific *Cr*RLK1L receptors ANX1, ANX2, BUPS1, and BUPS2 [15••,26,28], assuring proper pollen tube elongation at the tip. However, when a pollen tube enters the micropyle to reach the female gametophyte, ovule-expressed RALF34 was reported to compete with RALF4/19 for binding to the ANX1/2 and BUPS1/2 RLKs, inducing pollen tube rupture and the release of the two sperm cells for fertilization [15••]. Although FER is expressed in all tissues analyzed except for pollen, it also regulates pollen tube integrity during fertilization [33]. When a pollen tube approaches the synergid cells of the female gametophyte, the accumulation of reactive oxygen species (ROS) and Ca^{2+} oscillations are induced in a FER-dependent manner, which is important for the dialogue between the receptive synergid and the pollen tube, eventually leading to pollen tube rupture [5,33,35]. LORELEI (LRE), a small glycosylphosphatidylinositol (GPI)-anchored protein, is also involved in pollen tube reception and physically interacts with FER, possibly acting as chaperone during transport through the endomembrane system, but also, importantly, as a co-receptor of FER [36–38]. Similarly, during vegetative development LORELEI-LIKE GPI-ANCHORED PROTEIN 1 (LLG1), the closest relative of LRE, collaborates with the FER RLK [37,39] (Figure 1) by forming a RALF23-mediated complex, as recently shown [40]. Finally, a functionally redundant set of five ovule-expressed EARLY NODULIN-LIKE PROTEINs (ENODLs),

Table 1

Conservation of the RALF-*Cr*RLK1L signaling module in different contexts of plant development and physiology

Gene family	Reproduction	Root development	Cell expansion	Biotic/abiotic stress
LRX	LRX8-11 [13•,14••,16–18]	LRX1/2 [66,67]	LRX2-4 [19•,68]	LRX3/4/5 [20•]
RALF	RALF4/19 [14••,15••,16]	RALF1 [22,69–71]	RALF1 [19•]	RALF22/23 [20•,23,24,40]
	RALF34 [15••]	RALF34 [34]	RALF17/23/32/33 [23]	F-RALF [72]
*Cr*RLK1L	ANX1/2 [15••,26,28]	FER [22,45]	FER [19•,37,76,77]	FER [20•,22,23,25,40,72,77,80–82]
	BUPS1/2 [15••]	ERU [22,75]	THE [27,78]	MEDOS1/2/3/4 [29]
	FER [33,73,74]	THE [34]	HERK1 [76]	ANX1/2 [83]
			CVY [79]	
LRE	LRE [36,39]	LLG1 [37]	LLG1 [37]	LLG1 [40,84]
ROP	ROP1 [85]	ROP2/4 [45,50]	ROP2/4/6 [86,87]	
RBOH	RBOHH/J [52,54]	RBOHC [45,88,89]	RBOHD/F [90]	RBOHD/F [91–93]
MARIS	MRI [62,94]	MRI [62,94]		
ENODL	EN14 [41]			
ATUNIS	AUN1/2 [63••]	AUN1/2 [63••]		

encompassing a GPI anchor motif, a plastocyanin-like domain, and an arabinogalactan glycomodule, are required for pollen tube reception. In a yeast two-hybrid system and GST pull-down assays, ENODL14 interacts with the juxta-membrane region of FER [41], but it is unknown whether ENODLs also play a role in other *Cr*RLK1L-mediated processes (Figure 1).

Intracellular signaling events involve second messengers and protein (de)phosphorylation

Upon reception of the signals in the CWI pathway, intracellular events are triggered involving downstream effectors that are slowly being uncovered. In eukaryotes, small GTPases of the Ras and Rho subfamilies form molecular switches in many signal transduction cascades. In plants, there are no small G-proteins of the Ras family but the Rho family is represented by Rho of Plants (ROP) proteins also referred to as RACs [42,43]. In tip-growing root hairs, RAC/ROP proteins interact with ROP-GUANINE NUCLEOTIDE EXCHANGE FACTORs (GEFs), which switch between an inactive GDP-bound and an active GTP-bound state, to regulate the tip growth [44]. ROP-GEF1, in turn, was shown to bind to FER in yeast two-hybrid and bimolecular fluorescence complementation assays [45] (Figure 1). In roots, this eventually results in activating plasma membrane H^+-ATPases of the AHA family [46] (Table 1),which are essential to control the membrane potential and to power ion transport across the plasma membrane in order to maintain polar growth of tip growing cells [47,48].

Signal transduction processes usually rely on second messengers, small molecules like nitric oxide, ROS, and Ca^{2+}, whose levels and spatiotemporal patterns are specifically altered by external signals. These so-called signatures are detected and interpreted by the cell to elicit specific downstream responses. Both Ca^{2+} and ROS have been implicated in *Cr*RLK1L-mediated signaling; while the Ca^{2+}-channels involved have not yet been identified, ROS-producing NADPH oxidases known as RESPIRATORY BURST OXIDASE HOMOLOGUEs (Rbohs) [49], are direct targets of RAC/ROP G-proteins [37,50,51]. The genome of the model plant *Arabidopsis thaliana* contains 10 *Rboh* genes with versatile functions, with *RbohH* and *RbohJ* having been implicated in the ANX1/2 pathway regulating pollen tube growth [52–54] (Figure 1). Double mutant *rbohH rbohJ* pollen tubes show reduced ROS levels and an unsteady tip-focused Ca^{2+} gradient [52,54]. While this indicates that Ca^{2+} channels may be regulated by ROS levels, the cross-regulatory interactions between ROS, Ca^{2+}, and H^+ in controlling pollen tube growth are complex and need to be dissected further [52–56].

Plant RLKs often function as homodimers or heterodimers and can interact with receptor-like cytoplasmic kinases (RLCKs), which lack extracellular domains, to induce distinct responses in various processes during pollen tube growth. [57]. On the one hand, the RLCKs LOST IN POLLEN TUBE GUIDANCE1 (LIP1) and LIP2 are involved in the pollen tube's response to AtLURE1, a cysteine-rich peptide involved in pollen tube guidance [58,59]. LIP1/2 interact with the tip-localized POLLEN-SPECIFIC RECEPTOR-LIKE KINASE 6 (PRK6), one of the AtLURE1 receptors [60,61], and thus potentially underly receptor complex activation during pollen tube guidance to the micropyle. On the other hand, the RLCK MARIS (MRI) is directly involved in the control of CWI (Figure 1). A constitutively active form of MRI (MRI^{R240C}, *mri-3D*), which was identified in a suppressor screen of the *anx1/2* double mutant, acts as a positive regulator of RALF4/19-ANX1/2-dependent pollen tube growth and can suppress male sterility caused by RALF4/19 downregulation [14••] as well as the bursting phenotype observed in *rbohj/h* double mutant pollen tubes [62]. In contrast, *mri-3D* fails to suppress the reduced fertility of *lrx8/9/10/11* quadruple mutants [63••], suggesting that the intracellular response mediated by the ANX1/2 RLKs splits into distinct pathways in the regulation of pollen tube growth. Interestingly, expression of the mutant MRI^{R240C} protein can also suppress the bursting root hair phenotype observed in *fer* mutants, demonstrating that MRI acts downstream of diverse members of the *Cr*RLK1L family in the CWI pathway [62].

In the same *anx1/2* suppressor screen, the *atunis1* (*aun1*) mutant was recovered, rendering a member of the TYPE ONE PROTEIN PHOSPHATASE (TOPP) family inactive. AUN1 and its closest homolog AUN2 function redundantly as negative regulators of the ANX1/2-dependent CWI pathway [63••]. Genetic experiments showed that the mutant form of AUN1, $AUN1^{D94N}$, can suppress diverse mutants of the pollen tube CWI pathway, placing AUN1/2 downstream of LRX 8/9/10/11, RALF4/19, ANX1/2, and RbohH/J, but not of MRI [63••] (Figure 1). Thus, it was proposed that the AUN1/2 phosphatases may counterbalance the kinase activity of MRI and/or regulate the phosphorylation status of common or different target proteins to regulate pollen tube growth [63••]. However, how exactly AUN1/2 are activated and which target proteins they dephosophorylate requires further investigations. Moreover, AUN1/2 are localized to both the cytoplasm and the vegetative nucleus of growing pollen tubes, where they may have distinct functions. Indeed, TOPP4, another family member involved in gibberellic acid and auxin signaling, directly interacts with proteins at the plasma membrane and in the nucleus [64,65]. Although many of the players involved in *Cr*RLK1L signaling were initially identified through their role in plant reproduction, they or their homologs were found to play similar roles in diverse processes, including root growth, root hair development, cell expansion, innate immunity, and a variety of biotic

and abiotic stress responses (Table 1). It is thus probably only a matter of time until additional members of the ENODL and TOPP family will be implicated in other *Cr*RLK1L-mediated signaling transduction processes.

Signaling back to the cell wall

Although our knowledge about the regulation of the CWI pathway has increased a lot over the past few years, many interesting questions are still open. For example, it is still unclear how pollen tube rupture is induced once it reaches the embryo sac. The FER-mediated Ca^{2+}-dialogue between the pollen tube and the receptive synergid cell is important for the timely rupture of the pollen tube as in mutants affecting the *FER* pathway in synergids, most pollen tubes do not burst [5]. In maize, the synergid-expressed cysteine-rich protein ZmES4 induces the opening of the intrinsic rectifying K^+-channel KZM1 and it was proposed that K^+ influx leads to water uptake and osmotic burst [95]. However, it is currently unknown how the opening of KZM1 or similar channels is precisely timed during the rapid growth phase of the pollen tube across the receptive synergid cell [5] and whether the CWI pathway of the pollen tube is also affected by other mechanisms leading to pollen tube rupture and the release of the sperm cells.

As mentioned above, it was reported that the addition of RALF34 to growing pollen tubes in culture leads to instantaneous rupture. This indicates that the CWI pathway of the pollen tube is hijacked by ovule-produced RALF34, which competes for the RALF4/19 binding sites on pollen-expressed LRXs and/or *Cr*RLK1Ls, thus inducing rupture at a precise time and place [15••]. Several questions are still open. For instance, how does RALF34, which accumulates in the inner integuments of the ovules, end up on the pollen tube surface and how does the replacement of RALF4/19 with RALF34 disrupt the signaling cascade?

In fact, RALF4/19 being autocrine signals, they may have functions both in signaling the state of the cell wall back to the pollen tube via the ANX1/2 *Cr*RLK1Ls in conjunction with pollen-expressed LRXs, but also signal extracellularly via the LRXs, leading to changes in the pollen tube cell wall (Figure 1). The fact that */rx8/9/10/11* mutant can be suppressed by expression of $AUN1^{D94N}$ but not MRI^{R240C} [14••,16,63••], further indicates a complex CWI pathway that also branches intracellularly.

Finally, it will be interesting to connect mechanosensing with the CWI sensing. Several cues point towards a direct connection of mechanosensing and growth control. MSL8 is a mechanosensitive anion channel localized in the plasma membrane, where it has a proposed function as an osmotic safety valve that regulates turgor pressure. Although it is not required for normal pollen development, it is necessary to respond to osmotic stress [96,97••]. Mechanosensitive OSCA Ca^{2+} channels are another family of genes involved in osmosensing [98–100]. Despite the lack of data from pollen to date, the presence of pollen-specific OSCA family members suggests that they may play a role in germination or the regulation of pollen tube growth. Viewed from the perspective of growth orientation, the concept of a perceptive force has been established in *Arabidopsis* and lily pollen tubes. When growing into an obstacle, the pollen tubes push until they reach a force threshold at which growth stops. After a lag phase, during which the pollen tubes reorient themselves, they resume growth in another direction [101•]. The mechanosensor underlying this behavior is currently unknown. Davì *et al.* found that, in fission yeast, the strain in the cell wall is perceived as a mechanical signal. Rapid cell elongation leads to an increase in the strain rate, which activates cell wall synthesis via the CWI pathway and vice versa. Interestingly, they found the transmembrane protein Wsc1, which via its physical interaction with a Rho-GEF activates a Rho G-protein, to be implicated in cell wall thickness homeostasis, suggesting that it could act as a direct cell wall mechanical sensor [10].

Conflict of interest statement

Nothing declared.

Acknowledgements

We apologize to our colleagues whose work we could not cite due to the focus on recent publications and space constraints. Our work on the cytomechanics of pollen tube growth and *Cr*RLK1L signaling during plant reproduction is supported by the University of Zurich and the Research and Technology Development project MecanX of SystemsX.ch (51RT-0_145676 to U.G.), as well as past and current grants of the Swiss National Science Foundation (CR22I2_166110, 310030B_160336, 31003A_179553 to U.G.)

References and recommended reading

Papers of particular interest, published within the period of review, have been highlighted as:

- • of special interest
- •• of outstanding interest

1. Bedinger PA, Broz AK, Tovar-Mendez A, McClure B: **Pollen-pistil interactions and their role in mate selection**. *Plant Physiol* 2017, **173**:79-90 http://dx.doi.org/10.1104/pp.16.01286.
2. Nasrallah JB: **Plant mating systems: self-incompatibility and evolutionary transitions to self-fertility in the mustard family**. *Curr Opin Genet Dev* 2017, **47**:54-60 http://dx.doi.org/10.1016/j.gde.2017.08.005.
3. Mizuta Y, Higashiyama T: **Chemical signaling for pollen tube guidance at a glance**. *J Cell Sci* 2018, **131** http://dx.doi.org/10.1242/jcs.208447.
4. Kessler SA, Grossniklaus U: **She's the boss: signaling in pollen tube reception**. *Curr Opin Plant Biol* 2011, **14**:622-627 http://dx.doi.org/10.1016/j.pbi.2011.07.012.
5. Ngo QA, Vogler H, Lituiev DS, Nestorova A, Grossniklaus U: **A calcium dialog mediated by the *FERONIA* signal transduction pathway controls plant sperm delivery**. *Dev Cell* 2014, **29**:491-500 http://dx.doi.org/10.1016/j.devcel.2014.04.008.
6. Zhong S, Qu LJ: **Peptide/receptor-like kinase-mediated signaling involved in male-female interactions**. *Curr Opin Plant Biol* 2019, **51**:7-14 http://dx.doi.org/10.1016/j.pbi.2019.03.004.

7. Higashiyama T, Takeuchi H: **The mechanism and key molecules involved in pollen tube guidance**. *Annu Rev Plant Biol* 2015, **66**:393-413 http://dx.doi.org/10.1146/annurev-arplant-043014-115635.

8. Higashiyama T, Yang WC: **Gametophytic pollen tube guidance: attractant peptides, gametic controls, and receptors**. *Plant Physiol* 2017, **173**:112-121 http://dx.doi.org/10.1104/pp.16.01571.

9. Murphy E, De Smet I: **Understanding the RALF family: a tale of many species**. *Trends Plant Sci* 2014, **19**:664-671 http://dx.doi.org/10.1016/j.tplants.2014.06.005.

10. Davì V, Tanimoto H, Ershov D, Haupt A, De Belly H, Le Borgne R, Couturier E, Boudaoud A, Minc N: **Mechanosensation dynamically coordinates polar growth and cell wall assembly to promote cell survival**. *Dev Cell* 2018, **45**:170-182.e7 http://dx.doi.org/10.1016/j.devcel.2018.03.022.

11. Levin DE: **Cell wall integrity signaling in *Saccharomyces cerevisiae***. *Microbiol Mol Biol Rev* 2005, **69**:262-291 http://dx.doi.org/10.1128/MMBR.69.2.262-291.2005.

12. Ringli C: **Monitoring the outside: cell wall-sensing mechanisms**. *Plant Physiol* 2010, **153**:1445-1452 http://dx.doi.org/10.1104/pp.110.154518.

13. • Ndinyanka Fabrice T, Vogler H, Draeger C, Munglani G, Gupta S, Herger AG, Knox P, Grossniklaus U, Ringli C: **LRX proteins play a crucial role in pollen grain and pollen tube cell wall development**. *Plant Physiol* 2018, **176**:1981-1992 http://dx.doi.org/10.1104/pp.17.01374

Together with Sede *et al.* (2018) and Zhao *et al.* (2018), this study reveals that LRX proteins are important players in the regulation of cell wall composition, structure, and mechanical properties.

14. •• Mecchia MA, Santos-Fernandez G, Duss NN, Somoza SC, Boisson-Dernier A, Gagliardini V, Martínez-Bernardini A, Fabrice TN, Ringli C, Muschietti JP, Grossniklaus U: **RALF4/19 peptides interact with LRX proteins to control pollen tube growth in *Arabidopsis***. *Science* 2017, **358**:1600-1603 http://dx.doi.org/10.1126/science.aao5467

Together with Ge *et al.* (2017) this study shows that the redundant RALF4/19 peptides act through the ANX1/2 pathway to control pollen tube growth. Furthermore, it sheds light onto how pollen-expressed LRX proteins affect cell wall properties through their direct interaction with RALF4/19, which serve as an autocrine signal to monitor cell wall integrity.

15. •• Ge Z, Bergonci T, Zhao Y, Zou Y, Du S, Liu M-C, Luo X, Ruan H, García-Valencia LE, Zhong S *et al.*: ***Arabidopsis* pollen tube integrity and sperm release are regulated by RALF-mediated signaling**. *Science* 2017, **358**:1596-1600 http://dx.doi.org/10.1126/science.aao3642

This study, together with the work of Mecchia *et al.* (2017), sheds light on the CWI pathway and shows that, in addition to ANX1/2, also BUPS1/2 are involved in perceiving RALF4/19. Moreover, they report that the addition of ovule-expressed RALF34 leads to the bursting of pollen tubes growing *in vitro*, suggesting that RALF34 displaces RALF4/19 upon arrival of the pollen tube at the ovule.

16. Moussu S, Broyart C, Santos-Fernandez G, Augustin S, Wehrle S, Grossniklaus U, Santiago J: **Structural basis for recognition of RALF peptides by LRX proteins during pollen tube growth**. *BioRxiv* 2019:695874 http://dx.doi.org/10.1101/695874. [Preprint] July 08, 2019 [cited 2019 September 10].

17. Sede AR, Borassi C, Wengier DL, Mecchia MA, Estevez JM, Muschietti JP: ***Arabidopsis* pollen extensins LRX are required for cell wall integrity during pollen tube growth**. *FEBS Lett* 2018, **592**:233-243 http://dx.doi.org/10.1002/1873-3468.12947.

18. Wang X, Wang K, Yin G, Liu X, Liu M, Cao N, Duan Y, Gao H, Wang W, Ge W *et al.*: **Pollen-expressed leucine-rich repeat extensins are essential for pollen germination and growth**. *Plant Physiol* 2018, **176**:1993-2006 http://dx.doi.org/10.1104/pp.17.01241.

19. • Dünser K, Gupta S, Herger A, Feraru MI, Ringli C, Kleine-Vehn J: **Extracellular matrix sensing by FERONIA and leucine-rich repeat extensins controls vacuolar expansion during cellular elongation in *Arabidopsis thaliana***. *EMBO J* 2019:e100353 http://dx.doi.org/10.15252/embj.2018100353

In this publication, a direct link between vegetatively expressed LRX proteins and FER is demonstrated, coordinating the onset of cell wall acidification and loosening with an increase in vacuolar size.

20. • Zhao C, Zayed O, Yu Z, Jiang W, Zhu P, Hsu CC, Zhang L, Tao WA, Lozano-Durán R, Zhu JK: **Leucine-rich repeat extensin proteins regulate plant salt tolerance in *Arabidopsis***. *Proc Natl Acad Sci U S A* 2018, **115**:13123-13128 http://dx.doi.org/10.1073/pnas.1816991115

This study shows that the RALF-LRX interaction previously reported by Mecchia *et al.* (2017) also plays a role in sensing cell-wall signals to regulate plant growth and respond to salt stress.

21. Pearce G, Moura DS, Stratmann J, Ryan CA: **RALF, a 5-kDa ubiquitous polypeptide in plants, arrests root growth and development**. *Proc Natl Acad Sci U S A* 2001, **98**:12843-12847 http://dx.doi.org/10.1073/pnas.201416998.

22. Haruta M, Sabat G, Stecker K, Minkoff BB, Sussman MR: **A peptide hormone and its receptor protein kinase regulate plant cell expansion**. *Science* 2014, **343**:408-411 http://dx.doi.org/10.1126/science.1244454.

23. Stegmann M, Monaghan J, Smakowska-Luzan E, Rovenich H, Lehner A, Holton N, Belkhadir Y, Zipfel C: **The receptor kinase FER is a RALF-regulated scaffold controlling plant immune signaling**. *Science* 2017, **355**:287-289 http://dx.doi.org/10.1126/science.aal2541.

24. Srivastava R, Liu JX, Guo H, Yin Y, Howell SH: **Regulation and processing of a plant peptide hormone, AtRALF23, in *Arabidopsis***. *Plant J* 2009, **59**:930-939 http://dx.doi.org/10.1111/j.1365-313X.2009.03926.x.

25. Chen J, Yu F, Liu Y, Du C, Li X, Zhu S, Wang X, Lan W, Rodriguez PL, Liu X *et al.*: **FERONIA interacts with ABI2-type phosphatases to facilitate signaling cross-talk between abscisic acid and RALF peptide in *Arabidopsis***. *Proc Natl Acad Sci U S A* 2016, **113**:E5519-27 http://dx.doi.org/10.1073/pnas.1608449113.

26. Boisson-Dernier A, Roy S, Kritsas K, Grobei MA, Jaciubek M, Schroeder JI, Grossniklaus U: **Disruption of the pollen-expressed *FERONIA* homologs *ANXUR1* and *ANXUR2* triggers pollen tube discharge**. *Development* 2009, **136**:3279-3288 http://dx.doi.org/10.1242/dev.040071.

27. Hématy K, Sado PE, Van Tuinen A, Rochange S, Desnos T, Balzergue S, Pelletier S, Renou JP, Höfte H: **A receptor-like kinase mediates the response of *Arabidopsis* cells to the inhibition of cellulose synthesis**. *Curr Biol* 2007, **17**:922-931 http://dx.doi.org/10.1016/j.cub.2007.05.018.

28. Miyazaki S, Murata T, Sakurai-Ozato N, Kubo M, Demura T, Fukuda H, Hasebe M: **ANXUR1 and 2, sister genes to FERONIA/SIRENE, are male factors for coordinated fertilization**. *Curr Biol* 2009, **19**:1327-1331 http://dx.doi.org/10.1016/j.cub.2009.06.064.

29. Richter J, Watson JM, Stasnik P, Borowska M, Neuhold J, Berger M, Stolt-Bergner P, Schoft V, Hauser MT: **Multiplex mutagenesis of four clustered *Cr*RLK1L with CRISPR/Cas9 exposes their growth regulatory roles in response to metal ions**. *Sci Rep* 2018, **8**:12182 http://dx.doi.org/10.1038/s41598-018-30711-3.

30. Shih HW, Miller ND, Dai C, Spalding EP, Monshausen GB: **The receptor-like kinase FERONIA is required for mechanical signal transduction in *Arabidopsis* seedlings**. *Curr Biol* 2014, **24**:1887-1892 http://dx.doi.org/10.1016/j.cub.2014.06.064.

31. Stegmann M, Zipfel C: **Complex regulation of plant sex by peptides**. *Science* 2017, **358**:1544-1545 http://dx.doi.org/10.1126/science.aar4190.

32. Boisson-Dernier A, Kessler SA, Grossniklaus U: **The walls have ears: the role of plant *Cr*RLK1Ls in sensing and transducing extracellular signals**. *J Exp Bot* 2011, **62**:1581-1591 http://dx.doi.org/10.1093/jxb/erq445.

33. Escobar-Restrepo JM, Huck N, Kessler S, Gagliardini V, Gheyselinck J, Yang WC, Grossniklaus U: **The FERONIA receptor-like kinase mediates male-female interactions during pollen tube reception**. *Science* 2007, **317**:656-660 http://dx.doi.org/10.1126/science.1143562.

34. Gonneau M, Desprez T, Martin M, Doblas VG, Bacete L, Miart F, Sormani R, Hématy K, Renou J, Landrein B *et al.*: **Receptor kinase THESEUS1 is a RAPID ALKALINIZATION FACTOR34 receptor in *Arabidopsis***. *Curr Biol* 2018, **28**:2452-2458 http://dx.doi.org/10.1016/j.cub.2018.05.075.

35. Duan Q, Kita D, Johnson EA, Aggarwal M, Gates L, Wu HM, Cheung AY: **Reactive oxygen species mediate pollen tube rupture to release sperm for fertilization in *Arabidopsis***. *Nat Commun* 2014, **5**:3129 http://dx.doi.org/10.1038/ncomms4129.

36. Capron A, Gourgues M, Neiva LS, Faure JE, Berger F, Pagnussat G, Krishnan A, Alvarez-Mejia C, Vielle-Calzada JP, Lee YR *et al.*: **Maternal control of male-gamete delivery in *Arabidopsis* involves a putative GPI-anchored protein encoded by the *LORELEI* gene**. *Plant Cell* 2008, **20**:3038-3049 http://dx.doi.org/10.1105/tpc.108.061713.

37. Li C, Yeh F-L, Cheung AY, Duan Q, Kita D, Liu M-C, Maman J, Luu EJ, Wu BW, Gates L *et al.*: **Glycosylphosphatidylinositol-anchored proteins as chaperones and co-receptors for FERONIA receptor kinase signaling in *Arabidopsis***. *eLife* 2015, **4**:e06587 http://dx.doi.org/10.7554/eLife.06587.

38. Liu X, Castro C, Wang Y, Noble J, Ponvert N, Bundy M, Hoel C, Shpak E, Palanivelu R: **The role of LORELEI in pollen tube reception at the interface of the synergid cell and pollen tube requires the modified eight-cysteine motif and the receptor-like kinase FERONIA**. *Plant Cell* 2016, **28**:1035-1052 http://dx.doi.org/10.1105/tpc.15.00703.

39. Tsukamoto T, Qin Y, Huang Y, Dunatunga D, Palanivelu R: **A role for LORELEI, a putative glycosylphosphatidylinositol-anchored protein, in *Arabidopsis thaliana* double fertilization and early seed development**. *Plant J* 2010, **62**:571-588 http://dx.doi.org/10.1111/j.1365-313X.2010.04177.x.

40. Xiao Y, Stegmann M, Han Z, DeFalco TA, Parys K, Xu L, Belkhadir Y, Zipfel C, Chai J: **Mechanisms of RALF peptide perception by a heterotypic receptor complex**. *Nature* 2019, **572**:270-274 http://dx.doi.org/10.1038/s41586-019-1409-7.

41. Hou Y, Guo X, Cyprys P, Zhang Y, Bleckmann A, Cai L, Huang Q, Luo Y, Gu H, Dresselhaus T *et al.*: **Maternal ENODLs are required for pollen tube reception in *Arabidopsis***. *Curr Biol* 2016, **26**:2343-2350 http://dx.doi.org/10.1016/j.cub.2016.06.053.

42. Feiguelman G, Fu Y, Yalovsky S: **ROP GTPases structure-function and signaling pathways**. *Plant Physiol* 2018, **176**:57-79 http://dx.doi.org/10.1104/pp.17.01415.

43. Nibau C, Wu HM, Cheung AY: **RAC/ROP GTPases: 'hubs' for signal integration and diversification in plants**. *Trends Plant Sci* 2006, **11**:309-315 http://dx.doi.org/10.1016/j.tplants.2006.04.003.

44. Molendijk AJ, Bischoff F, Rajendrakumar CS, Friml J, Braun M, Gilroy S, Palme K: ***Arabidopsis thaliana* Rop GTPases are localized to tips of root hairs and control polar growth**. *EMBO J* 2001, **20**:2779-2788 http://dx.doi.org/10.1093/emboj/20.11.2779.

45. Duan Q, Kita D, Li C, Cheung AY, Wu HM: **FERONIA receptor-like kinase regulates RHO GTPase signaling of root hair development**. *Proc Natl Acad Sci U S A* 2010, **107**:17821-17826 http://dx.doi.org/10.1073/pnas.1005366107.

46. Yuan W, Zhang D, Song T, Xu F, Lin S, Xu W, Li Q, Zhu Y, Liang J, Zhang J: ***Arabidopsis* plasma membrane H^+-ATPase genes AHA2 and AHA7 have distinct and overlapping roles in the modulation of root tip H^+ efflux in response to low-phosphorus stress**. *J Exp Bot* 2017, **68**:1731-1741 http://dx.doi.org/10.1093/jxb/erx040.

47. Chen W, Gong P, Guo J, Li H, Li R, Xing W, Yang Z, Guan Y: **Glycolysis regulates pollen tube polarity via Rho GTPase signaling**. *PLoS Genet* 2018, **14**:e1007373 http://dx.doi.org/10.1371/journal.pgen.1007373.

48. Hu C, Vogler H, Aellen M, Shamsudhin N, Jang B, Burri JT, Läubli N, Grossniklaus U, Pané S, Nelson BJ: **High precision, localized proton gradients and fluxes generated by a microelectrode device induce differential growth behaviors of pollen tubes**. *Lab Chip* 2017, **17**:671-680 http://dx.doi.org/10.1039/c6lc01307d.

49. Suzuki N, Miller G, Morales J, Shulaev V, Torres MA, Mittler R: **Respiratory burst oxidases: the engines of ROS signaling**. *Curr Opin Plant Biol* 2011, **14**:691-699 http://dx.doi.org/10.1016/j.pbi.2011.07.014.

50. Carol RJ, Takeda S, Linstead P, Durrant MC, Kakesova H, Derbyshire P, Drea S, Zarsky V, Dolan L: **A RhoGDP dissociation inhibitor spatially regulates growth in root hair cells**. *Nature* 2005, **438**:1013-1016 http://dx.doi.org/10.1038/nature04198.

51. Wong HL, Pinontoan R, Hayashi K, Tabata R, Yaeno T, Hasegawa K, Kojima C, Yoshioka H, Iba K, Kawasaki T, Shimamoto K: **Regulation of rice NADPH oxidase by binding of Rac GTPase to its N-terminal extension**. *Plant Cell* 2007, **19**:4022-4034 http://dx.doi.org/10.1105/tpc.107.055624.

52. Boisson-Dernier A, Lituiev DS, Nestorova A, Franck CM, Thirugnanarajah S, Grossniklaus U: **ANXUR receptor-like kinases coordinate cell wall integrity with growth at the pollen tube tip via NADPH oxidases**. *PLoS Biol* 2013, **11**:e1001719 http://dx.doi.org/10.1371/journal.pbio.1001719.

53. Kaya H, Nakajima R, Iwano M, Kanaoka MM, Kimura S, Takeda S, Kawarazaki T, Senzaki E, Hamamura Y, Higashiyama T *et al.*: **Ca^{2+}-activated reactive oxygen species production by *Arabidopsis* RbohH and RbohJ is essential for proper pollen tube tip growth**. *Plant Cell* 2014, **26**:1069-1080 http://dx.doi.org/10.1105/tpc.113.120642.

54. Lassig R, Gutermuth T, Bey TD, Konrad KR, Romeis T: **Pollen tube NAD(P)H oxidases act as a speed control to dampen growth rate oscillations during polarized cell growth**. *Plant J* 2014, **78**:94-106 http://dx.doi.org/10.1111/tpj.12452.

55. Behera S, Zhaolong X, Luoni L, Bonza MC, Doccula FG, De Michelis MI, Morris RJ, Schwarzländer M, Costa A: **Cellular Ca^{2+} signals generate defined pH signatures in plants**. *Plant Cell* 2018, **30**:2704-2719 http://dx.doi.org/10.1105/tpc.18.00655.

56. Michard E, Simon AA, Tavares B, Wudick MM, Feijó JA: **Signaling with ions: the keystone for apical cell growth and morphogenesis in pollen tubes**. *Plant Physiol* 2017, **173**:91-111 http://dx.doi.org/10.1104/pp.16.01561.

57. Liang X, Zhou JM: **Receptor-like cytoplasmic kinases: central players in plant receptor kinase-mediated signaling**. *Annu Rev Plant Biol* 2018, **69**:267-299 http://dx.doi.org/10.1146/annurev-arplant-042817-040540.

58. Liu J, Zhong S, Guo X, Hao L, Wei X, Huang Q, Hou Y, Shi J, Wang C, Gu H, Qu LJ: **Membrane-bound RLCKs LIP1 and LIP2 are essential male factors controlling male-female attraction in *Arabidopsis***. *Curr Biol* 2013, **23**:993-998 http://dx.doi.org/10.1016/j.cub.2013.04.043.

59. Takeuchi H, Higashiyama T: **A species-specific cluster of defensin-like genes encodes diffusible pollen tube attractants in *Arabidopsis***. *PLoS Biol* 2012, **10**:e1001449 http://dx.doi.org/10.1371/journal.pbio.1001449.

60. Takeuchi H, Higashiyama T: **Tip-localized receptors control pollen tube growth and LURE sensing in *Arabidopsis***. *Nature* 2016, **531**:245-248 http://dx.doi.org/10.1038/nature17413.

61. Wang T, Liang L, Xue Y, Jia PF, Chen W, Zhang MX, Wang YC, Li HJ, Yang WC: **A receptor heteromer mediates the male perception of female attractants in plants**. *Nature* 2016, **531**:241-244 http://dx.doi.org/10.1038/nature16975.

62. Boisson-Dernier A, Franck CM, Lituiev DS, Grossniklaus U: **Receptor-like cytoplasmic kinase MARIS functions downstream of *Cr*RLK1L-dependent signaling during tip growth**. *Proc Natl Acad Sci U S A* 2015, **112**:12211-12216 http://dx.doi.org/10.1073/pnas.1512375112.

63. •• Franck CM, Westermann J, Bürssner S, Lentz R, Lituiev DS, Boisson-Dernier A: **The protein phosphatases ATUNIS1 and ATUNIS2 regulate cell wall integrity in tip-growing cells**. *Plant Cell* 2018, **30**:1906-1923 http://dx.doi.org/10.1105/tpc.18.00284

The AUN1/2 phosphatases were identified as negative regulators of the tip growth in pollen tubes and root hairs. By placing AUN1/2 into the *Cr*RLK1L signaling pathway, the authors show that pollen-expressed LRX proteins and the ANX1/2 *Cr*RLK1Ls function in distinct but converging pathways to fine-tune cell wall integrity.

64. Guo X, Qin Q, Yan J, Niu Y, Huang B, Guan L, Li Y, Ren D, Li J, Hou S: **TYPE-ONE PROTEIN PHOSPHATASE4 regulates pavement cell interdigitation by modulating PIN-FORMED1 polarity and trafficking in *Arabidopsis***. *Plant Physiol* 2015, **167**:1058-1075 http://dx.doi.org/10.1104/pp.114.249904.

65. Qin Q, Wang W, Guo X, Yue J, Huang Y, Xu X, Li J, Hou S: ***Arabidopsis* DELLA protein degradation is controlled by a**

type-one protein phosphatase, TOPP4. *PLoS Genet* 2014, **10**: e1004464 http://dx.doi.org/10.1371/journal.pgen.1004464.

66. Baumberger N, Ringli C, Keller B: **The chimeric leucine-rich repeat/extensin cell wall protein LRX1 is required for root hair morphogenesis in *Arabidopsis thaliana***. *Genes Dev* 2001, **15**:1128-1139 http://dx.doi.org/10.1101/gad.200201.

67. Baumberger N, Doesseger B, Guyot R, Diet A, Parsons RL, Clark MA, Simmons MP, Bedinger P, Goff SA, Ringli C, Keller B: **Whole-genome comparison of leucine-rich repeat extensins in *Arabidopsis* and rice. A conserved family of cell wall proteins form a vegetative and a reproductive clade**. *Plant Physiol* 2003, **131**:1313-1326 http://dx.doi.org/10.1104/pp.102.014928.

68. Draeger C, Ndinyanka Fabrice T, Gineau E, Mouille G, Kuhn BM, Moller I, Abdou MT, Frey B, Pauly M, Bacic A, Ringli C: ***Arabidopsis* leucine-rich repeat extensin (LRX) proteins modify cell wall composition and influence plant growth**. *BMC Plant Biol* 2015, **15**:155 http://dx.doi.org/10.1186/s12870-015-0548-8.

69. Bergonci T, Silva-Filho MC, Moura DS: **Antagonistic relationship between AtRALF1 and brassinosteroid regulates cell expansion-related genes**. *Plant Signal Behav* 2014, **9**:e976146 http://dx.doi.org/10.4161/15592324.2014.976146.

70. Bergonci T, Ribeiro B, Ceciliato PH, Guerrero-Abad JC, Silva-Filho MC, Moura DS: ***Arabidopsis thaliana* RALF1 opposes brassinosteroid effects on root cell elongation and lateral root formation**. *J Exp Bot* 2014, **65**:2219-2230 http://dx.doi.org/10.1093/jxb/eru099.

71. Morato do Canto A, Ceciliato PH, Ribeiro B, Ortiz Morea FA, Franco Garcia AA, Silva-Filho MC, Moura DS: **Biological activity of nine recombinant AtRALF peptides: Implications for their perception and function in *Arabidopsis***. *Plant Physiol Biochem* 2014, **75**:45-54 http://dx.doi.org/10.1016/j.plaphy.2013.12.005.

72. Masachis S, Segorbe D, Turrà D, Leon-Ruiz M, Fürst U, El Ghalid M, Leonard G, López-Berges MS, Richards TA, Felix G, Di Pietro A: **A fungal pathogen secretes plant alkalinizing peptides to increase infection**. *Nat Microbiol* 2016, **1**:16043 http://dx.doi.org/10.1038/nmicrobiol.2016.43.

73. Huck N, Moore JM, Federer M, Grossniklaus U: **The *Arabidopsis* mutant feronia disrupts the female gametophytic control of pollen tube reception**. *Development* 2003, **130**:2149-2159 http://dx.doi.org/10.1242/dev.00458.

74. Rotman N, Rozier F, Boavida L, Dumas C, Berger F, Faure JE: **Female control of male gamete delivery during fertilization in *Arabidopsis thaliana***. *Curr Biol* 2003, **13**:432-443 http://dx.doi.org/10.1016/s0960-9822(03)00093-9.

75. Bai L, Ma X, Zhang G, Song S, Zhou Y, Gao L, Miao Y, Song CP: **A receptor-like kinase mediates ammonium homeostasis and is important for the polar growth of root hairs in *Arabidopsis***. *Plant Cell* 2014, **26**:1497-1511 http://dx.doi.org/10.1105/tpc.114.124586.

76. Guo H, Li L, Ye H, Yu X, Algreen A, Yin Y: **Three related receptor-like kinases are required for optimal cell elongation in *Arabidopsis thaliana***. *Proc Natl Acad Sci U S A* 2009, **106**:7648-7653 http://dx.doi.org/10.1073/pnas.0812346106.

77. Kessler SA, Shimosato-asano H, Keinath NF, Wuest SE, Ingram G, Panstruga R, Grossniklaus U: **Conserved molecular components for pollen tube reception and fungal invasion**. *Science* 2010, **330**:968-971 http://dx.doi.org/10.1126/science.1195211.

78. Merz D, Richter J, Gonneau M, Sanchez-Rodriguez C, Eder T, Sormani R, Martin M, Hématy K, Höfte H, Hauser MT: **T-DNA alleles of the receptor kinase THESEUS1 with opposing effects on cell wall integrity signaling**. *J Exp Bot* 2017, **68**:4583-4593 http://dx.doi.org/10.1093/jxb/erx263.

79. Gachomo EW, Jno Baptiste L, Kefela T, Saidel WM, Kotchoni SO: **The *Arabidopsis CURVY1 (CVY1)* gene encoding a novel receptor-like protein kinase regulates cell morphogenesis, flowering time and seed production**. *BMC Plant Biol* 2014, **14**:221 http://dx.doi.org/10.1186/s12870-014-0221-7.

80. Huang GQ, Li E, Ge FR, Li S, Wang Q, Zhang CQ, Zhang Y: ***Arabidopsis* RopGEF4 and RopGEF10 are important for FERONIA-mediated developmental but not environmental regulation of root hair growth**. *New Phytol* 2013, **200**:1089-1101 http://dx.doi.org/10.1111/nph.12432.

81. Keinath NF, Kierszniowska S, Lorek J, Bourdais G, Kessler SA, Shimosato-Asano H, Grossniklaus U, Schulze WX, Robatzek S, Panstruga R: **PAMP (Pathogen-Associated Molecular Pattern)-induced changes in plasma membrane compartmentalization reveal novel components of plant immunity**. *J Biol Chem* 2010, **285**:39140-39149 http://dx.doi.org/10.1074/jbc.M110.160531.

82. Yang T, Wang L, Li C, Liu Y, Zhu S, Qi Y, Liu X, Lin Q, Luan S, Yu F: **Receptor protein kinase FERONIA controls leaf starch accumulation by interacting with glyceraldehyde-3-phosphate dehydrogenase**. *Biochem Biophys Res Commun* 2015, **465**:77-82 http://dx.doi.org/10.1016/j.bbrc.2015.07.132.

83. Mang H, Feng B, Hu Z, Boisson-Dernier A, Franck CM, Meng X, Huang Y, Zhou J, Xu G, Wang T *et al.*: **Differential regulation of two-tiered plant immunity and sexual reproduction by ANXUR receptor-like kinases**. *Plant Cell* 2017, **29**:3140-3156 http://dx.doi.org/10.1105/tpc.17.00464.

84. Shen Q, Bourdais G, Pan H, Robatzek S, Tang D: ***Arabidopsis* glycosylphosphatidylinositol-anchored protein LLG1 associates with and modulates FLS2 to regulate innate immunity**. *Proc Natl Acad Sci U S A* 2017, **114**:5749-5754 http://dx.doi.org/10.1073/pnas.1614468114.

85. Wu G, Gu Y, Li S, Yang Z: **A genome-wide analysis of *Arabidopsis* Rop-interactive CRIB motif-containing proteins that act as Rop GTPase targets**. *Plant Cell* 2001, **13**:2841-2856 http://dx.doi.org/10.1105/tpc.010218.

86. Fu Y, Gu Y, Zheng Z, Wasteneys G, Yang Z: ***Arabidopsis* interdigitating cell growth requires two antagonistic pathways with opposing action on cell morphogenesis**. *Cell* 2005, **120**:687-700 http://dx.doi.org/10.1016/j.cell.2004.12.026.

87. Xu T, Wen M, Nagawa S, Fu Y, Chen JG, Wu MJ, Perrot-Rechenmann C, Friml J, Jones AM, Yang Z: **Cell surface- and rho GTPase-based auxin signaling controls cellular interdigitation in *Arabidopsis***. *Cell* 2010, **143**:99-110 http://dx.doi.org/10.1016/j.cell.2010.09.003.

88. Foreman J, Demidchik V, Bothwell JH, Mylona P, Miedema H, Torres MA, Linstead P, Costa S, Brownlee C, Jones JD *et al.*: **Reactive oxygen species produced by NADPH oxidase regulate plant cell growth**. *Nature* 2003, **422**:442-446 http://dx.doi.org/10.1038/nature01485.

89. Monshausen GB, Bibikova TN, Messerli MA, Shi C, Gilroy S: **Oscillations in extracellular pH and reactive oxygen species modulate tip growth of *Arabidopsis* root hairs**. *Proc Natl Acad Sci U S A* 2007, **104**:20996-21001 http://dx.doi.org/10.1073/pnas.0708586104.

90. Denness L, McKenna JF, Segonzac C, Wormit A, Madhou P, Bennett M, Mansfield J, Zipfel C, Hamann T: **Cell wall damage-induced lignin biosynthesis is regulated by a reactive oxygen species- and jasmonic acid-dependent process in *Arabidopsis***. *Plant Physiol* 2011, **156**:1364-1374 http://dx.doi.org/10.1104/pp.111.175737.

91. Kwak JM, Mori IC, Pei ZM, Leonhardt N, Torres MA, Dangl JL, Bloom RE, Bodde S, Jones JD, Schroeder JI: **NADPH oxidase *AtrbohD* and *AtrbohF* genes function in ROS-dependent ABA signaling in *Arabidopsis***. *EMBO J* 2003, **22**:2623-2633 http://dx.doi.org/10.1093/emboj/cdg277.

92. Mersmann S, Bourdais G, Rietz S, Robatzek S: **Ethylene signaling regulates accumulation of the FLS2 receptor and is required for the oxidative burst contributing to plant immunity**. *Plant Physiol* 2010, **154**:391-400 http://dx.doi.org/10.1104/pp.110.154567.

93. Torres MA, Dangl JL, Jones JD: ***Arabidopsis* gp91^{phox} homologues *AtrbohD* and *AtrbohF* are required for accumulation of reactive oxygen intermediates in the plant defense response**. *Proc Natl Acad Sci U S A* 2002, **99**:517-522 http://dx.doi.org/10.1073/pnas.012452499.

94. Liao HZ, Zhu MM, Cui HH, Du XY, Tang Y, Chen LQ, Ye, D, Zhang XQ: **MARIS plays important roles in *Arabidopsis* pollen tube and root hair growth**. *J Integr Plant Biol* 2016, **58**:927-940 http://dx.doi.org/10.1111/jipb.12484.

95. Amien S, Kliwer I, Márton ML, Debener T, Geiger D, Becker D, Dresselhaus T: **Defensin-like ZmES4 mediates pollen tube burst in maize via opening of the potassium channel KZM1**. *PLoS Biol* 2010, **8**:e1000388 http://dx.doi.org/10.1371/journal.pbio.1000388.

96. Hamilton ES, Jensen GS, Maksaev G, Katims A, Sherp AM, Haswell ES: **Mechanosensitive channel MSL8 regulates osmotic forces during pollen hydration and germination**. *Science* 2015, **350**:438-441 http://dx.doi.org/10.1126/science.aac6014.

97. •• Hamilton ES, Haswell ES: **The tension-sensitive ion transport activity of MSL8 is critical for its function in pollen hydration and germination**. *Plant Cell Physiol* 2017, **58**:1222-1237 http://dx.doi.org/10.1093/pcp/pcw230

In this study, the authors demonstrate that intact MSL8 channels are crucial for normal pollen function during germination and growth. Following up their previous work reported in Hamilton *et al.* (2015), they establish MSL8 as the first plant mechanosensitive channel that transduces mechanical stimuli into physiological responses.

98. Yuan F, Yang H, Xue Y, Kong D, Ye R, Li C, Zhang J, Theprungsirikul L, Shrift T, Krichilsky B *et al.*: **OSCA1 mediates osmotic-stress-evoked Ca^{2+} increases vital for osmosensing in *Arabidopsis***. *Nature* 2014, **514**:367-371 http://dx.doi.org/10.1038/nature13593.

99. Murthy SE, Dubin AE, Whitwam T, Jojoa-Cruz S, Cahalan SM, Mousavi SAR, Ward AB, Patapoutian A: **OSCA/TMEM63 are an evolutionarily conserved family of mechanically activated ion channels**. *eLife* 2018, **7**:e41844 http://dx.doi.org/10.7554/eLife.41844.

100. Gu X, Wang P, Liu Z, Wang L, Huang Z, Zhang S, Wu J: **Genome-wide identification and expression analysis of the OSCA gene family in *Pyrus bretschneideri***. *Can J Plant Sci* 2018, **98**:918-929 http://dx.doi.org/10.1139/cjps-2017-0115.

101. • Burri JT, Vogler H, Läubli NF, Hu C, Grossniklaus U, Nelson BJ: **Feeling the force: how pollen tubes deal with obstacles**. *New Phytol* 2018, **220**:187-195 http://dx.doi.org/10.1111/nph.15260

Using microfluidic channels and microrobotic force sensors, this study provides evidence that pollen tubes can haptically perceive their environment. After encountering an obstacle, they push against it until a certain force threshold is reached, at which point the pollen tubes stop growing, reorient themselves, and resume growth in a new direction.

www.sciencemag.org/cgi/content/full/science.aao5467/DC1

Supplementary Materials for

RALF4/19 peptides interact with LRX proteins to control pollen tube growth in *Arabidopsis*

Martin A. Mecchia, Gorka Santos-Fernandez, Nadine N. Duss, Sofia C. Somoza, Aurélien Boisson-Dernier, Valeria Gagliardini, Andrea Martínez-Bernardini, Tohnyui Ndinyanka Fabrice, Christoph Ringli, Jorge P. Muschietti,* Ueli Grossniklaus*

*Corresponding author. Email: grossnik@botinst.uzh.ch (U.G.); prometeo@dna.uba.ar (J.P.M.)

Published 14 December 2017 on *Science* First Release
DOI: 10.1126/science.aao5467

This PDF file includes:

Other supplementary material for this manuscript includes the following:

Movies S1 and S2

Materials and Methods

Plant material

Wild-type (WT) plants in all experiments were *Arabidopsis thaliana* L. (Heyn) accession Col-0. The *ralf4-1* mutant (see Table S5) was obtained from the Signal Collection at the Salk Institute (*29*), and the *rbohH/J* double and *lrx* mutants are in the same genetic background and were described previously (*13,23*). Gene identity numbers, allele designations, and stock numbers are summarized in Table S1. Plants were grown in soil (ED73; Universalerde), covered with a thin quartz sand layer, under long photoperiods (16 hs light/8 hs dark) at 23°C and 60% relative humidity.

Genotyping and gene expression analysis

Genotyping PCR reactions for the *ralf4-1* mutant were performed using LP-RALF4 and RP-RALF4 primers for the wild-type *RALF4* allele, whereas RP-RALF4 and LBa1 primers were used for the mutant *ralf4-1* allele (Table S4). Amplified products were analysed by agarose gel electrophoresis.

Total RNA was extracted from indicated *Arabidopsis* tissues with the Trizol reagent (Life Technologies). After DNase I treatment (Promega), reverse transcription (First-strand cDNA Synthesis Kit, Amersham Bioscience) was performed on 2.5 mg RNA, and 2 µl were used for PCR reactions. Samples were withdrawn after 31 cycles, and products were analysed by agarose gel electrophoresis. Primers used are listed in Table S4.

Droplet digital PCR (ddPCR) assays using the QX200 Droplet Digital PCR System (Bio-Rad) were performed according to the manufacturer's instructions. PCR reactions (25 µl) were prepared with 1× EvaGreen ddPCR Supermix (Bio-Rad), primers (Table S4) at a

final concentration of 100 nM, and 5 µl of cDNA. Droplets were generated according to the manufacturer's recommendation. PCR products were amplified under the following conditions: 95°C for 5 min, 40 cycles of 96°C for 30 s and 60°C for 60 s, followed by 4°C for 5 min, 90°C for 5 min, and held at 4°C until processing. PCR-amplified droplets were read individually with the QX200 droplet reader, and the results were analyzed with QuantaSoft software, version 1.4 (Bio-Rad).

Bioinformatic analyses

Microarray data expression was obtained from the Genevestigator website (www.genevestigator.com).

Multiple sequence alignment of mature RALF peptides (*4*) was performed using CLUSTALW with default parameters. Phylogenetic trees were generated by the neighbour-joining method (*30*), using MEGA 7.0 with 1000 bootstrap and the Poisson correction model (*31-33*).

Generation of transgenic lines

See Supplementary Table S4 and S5 for a list of binary plasmids and primers employed to generate the transgenic lines used in this study. All transgenic lines were generated using the floral dip method (*34*) with the *Agrobacterium tumefaciens* strain GV3101. The constructs p*LAT52:ANX1-YFP*, p*LAT52:MRI-YFP*, and p*LAT52:MRI*^{R240C}*-YFP* were described previously (*11,14*). Gene-specific artificial microRNAs (amiRs) were designed with the phantom database (http://phantomdb.ucsd.edu/) and the WMD3 designer (http://wmd3.weigelworld.org/). amiRs were cloned by site-directed mutagenesis into the

endogenous *miR319a* precursor as previously described (*35*). *rRALF4* was generated through PCR-driven overlap extension (Table S4). The *RALF4* and *RALF19* promoter fragments were amplified and cloned into pGEM-T Easy and then transferred to the pMDC162 destination vector (*36*). The resulting expression vectors pMDC162-pRALF4:GUS and pMDC162-pRALF19:GUS were confirmed by sequencing and transformed into wild-type (Col-0) background. Transformants were selected by screening for hygromicin resistance and confirmed by PCR genotyping. For RALF4ox, the RALF4 coding region was amplified and cloned into pENTR1A, and recombined into pK7WG2D-LAT52p to express *RALF4* under the control of the p*LAT52* promoter. After sequencing, the construct was introduced into *quartet* (*qrt*) mutant plants.

Pollen germination *in vitro* and semi-*in vivo*

Open flowers were incubated at 22°C for 30 min in moist incubation boxes. Then, pollen was bound to xilane-coated slides containing germination medium [0.01% boric acid (w/v), 5 mM $CaCl_2$, 5 mM KCl, 1 mM $MgSO_4$, 10% sucrose, pH 7.5]. Pollen grains were pre-incubated in moist incubation boxes for 30-45 min at 30°C and then transferred to 22°C from 30 min to 5 h as indicated.

For semi-*in vivo* germination assays, stigmas were pollinated and, after a short time, styles were cut off and put onto growth medium in moist incubation boxes at 22°C for up to 3 h.

Synthetic peptides

RALF1, RALF4, RALF4 scrambled, FITC-RALF4 scrambled, FITC-RALF4, and FITC-RALF19 synthetic peptides were obtained from PHTDPeptides Industrial Co, Ltd. (Zhengzhou City, China). After 2 h of *in vitro* pollen germination (see above), peptides were added to pollen germination medium to a concentration of 250nM, the effect on pollen tube growth was imaged using a Leica DM6000 microscope and analysed using the ImageJ 1.40g software (rsb.info.nih.gov/ij).

Aniline blue, ruthenium red, JIM5, and JIM7 staining

To analyse callose deposition, pollen tubes were fixed 2 h after germination in 30 mg ml^{-1} freshly prepared formaldehyde in Pipes buffer (1 mM EGTA, 0.5 mM $MgCl_2$, 50 mM PIPES) for 30 min. After two washes, pollen tubes were incubated for 15 min with 1 mg ml^{-1} aniline blue in 0.15 M K_2HPO_4, mounted, and observed under UV light excitation.

To analyse pectin, ruthenium red staining and immunocytochemical analyses using JIM5 and JIM7 antibodies were performed. For ruthenium red staining, pollen tubes were incubated *in vitro* on liquid germination medium for 2 h, and 0.01% of Ruthenium red was applied for 5 min. For immunocytochemistry with JIM5 and JIM7 antibodies, pollen tubes were fixed overnight in PEM buffer (4% paraformaldehyde in 1 M NaOH, 50 mM PIPES, 1 mM EGTA, and 5 mM $MgSO_4$, pH6.9). After washing with 1x PBS buffer (137 mM NaCl, 10 mM Phosphate, 2.7 mM KCl, pH7.4) and incubation with 1x PBS/MP buffer (1x PBS + 3-5% milk protein) for 1h, a 1:100 dilution of the corresponding antibody in 1x PBS/MP was added to the slide for 1h at room temperature (RT); then, it was washed 3 times with 1x PBS, followed by a 1h incubation with a 1:1000 dilution of AK2 antibody (Anti-Rat IgG (whole molecule)-FITC antibody produced in rabbit, Sigma

F1763) in 1x PBS/MP. After 3 more washes of 10 min in PBS, pollen grains and pollen tubes were transferred into a glycerol-based anti-fade solution and imaged with a Leica DM6000 digital microscope, using the Leica Application Suite Advanced Fluorescence software (Leica Microsystems, Mannheim, Germany). Pollen germination counts and pollen tube length measurements were performed manually using ImageJ 1.40g software (http://rsb.info.nih.gov/ij).

Transient expression of LRX8, LRX10, LRX11, RALF4, and scrambled RALF4 fusion proteins in *Nicotiana benthamiana*

The intron-less *LRX* coding sequences from the start to the end of the sequenced encoding the LRR domain were amplified from genomic DNA (Table S4) with *Pfu*II ultra polymerase (Strataclone), and the PCR products were cloned into the pSC blunt cloning vector (Stratagene) for sequencing. Correct clones were cut with *Xho*I and *Pst*I (*LRX8* and *LRX11*) or *Kpn*I and *Pst*I (*LRX10*), and the *LRX*-coding fragment, together with a *Citrine* clone containing *Pst*I and *Spe*I sites at the 5' and 3' end, respectively, were used for triple ligation into the overexpression vector *pART7*, cut with *Xho*I and *Xba*I or *Kpn*I and *Xba*I respectively (*37*). The resulting *35S:LRX-CIT* cassettes were cloned into the binary vector *pART27*.

The sequences encoding the RALF4 and scrambled RALF4 peptides, together with sequenced coding for a 2xHA-epitope tag flanked by att sites (Gateway, Life Technologies), were synthesized using Genscript technology (Genscript, NJ, USA):

5'GGGGACAAGTTTGTACAAAAAAGCAGGCTAGGGCGTAGAAGAACCAAAAC

CTAAACAAAAGAGCAATAATAACTCATTAAAAAACCAAAACCAAAAAAAAA

CAAAATGGGTGTCAAAATGTTATTAATCTTTGGTCTCTTGATCTTAGCTATGG

TAGCTAAATCCGTCAATGCAACCTACCCTTTAACCAAATCTTGCATCAACGGG

CAAGGTTGCATCGGGGAAGACGATGAGCTCGAATCTCTAATGGATTCAGAGA

CAAACCGTCGTCAACTCGCAAGAGGACGTCGTTACATTGGCTACGATGCTCT

CAAAAAGAACAATGTGCCTTGCAGTAGACGTGGCCGATCCTACTACGATTGC

AAGAAGAGAAGAAGGAATAATCCTTACAGGCGTGGATGCAGTGCCATCACG

CATTGCTATAGGTACGCTCGCTACCCATACGATGTTCCAGATTACGCTTACCC

ATACGATGTTCCAGATTACGCTTAAACCCAGCTTTCTTGTACAAAGTGGTCCC

C3’ and

5’CAAATAATGATTTTATTTTGACTGATAGTGACCTGTTCGTTGCAACAAATTG

ATGAGCAATGCTTTTTTATAATGCCAACTTTGTACAAAAAAGCAGGCTAGGG

CGTAGAAGAACCAAAACCTAAACAAAAGAGCAATAATAACTCATTAAAAAA

CCAAAACCAAAAAAAAACAAAATGGGTGTCAAAATGTTATTAATCTTTGGTC

TCTTGATCTTAGCTATGGTAGCTAAATCCGTCAATGCAACCTACCCTTTAACC

AAATCTTGCATCAACGGGCAAGGTTGCATCGGGGAAGACGATGAGCTCGAAT

CTCTAATGGATTCAGAGACAAACCGTCGTCAACTCGCAAGAGGACCTACGTA

CAACAGTTGCCGTCGTAAGTGCAAGAGAGATAGAGGCTACGCTGCCAGGCGT

TACAAGCGATACAGGTATGTGAATGCTGATATTAAACGCAATCATTCCGGCT

ACCCTTGCAGGATCTGCAGTAGACTCTACGGACGTAATTACCCATACGATGTT

CCAGATTACGCTTACCCATACGATGTTCCAGATTACGCTTAAACCCAGCTTTC

TTGTACAAAGTTGGCATTATAAGAAAGCATTGCTTATCAATTTGTTGCAACGA

ACAGGTCACTATCAGTCAAAATAAAATCATTATTT3’, respectively. The

7

sequences were inserted into the pMDC32 vector (*36*) for *Agrobacterium*-mediated transformation (*34*) using Gateway technology (Life Technologies).

A culture of *Agrobacterium* cells containing one or both expression vectors (1ml LB media including resistance antibiotics) was inoculated at 28C overnight and transferred to 30 mL LB media with the same antibiotics. The culture was grown to a final optical density OD_{600} of ~1.5. Cells were harvested by centrifugation at 3000 rpm for 20 min, resuspended in infiltration buffer (10 mM MES- KOH pH5.6, 10 mM MgCl2) to an OD_{600} of ~0.8, and activated by incubating at C24 for 1 hr. Three leaves of a *N. benthamiana* plant were infiltrated (~six spots per leaf) and the leaf discs were recovered three days after inoculation.

Leaf discs were ground in liquid nitrogen and resuspended in 500 µL of 50 mM Tris-HCl pH7.5 buffer supplemented with 0.5% Triton-X100 (v/v), 150 mM NaCl, and Protease Inhibitor Cocktail Mini (Roche). After centrifugation at 13,000 rpm for 16 min â€¡4 the supernatant was recovered. Protein accumulation was confirmed by Western blotting, using the anti-GFP antibody (1:3000, Torrey Pines Biolabs) and the anti-HA antibody (1:5000, Abcam). As secondary antibodies, the Agrisera S09602 goat anti-rabbit antibody was used with the ECL-chemistry of FUSION FX - Western Blot & Chemi Imaging (Vilber Lourmat).

Co-immunoprecipitation assays with RAL4-HA, scrambled RALF4-HA, and LRX-CIT

N. benthamiana plant extracts (1 mL) obtained from the leaf discs that were infiltrated by *Agrobacterium* carrying RALF-HA, LRX-CIT, or a mix of both constructs, were incubated with 100 µl Anti-HA−agarose beads carrying monoclonal anti-HA antibody

produced in mouse (A2095 SIGMA) at 4°C overnight. The bound fraction was washed with 1 mL 1x PBS three times. Bound proteins were eluted and denatured by incubation for 3 mins at 98 °C in 2x SDS L aemmli buffer (4% SDS (w/v), 20% glycerol (v/v), 10% β-mercaptoethanol (v/v), 0.004% bromphenol blue (w/v), 0.125 M Tris-HCl pH 6.8) (*14*). RALF-HA_LRX-CIT complexes detached from the beads were analysed in a 10% polyacrylamide gel (30% Acrylamide/Bis Solution, 19:1, Bio-Rad) run in 1x Tris-HCl pH 7.5, SDS, glycine buffer, and subsequently blotted onto an Immobilion® PVDF membrane (Merck Millipore). Binding of RALF-HA and LRX-CIT was detected with rabbit anti-HA antibody (1:1000, Abcam), a rabbit anti-GFP antibody (1:3000, Torrey Pines Biolabs), and secondary goat-anti-rabbit antibodies (1:40,000, Agrisera, AS09602). GFP-Trap®_A (Chromotek) agarose beads were used to immunoprecipitate RALF-HA, LRX-CIT, and RALF-HA_LRX-CIT complexes as described above. The bound fraction was washed with 1 mL 10mM Tris-HCl pH 7.5, 150 mM NaCl, 0.5 mM EDTA three times, followed by 10 min incubation at 98 °C in 2x SDS Laemmli buffer (*38*).

Yeast 2-hybrid assays

The sequences encoding the mature RALF4 peptide was cloned into the pDEST32 vector to generate GAL4:AD-RALF4. Sequences coding for the LRR domain of LRX8 and LRX9 were inserted into the pDEST22 vector to generate GAL4:DBD-LRX8 and GAL4:DBD-LRX9 (Invitrogen). The constructs were co-transformed into yeast strain PJ69-4A and the resulting transformants were selected on SC -Leu/-Trp plates. Interaction between the two proteins was monitored by growing colonies on SC -Leu/-Trp/-His plates. pEXP™32/Krev1 + pEXP™22/RalGDS-wt and pEXP™32/Krev1 +

pEXP™22/RalGDS-m2 (Invitrogen) were used as positive and negative interaction controls, respectively.

Quantitation of binding of LRX8-CIT to RALF4 and RALF1 by biolayer interferometry using the BLItz® system (Pall FortéBio)

N. benthamiana plant extracts (1 mL) obtained from the leaf discs that were infiltrated by *Agrobacterium* carrying LRX8-CIT plasmid were incubated with 40 µl GFP-Trap®_A (Chromotek) agarose beads 3hrs at 4°C under constant mixing. After washing 3 times with protein extraction buffer (50 mM Tris-HCl pH7.5, 50 mM NaCl, 10% glycerol (v/v), 0.5% NP-40 (v/v), 5mM DTT, 1x Protease Inhibitor Cocktail Mini (Roche), 2mM Na_2MoO_4, 2.5mM NaF), elution was performed with 30µl (1bed) of 1M Glycine pH2.0 buffer for 2min in a Thermomixer (Eppendorf) at 1200 rpm, then beads were spun down for 2min at 1300xg at RT, and the supernatant neutralized with 30µl of 1M Tris-HCl pH9.5.

Protein concentration was established by a Qubit measurement (Quant-iT™ Protein Assay kit, Invitrogen). Samples were diluted 1:1 with sample diluent buffer (Pall FortéBio cat18-1091) to a concentration of 0.142 mg/ml for analysis using the BLItz® system. The same buffer was used to dilute the anti-GFP antibody (Torrey Pines Biolabs) 1:50 to a final concentration of 4 µg/ml. A 1:1 mix of sample:antibody was then incubated for 30 minutes at RT, and loaded into the protein A biosensor (Pall FortéBio cat 18-5010). The experiment was divided into 5 different steps: Initial baseline duration (30 s), Loading duration (120 s), Baseline duration (30 s), Association duration (120 s), and Dissociation duration (120 s). Different RALF4 synthetic peptide concentrations; 150

µM, 100 µM, 50 µM, 20 µM, 15 µM, 10 µM, 4 µM, 2 µM and 0.2 µM, were added to quantify the protein interaction.

Interaction between LRX8-CIT and RALF4 molecules analysed by MicroScale Thermophoresis (MST) using the Monolith system (NanoTemper Technologies)

For MST using the Monolith technology, LRX8-CIT total protein extract was isolated as described above, and diluted in a 2x protein extraction buffer to a final concentration of 0.2 mg/ml (dilution 1:20 from total lysate). RALF4 synthetic peptide was titrated in a 2:1 dilution series to concentrations between 100 and 0.2 µM for molecule interaction analysis. Samples were loaded into Monolith™ NT.115 MST standard Coated Capillaries (NanoTemper Technologies), and measured using Monolith NT.115 with MO.Control software at RT (LED/excitation blue power setting 5%, MST power setting High). Data was analysed using MO.Affinity Analysis software (version 2.2.5, NanoTemper Technologies) at the standard MST-on time of 5 s.

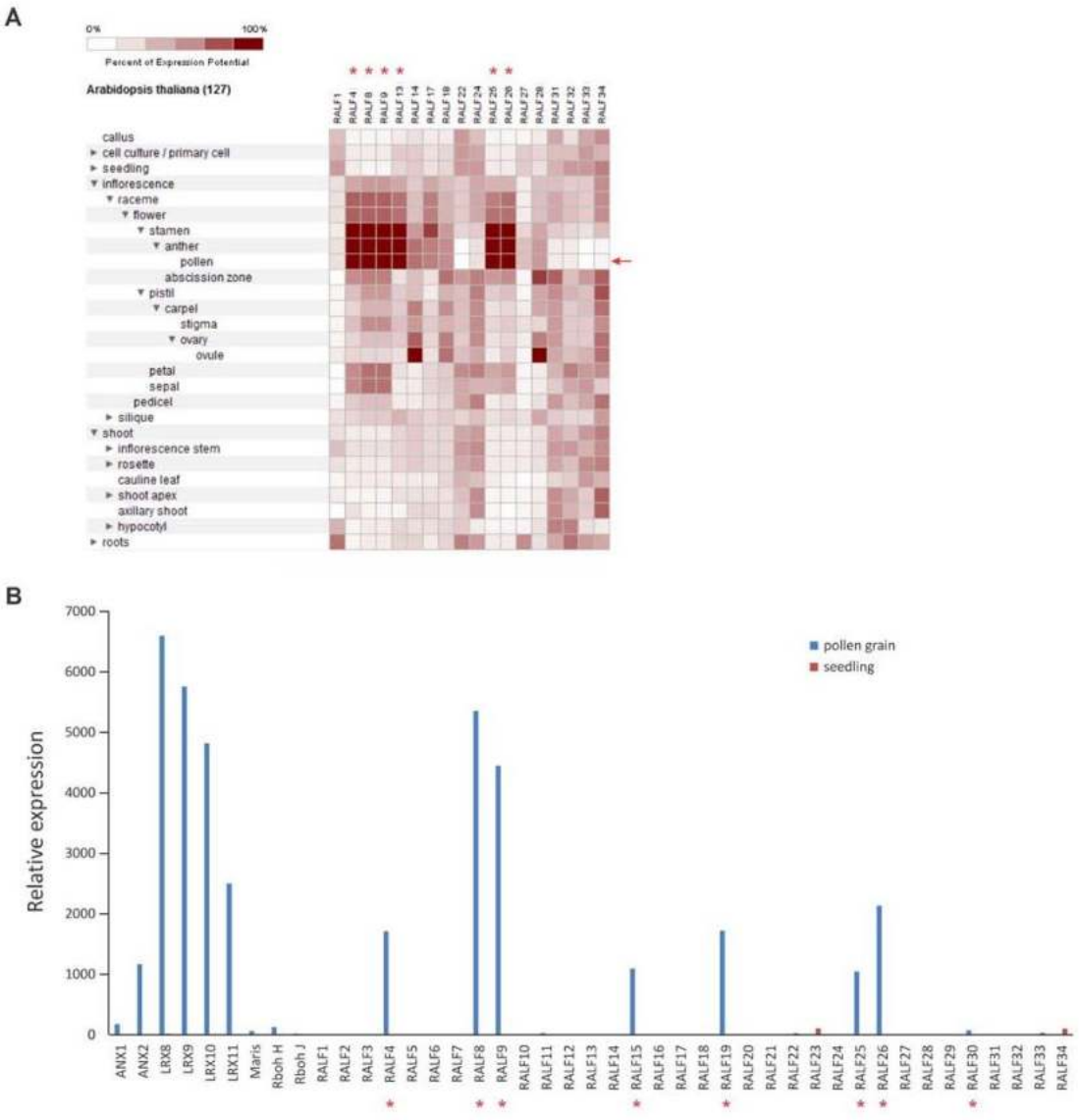

Fig. S1. Microarray expression data of *RALF* family members.

Microarray expression analysis of *RALF* genes in various *Arabidopsis* tissues (www.genevestigator.com). Red asterisks indicate *RALF* genes with high expression in pollen. *RALF19* and *RALF30* are not on the ATH1 array. **(B)** RNAseq expression analysis of *RALF* genes in mature pollen grains and seedlings of *Arabidopsis (39)*. Red asterisks indicate *RALF* genes with high expression in pollen. Unlike in the microarray data, *RALF13* was not found to expressed in pollen by RNAseq. In the main text, we use this RNAseq data as our reference.

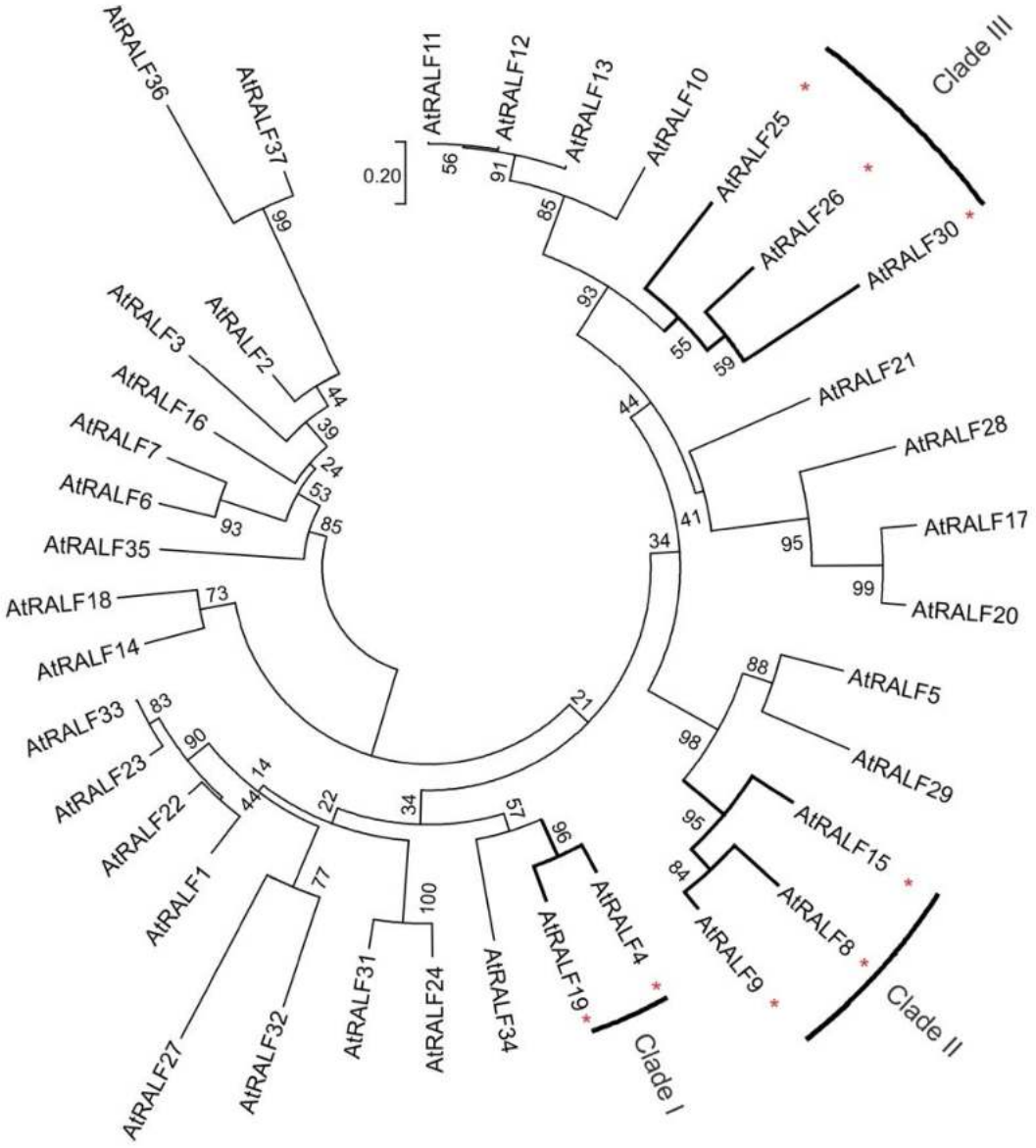

Fig. S2. Three clades of RALF peptides contain members with high expression in pollen.

Phylogenetic tree of *Arabidopsis* RALF peptides. Alignment of mature amino acid sequences were used (*4*). Three clades containing pollen-expressed *RALF* genes were identified. Clade I: RALF4 and RALF19; Clade II: RALF8, RALF9, and RALF15; Clade III: RALF25, RALF26, and RALF30. Red asterisks indicate *RALF* genes expressed in pollen based on publically available expression data (fig. S1).

A

```
AtRALF1          RRILATTKYISYQSLKRNSVPCSRRGASYYNCQNGAQANPYSRGCSKIARCRS

AtRALF4                RRYIGYDALKKNNVPCSRRGRSYYDCKKRRRNNPYRRGCSAITHCYRYAR
                       * ** * ** ******************** * ******** ******
AtRALF19         RRQLAARRSYISYGALRKNNVPCSRRGRSYYDCKKRKRANPYRRGCSVITHCYRQTS
```

B

Identity	AtRALF4	AtRALF19
AtRALF1	59 %	57 %
AtRALF4	-	85 %

Fig. S3. Amino acid identity of *RALF4* and *RALF19*.
(A) Alignment of the mature sequences of RALF1, RALF4, and RALF19. Cysteins are in red and bold. Asterisks indicate amino acid conservation between RALF4 and RALF19.
(B) Percentage of amino acid identity between RALF1, RALF4, and RALF19. RALF1 was used as a reference.

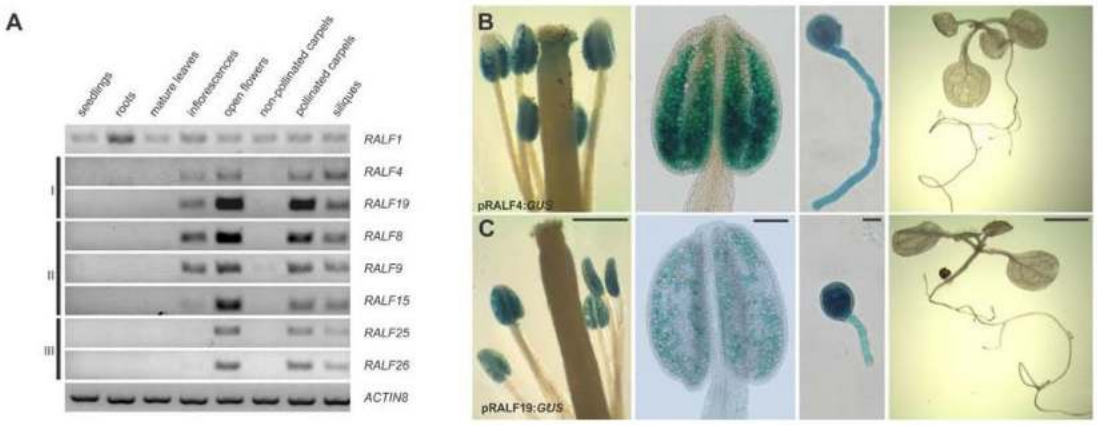

Fig. S4. Confirmation of pollen-expressed *RALF* genes by RT-PCR and *GUS* reporter gene analysis.

(A) RT-PCR was used to validate expression of pollen expressed RALF*s* in different tissues of wild-type *Arabidopsis* plants. The *ACTIN8* and *RALF1* genes were used as control. **(B-C)** GUS activity in transgenic plants carrying a pRALF4:*GUS* **(B)** and pRALF19:*GUS* **(C)** reporter gene construct, respectively. Open flower, anther, *in vitro* germinated pollen, and seedling are shown. Scale bars: 0.5 cm (flower), 100 µm (stamen), 10 µm (germinated pollen), 2 mm (seedling).

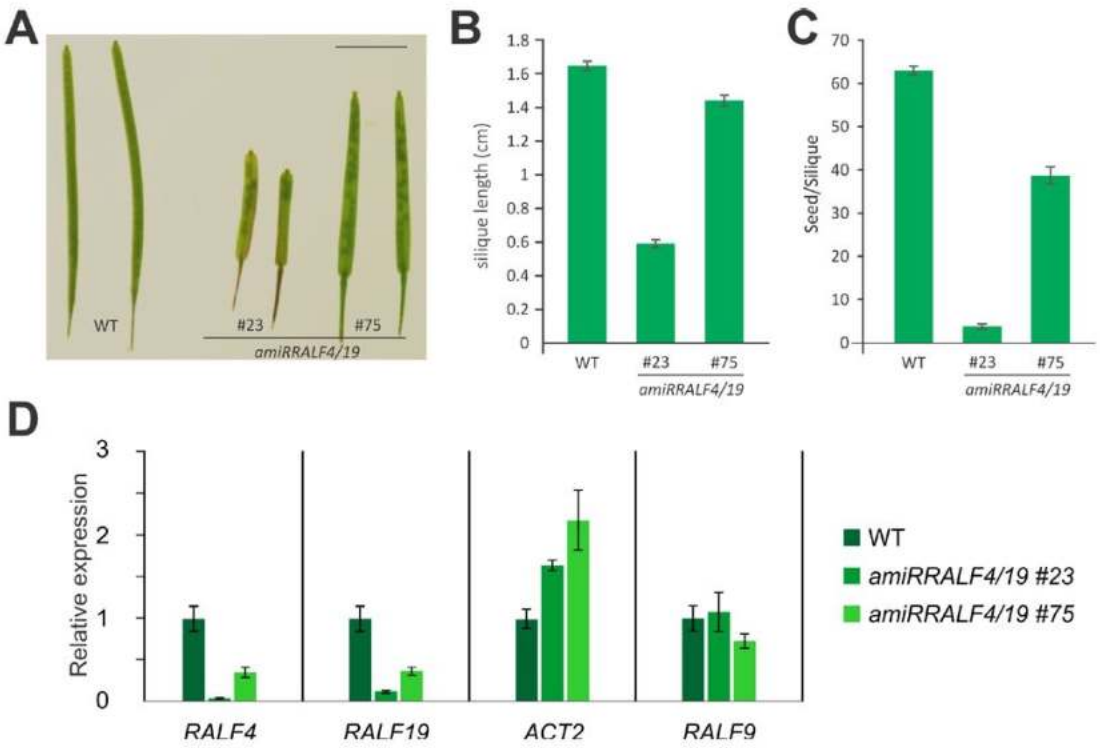

Fig. S5. Characterization of *amiRRALF4/19* lines.
(A) Siliques from the primary inflorescence of WT and amiRRALF4/19 lines #23 and #75. Scale bar: 0.5 cm. **(B)** Silique length of WT and amiRRALF4/19 lines #23 and #75. The data shown are mean ± s.e.m. of three biological replicates with 20 siliques analyzed per experiment. **(C)** Seeds per silique of WT and amiRRALF4/19 lines #23 and #75. The data shown are mean ± s.e.m. of three biological replicates with 20 siliques analyzed per experiment. **(D)** ddPCR of RALF4 and RALF19 levels in open flowers of WT and amiRRALF4/19 lines #23 and #75. Expression was calculated as copies relative to ARTUMES (40), WT was used as reference. RALF9 and ACT2 were used as internal reference genes. The data shown are mean ± s.e.m. of three biological replicates.

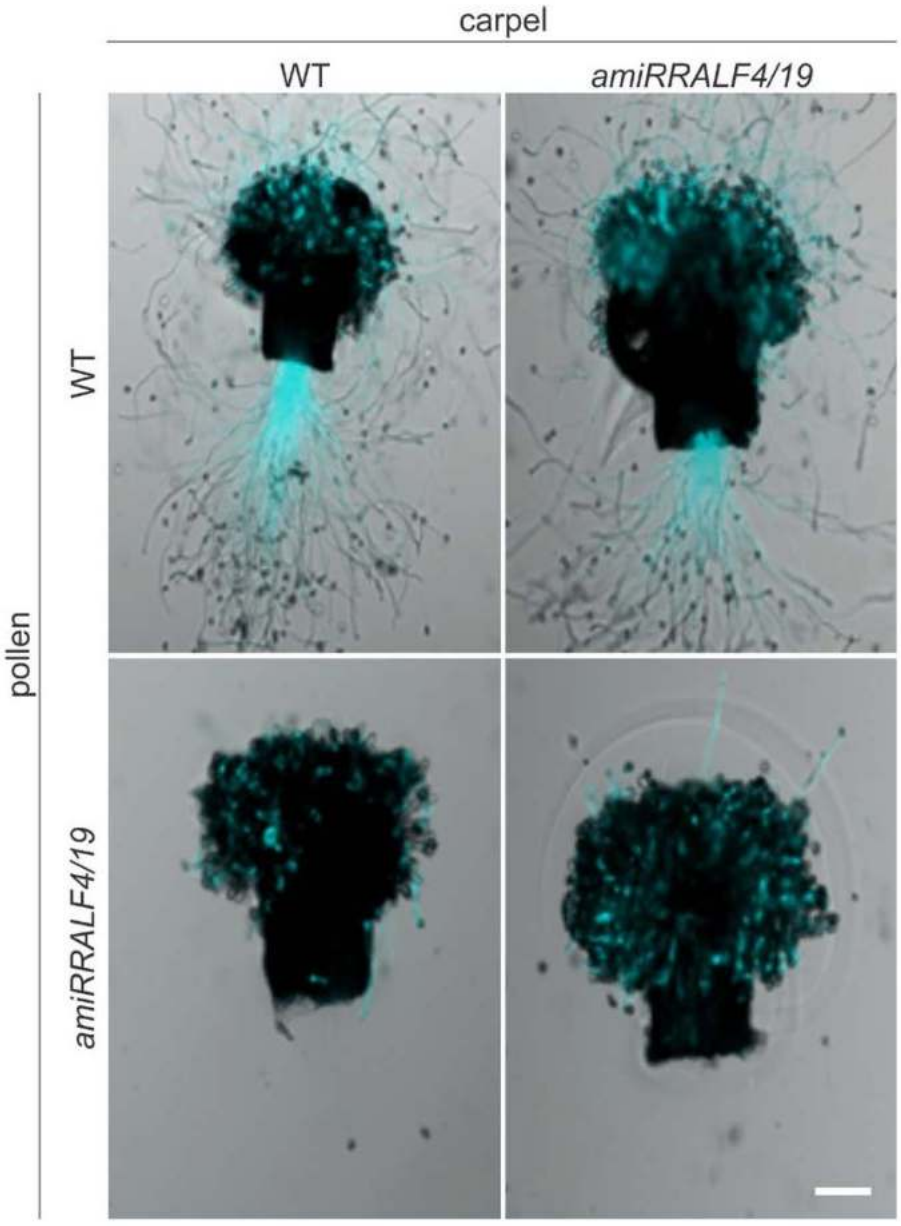

Fig. S6. Downregulation of *RALF4* and *RALF19* result in male sterility.

Semi-*in vivo* pollen germination of crosses using WT and *amiRRALF4/19* pollen in crosses with WT and *amiRRALF4/19* carpels, respectively. Scale bar: 100 µM

Fig. S7. Downregulation of *RALF4* and *RALF19* produce reduce ovule targeting in vivo.

Hand-pollination of WT and *amiRRALF4/19* carpels with minimal amounts of self-pollen. 15-20 pollen grains were added to each carpel (n=6). Samples were collected and stained with aniline blue 24 h after pollination. Light blue asterisks indicate ovules that were targeted by a pollen tube. Scale bar: 250 μm.

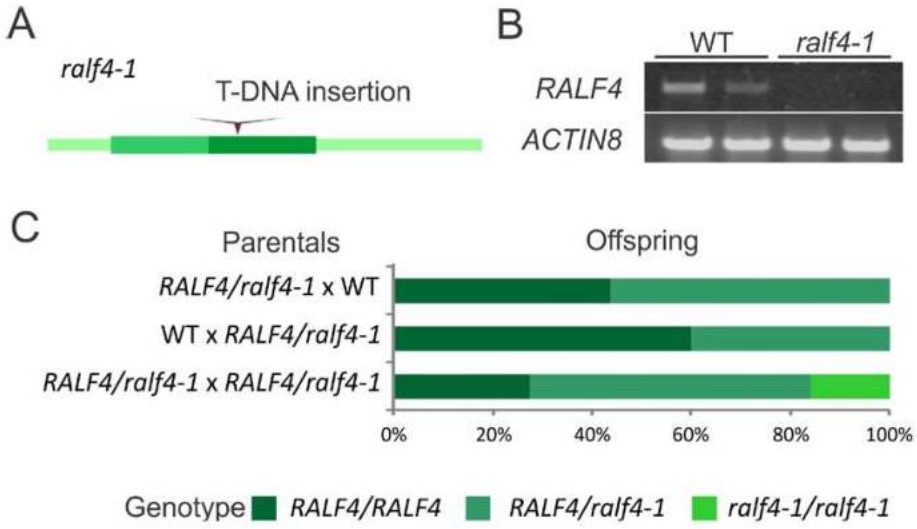

Fig. S8. *ralf4-1* single mutant plants display a phenotype indistinguishable from the wild type.

(A) Diagram of the T-DNA insertion in the *ralf4-1* mutant (SALK_016969). **(B)** RT-PCR of *RALF4* levels in open flowers of WT and *ralf4-1* mutant lines. *ACTIN8* was used as control. **(C)** Segregation analysis of backcrosses and F2 progenies of heterozygous *ralf4-1* mutant plants (100 progeny per cross were analysed).

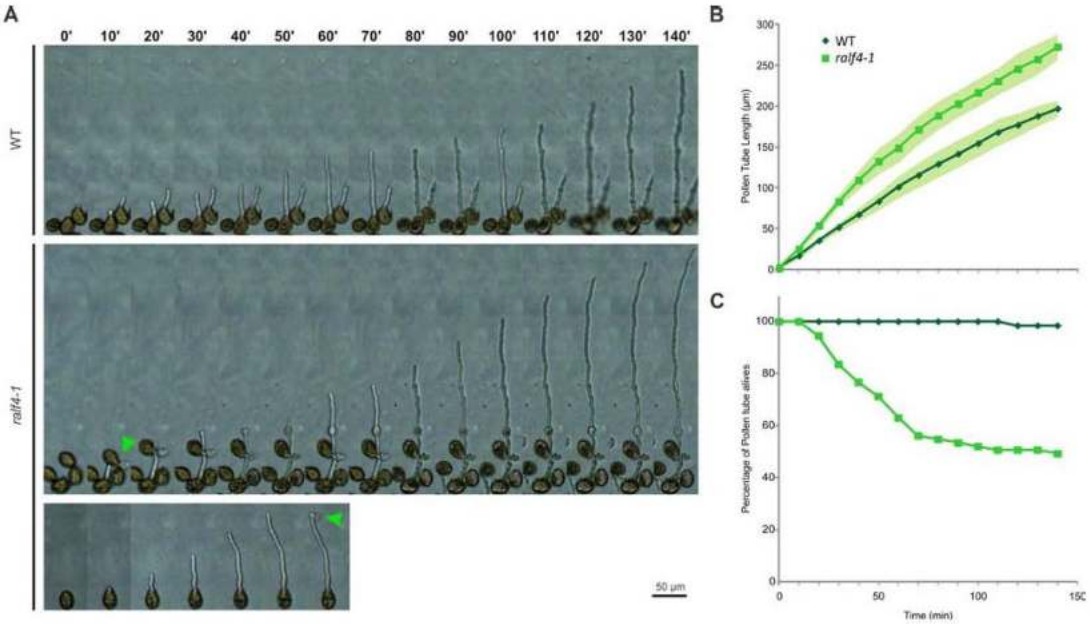

Fig. S9: *ralf4-1* pollen tubes growth initially faster than wild-type controls.

(A) Time course of growing WT and *ralf4-1* pollen tubes growing *in vitro*. Green triangles indicate pollen tube bursting. **(B)** Lengths of WT and *ralf4-1* pollen tubes over the time course (data points are mean ± s.e.m. of three biological replicates, n=20 each). **(C)** Percentage of living WT and *ralf4-1* pollen tubes over the time course (n=60).

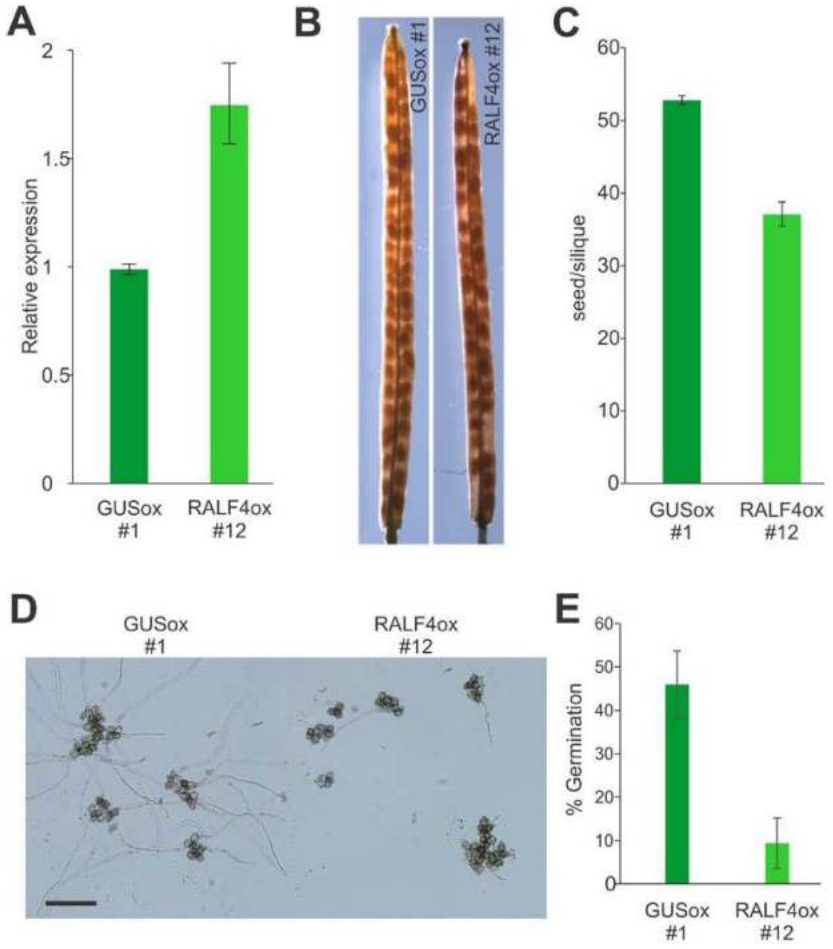

Fig. S10. Overexpression of *RALF4* reduces seed set and pollen germination.
(A) RNA levels of *RALF4* in GUSox #1 and RALF4ox #12 open flowers. Expression was normalized to *ARTUMES* (*40*) expression. The data shown are mean ± s.e.m. of three biological replicates. **(B)** Representative siliques of the GUSox #1 and RALF4ox #12 line. **(C)** Number of seeds per silique in GUSox #1 and RALF4ox #12 lines (n =20). **(D)** *In vitro* germination of pollen from GUSox #1 and RALF4ox #12 transgenic lines. Scale bar: 200 µm. **(E)** Percentage of germinated pollen 3 h after germination of homozygous GUSox #1 and RALF4ox #12 transgenic lines. The data shown are mean ± s.e.m. of three biological replicates.

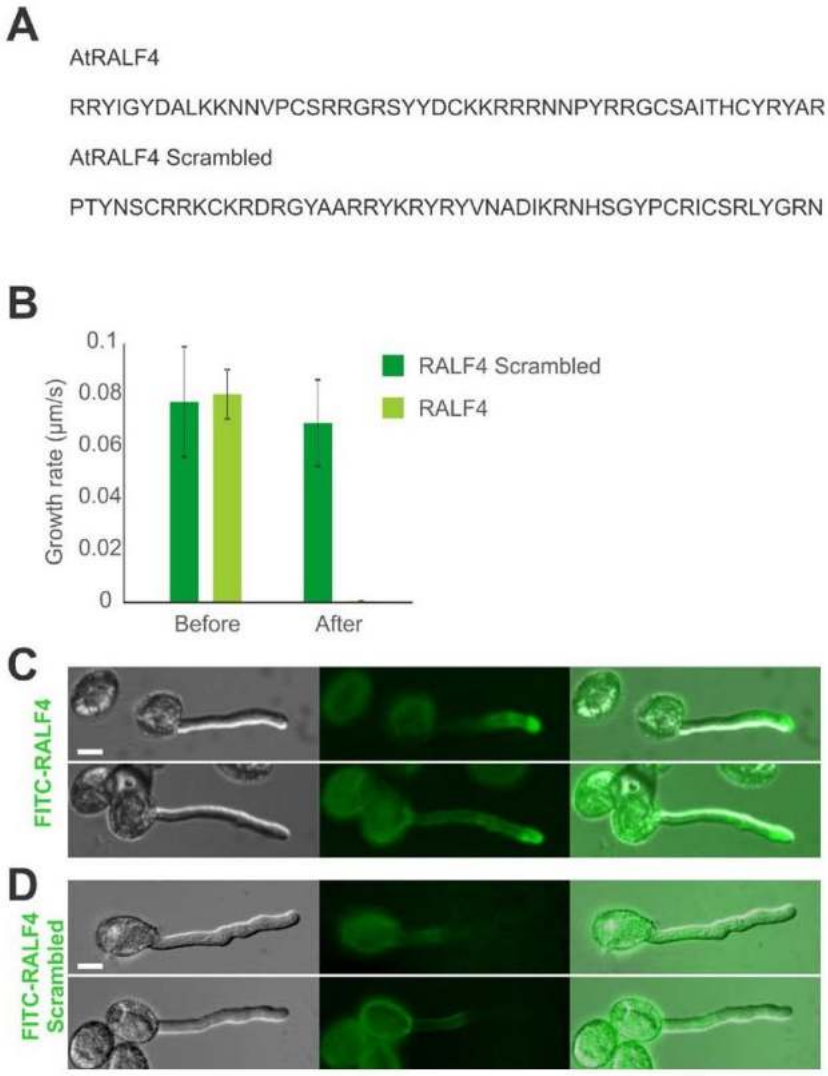

Fig. S11. High concentrations of exogenously applied RALF4 peptide reduce pollen tube growth.

(A) Amino acid sequence of synthetic RALF4 and scrambled RALF4 peptides used in pollen tube growth assays. **(B)** Growth rate of WT pollen tubes 20 s before and after the addition of the RALF4 and RALF4 Scrambled peptides, respectively (data shown are mean ± s.e.m. of three biological replicates, n=20 each). **(C-D)** Binding of FITC conjugated RALF4 peptides on WT pollen tubes. FITC-RALF4 peptide **(C)**, but not FITC-RALF4 Scrambled **(D)**, bound to growing pollen tubes. Scale bar: 10 µm.

Fig. S12. *amiRRALF4/19* pollen tubes accumulate pectin in bulges.
Ruthenium red staining for pectin in WT and *amiRRALF4/19* pollen tubes. Scale bar: 20 μm

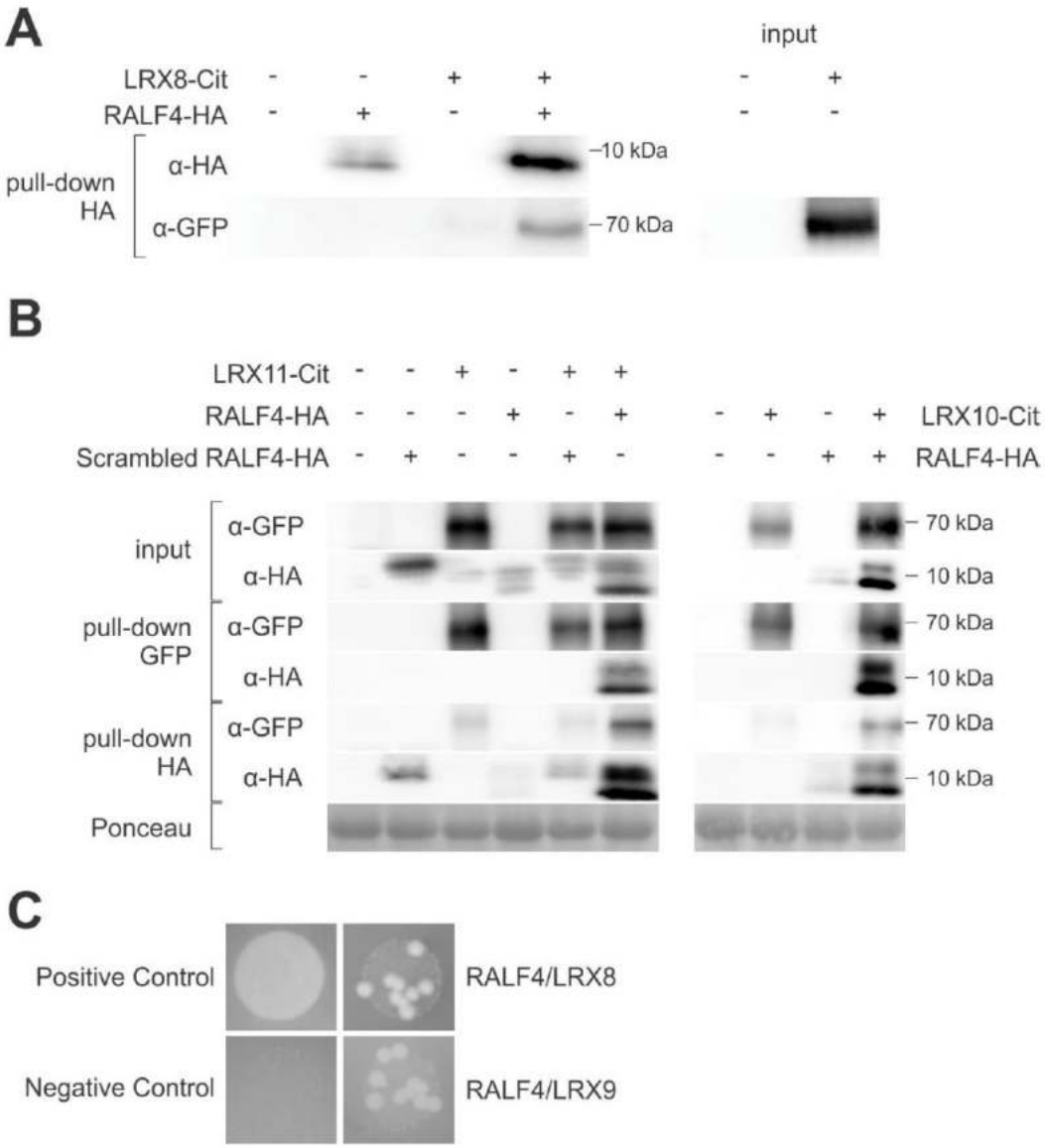

Fig. S13. RALF4 interact with LRX proteins.

(A) Western blot analysis after co-immunoprecipitation of LRX8-CIT and RALF4-HA using anti-HA agarose beads. **(B)** Western blot analysis of co-immunoprecipitated RALF4-HA with LRX11-CIT or LRX10-CIT using anti-GFP and anti-HA agarose beads. Membranes were probed with anti-GFP (α-GFP) and anti-HA (α-HA) antibodies. The predicted size of RALF4-HA and Scrambled RALF4-HA propeptide is14.8 kDa, of mature RALF4-HA 8.3 kDa, and of LRX8-Cit, LRX10-Cit, and LRX11-Cit ~70kDa. Ponceau staining was used as a loading control **(C)** Yeast-two-hybrid analysis of interactions between RALF4 with LRX8 and LRX9, respectively.

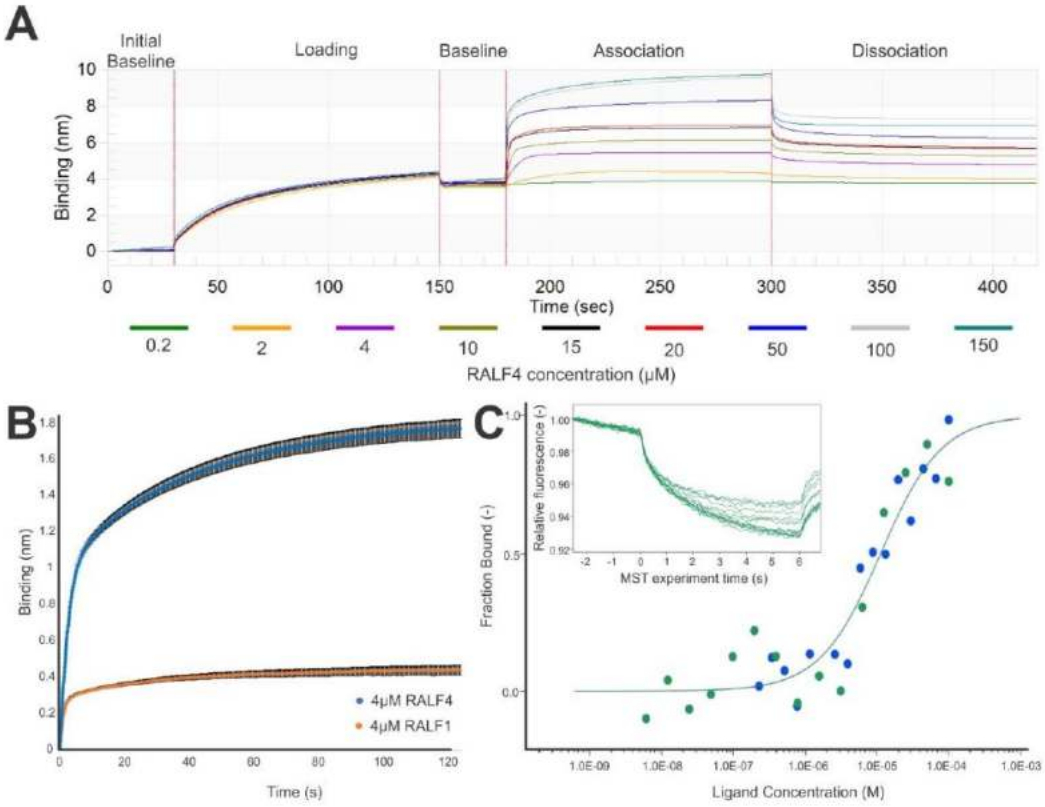

Fig. S14. Quantitative analysis of LRX8-RALF4 binding.
(A, B) Characterization of the binding of synthetic RALF4 peptide at increasing concentrations to LRX8 using the BLItz® system. (A) LRX8-RALF4 binding shows a stable equilibrium dissociation constant KD=900 nM R^2= 0.9716. (B) Binding of RALF4 and RALF1 synthetic peptides to LRX8 at a given concentration (4µM). RALF1, not expressed in pollen (Fig. S1), was used as a negative control. The graph shows the mean ± standard deviation of 4 independent biological replicates at each time point. **(C)** Characterization of molecular interaction between LRX8-CIT and RALF4 molecules by MicroScale Thermophoresis using the Monolith system. Interaction of the synthetic RALF4 peptide at different concentrations to the LRX8 target protein is shown. Green and blue dots represent independent biological replicates.

Table S1. List of genes and mutants used in the study

Gene name	Locus	Mutant name	T-DNA line	Reference
RALF4	AT1G28270	*ralf4-1*	*SALK_016969*	*this study*
RALF19	AT2G33775	-	-	*this study*
RBOHH	AT5G60010	*rbohH-3*	*SALK_136917*	*(2)*
RBOHJ	AT3G45810	*rbohJ-3*	*SALK_050665*	*(2)*
LRX8	AT3G19020	*lrx8*	*SALK_001367*	*(3)*
LRX9	AT1G49490	*lrx9*	*SALK_136073*	*(3)*
LRX10	AT2G15880	*lrx10*	*SALK_087083*	*(3)*
LRX11	AT4G33970	*lrx11*	*SALK_030664*	*(3)*

Table S2. Segregation ratio analysis in RALF4ox transgenic lines.

Segregation ratio analysis of the kanamycin resistance gene in GUSox and RALF4ox transgenic T1 lines. Sensitivity to kanamycin was tested in T2 plants and showed a distorted segregation ratio in RALF4ox lines, indicating a defect in pollen development or pollen tube growth.

	#	Resistant	Sensitive	Ratio
GUSox	1	202	54	3.74
	2	483	148	3.26
	3	388	130	2.98
	4	144	49	2.94
RALF4ox	1	46	21	2.19
	2	913	994	0.92
	3	254	278	0.91
	4	150	53	2.83
	5	288	102	2.82
	6	130	141	0.92
	7	103	116	0.89
	8	113	59	1.92
	9	90	50	1.80
	10	520	184	2.83
	11	450	138	3.26
	12	599	433	1.38
	13	315	101	3.12
	14	134	58	2.31
	15	100	37	2.70
	16	90	21	4.29
	17	60	52	1.15
	18	262	184	1.42
	19	104	24	4.33
	20	73	17	4.29
	21	54	34	1.59
	22	48	37	1.30
	23	117	60	1.95

Table S3. Backcross test of hemizygous RALF4ox #2 plants.

Sensitivity to kanamycin was tested in the progeny of the crosses, indicating that pollen tubes carrying the RALF4ox construct do not contribute to the progeny.

	Resistant	Sensitive
RALF4ox #2 x WT	34	36
WT x RALF4ox #2	0	20

Table S4. List of primers used in this study

Name	Sequence	Observation
RALF1F	GGAATTCAAAGAAGAATATTGGCGACCAC	RT-PCR
RALF1R	CCTCGAGCTAACTCCTGCAACGAGCAA	RT-PCR
RALF4F	GGAATTCAACGTCGTCAACTCGCAAGAGG	RT-PCR
RALF4R	CCTCGAGTTAGCGAGCGTACCTATAGC	RT-PCR
RALF8F	GGAATTCAATCCGTAAGATACATAACTTA	RT-PCR
RALF8R	CCTCGAGTTAGGTGGGCTTTGGACCTG	RT-PCR
RALF9F	GGAATTCAAACAAGATACATAACTTATCC	RT-PCR
RALF9R	CCTCGAGCTATCCACCACGGCAACGAT	RT-PCR
RALF14F	GGAATTCAACGTAGGATTCTACAAGCATC	RT-PCR
RALF14R	CCTCGAGCTAATTCGTAAACCGGTAAC	RT-PCR
RALF15F	GGAATTCAAACAAGATACATAAGTTATCG	RT-PCR
RALF15R	CCTCGAGTCATTTTCTACCTGTATCAC	RT-PCR
RALF18F	GGAATTCAACATAGGATACTTCAAGCTAAG	RT-PCR
RALF18R	CCTCGAGTTAATTTGTAAAGCGGTAAC	RT-PCR
RALF19F	GGAATTCAACGGCGCCAACTAGCCGCGAG	RT-PCR
RALF19R	CCTCGAGTTAAGAAGTTTGCCTGTAGC	RT-PCR
RALF25F	GGAATTCAAAACGATAACAAGAGAAAATATC	RT-PCR
RALF25R	CCTCGAGTCACGGATTCTGCACTCGGC	RT-PCR
RALF26F	GGAATTCAACGCAAAGGTCGAAAGTATTT	RT-PCR
RALF26R	CCTCGAGCTAGGCATCTCGTCTGCACC	RT-PCR
RALF28F	GGAATTCAAAATGAGATTGGCTATCCAGG	RT-PCR
RALF28R	CCTCGAGTTATATCATCTTTCGAGGAA	RT-PCR
RALF34F	GGAATTCAACGACGGTCATTGTACTGGCG	RT-PCR

RALF34R	CCTCGAGCTATCTCCGGCATCGAGTGA	RT-PCR
ACTIN8F	ATGAAGATTAAGGTCGTGGCAC	RT-PCR
ACTIN8R	GTTTTTATCCGAGTTTGAAGAGGC	RT-PCR
qRALF4F	AGGGCGTAGAAGAACCAAAACCT	ddPCR
qRALF4R	CTTGCGAGTTGAGCACGGT	ddPCR
MFB RALF4	FAM_ AACAAAAGAGCAATAATAAC	ddPCR
qRALF9	Biorad. Unique assay ID:qAthCEP0018283	ddPCR
qRALF19F	GAGAGCACCGTAACTGATGTAGCTG	ddPCR
qRALF19R	GAGGATGGTGAGCTTGACTACTTG	ddPCR
MFB RALF19	VIC-CCTCGCGGCTAGTT	ddPCR
qACT1F	GAGACTTTCAATGCCCCTGC	ddPCR
qACT1R	CCATCTCCAGAGTCGAGCACA	ddPCR
MFB ACT1	FAM-CAGTGGTCGTACTACCGGT	ddPCR
qARUF	GTTTGTTACCAATGTGCTTGTTCG	ddPCR
qARUR	TCCATATCCAGTCTTCCAGTTATCC	ddPCR
MFB ARU	FAM-TACTGCACAAAGGTTG	ddPCR
RP-RALF4	AGGGCGTAGAAGAACCAAAAC	*RALF4* genotyping
LP-RALF4	AAAACCTTCCTCTCGACTTGG	*ralf4-1* genotyping
LBa1	TGGTTCACGTAGTGGGCCATCG	*ralf4-1* genotyping
Resc_R4A	GGGGACAAGTTTGTACAAAAAAGCAGGCTTCagttgtt cgctacgtgattt	*rRALF4*
Resc_R4D	GGGGACCACTTTGTACAAGAAAGCTGGGTTGTCGA Cactgtagaaataacggacgg	*rRALF4*
Resc_R4B	TACAGTCATAATAACTCCTTCCACGTCTACTGCAA	*rRALF4*

	GGC	
Resc_R4C	AAGGAGTTATTATGACTGTAAGAAGAGAAGAAGG AATAATCC	*rRALF4*
RALF4oxF	GGAATTCCTGCATAATCTCTCACACACTTCTATTTC	p*LAT52:RALF4*
RALF4oxR	CCTCGAGAAGAAGAAATAGGTCTCATTTGATCCC	p*LAT52:RALF4*
LRX8F	TGACTCGAGATGACCCGAAGAACAATGGAG	Co-IP LRX8-CIT
LRX8R	TGACTGCAGCTGCAATCCACAGGACGGC	Co-IP LRX8-CIT
LRX10F	AGAGGTACCGTTCCAAGTCATGACTAAACCTCC	Co-IP LRX10-CIT
LRX10R	GATCTGCAGCTACAATCAACTGGACGGCTAATC	Co-IP LRX10-CIT
LRX11F	AGACTCGAGATGCCCTTCTATAAGCAGCC	Co-IP LRX11-CIT
LRX11R	TCTCTGCAGCTACAATCAACCGGGCGGTTGCTA	Co-IP LRX11-CIT
RALF4PDR	TCGTATGGGTAGCGAGCGTA	Co-IP RALF4-HA
RALF4PDR	TCGTATGGGTAGCGAGCGTA	Co-IP RALF4-HA

Table S5. Transgenic lines used in this study

Name	Construct	Backbone
amiRRALF4/19	p*ACA9:amiRRALF4/19*	pGreen
rRALF4	p*RALF4:rRALF4*	pMDC100
p*RALF4:GUS*	p*RALF4:GUS*	pMDC162
p*RALF19:GUS*	p*RALF19:GUS*	pMDC162
RALF4ox	p*LAT52:RALF4*	pK7WG2D
GUSox	p*LAT52:GUS*	pK7WG2D
ANX1-YFP	p*LAT52:ANX1-YFP*	pB7YWG2
MRI-YFP	p*LAT52:MRI-YFP*	pB7YWG2
MRI^{R240C}*-YFP*	p*LAT52:*MRI^{R240C}*-YFP*	pB7CWG2

Movie S1

Effect of RALF4 synthetic peptides on wild-type and *lrx8/9/11* mutant pollen tubes as monitored in a lab-on-chip device. Pollen tubes were grown in a microfluidics chamber allowing for precise imaging of pollen tubes and manipulation of the growth medium (*41*). Synthetic RALF4 peptides (250 nM) were mixed with fluorescent beads (1:1000) to allow the monitoring of when the solution reaches the pollen tubes in a real-time analysis. The response of *lrx8/9/11* triple mutant (left) and WT (right) pollen tubes is shown. Scale bar: 10 μm.

Movie S2

Effect of RALF4 synthetic peptides on wild-type and *lrx8/9/11* mutant pollen tubes growing in semi-soft medium. Response of WT (up) and *lrx8/9/11* (down) pollen tubes after the addition of synthetic RALF4 peptides (250 nM) to pollen tube
s growing in semi-solid pollen germination medium. Scale bar: 10 μm.

References

1. E. Murphy, I. De Smet, Understanding the RALF family: A tale of many species. *Trends Plant Sci.* **19**, 664–671 (2014). doi:10.1016/j.tplants.2014.06.005

2. G. Pearce, D. S. Moura, J. Stratmann, C. A. Ryan Jr., RALF, a 5-kDa ubiquitous polypeptide in plants, arrests root growth and development. *Proc. Natl. Acad. Sci. U.S.A.* **98**, 12843–12847 (2001). doi:10.1073/pnas.201416998 Medline

3. M. Stegmann, J. Monaghan, E. Smakowska-Luzan, H. Rovenich, A. Lehner, N. Holton, Y. Belkhadir, C. Zipfel, The receptor kinase FER is a RALF-regulated scaffold controlling plant immune signaling. *Science* **355**, 287–289 (2017). doi:10.1126/science.aal2541 Medline

4. A. Morato do Canto, P. H. O. Ceciliato, B. Ribeiro, F. A. Ortiz Morea, A. A. Franco Garcia, M. C. Silva-Filho, D. S. Moura, Biological activity of nine recombinant AtRALF peptides: Implications for their perception and function in *Arabidopsis*. *Plant Physiol. Biochem.* **75**, 45–54 (2014). doi:10.1016/j.plaphy.2013.12.005 Medline

5. R. Srivastava, J. X. Liu, H. Guo, Y. Yin, S. H. Howell, Regulation and processing of a plant peptide hormone, AtRALF23, in *Arabidopsis*. *Plant J.* **59**, 930–939 (2009). doi:10.1111/j.1365-313X.2009.03926.x Medline

6. J. Wu, E. L. Kurten, G. Monshausen, G. M. Hummel, S. Gilroy, I. T. Baldwin, NaRALF, a peptide signal essential for the regulation of root hair tip apoplastic pH in *Nicotiana attenuata*, is required for root hair development and plant growth in native soils. *Plant J.* **52**, 877–890 (2007). doi:10.1111/j.1365-313X.2007.03289.x Medline

7. M. Haruta, G. Sabat, K. Stecker, B. B. Minkoff, M. R. Sussman, A peptide hormone and its receptor protein kinase regulate plant cell expansion. *Science* **343**, 408–411 (2014). doi:10.1126/science.1244454 Medline

8. P. A. Covey, C. C. Subbaiah, R. L. Parsons, G. Pearce, F. T. Lay, M. A. Anderson, C. A. Ryan, P. A. Bedinger, A pollen-specific RALF from tomato that regulates pollen tube elongation. *Plant Physiol.* **153**, 703–715 (2010). doi:10.1104/pp.110.155457 Medline

9. G. Y. Zhang, J. Wu, X. W. Wang, Cloning and expression analysis of a pollen preferential rapid alkalinization factor gene, BoRALF1, from broccoli flowers. *Mol. Biol. Rep.* **37**, 3273–3281 (2010). doi:10.1007/s11033-009-9912-9 Medline

10. M. Schiøtt, S. M. Romanowsky, L. Baekgaard, M. K. Jakobsen, M. G. Palmgren, J. F. Harper, A plant plasma membrane Ca^{2+} pump is required for normal pollen tube growth and fertilization. *Proc. Natl. Acad. Sci. U.S.A.* **101**, 9502–9507 (2004). doi:10.1073/pnas.0401542101 Medline

11. A. Boisson-Dernier, S. Roy, K. Kritsas, M. A. Grobei, M. Jaciubek, J. I. Schroeder, U. Grossniklaus, Disruption of the pollen-expressed FERONIA homologs ANXUR1 and

ANXUR2 triggers pollen tube discharge. *Development* **136**, 3279–3288 (2009). doi:10.1242/dev.040071 Medline

12. S. Miyazaki, T. Murata, N. Sakurai-Ozato, M. Kubo, T. Demura, H. Fukuda, M. Hasebe, ANXUR1 and 2, sister genes to FERONIA/SIRENE, are male factors for coordinated fertilization. *Curr. Biol.* **19**, 1327–1331 (2009). doi:10.1016/j.cub.2009.06.064 Medline

13. A. Boisson-Dernier, D. S. Lituiev, A. Nestorova, C. M. Franck, S. Thirugnanarajah, U. Grossniklaus, ANXUR receptor-like kinases coordinate cell wall integrity with growth at the pollen tube tip via NADPH oxidases. *PLOS Biol.* **11**, e1001719 (2013). doi:10.1371/journal.pbio.1001719 Medline

14. A. Boisson-Dernier, C. M. Franck, D. S. Lituiev, U. Grossniklaus, Receptor-like cytoplasmic kinase MARIS functions downstream of *Cr*RLK1L-dependent signaling during tip growth. *Proc. Natl. Acad. Sci. U.S.A.* **112**, 12211–12216 (2015). doi:10.1073/pnas.1512375112 Medline

15. M. L. Márton, A. Fastner, S. Uebler, T. Dresselhaus, Overcoming hybridization barriers by the secretion of the maize pollen tube attractant ZmEA1 from *Arabidopsis* ovules. *Curr. Biol.* **22**, 1194–1198 (2012). doi:10.1016/j.cub.2012.04.061 Medline

16. S. Okuda, T. Suzuki, M. M. Kanaoka, H. Mori, N. Sasaki, T. Higashiyama, Acquisition of LURE-binding activity at the pollen tube tip of *Torenia fournieri*. *Mol. Plant* **6**, 1074–1090 (2013). doi:10.1093/mp/sst050 Medline

17. H. Vogler, D. Felekis, B. J. Nelson, U. Grossniklaus, Measuring the mechanical properties of plant cell walls. *Plants* **4**, 167–182 (2015). doi:10.3390/plants4020167 Medline

18. Y. Chebli, M. Kaneda, R. Zerzour, A. Geitmann, The cell wall of the *Arabidopsis* pollen tube—spatial distribution, recycling, and network formation of polysaccharides. *Plant Physiol.* **160**, 1940–1955 (2012). doi:10.1104/pp.112.199729 Medline

19. H. Höfte, The yin and yang of cell wall integrity control: Brassinosteroid and FERONIA signaling. *Plant Cell Physiol.* **56**, 224–231 (2015). doi:10.1093/pcp/pcu182 Medline

20. P. K. Hepler, C. M. Rounds, L. J. Winship, Control of cell wall extensibility during pollen tube growth. *Mol. Plant* **6**, 998–1017 (2013). doi:10.1093/mp/sst103 Medline

21. J. Chen, F. Yu, Y. Liu, C. Du, X. Li, S. Zhu, X. Wang, W. Lan, P. L. Rodriguez, X. Liu, D. Li, L. Chen, S. Luan, FERONIA interacts with ABI2-type phosphatases to facilitate signaling cross-talk between abscisic acid and RALF peptide in *Arabidopsis*. *Proc. Natl. Acad. Sci. U.S.A.* **113**, E5519–E5527 (2016). doi:10.1073/pnas.1608449113 Medline

22. A. Boisson-Dernier, S. A. Kessler, U. Grossniklaus, The walls have ears: The role of plant CrRLK1Ls in sensing and transducing extracellular signals. *J. Exp. Bot.* **62**, 1581–1591 (2011). doi:10.1093/jxb/erq445 Medline

23. N. Baumberger, C. Ringli, B. Keller, The chimeric leucine-rich repeat/extensin cell wall protein LRX1 is required for root hair morphogenesis in *Arabidopsis thaliana*. *Genes Dev.* **15**, 1128–1139 (2001). doi:10.1101/gad.200201 Medline

24. N. Baumberger, B. Doesseger, R. Guyot, A. Diet, R. L. Parsons, M. A. Clark, M. P. Simmons, P. Bedinger, S. A. Goff, C. Ringli, B. Keller, Whole-genome comparison of leucine-rich repeat extensins in *Arabidopsis* and rice. A conserved family of cell wall proteins form a vegetative and a reproductive clade. *Plant Physiol.* **131**, 1313–1326 (2003). doi:10.1104/pp.102.014928 Medline

25. T. Ndinyanka Fabrice, H. Vogler, C. Draeger, G. Munglani, S. Gupta, A. G. Herger, P. Knox, U. Grossniklaus, C. Ringli, LRX proteins play a crucial role in pollen grain and pollen tube cell wall development. bioRxiv:10.1101/223008 (2017).

26. T. Schallus, C. Jaeckh, K. Fehér, A. S. Palma, Y. Liu, J. C. Simpson, M. Mackeen, G. Stier, T. J. Gibson, T. Feizi, T. Pieler, C. Muhle-Goll, Malectin: A novel carbohydrate-binding protein of the endoplasmic reticulum and a candidate player in the early steps of protein N-glycosylation. *Mol. Biol. Cell* **19**, 3404–3414 (2008). doi:10.1091/mbc.E08-04-0354 Medline

27. C. Li, F.-L. Yeh, A. Y. Cheung, Q. Duan, D. Kita, M.-C. Liu, J. Maman, E. J. Luu, B. W. Wu, L. Gates, M. Jalal, A. Kwong, H. Carpenter, H.-M. Wu, Glycosylphosphatidylinositol-anchored proteins as chaperones and co-receptors for FERONIA receptor kinase signaling in *Arabidopsis*. *eLife* **4**, e06587 (2015). doi:10.7554/eLife.06587

28. H. Liao, R. Tang, X. Zhang, S. Luan, F. Yu, FERONIA receptor kinase at the crossroads of hormone signaling and stress responses. *Plant Cell Physiol.* **58**, 1143–1150 (2017). doi:10.1093/pcp/pcx048

29. J. M. Alonso, A. N. Stepanova, T. J. Leisse, C. J. Kim, H. Chen, P. Shinn, D. K. Stevenson, J. Zimmerman, P. Barajas, R. Cheuk, C. Gadrinab, C. Heller, A. Jeske, E. Koesema, C. C. Meyers, H. Parker, L. Prednis, Y. Ansari, N. Choy, H. Deen, M. Geralt, N. Hazari, E. Hom, M. Karnes, C. Mulholland, R. Ndubaku, I. Schmidt, P. Guzman, L. Aguilar-Henonin, M. Schmid, D. Weigel, D. E. Carter, T. Marchand, E. Risseeuw, D. Brogden, A. Zeko, W. L. Crosby, C. C. Berry, J. R. Ecker, Genome-wide insertional mutagenesis of *Arabidopsis thaliana*. *Science* **301**, 653–657 (2003). doi:10.1126/science.1086391 Medline

30. N. Saitou, M. Nei, The neighbor-joining method: A new method for reconstructing phylogenetic trees. *Mol. Biol. Evol.* **4**, 406–425 (1987). Medline

31. J. Felsenstein, Confidence limits on phylogenies: An approach using the bootstrap. *Evolution* **39**, 783–791 (1985). doi:10.1111/j.1558-5646.1985.tb00420.x Medline

32. E. Zuckerkandl, L. Pauling, Evolutionary divergence and convergence in proteins. In *Evolving Genes and Proteins*, V. Bryson, H. J. Vogel, Eds. (Academic Press, 1965), pp. 97–166.

33. S. Kumar, G. Stecher, K. Tamura, MEGA7: Molecular evolutionary genetics analysis version 7.0 for bigger datasets. *Mol. Biol. Evol.* **33**, 1870–1874 (2016). doi:10.1093/molbev/msw054 Medline

34. S. J. Clough, A. F. Bent, Floral dip: A simplified method for *Agrobacterium*-mediated transformation of *Arabidopsis thaliana*. *Plant J.* **16**, 735–743 (1998). doi:10.1046/j.1365-313x.1998.00343.x Medline

35. R. Schwab, S. Ossowski, M. Riester, N. Warthmann, D. Weigel, Highly specific gene silencing by artificial microRNAs in *Arabidopsis*. *Plant Cell* **18**, 1121–1133 (2006). doi:10.1105/tpc.105.039834 Medline

36. M. D. Curtis, U. Grossniklaus, A gateway cloning vector set for high-throughput functional analysis of genes in planta. *Plant Physiol.* **133**, 462–469 (2003). doi:10.1104/pp.103.027979 Medline

37. A. P. Gleave, A versatile binary vector system with a T-DNA organisational structure conducive to efficient integration of cloned DNA into the plant genome. *Plant Mol. Biol.* **20**, 1203–1207 (1992). doi:10.1007/BF00028910 Medline

38. U. K. Laemmli, Cleavage of structural proteins during the assembly of the head of bacteriophage T4. *Nature* **227**, 680–685 (1970). doi:10.1038/227680a0 Medline

39. A. E. Loraine, S. McCormick, A. Estrada, K. Patel, P. Qin, RNA-seq of *Arabidopsis* pollen uncovers novel transcription and alternative splicing. *Plant Physiol.* **162**, 1092–1109 (2013). doi:10.1104/pp.112.211441 Medline

40. L. M. Müller, H. Lindner, N. D. Pires, V. Gagliardini, U. Grossniklaus, A subunit of the oligosaccharyltransferase complex is required for interspecific gametophyte recognition in *Arabidopsis*. *Nat. Commun.* **7**, 10826 (2016). doi:10.1038/ncomms10826 Medline

41. N. Shamsudhin, N. Laeubli, H. B. Atakan, H. Vogler, C. Hu, W. Haeberle, A. Sebastian, U. Grossniklaus, B. J. Nelson, Massively parallelized pollen tube guidance and mechanical measurements on a lab-on-a-chip platform. *PLOS ONE* **11**, e0168138 (2016). doi:10.1371/journal.pone.0168138 Medline

PNAS
www.pnas.org

Supplementary Information for

Structural basis for recognition of RALF peptides by LRX proteins during pollen tube growth

Steven Moussu[1‡], Caroline Broyart[1‡], Gorka Santos-Fernandez[‡2], Sebastian Augustin[1], Sarah Wehrle[3], Ueli Grossniklaus[2], Julia Santiago[1*].

[1]The Plant Signaling Mechanisms Laboratory, Department of Plant Molecular Biology, University of Lausanne, 1015 Lausanne, Switzerland.
[2]Department of Plant and Microbial Biology and Zurich-Basel Plant Science Center, University of Zurich, 8008 Zurich, Switzerland.
[3]Institute of Bioengineering, École Polytechnique Fédérale de Lausanne, 1015 Lausanne, Switzerland.

[*]Corresponding author: julia.santiago@unil.ch (J.S)

[‡]These authors contributed equally to this work

This PDF file includes:

Figs. S1 to S22
Table S1 and S2

www.pnas.org/cgi/doi/10.1073/pnas.2000100117

Figure S1. RALF4/19 form a tight complex with the LRR core of pollen LRX proteins.

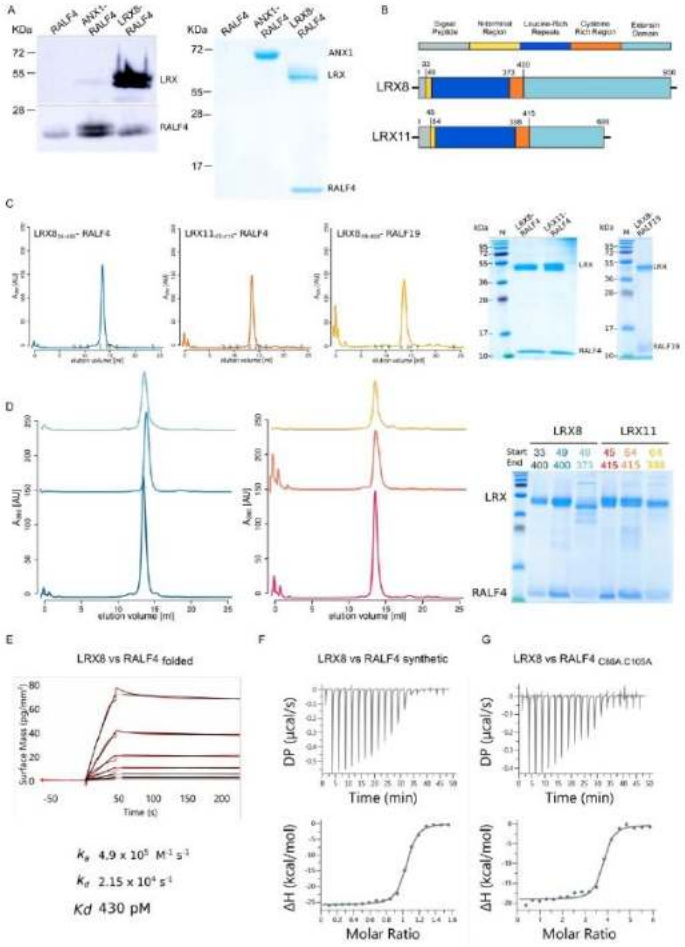

(*A*) Anti-HIS Western blot (left) of insect-cell culture pellets expressing or co-expressing RALF4, ANX1-RALF4 and LRX8-RALF4. SDS-PAGE of corresponding secreted protein fractions (right). (*B*) Schematic overview of LRX8 and LRX11 domains, including the amino acid coordinates according to structural data. (*C*) Analytical size exclusion chromatography (SEC) of $LRX8_{33-400}$-RALF4, $LRX11_{45-415}$-RALF4, and $LRX8_{49-400}$-RALF19 complexes (left). SDS-PAGE (right) of the different peaks corresponding to the SEC experiments. (*D*) Mapping of the LRX8/LRX11 domain interacting with RALF4 according to the schematic diagram in (*B*). SEC (left) of the LRX8/11-RALF4 complexes. SDS-PAGE (right) of the different SEC peaks. Colors of the SEC plots and the corresponding peak legends are matching. (*E*) Grating-coupled interferometry (GCI)-derived binding kinetics for LRX8 *vs* $RALF4_{folded}$. Shown are the sensogram with data in red and the respective curve fits in black. Table summaries of kinetic parameters are shown below (k_a, association rate constant; k_d, dissociation rate constant; K_D, dissociation constant). (*F*) and (*G*) Isothermal titration calorimetry thermogram (ITC) of the LRX8 protein *vs* $RALF4_{synthetic}$ and $RALF4_{C86A.C105A}$, respectively.

Figure S2. LRX8-RALF4 and LRX11-RALF4 mass spectrometry sequence determination.

A

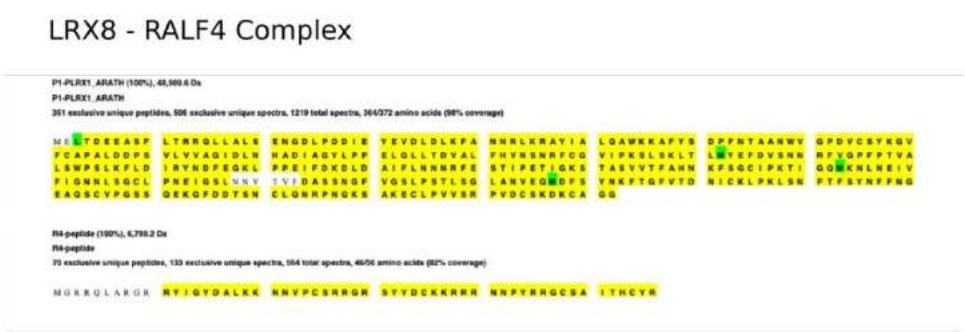

B

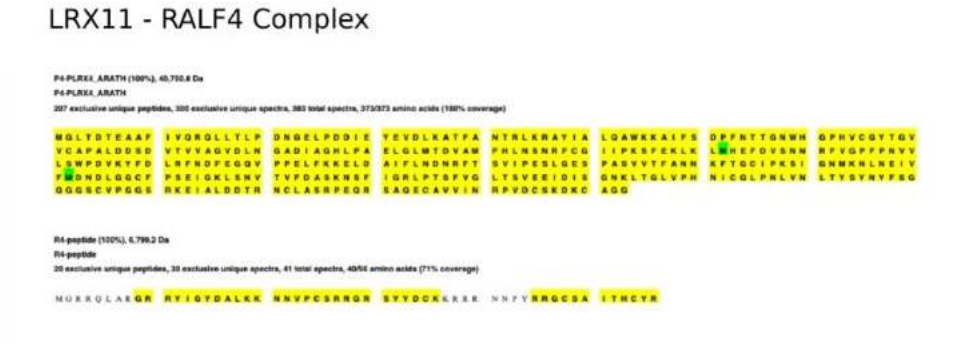

C

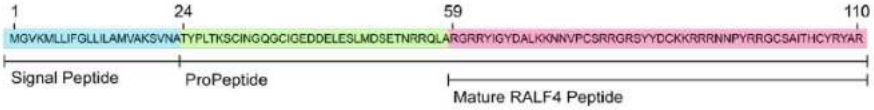

(A) and *(B)* Results from LC-MS/MS analysis of LRX8-RALF4 and LRX11-RALF4 protein complexes. Number of peptides and coverage for each component of the complex is highlighted in yellow. Oxidised methionines are highlighted in green. Leu 3 of LRX8 was identified as the N-terminal, N-acetylated residue, although the modification was only sporadically identified and was thus partial. Cys residues were reduced and alkylated (carbamidomethyl, not shown) and searched as fixed modification. All the sequence coverages are the combined results of tryptic and chymotryptic digestions and separate LC-MS/MS analyses on a high resolution orbitrap Fusion instrument. Samples in (*A*) were analysed by both HCD and EThcD fragmentation, while for results in (*B*) only HCD fragmentation was used. For more details see the Materials and Methods section. *(C)* Sequence map of full length RALF4 indicating the amino acid coordinates corresponding to the different signatures of the protein.

Figure S3. Isothermal titration calorimetry assays of LRX8 *vs* $RAL4_{folded}$, $RALF4_{CCCC}$ and $RALF4_{sythetic}$.

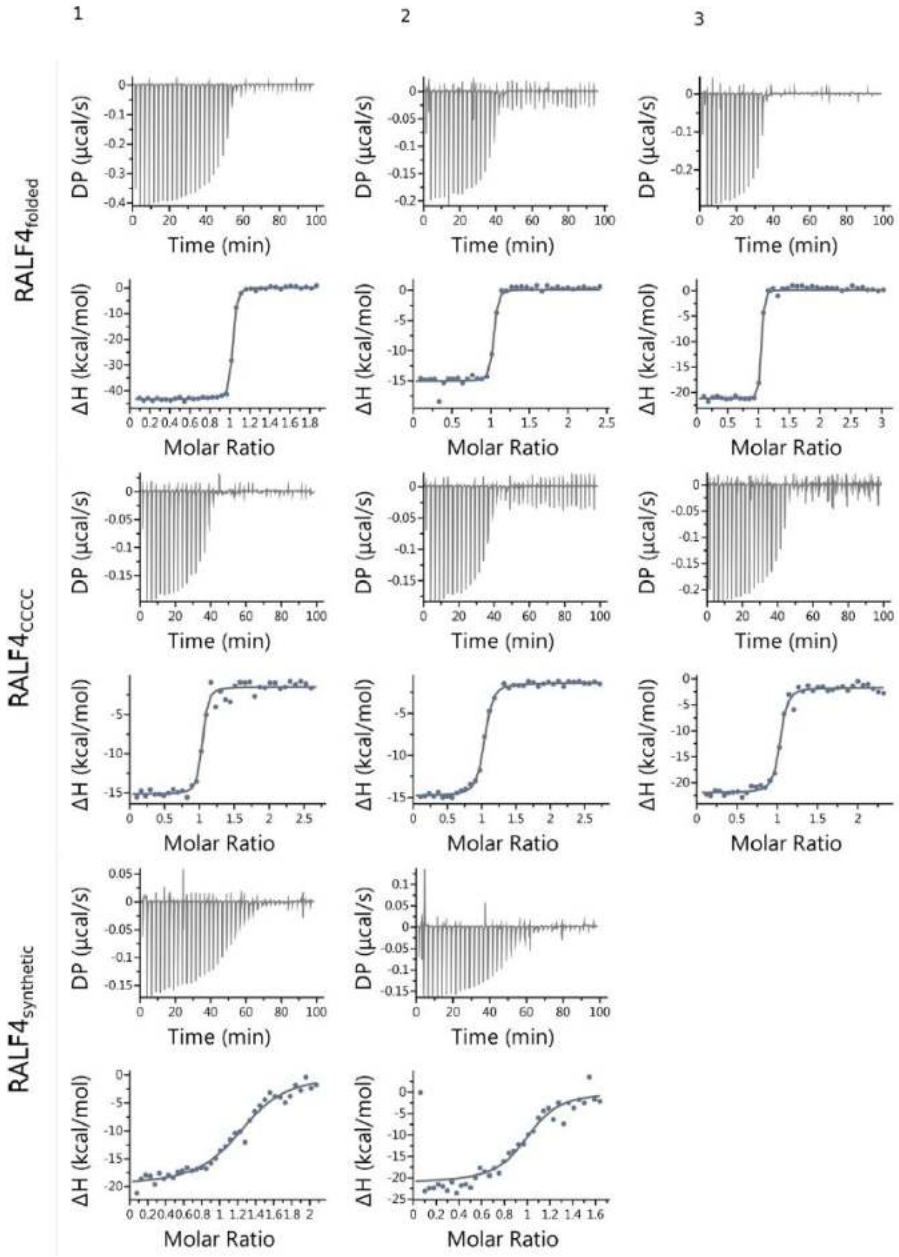

ITC thermograms of the independent experiments performed for each peptide.

Figure S4. Near-UV Circular Dichroism on different RALF4 peptides.

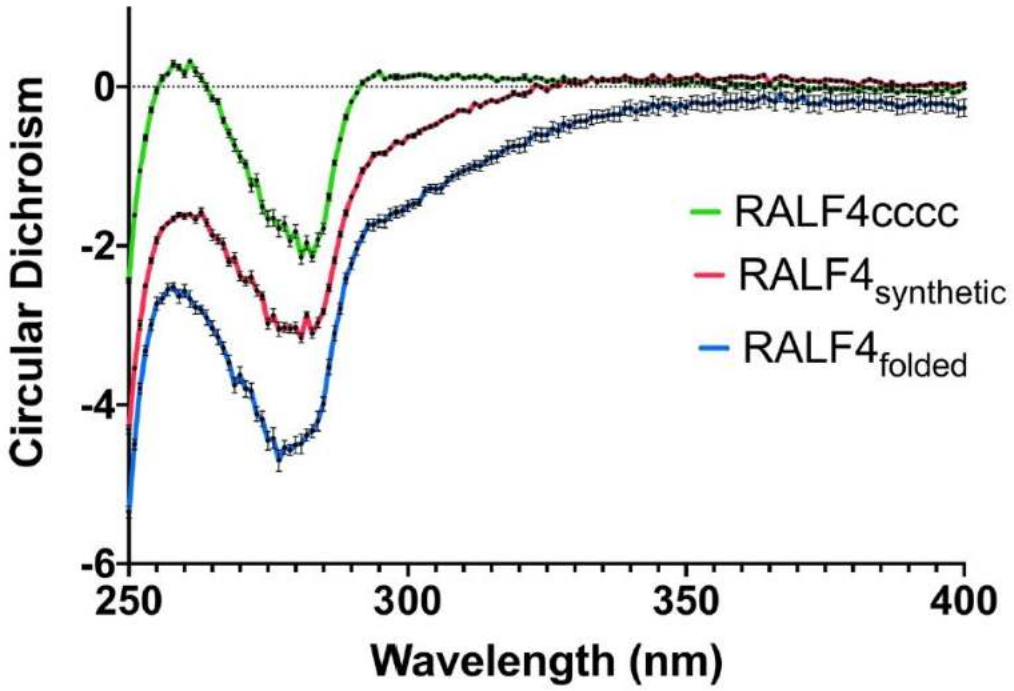

Circular dichroism near-UV spectra corresponding to different RALF4 peptides in solution. Depicted are the spectra for $RALF4_{folded}$ (blue), $RALF4_{synthetic}$ (red) and $RALF4_{CCCC}$ (green). Broad increase in signal (y-axes) indicates an increase in disulfide bonds abundance. Error bars represent the SEM over 10 measures.

Figure S5. LRX8 and 11 are constitutive dimers in their apo form or in complex with RALF4.

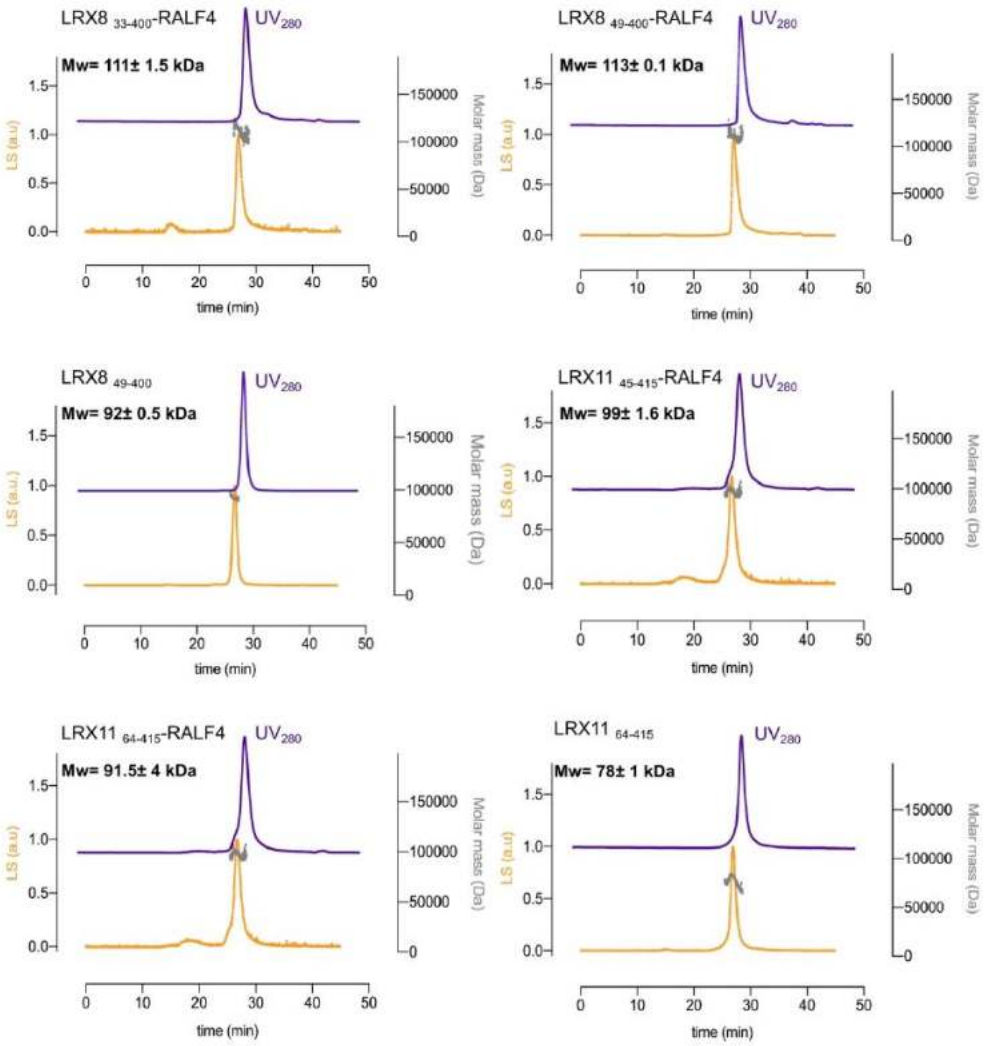

Molecular weight determination of the respective complexes using Multi Angle Light Scattering (MALS). UV_{280} absorption is plotted in purple, light scattering (LS) in orange, and the determined molecular weight (Da) in grey. The molecular weight indicated on each plot is the mean ± SD of two independent measurements.

Figure S6. LRX8-RALF4 and LRX2-RALF4 complexes share a common architecture.

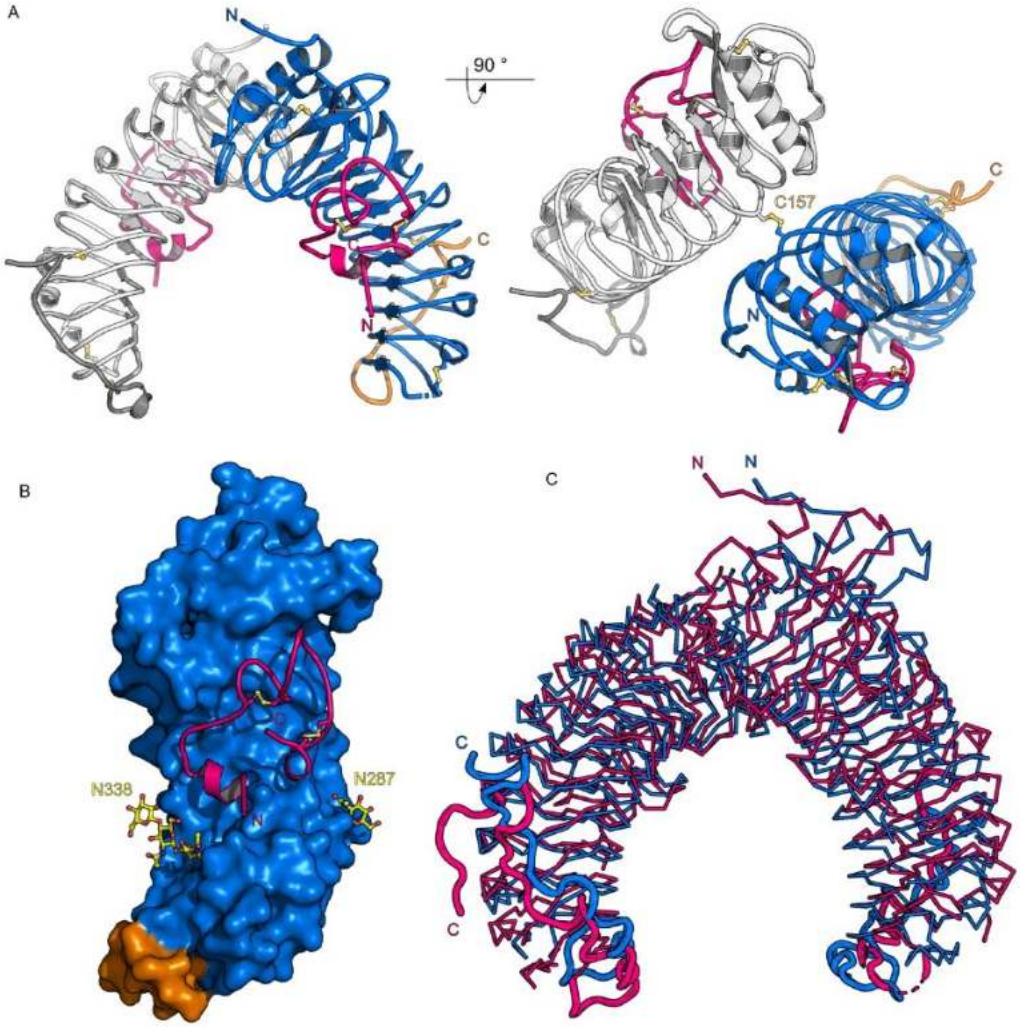

(*A*) Front and 90° x-axis rotated view of LRX8 covalently linked homodimer in complex with RALF4 (ribbon diagram). The LRR domain is depicted in blue, the Cys-rich tail in orange, and the RALF4 peptide is highlighted in pink. The disulfide bridge covalently linking the two LRX protomers is highlighted in yellow. (*B*) Surface view of LRX8 (color code as in *A*) along with cartoon representation of RALF4 peptide (in pink), highlighting the binding surface of the peptide. N-glycosylations are depicted in yellow. (*C*) Structural superimposition of the LRX2-RALF4 (Cα trace in pink) and LRX8-RALF4 (in blue) complexes. r.m.s.d. of ~ 0.8 Å comparing 357 pairs of corresponding Cα atoms between LRX2-RALF4 and LRX8-RALF4 complexes.

Figure S7. The LRX2/8-RALF4 complex interfaces are conserved among the LRX protein family.

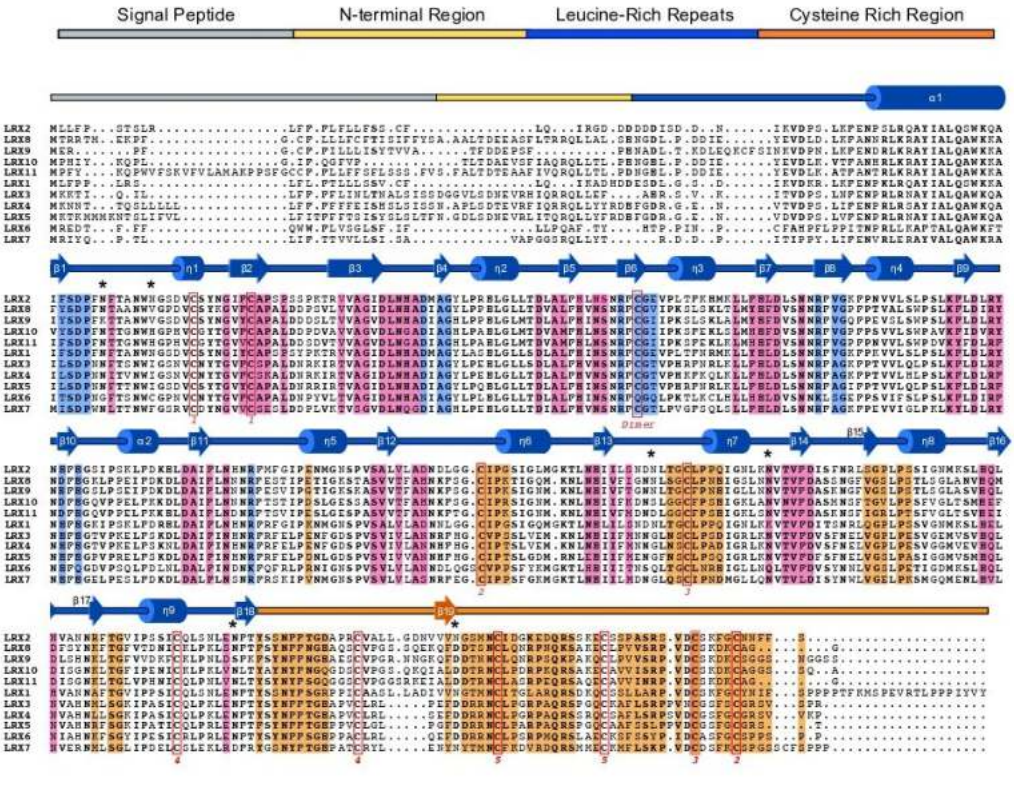

Structure-based sequence alignment of the LRX family members. The alignment includes a secondary structure assignment calculated with the program DSSP and colored according to Fig. 2 and Fig. S1*B*. Cys residues engaged in disulfide bonds are squared in red, with matching pairs indicated by numbers. Predicted and experimentally verified N-glycosylation sites are depicted by black stars. The various interaction surfaces in the LRX2/8-RALF4 complex structures are highlighted according to the following color code: LRX dimer interface in blue, LRX-RALF4 binding pocket in pink, and the interaction surface of the LRX Cys extension with the LRR core of the protein is highlighted in light orange.

Figure S8. RALF4 omit map and surface electrostatic potential of the peptide exposed surface.

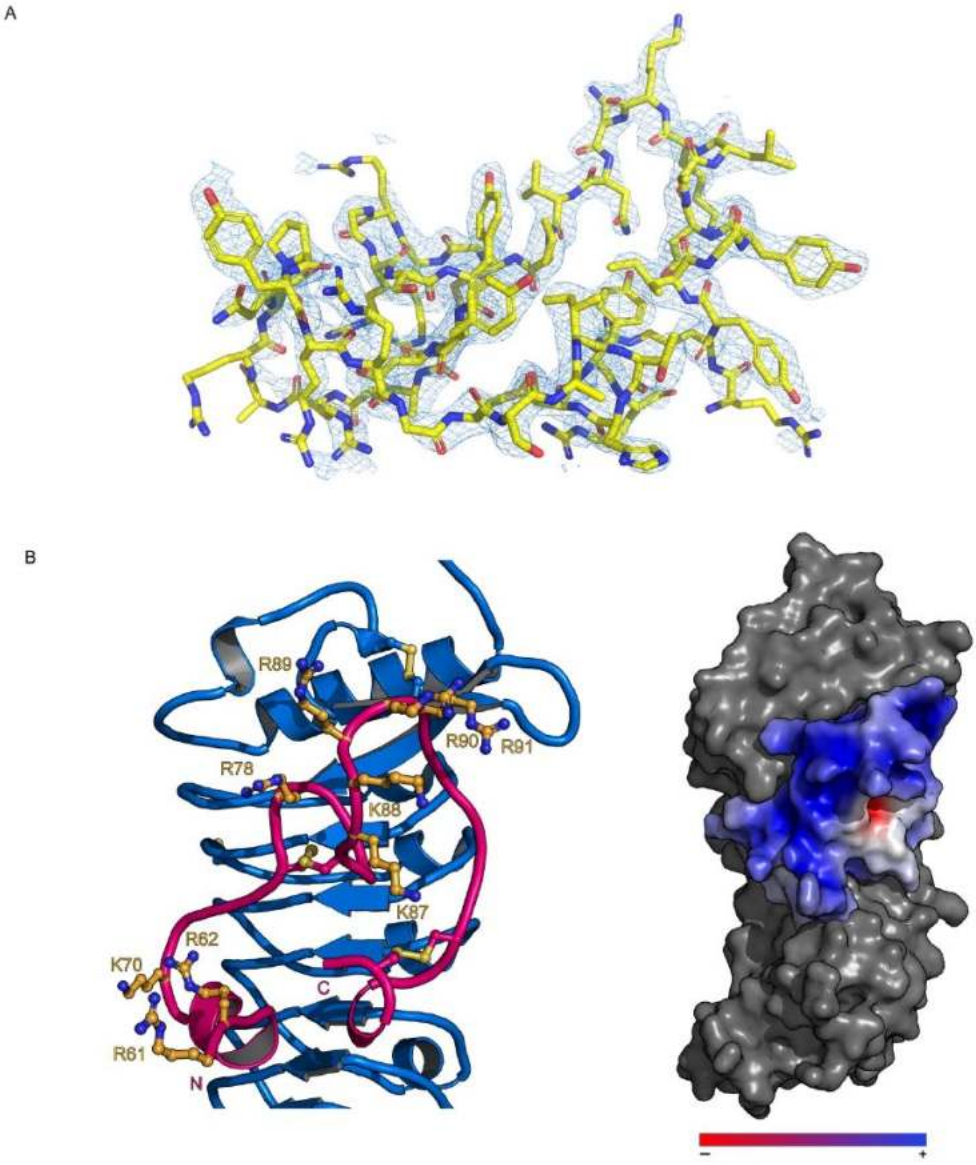

(*A*) RALF4 simulated annealing 2Fo-Fc omit electron density map contoured at 1.5 σ. (*B*) RALF4 reveals a positively-charged surface when bound to LRX. Details of the basic nature of RALF4 exposed surface (left). Arg (R) and Lys (K) free residues are shown as sticks in light orange. Electrostatic surface representation of RALF4 when in complex with LRX2 (right). LRX2 is shown in grey and RALF4 solvent-accessible surface electrostatic potential has been calculated using APBS plugin (PyMOL). The potential is given with the negative (red) and positive (blue) contour levels in the range from -8.0 to +8.0 kBT, respectively.

Figure S9. RALF4 binding interface to LRX is conserved among closely related RALF family members.

A

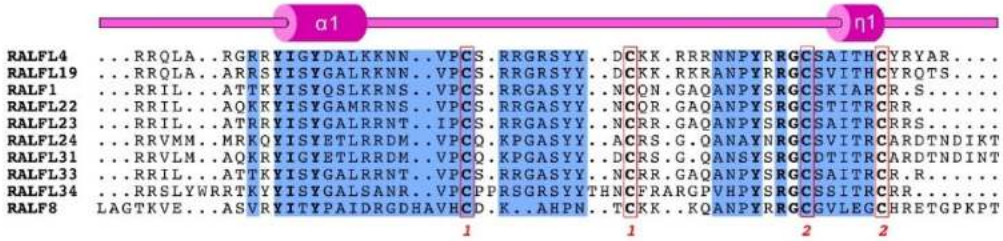

B

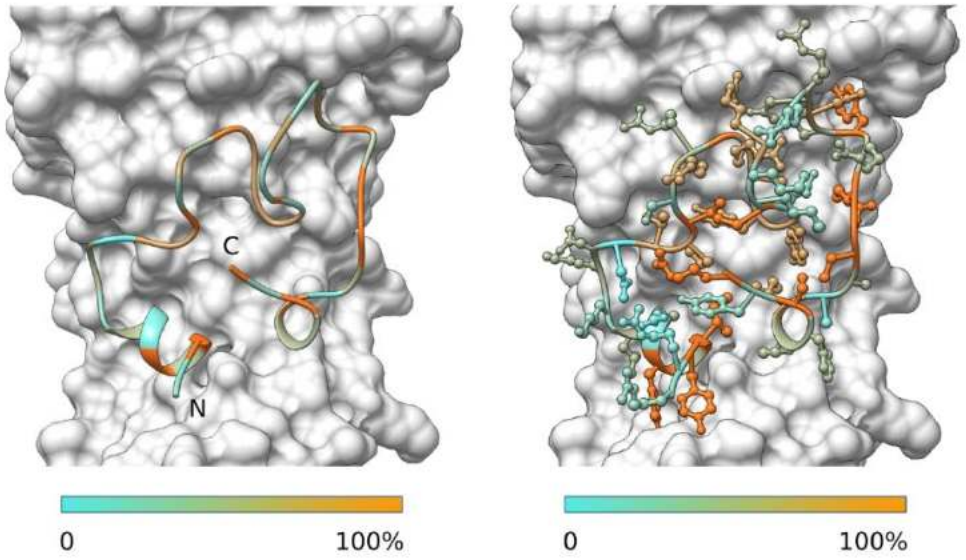

(*A*) Structure-based sequence alignment of RALF4 family related members. The alignment includes a secondary structure assignment calculated with the program DSSP and colored according to Fig. 2. Cys residues engaged in disulfide bonds are squared in red, with matching pairs indicated by numbers. The RALF4-LRX2 interaction surface is highlighted in blue. (*B*) The RALF4 regions directly interacting with the LRX binding pocket (highlighted in blue above) are conserved among RALF4-related family members. RALF4 ribbon representation (left) and depicting the amino acid lateral-chains (right) colored according to sequence conservation among RALF peptides indicated in the alignment above.

Figure S10. Ligplot representation of the interactions occurring in the LRX8-RALF4 interface.

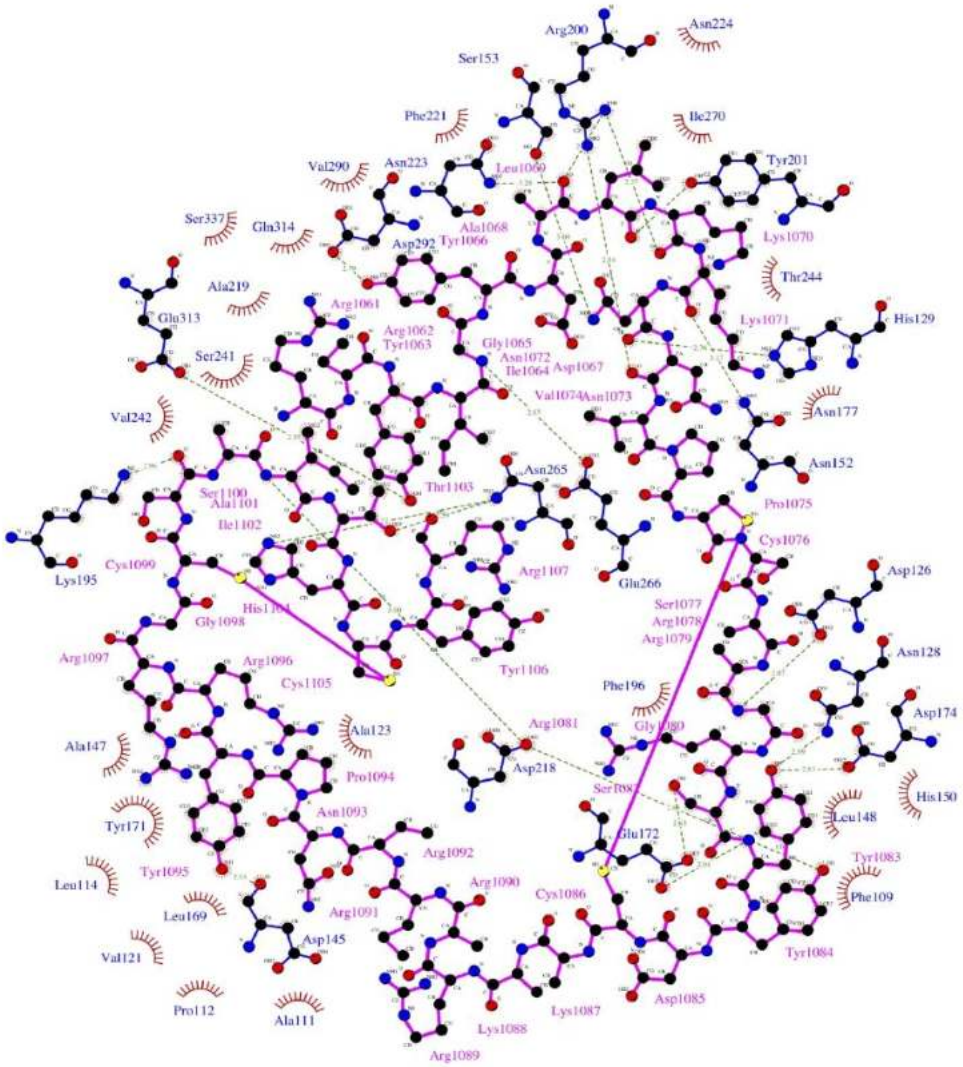

2-D ligand-interaction diagram of RALF4 (pink) and LRX8 (blue) generated with Ligplot. Hemispheres represent hydrophobic interactions. Disulfide bonds are depicted with a pink solid line and hydrogen bonds are represented in green.

Figure S11. *In vitro* and *in vivo* validation of the LRX8-RALF4 structure complex.

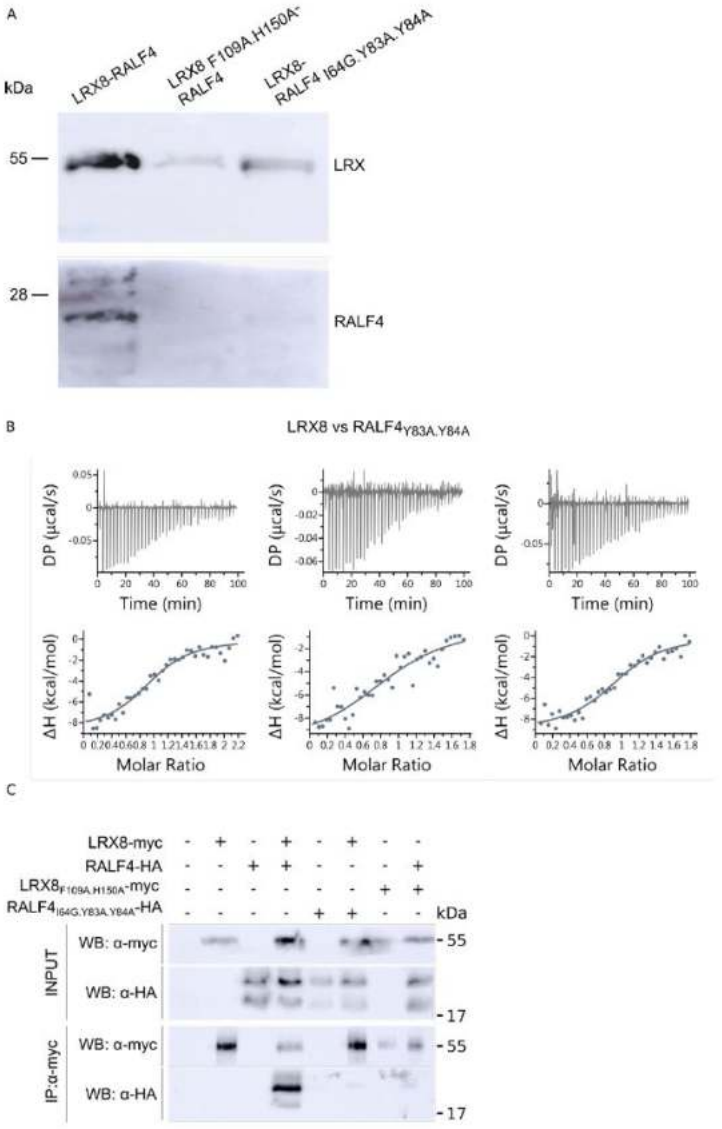

(*A*) *In vitro* validation of the LRX8-RALF4 complex. Western blot from insect cell co-expression cultures of LRX8-RALF4, LRX8$_{F109A.H150A}$-RALF4 (LRX peptide binding-pocket mutant), and LRX8-RALF4$_{I64A.Y83A.Y84A}$ (peptide binding mutant). (*B*) ITC thermograms of LRX8 *vs* RALF4$_{Y83A.Y84A}$. (C) *In vivo* validation of the LRX8-RALF4 complex structure. Co-immunoprecipitation (Co-IP) of LRX8-myc and RALF4-HA proteins transiently expressed in tobacco were performed using an anti-myc antibody (IP:α-myc). RALF4-HA peptides were detected with an anti-HA antibody in the IP elution.

Figure S12. Characterization of LRX8 complementation lines.

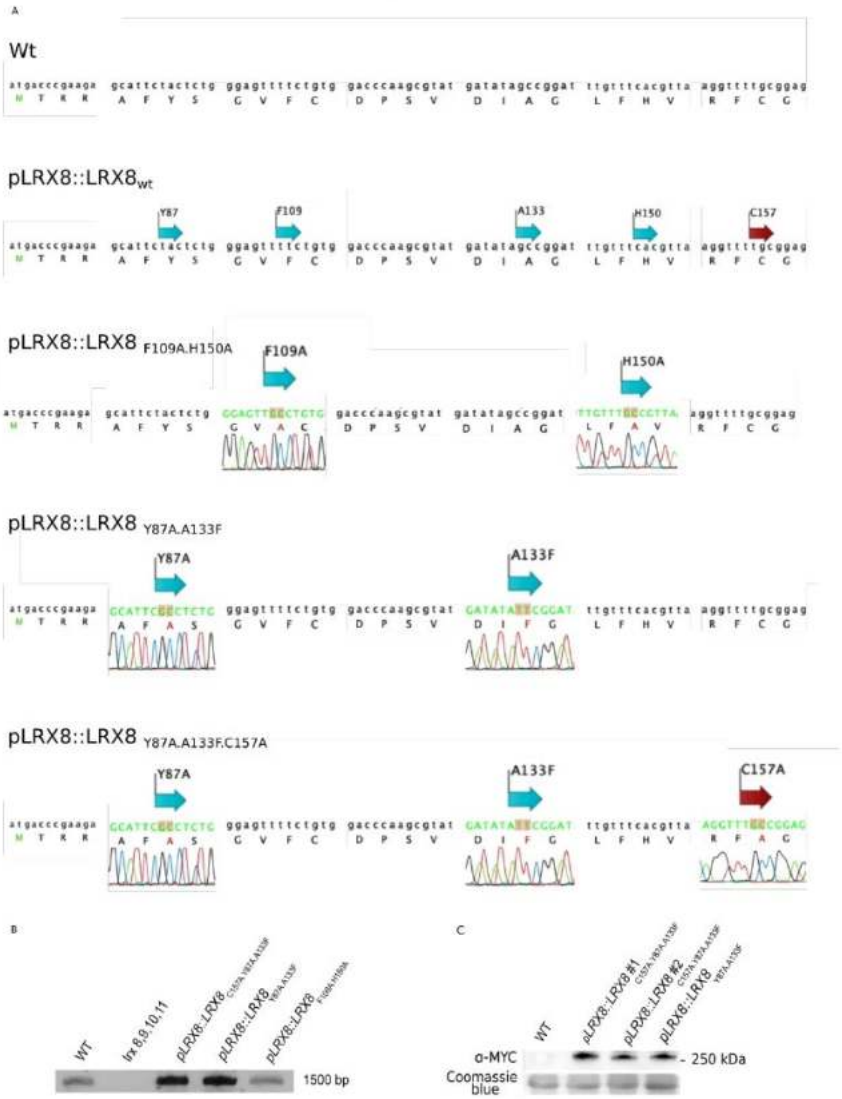

(*A*) Sequencing data of cDNA amplification of LRX8 in WT and *lrx8,9,10,11* complemented with either *pLRX8::LRX8*$_{C157A.Y87A.A133F}$, *pLRX8::LRX8*$_{Y87A.A133F}$ or *pLRX8::LRX8*$_{F109A.H150A}$, showing that the expression of the LRX8 band in (*B*) corresponds to the expression of the inserted mutant versions. (*B*) cDNA amplification of LRX8 in WT, *lrx8,9,10,11*, and *lrx8,9,10,11* complemented by either *pLRX8::LRX8*$_{C157A.Y87A.A133F}$, *pLRX8::LRX8*$_{Y87A.A133F}$, or *pLRX8::LRX8*$_{F109A.H150A}$, showing restoration of LRX8 expression in the complemented lines. (*C*) α-myc protein detection of LRX8 mutants in pollen.

Figure S13. *In planta* cell wall localization of LRX8 wild type and oligomeric mutants.

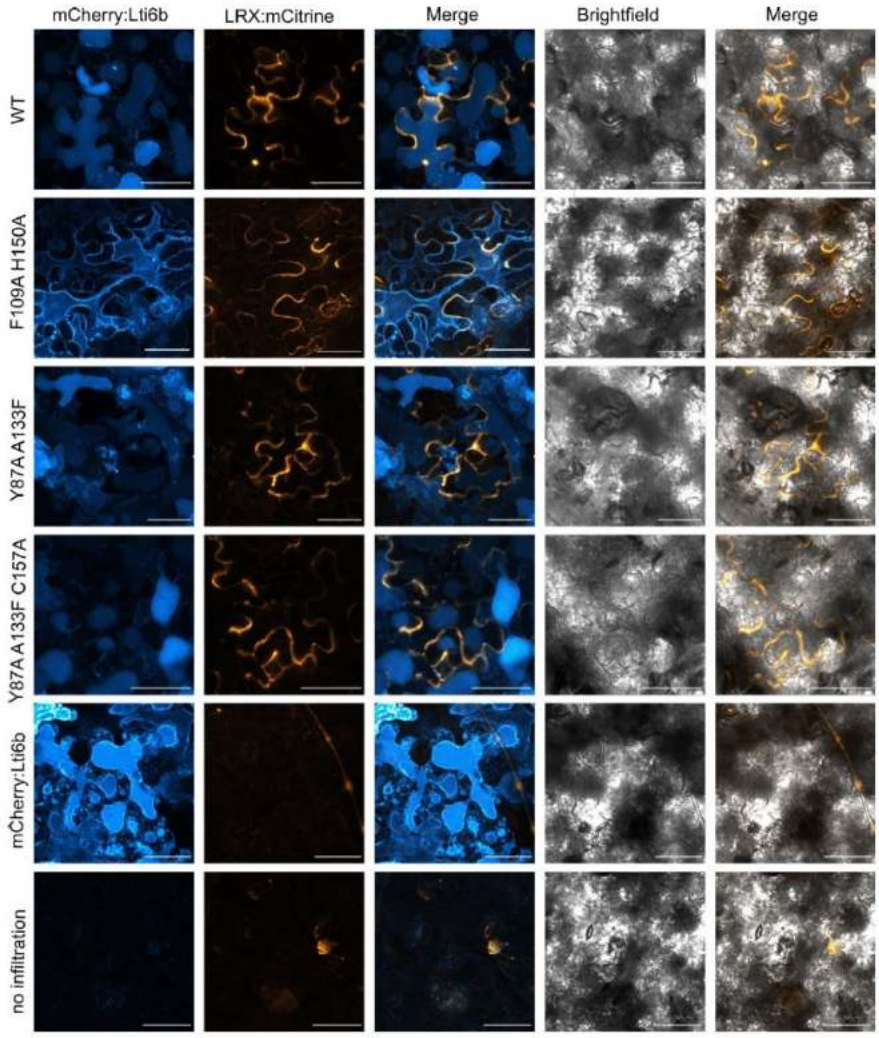

Subcellular localization of LRX8-mCitrine mutants. Plasmolysis experiments were performed on *N. benthamiana* leaves transiently transformed with mCitrine tagged LRX8 WT and mutants: *LRX8*$_{F109A.H150A}$-mCitrine, *LRX8*$_{Y87A.A133F}$-mCitrine, *LRX8*$_{C157A.Y87A.A133F}$-mCitrine, to check for proper cell wall localization. mCherry-Lti6b plasma membrane marker, depicted in blue, is used to properly visualize the shrinking of plasma membrane upon plasmolysis. The last two rows represent controls with only the plasma membrane marker or no infiltrated samples. Scale bar = 50 µm.

Figure S14. Purified proteins used in ITC experiments and ITC binding matrix of LRX8 and LRX8-RALF4$_{folded}$ *vs* pollen *Cr*RLK1L and LLGs.

A

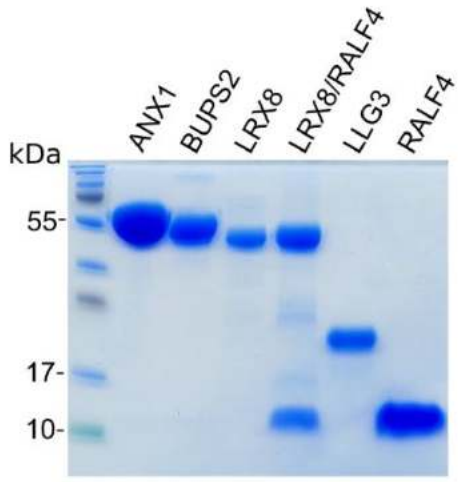

B

Ligand (Syringe)	Protein (Cell)	pH	Kd (nM)	ΔH (kcal/mol)	N
ANX1	LRX8	5		no binding detected	
BUPS2	LRX8	5		no binding detected	
LRX8	LLG3	5		no binding detected	
ANX1	LRX8-RALF4	5		no binding detected	
BUPS2	LRX8-RALF4	5		no binding detected	
LRX8-RALF4	LLG3	5		no binding detected	

Ligand (Syringe)	Protein (Cell)	pH	Kd (nM)	ΔH (kcal/mol)	N
ANX1	LRX8	7.5		no binding detected	
BUPS2	LRX8	7.5		no binding detected	
LRX8	LLG3	7.5		no binding detected	
ANX1	LRX8-RALF4	7.5		no binding detected	
BUPS2	LRX8-RALF4	7.5		no binding detected	
LRX8-RALF4	LLG3	7.5		no binding detected	

(*A*) SDS-PAGE of the purified proteins used in the ITC binding matrix. (*B*) ITC binding matrix of LRX8 and LRX8-RALF4 complex *vs* *Cr*RLK1L and LLGs in alkaline and acidic conditions.

Figure S15. Isothermal titration calorimetry thermograms of RALF4$_{folded}$ and LRX8 *vs* *Cr*RLK1Ls/LLGs at pH 7.5.

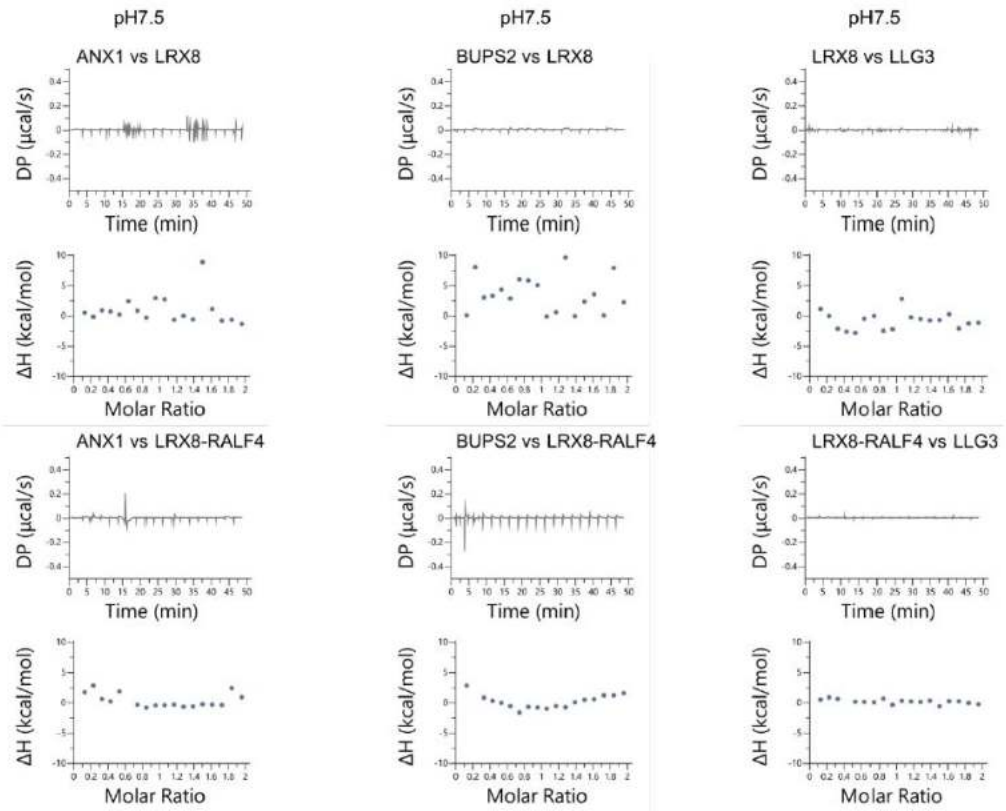

ITC thermograms of the independent experiments analyzed in Fig. S14B at pH 7.5.

Figure S16. Isothermal titration calorimetry thermograms of RALF4$_{folded}$ and LRX8 *vs* *Cr*RLK1Ls/LLGs at pH 5.

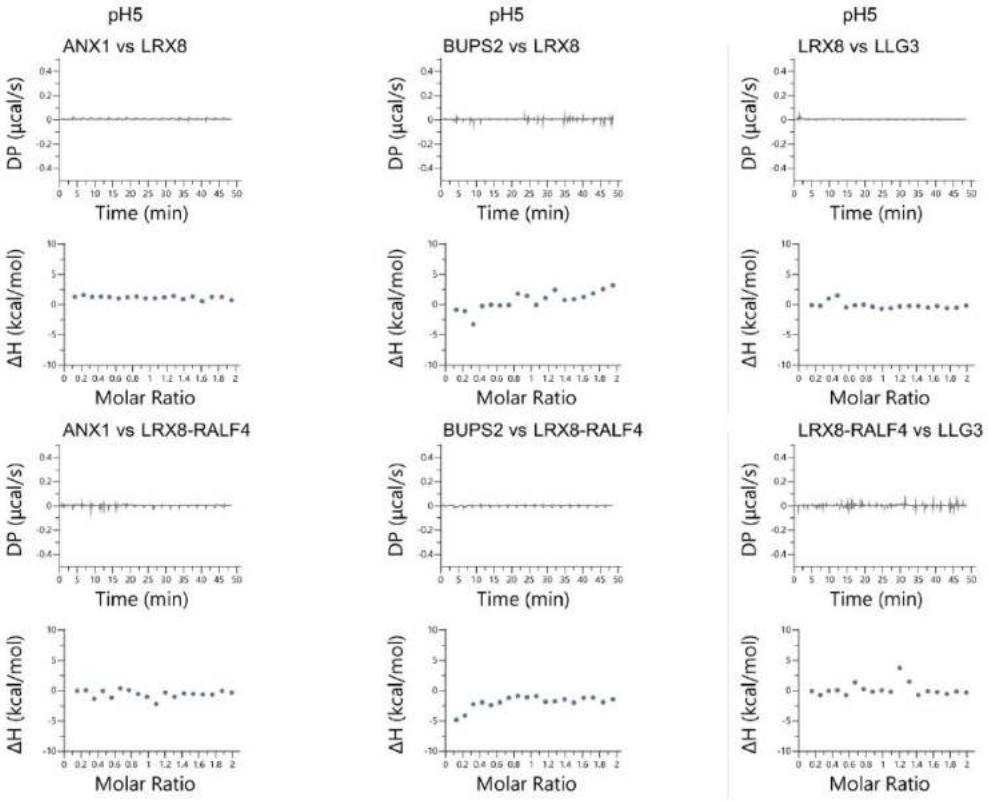

ITC thermograms of the independent experiments analyzed in Fig. S14B at pH 5.

Figure S17. Isothermal titration calorimetry thermograms of LRX8 and LLGs *vs* RAL4$_{folded}$ in alkaline and acidic conditions.

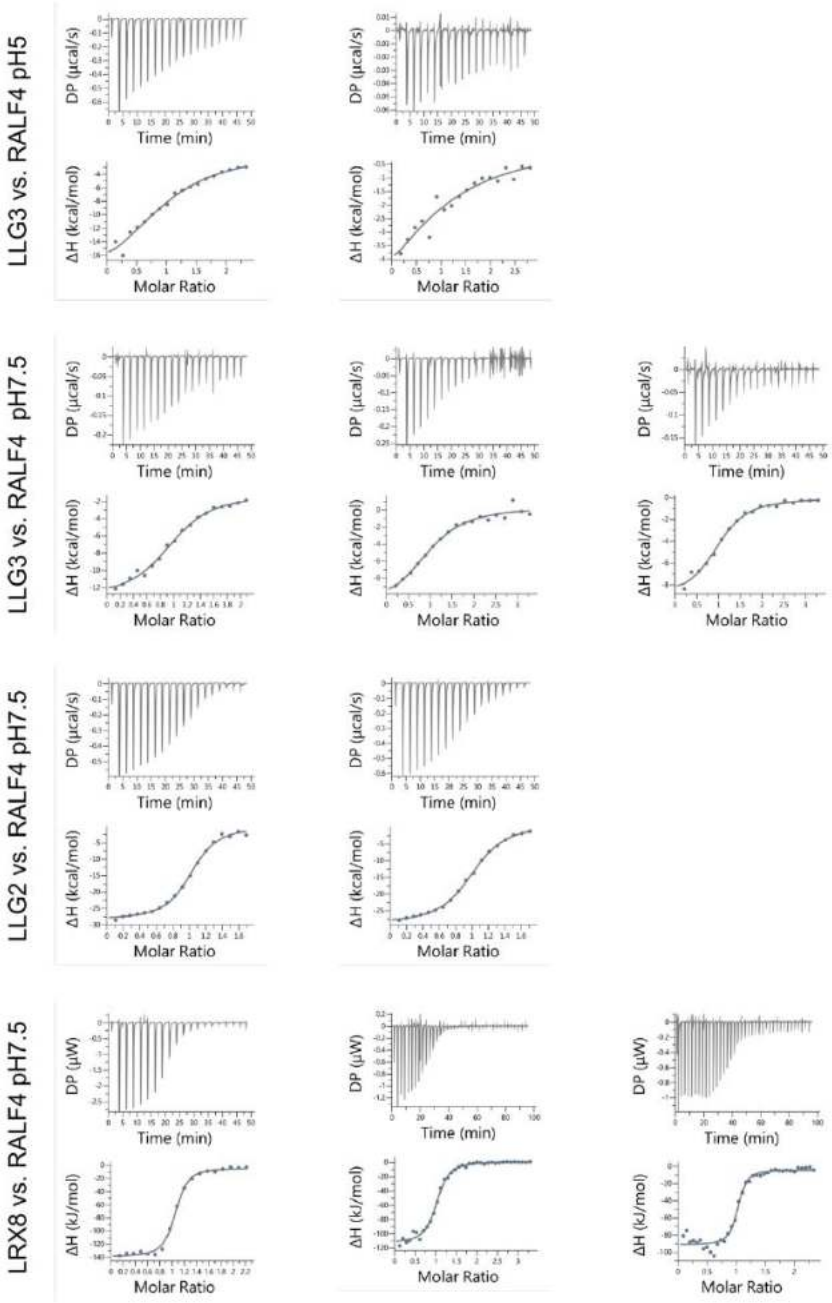

ITC thermograms of the independent experiments analyzed in Fig. 3*F*

Figure S18. Isothermal titration calorimetry thermograms of LRX8 and LLG3 *vs* RAL4$_{folded}$ Y63AY66A mutant in acidic conditions and alkaline conditions.

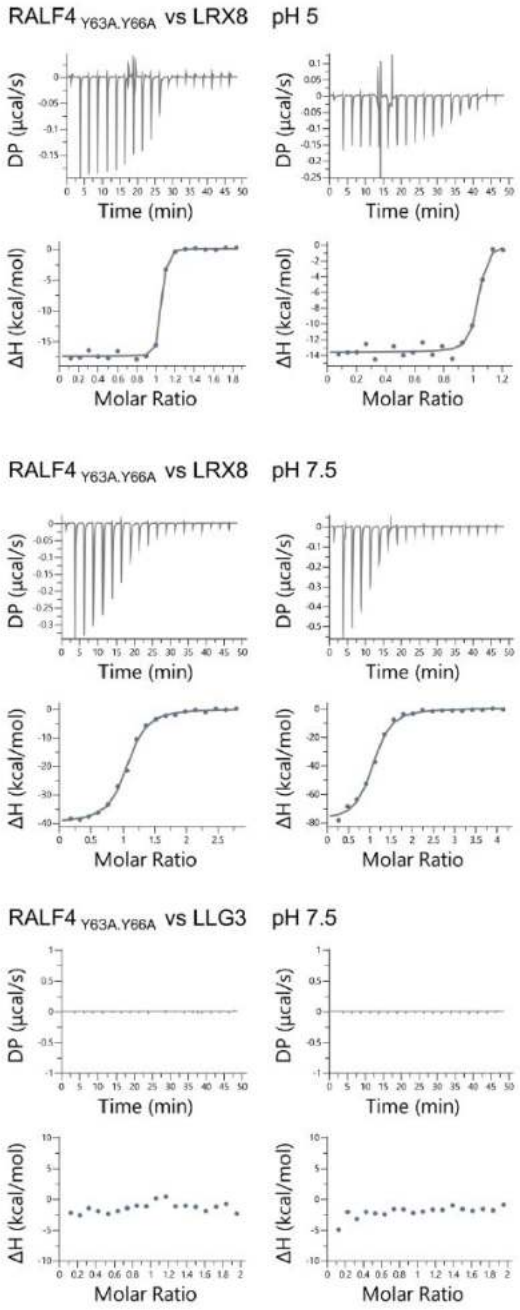

ITC thermograms of the independent experiments analyzed in Fig. 3*F*

Figure S19. Quantitative SEC-MALS analysis of the LRX-RALF dimer interface mutants and binding analysis of RALF4 to LRX8 monomer.

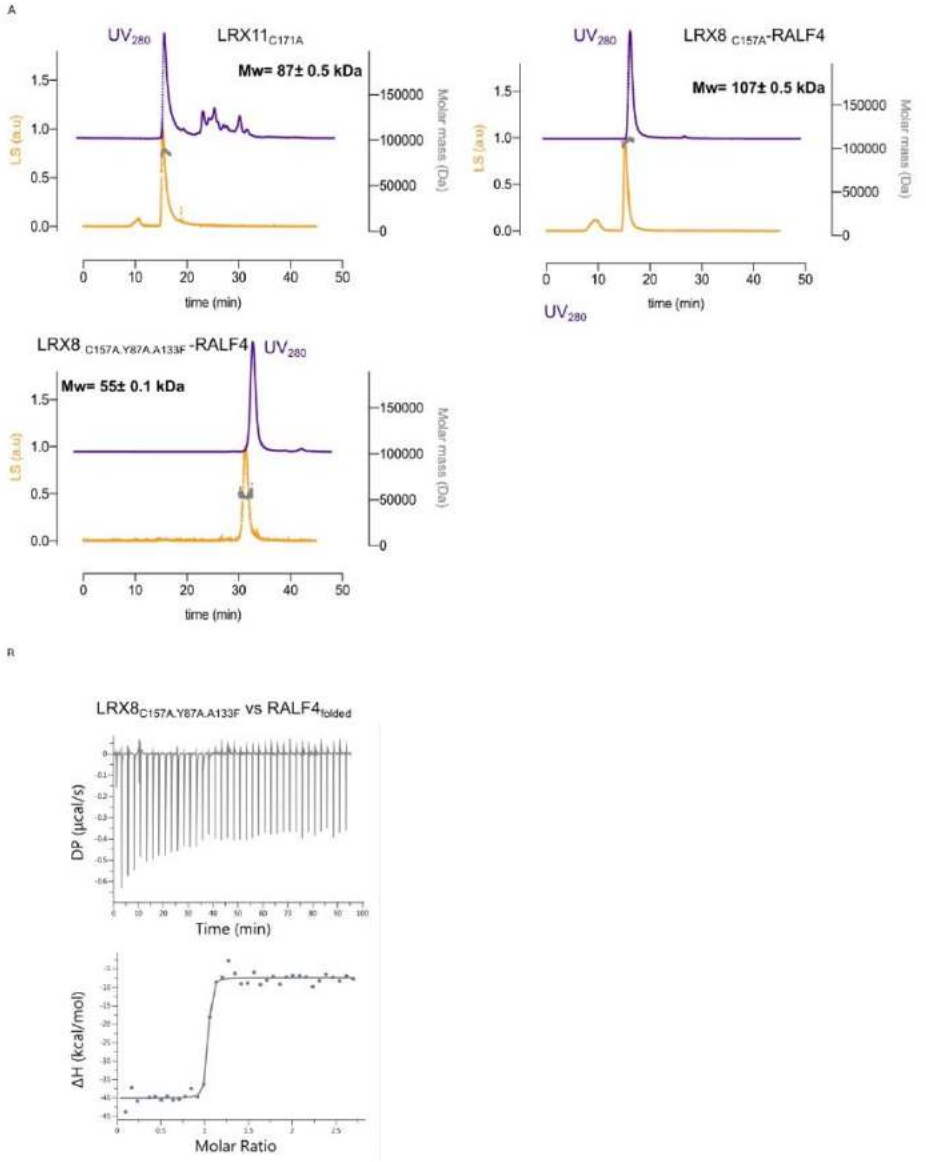

(*A*) Molecular weight determination of the respective complexes using MALS. UV_{280} absorption is plotted in purple, light scattering (LS) in orange, and the determined molecular weight (Da) in grey. The molecular weight indicated on each plot is the mean ± SD of two independent measurements. (*B*) ITC thermogram of $RALF4_{folded}$ *vs* $LRX8_{C157A,Y87A,A133F}$.

Figure S20. Monomeric LRX8 in complex with RALF4 shares a common architecture with the wild-type dimeric complex.

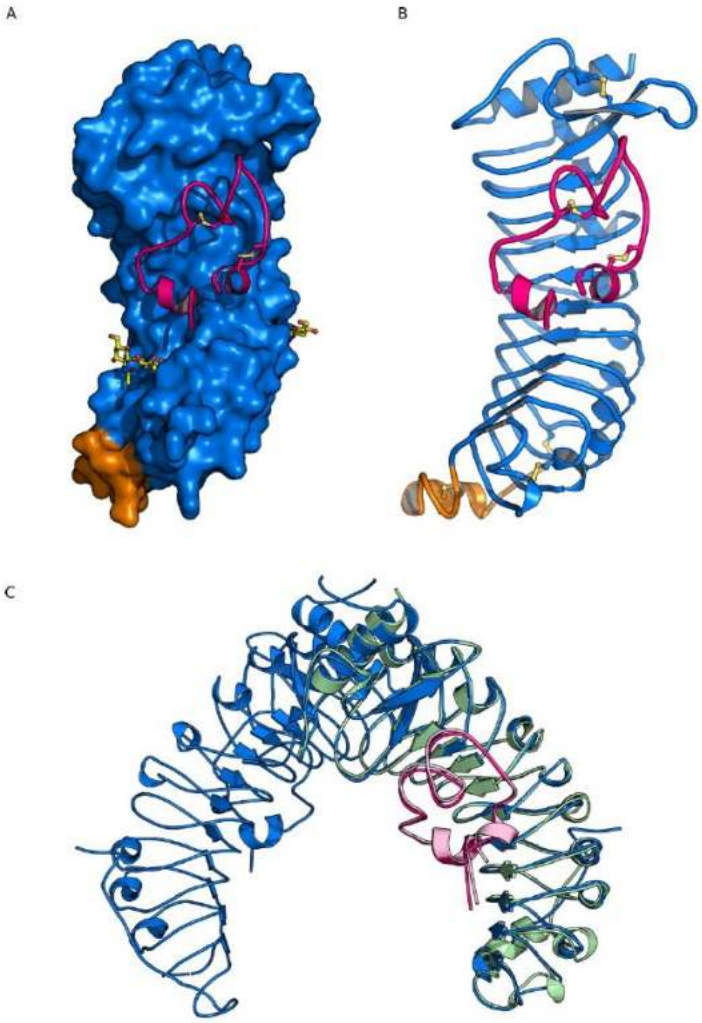

(*A*) Surface view of LRX8 (color code as in Fig. 2) along with cartoon representation of RALF4 peptide (in pink), highlighting the binding surface of the peptide. N-glycosylations are depicted in yellow. (*B*) Front view of LRX8 monomer in complex with RALF4 (ribbon diagram). The LRR domain is depicted in blue, the Cys-rich tail in orange, and the RALF4 peptide is highlighted in pink. (*C*) Structural superimposition of the LRX8-RALF4 dimer (Cα trace in blue, with the peptide in pink) and LRX8-RALF4 monomer (Cα trace in green, with the peptide depicted in light pink) complexes. R.m.s.d. of ~ 0.65 Å comparing 327 corresponding Cα atoms between the two proteins.

Figure S21. *In vivo* and *in vitro* confirmation of disulfide bonded LRX8 dimers.

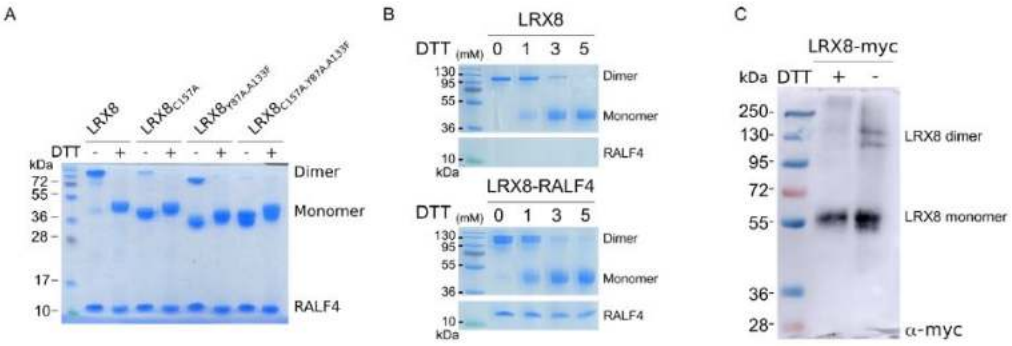

(A) SDS-PAGE analysis in the presence/absence of DTT of the mutants shown in Fig 4*C*. (*B*) *In vitro* validation of covalently linked LRX8 homodimers in denaturing conditions. SDS-PAGE gels of LRX8 alone (left) and in complex with RALF4 (right), treated with increasing DTT concentrations (0, 1, 3, and 5 mM). Dimers run above 100kDa while monomers run around 50kDa. (*C*) Detection of monomer and dimer species of transiently expressed $LRX8_{1\text{-}400}$ in tobacco leaves, ± DTT.

Figure S22. Dominant active MRI_{R240C} does not suppress the mutant phenotype of multiple *lrx* mutants.

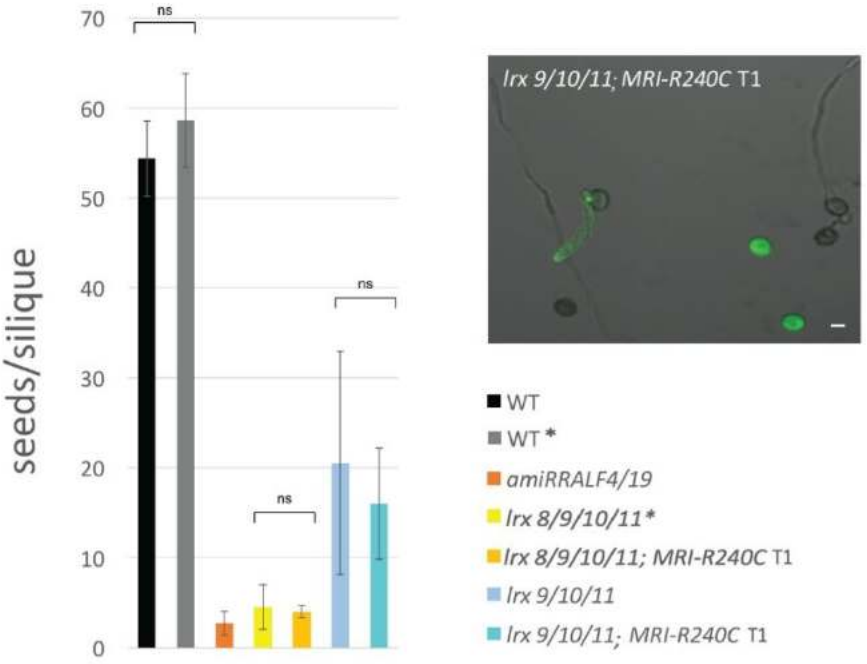

Introduction of the dominant active MRI_{R240C} kinase does not suppress the pollen tube defects of *lrx8/9/10/11* quadruple and *lrx9/10/11* triple mutants, as evidenced by the strongly reduced seed set per silique. Mutants with or without the MRI_{R240C} transgene (3 independent T1 lines) show no statistically significant (ns) difference in seed set. Six to eight siliques of three plants were analyzed per genotype. The plants marked by * were not grown at the same time (data from ref[5]) but since the wild-type (wt) controls showed no statistically significant difference, they are shown in the same graph. The inlet shows that although MRI_{R240C}-CFP was expressed in pollen grains and pollen tubes of the T1 plants, it did not suppress the *lrx9/10/11* mutant phenotype. Scale bar, 10 μm.

Table S1. Crystallographic data-collection and refinement statistics.

	LRX2-RALF4 *native*	LRX8-RALF4 *native*	$LRX8_{monomer}$-RALF4 *native*
Data collection			
Space group	*P 41*	*C 1 2 1*	*P1*
Cell dimensions			
a, *b*, *c* (Å)	119.99, 119.99, 305.73	205.84, 114.09, 146.97	51.8, 65.54, 83.7
α, β, γ (°)	90, 90, 90	90, 116.25, 90	72.12, 87.62, 68.36
Resolution (Å)	59.99 – 3.20 (3.31 – 3.20)	49.44 – 3.89 (4.13 – 3.89)	48 – 2.33 (2.47-2.33)
R_{meas}[#]	0.413 (2.79)	0.457 (2.15)	0.149 (1.02)
CC(1/2)[#] *(%)*	99.7 (58.1)	97.8 (34.8)	99 /42.5)
$I/\sigma I$[#]	10.82 (1.33)	4.44 (1.06)	5.21(1.14)
Completeness (%)[#]	99.82 (99.49)	99.6 (99.2)	97.2 (90.6)
Redundancy[#]	26.66 (27.55)	6.7 (6.7)	1.8 (1.77)
Wilson B-factor[#]	78.54	93.85	34.6
Refinement			
Resolution (Å)	59.99 – 3.20 (3.31 – 3.20)	49.44 – 3.89 (4.13 – 3.89)	48-2.33 (2.47-2.33)
No. reflections	1,212,145 (184,586)	191,042 (30,086)	142,294 (78,713)
R_{work}/ R_{free}[$]	0.223/0.272 (0.370/0.424)	0.281/0.329 (0.326/0.379)	0.172/0.228 (0.251/0.319)
No. atoms			
Protein	23,520	14,844	5,752
Glycan	773	226	84
R.m.s deviations[$]			
Bond lengths (Å)	0.003	0.003	0.008
Bond angles (°)	0.75	0.76	0.9
Molprobity results			
Ramachandran outliers (%)[‡]	0.27	0.32	0.00
Ramachandran favored (%)[‡]	90.62	87.54	92.63
Molprobity score[‡]	2.16	2.22	1.74
PDB-ID	**6QXP**	**6QWN**	**6TME**

[#] XDS (54), [$] PHENIX (49), [‡] MOLPROBITY (52)

Table S2. Correspondence between amino acids of LRX2, LRX8, and LRX11.

Surface	LRX2	LRX8	LRX11
Homodimer	C138	C157	C171
	F68	Y87	F101
	A114	A133	A147
	Y116	Y135	Y149
	R136	R155	R169
	R160	R179	R193
	E184	D203	D217
LRX/RALF	F90	F109	V123
	H131	H150	H164
	E153	E172	E186
	D155	D174	D188
	D199	D218	D232
	E248	E266	E280
	E295	E313	E327
	Q296	Q314	E328
Cysteine Tail	C364	C382	C397
	C374	C392	C407
	C379	C397	C412
	C324	C253	C267
	C259	C277	C291
	C351	C369	C384
	I235	I254	I268
	Q263	E281	E295
	N326	N344	N358
	D331	E349	Q363
	N350	N368	N363
	K355	R373	R388
	R359	K377	R392
	E363	E381	E396
	N381	G399	G414
N-Glycosylations	N73	N92	N106
	N269	N287	N301
	N320	N338	N352
	N346	D364	D379

Table indicating the equivalent amino acids involved in the different interaction surfaces among LRX2, LRX8, and LRX11.